

**MITIGATION OF PLATE END DEBONDING IN CFRP
STRENGTHENED WIDE-FLANGE STEEL I-BEAMS UNDER
MONOTONIC AND FATIGUE LOADING**

MOHAMED KAMRUZZAMAN

**FACULTY OF ENGINEERING
UNIVERSITY OF MALAYA
KUALA LUMPUR**

2017

**MITIGATION OF PLATE END DEBONDING IN CFRP
STRENGTHENED WIDE-FLANGE STEEL I-BEAMS
UNDER MONOTONIC AND FATIGUE LOADING**

MOHAMED KAMRUZZAMAN

**THESIS SUBMITTED IN FULFILMENT OF THE
REQUIREMENT FOR THE DEGREE OF DOCTOR OF
PHILOSOPHY**

**FACULTY OF ENGINEERING
UNIVERSITY OF MALAYA
KUALA LUMPUR**

2017

UNIVERSITY OF MALAYA

ORIGINAL LITERARY WORK DECLARATION

Name of Candidate: MOHAMED KAMRUZZAMAN

Registration/Matric No:

Name of Degree: DOCTOR OF PHILOSOPHY

Title of Project Paper/Research Report/Dissertation/Thesis ("this Work"):

**MITIGATION OF PLATE END DEBONDING IN CFRP STRENGTHENED
WIDE-FLANGE STEEL I-BEAMS UNDER MONOTONIC AND FATIGUE
LOADING**

Field of Study: STRUCTURAL ENGINEERING & MATERIALS

I do solemnly and sincerely declare that:

- (1) I am the sole author/writer of this Work;
- (2) This Work is original;
- (3) Any use of any work in which copyright exists was done by way of fair dealing and for permitted purposes and any excerpt or extract from, or reference to or reproduction of any copyright work has been disclosed expressly and sufficiently and the title of the Work and its authorship have been acknowledged in this Work;
- (4) I do not have any actual knowledge nor do I ought reasonably to know that the making of this work constitutes an infringement of any copyright work;
- (5) I hereby assign all and every rights in the copyright to this Work to the University of Malaya ("UM"), who henceforth shall be owner of the copyright in this Work and that any reproduction or use in any form or by any means whatsoever is prohibited without the written consent of UM having been first had and obtained;
- (6) I am fully aware that if in the course of making this Work I have infringed any copyright whether intentionally or otherwise, I may be subject to legal action or any other action as may be determined by UM.

Candidate's Signature

Date:

Subscribed and solemnly declared before,

Witness's Signature

Date:

Name:

Designation:

ABSTRACT

The use of the externally bonded reinforcement (EBR) technique with carbon fiber reinforced polymer (CFRP) is a recent and promising method for increasing the flexural capacity and fatigue life of steel structural elements. However, plate end-debonding is one of the main problems of CFRP strengthened steel beams. The CFRP end-debonding and end-delamination (EDL) causes premature failures for strengthened steel beams subjected to monotonic and cyclic loading, which is an essential issue that needs to be resolved. The aim of this study is to investigate the effectiveness of strengthening wide-flange steel I-beams using CFRP in order to increase the monotonic and fatigue flexural strength of the beams and improve against CFRP end debonding. This research highlights various approaches to improve the resistance against debonding by studying the CFRP in-plane end cutting shape, the combination of CFRP in-plane and tapering end shape, end anchorage, as well as the triangular spew fillet of adhesive at the tips of the CFRP plate. In addition, the effect of lateral bracing and stiffeners on the CFRP failure modes was also investigated. A total of twenty-five beams were fabricated and divided into two categories for the investigation, i.e. flexural monotonic and fatigue specimens. Furthermore, detailed finite element (FE) simulations have been conducted for the tested specimens. FE non-linear analyses has been carried out to simulate the flexural behavior of the beams under monotonic loading. The fatigue life was also predicted at constant load ranges for all tested steel beams using the FE simulations. The use of plate stiffeners and lateral bracing improve the overall performance of the strengthened beams. The application of the trapezoidal in-plane CFRP end cutting shape was found to be the best configuration for delaying the plate end debonding failure compared to the other end cutting shapes under both monotonic loadings and fatigue. Applying the combined trapezoidal in-plane and tapered CFRP end shape with triangular spew fillets of adhesive increased the load bearing capacity and delayed the plate debonding failure

mode. Anchorage using CFRP fabrics at the end of CFRP plates mitigated the CFRP end problems, particularly end-debonding and EDL of strengthened beams. The FE simulation also showed that the trapezoidal is the best end cutting shape to delay plate debonding and the plate end anchorage using three layers with 220 x 175 mm CFRP fabrics is effective in mitigating end debonding initiation for monotonic and fatigue loading. The correlation between the results of the experiment and numerical modelling presented good agreements in this study.

University of Malaya

ABSTRAK

Penggunaan externally bonded reinforcement (EBR) dengan gentian karbon polimer (CFRP) merupakan kaedah terbaru danberpotensi untuk meningkatkan kapasiti lenturan dan juga jangka hayat lesu bahan struktur keluli. Tetapi, plate end-debonding adalah satu daripada masalah utama dalam penguatan struktur keluli menggunakan CFRP. Nyahikatan hujung CFRP dan hujung tertanggal (EDL) merupakan kerosakan awal bagi rasuk keluli yang dikuatkan di bawah beban monotonic dan kitaran, yang merupakan masalah utama untuk diselesaikan. Objektif dalam kajian ini adalah untuk mengenalpasti keberkesanan penguatan rasuk keluli jenis I yang dikuatkan dengan CFRP untuk meningkatkan kekuatan monotonic dan kekuatan lesu lenturan rasuk dan juga menyelesaikan nyahikatan hujung CFRP. Kajian ini meliputi beberapa kaedah untuk meningkatkan keupayaan terhadap nyahikatan dengan mengkaji bentuk pemotongan hujung planar CFRP, kombinasi CFRP planar dan bentuk hujung tirus, ikatan hujung, dan juga kambi spew segitiga bagi perekat pada hujung plat CFRP. Di samping itu, kesan perembatan sisi dan pengkaku pada mod kegagalan CFRP juga disiasat. Sejumlah dua puluh lima rasuk telah difabrikasi dan dibahagikan kepada dua kategori untuk penyiasatan, iaitu specimen monotonik lentur dan specimen lesu. Tambahan pula, simulasi unsur terhingga (FE) terperinci telah dijalankan untuk spesimen yang diuji. Analisis tak lurus FE telah dijalankan untuk mensimulasikan kelakuan lenturan rasuk di bawah beban monotonik. Hayat lesu juga diramalkan pada julat beban berterusan untuk semua rasuk keluli yang diuji menggunakan simulasi unsur terhingga. Penggunaan pengukuh plat dan perembatan sisi meningkatkan prestasi keseluruhan rasuk yang diperkuat. Penggunaan bentuk pemotongan hujung CFRP planar trapezoid didapati adalah konfigurasi terbaik untuk melambatkan kegagalan nyahikatan akhir plat berbanding dengan bentuk pemotongan hujung yang lain di bawah kedua-dua beban monotonik dan lesu. Dengan menggunakan gabungan hujung planar dan trapezoid bentuk

hujung CFRP dengan perekat berbentuk kambi spew segitiga dapat meningkatkan kapasiti galas beban dan menanggukkan mod kegagalan nyahikatan plat. Tambatan hujung menggunakan fabrik CFRP pada akhir plat CFRP dapat mengurangkan masalah hujung CFRP, terutamanya nyahikatan hujung dan EDL pada rasuk yang diperkuat. Simulasi FE juga menunjukkan bahawa trapezoid adalah bentuk pemotongan akhir yang terbaik untuk melambatkan nyahikatan plat dan tambatan akhir plat dengan menggunakan tiga lapisan fabrik CFRP bersaiz 220 x 175 mm berkesan dalam mengurangkan permulaan penyingkiran debonding di bawah beban monotonik dan lesu. Hubungan antara hasil ujikaji eksperimen dan kaedah berangka memberikan persetujuan yang baik dalam kajian ini.

University of Malaya

ACKNOWLEDGEMENTS

In the Name of Allah, The Beneficent, The Merciful, I would like to express my utmost gratitude and thanks to the almighty Allah (s.w.t) for providing me the opportunity to pursue my studies as well as instilling the patience and persistence during my research work. I am also thankful to my mother for her encouragement in every step of getting education.

I wish to express my sincere thanks and profound appreciation to my supervisor, Professor Dr. Mohd Zamin Jumaat and Associate Professor Dr. Nor Hafizah Ramli for their excellent supervision, guidance, encouragement and valuable time spent on the fruitful discussion throughout the work, which was extremely valuable in conducting this research work. Their fervent guidance in every aspect of this work was the most valuable experience of my life and also would remain so forever.

Sincere and great appreciation goes to University Malaya High Impact Research Grant under Grant Account No-UM.C/HIR/MOHE/ENG/36 (D000036-160001) for funding this research work.

Finally, special thanks are offered to all the researchers, lab assistants, lab technicians, and all the members linking to CICT (Centre for Innovative Construction Technology).

TABLE OF CONTENTS

ABSTRACT	iii
ABSTRAK	v
ACKNOWLEDGEMENTS	vii
TABLE OF CONTENTS	viii
LIST OF FIGURES	xv
LIST OF TABLES	xxiv
LIST OF SYMBOLS	xxvi
LIST OF ABBREVIATIONS	xxviii
CHAPTER 1: INTRODUCTION	1
1.1 Background and problem statement.....	1
1.2 Objectives	4
1.3 Scope of work	4
1.4 Originality and contribution of work	5
1.5 Outline of thesis	6
CHAPTER 2: LITERATURE REVIEW	8
2.1 Introduction.....	8
2.2 FRP materials.....	8
2.3 Adhesive	10
2.4 Cover plate and stiffener	11

2.5 Prevention of galvanic corrosion	12
2.6 Surface treatment	13
2.7 Basis of flexural design.....	15
2.8 Flexural strengthening techniques	17
2.8.1 CFRP end shapes	19
2.8.2 End anchoring	21
2.8.3 Plate configurations	23
2.8.4 Pre-stressed FRP plates	25
2.9 Adhesive curing	26
2.10 Support systems and instrumentations.....	28
2.11 Fatigue performance of reinforced steel beams	32
2.11.1 Reinforced with fibre polymer composite	32
2.11.2 Reinforced with prestressed polymer composite	38
2.11.3 Fatigue in hybrid joint and Nano-adhesive	40
2.12 Failure modes of reinforced steel beams.....	41
2.12.1 Debonding failures	41
2.12.2 Lateral torsional buckling	47
2.13 Finite Element (FE) simulation.....	48

2.14 Literature review summary	54
CHAPTER 3: METHODOLOGY.....	56
3.1 Introduction.....	56
3.2 Experimental program	57
3.2.1 Materials	58
3.2.1.1 Wide-flange steel I-beam (W-section).....	58
3.2.1.2 CFRP.....	61
3.2.1.3 Adhesive	62
3.2.1.4 Steel stiffener plates	63
3.2.2 Test specimens	66
3.2.2.1 Effect of lateral bracing and stiffeners	72
3.2.2.2 In-plane end cutting shapes.....	72
3.2.2.3 In-plane and tapering combined end shape with spew fillet.....	74
3.2.2.4 CFRP fabrics anchoring.....	76
3.2.3 Preparation of the specimens	79
3.2.4 Test setup	83
3.2.5 Test equipment.....	85
3.2.5.1 Instron-8505 universal testing machine	87

3.2.5.2 Support system.....	87
3.2.5.3 Spreader beam.....	87
3.2.5.4 Strain gauge	89
3.2.5.5 Linear Variable Displacement Transducers (LVDTs).....	90
3.2.5.6 Data logger.....	91
3.2.6 Test procedures	91
3.2.6.1 Monotonic	92
3.2.6.2 Fatigue.....	93
3.3 Numerical simulation.....	95
3.3.1 Finite element simulation.....	96
3.3.2 Modelling method	96
3.3.2.1 3D Modelling	97
3.3.3 Element selection	99
3.3.4 Materials property	99
3.3.5 Boundary conditions with lateral bracing against buckling instability.....	101
3.3.6 Meshing method.....	102
3.3.7 CFRP–steel interface and debonding modelling.....	103
3.3.8 Proposed anchorage design.....	105

3.3.9 Monotonic loading model	107
3.3.10 Fatigue loading model.....	107
3.3.11 Specification of the simulated models	108
CHAPTER 4: RESULTS AND DISCUSSIONS	109
4.1 Introduction.....	109
4.2 Monotonic flexural strengthening.....	109
4.2.1 Effect of lateral bracing and stiffeners	110
4.2.1.1 Load-deflection relationship and failure mode	110
4.2.1.2 Lateral displacement	115
4.2.1.3 Ductility	116
4.2.2 Different in-plane end cutting shapes	117
4.2.2.1 Failure mode	118
4.2.2.2 Load-deflection relationship	121
4.2.2.3 Ductility	123
4.2.2.4 Measured strains	125
4.2.3 Tapering end shape with spew fillet of adhesive	127
4.2.3.1 Failure mode	127
4.2.3.2 Load deflection relationship	130

4.2.3.3 Ductility	133
4.2.3.4 Measured strains	135
4.2.4 CFRP fabrics anchoring	136
4.2.4.1 Failure mode	137
4.2.4.2 Load deflection relationship	140
4.2.4.3 Ductility	142
4.2.4.4 Measured strains	143
4.2.5 Numerical simulation	145
4.2.6 Parametric study using FE modelling	154
4.3 Fatigue Performance	155
4.3.1 Different in-plane end cutting shapes	157
4.3.1.1 Failure mode	157
4.3.1.2 Fatigue life and failure initiation life	161
4.3.1.3 Deflection versus number of cycles	164
4.3.1.4 Strain versus life	167
4.3.2 CFRP fabrics anchoring	174
4.3.2.1 Failure mode	176
4.3.2.2 Fatigue life and failure initiation life	177

4.3.2.3 Deflection versus number of cycles	179
4.3.2.4 Strain versus life	181
4.3.3 Comparison of predicted and experimental fatigue data	184
CHAPTER 5: CONCLUSIONS	188
5.1 Monotonic strength	188
5.2 Fatigue performance	189
5.3 Recommendations for future work	190
REFERENCES.....	191
LIST OF PUBLICATIONS AND PAPERS PRESENTED	204
APPENDIX A	205
APPENDIX B	213
APPENDIX C	217

LIST OF FIGURES

Figure 1.1: CFRP end debonding (Deng & Lee, 2007b)	3
Figure 2.1: Diagram for calculating flexural capacity	15
Figure 2.2: Reverse tapering CFRP end (Schnerch et al., 2007)	20
Figure 2.3: Triangular spew fillet of adhesive at the end of the composite plate (Hildebrand, 1994)	21
Figure 2.4: CFRP end anchorage using steel plate and bolts	23
Figure 2.5: Strengthening technique with steel cover plate, stiffener and different CFRP plate configuration (Wu et al., 2012)	24
Figure 2.6: Support condition for monotonic and fatigue test set-up	30
Figure 2.7: S-N curve for steel beam strengthened with non-prestressed CFRP (Jiao, Mashiri, & Zhao, 2012; Tavakkolizadeh & Saadatmanesh, 2003)	33
Figure 2.8: Fatigue crack growth curve for unreinforced and reinforced steel beams (Tavakkolizadeh & Saadatmanesh, 2003)	34
Figure 2.9: Effect of layers of strengthening material (Wu et al., 2012)	36
Figure 2.10: Stress behaviour in fatigue for different notch categories	37
Figure 2.11: FCG curves for strengthened with non-prestressed and prestressed CFRP plates (Ghafoori, Schumacher, & Motavalli, 2012)	39
Figure 2.12: Deflection vs. number of cycle curves for strengthened steel beam using 14%, 15%, 35%, 0% and 37% prestressed CFRP plates (Vatandoost, 2010)	40

Figure 2.13: Failure modes of retrofitted beams using FRP plates (a) (Tavakkolizadeh & Saadatmanesh, 2003), (b) (Wu et al., 2012).....	43
Figure 2.14: CFRP end debonding due to cyclic loadings.....	44
Figure 2.15: End debonding under monotonic loads.....	45
Figure 2.16: Debonding interface of retrofitted beams using (a) CFRP plates; (b) CFRP sheets (Jiao, Mashiri, & Zhao, 2012).....	46
Figure 2.17: The failure modes for (a) PUR technique and (b) PBR technique.....	46
Figure 2.18: Performance of end anchorage after failure for steel beam strengthened with prestressedstrips to the cover plate (a) Removable end anchor, (b) Fixed end anchor (Vatandoost, 2010).....	47
Figure 2.19: (a) A geometrical model using ABAQUS in the FE analysis and (b) the mesh refinement around the loading, anchorage and crack tips (Ghafoori et al., 2012).....	49
Figure 2.20: Load deflection relationship in experimental and numerical studies (static) (Narmashiri & Jumaat, 2011).....	51
Figure 2.21: S-N curve in experimental and numerical studies (Kim & Harries, 2011)	52
Figure 3.1: Flow chart of the methods.....	57
Figure 3.2: Dimensions of the tensile test specimens.....	59
Figure 3.3: Tensile test coupon (a) Sample cutting, (b) Preparation and (c) Coupon with strain gauge.....	60
Figure 3.4: (a) Tensile coupon test set-up, (b) Failure mode.....	60

Figure 3.5: Carbon fiber reinforced polymer (CFRP) materials	61
Figure 3.6: Elevation projection of the specimens	68
Figure 3.7: Cross section of the specimens	68
Figure 3.8: Different in-plane end cutting shapes with measurements: (a) rectangular, (b) trapezoidal, (c) semi-circular, (d) semi-ellipse	73
Figure 3.9: (a) rectangular, (b) trapezoidal, (c) semi-circular and (d) semi-ellipse in-plane CFRP end cutting shapes	73
Figure 3.10: Specimen with a tapered CFRP end shape	74
Figure 3.11: Tapered end shapes	75
Figure 3.12: In-plane CFRP end cutting shapes with triangular adhesive fillets.....	75
Figure 3.13: CFRP tapered ends with triangular adhesive fillets	76
Figure 3.14: Reverse tapered CFRP end with a triangular adhesive fillet.....	76
Figure 3.15: Length and width of the CFRP fabrics	78
Figure 3.16: Dimensions and positions of end-anchorage using CFRP fabrics.....	78
Figure 3.17: Attachment of CFRP fabrics to specimens for anchorage using adhesive .	78
Figure 3.18: Sand blasted steel beams	80
Figure 3.19: Applying adhesive on the surface of the beam flange.....	81
Figure 3.20: Placing of the CFRP plate	82

Figure 3.21: Clamping the strengthened beams using fastening clamps	82
Figure 3.22: Schematic four-point bending setup (a) without and (b) with lateral bracing	83
Figure 3.23: Test set-up	84
Figure 3.24: Position of the strain gauges.....	86
Figure 3.25: Strain gauges at mid-span.....	86
Figure 3.26: Spreader beam	88
Figure 3.27: Span length of the spreader beam.....	89
Figure 3.28: Strain gauge	89
Figure 3.29: Linear Variable Deformation Transducer (LVDT)	90
Figure 3.30: Dynamic data logger connected with laptop	91
Figure 3.31: Cyclic loading parameters	94
Figure 3.32: Fatigue cyclic loading.....	94
Figure 3.33: Part of the steel beam	98
Figure 3.34: Part of the CFRP strip	98
Figure 3.35: Assembly of different parts	98
Figure 3.36: Stress-strain diagram	100
Figure 3.37: support and loading condition position of strengthened steel beams	101

Figure 3.38: Boundary condition with lateral constraint	102
Figure 3.39: Meshing of the strengthened beams	103
Figure 3.40: Meshing of anchored specimen with CFRP fabrics	103
Figure 3.41: ABAQUS traction-separation cohesive material law	104
Figure 3.42: Shear friction mechanism in the transverse CFRP	106
Figure 4.1: Load-deflection diagram of un-strengthened specimens.....	111
Figure 4.2: Stress concentration and local buckling failure below the loading plate ...	111
Figure 4.3: Load-deflection diagram of strengthened beams	113
Figure 4.4: Variation of deflection values of un-strengthened (M0, M1 and M2) and strengthened beams (M2, M3, M4) at peak load (kN).....	114
Figure 4.5: Splitting failure mode of CFRP plate (specimen M3).....	114
Figure 4.6: Load-lateral displacement relationships of strengthened beams	115
Figure 4.7: CFRP end debonded steel surface	118
Figure 4.8: CFRP plate with ED	119
Figure 4.9: CFRP debonding failure mode of a strengthened specimen	121
Figure 4.10: Load deflection diagrams of strengthened beams using different CFRP end shapes.....	122
Figure 4.11: Variation of deflection values of the control beam and strengthened beams using different CFRP in-plane end cutting shapes at peak load	123

Figure 4.12: Variation of ductility indices of strengthened specimens with different CFRP in-plane end shapes at debonding load	125
Figure 4.13: Strain distribution along the CFRP plate for specimens with different in-plane end shapes	126
Figure 4.14: End delamination failure mode of a reverse taper CFRP plate	128
Figure 4.15: Load-deflection plots of specimens M13, M14 and M15 are compared with control beam.....	130
Figure 4.16: Load- deflection curve for specimens with and without of taper CFRP plates or spew fillet of adhesive	132
Figure 4.17: Variation of deflection values at peak loads of control beam and strengthened specimens with and without of taper CFRP plates or spew fillet of adhesive	133
Figure 4.18: Variation of the ductility indices at debonding loads of strengthened specimens with and without tapered CFRP plates or spew fillets of adhesive	135
Figure 4.19: Strain distribution along the CFRP plate for specimens with and without tapered CFRP plates or spew fillets of adhesive.....	136
Figure 4.20: IC debonding failure mode of CFRP fabrics anchored specimens under monotonic loadings	139
Figure 4.21: Load-deflection curve of control beam and strengthened anchored specimens	140
Figure 4.22: Variation of deflection at peak loads of control beam and strengthened specimens with and without anchoring.....	141

Figure 4.23: Effect of CFRP fabrics anchorage on ductility indices	143
Figure 4.24: Strain distribution along the CFRP composite plate for specimens with and without CFRP fabrics anchorage at a 215 kN load	144
Figure 4.25: Strains in the mid-span tension flange versus applied load.....	145
Figure 4.26: (a) Stress concentration and local buckling at below the loading point and (b) Lateral torsional buckling of specimen M0.....	147
Figure 4.27: Lateral torsional buckling failure mode of specimen M1	147
Figure 4.28: Lateral torsional buckling in specimen M4: (a) experimental, (b) FE	148
Figure 4.29: Effect of stiffeners and lateral bracing with ED initiation of the CFRP plate in specimen M5	149
Figure 4.30: End debonding failure mode (FEM).....	150
Figure 4.31: Simulation of the IC debonding (anchored specimen, M17)	150
Figure 4.32: Load-deflection diagram between experimental (Deng & Lee, 2007a) and FEM	151
Figure 4.33: Load-deflection diagram of un-strengthened specimen	152
Figure 4.34: FEM and experimental load-deflection diagram of strengthened specimens	153
Figure 4.35: Fracture of the wrapping failure mode (FEM)	155
Figure 4.36: Strain profile at mid-span of strengthened specimen F3	156

Figure 4.37: ED of the CFRP plate	159
Figure 4.38: Failure mode of fatigue strengthened specimens with different in-plane CFRP end cutting shapes under fatigue	160
Figure 4.39: Comparison of ED initiation life and fatigue life of strengthened specimens with CFRP end shapes	163
Figure 4.40: Deflection versus number of cycles.	165
Figure 4.41: Maximum deflection versus number of cycles for strengthened beams with different CFRP end shapes.....	166
Figure 4.42: Strain in the tension plate versus number of cycles for specimen with a rectangular shape (F3).....	168
Figure 4.43: Strain in the tension plate versus number of cycles for specimen with a semi-ellipse end shape (F4)	169
Figure 4.44: Strain in the tension plate versus number of cycles for specimen with a semi-circular end shape (F5).....	171
Figure 4.45: Strain in the tension plate versus number of cycles for specimen with a trapezoidal shape (F6).....	172
Figure 4.46: Strain on CFRP plate for different in-plane CFRP end shapes at the level of 279500 cycles.....	174
Figure 4.47: Failure mode of anchored specimen with CFRP fabrics (F7) under fatigue	176

Figure 4.48: Comparison of ED initiation life and fatigue life of specimens with and without anchorage	178
Figure 4.49: Deflection ranges versus number of cycles of an anchored specimen (F7)	180
Figure 4.50: Maximum deflection versus number of cycles curve for strengthened specimens with and without anchorage	181
Figure 4.51: Strain in the tension plate versus number of cycles for an anchored specimen (F7).....	182
Figure 4.52: Maximum strain on CFRP plates for specimens with and without anchorage at 279500 cycles	183
Figure 4.53: End-debonding and steel beam fracture initiation at below point load under fatigue (FEM).....	185
Figure 4.54: Fatigue failure of anchored specimen, F7 (FEM)	186
Figure 4.55: Load versus deflection for strengthened beam with in-plane end cutting shape (specimen F6)	187

LIST OF TABLES

Table 2.1: Strengthening techniques.....	18
Table 3.1: Dimensions and material properties of wide-flange steel I-beams (W-beam)	64
Table 3.2: Dimensions and material properties of CFRP plates Sika CarboDur® S1014 (Sika®CarboDurPlates, 2013)	64
Table 3.3: Dimensions and material properties of CFRP fabrics SikaWrap®-301 C	65
Table 3.4: Dimensions and material properties of adhesive: SikaDur® 30.....	65
Table 3.5: Dimensions and material properties of Sikadur®-330 epoxy	65
Table 3.6: Test matrix of the experimental program	66
Table 3.7: Specifications of the monotonic specimens.....	69
Table 3.8: Specifications of the anchored specimens under monotonic loading for parametric studies using numerical modeling.....	70
Table 3.9: Specifications of the fatigue specimens.....	71
Table 4.1: Monotonic strength with ductility and failure modes (effect of stiffeners and lateral bracing related specimens).....	112
Table 4.2: Specifications, load carrying capacity and failure modes of strengthened specimens with different CFRP in-plane end shapes.....	120
Table 4.3: Ductility indices of specimens with in-plane CFRP end cutting shapes	124

Table 4.4: Specifications, load carrying capacity and failure modes of strengthened specimens with tapered CFRP end shapes and spew fillets.....	129
Table 4.5: Ductility indices of specimens with tapered CFRP plate ends and spew fillets	134
Table 4.6: Specifications, load carrying capacity and failure modes of specimens with and without anchorage	138
Table 4.7: Ductility indices of specimens with and without anchorage.	142
Table 4.8: Comparison of yield load and peak load between numerical and experimental results of monotonic specimens	146
Table 4.9: Failure load and failure mode of anchored specimens (FEM).....	154
Table 4.10: Fatigue test result of strengthened specimens with in-plane CFRP end cutting shapes	158
Table 4.11: Failure initiation life of specimens with different CFRP end shapes	163
Table 4.12: Fatigue test result of specimens with and without anchorage	175
Table 4.13: Failure initiation life of specimens with and without anchorage.....	178
Table 4.14: Comparison of predicted fatigue life with experimental result	184
Table 4.15: Predicted fatigue life and failure mode of anchored beams (FEM).....	186

LIST OF SYMBOLS

b_f	Width of flange
d	Effective height of section
ε_0	Initial strain
$\varepsilon_d^{(t)}$	Design tensile strain
$\varepsilon_d^{(c)}$	Design tensile strain
$\varepsilon_{fd}^{(t)}$	Design tensile strain of the strengthening FRP
$\varepsilon_{sd}^{(t)}$	Design tensile strain of steel
f_f	Strength of the CFRP
f_y	Yield strength of the steel
h	Height of beam section
L	Span length
P	Total vertical load
P_a	Amplitude load
P_{Max^m}	Maximum load
P_{Min^m}	Minimum load
P_m	Mean load
P_u	Ultimate load
P_y	Yield load
ΔP	Load range
R	Load ratio

t_f Thickness of flange

t_w Thickness of web

L_{CFRP} Length of CFRP plate

t_{CFRP} Thickness of CFRP plate

t_{adh} Thickness of adhesive

ε Strain

T_g Glass transition temperature (adhesive)

University of Malaya

LIST OF ABBREVIATIONS

AASHTO	American Association of State Highway and Transportation Officials
AFRP	Aramid Fibre Reinforced Polymer
BFRP	Basalt Fibre Reinforced Polymer
CFRP	Carbon Fibre Reinforced Polymer
EBR	Externally Bonded Reinforcement
ED	End Debonding
EDL	End Delamination
FL	Flexural Failure
FRP	Fibre Reinforced Polymer
GFRP	Glass Fibre Reinforced Polymer
GPa	Giga-pascal
ICD	Intermediate Crack Debonding
kN	Kilo Newton
LDT	Laser Displacement Transducer
LVDT	Linear Variable Displacement Transducer
MPa	Mega-pascal
PL	Peeling-off Failure
W-beam	Wide-flange steel I-beam

CHAPTER 1: INTRODUCTION

1.1 Background and problem statement

In recent decades, the installation of fiber-reinforced polymer (FRP) composites for strengthening structural elements has become an efficient method to meet the increased loads, or repair due to fatigue crack or corrosion. The application of FRP composites to increase monotonic and fatigue strength of damaged steel beams is an attractive substitute to traditional approaches like steel-plating. FRP possesses outstanding advantages as a structural strengthening material, including high strength, anticorrosion properties, high durability and restoration of the lost capacity of damaged structures (Kim & Heffernan, 2008). FRP plates/fabrics are also effective in strengthening or retrofitting of steel structural elements to extend their fatigue life and decrease crack or fracture propagation (Wu et al., 2012; Yu et al., 2013), if galvanic corrosion is avoided and sufficient bond is provided (Harries et al., 2011). The two main types of FRP strips are Carbon Fiber Reinforced Polymer (CFRP) and Glass Fiber Reinforced Polymer (GFRP).

CFRP is a polymer matrix composite material that is reinforced using carbon fibers. CFRP is more commonly used for strengthening and retrofitting of steel structures than GFRP because of its strength. Recent retrofitting works in Japan, the United Kingdom, America, Switzerland, and China showed that there was great potential in using CFRP composites for strengthening of steel structures (Hu, Zhao, & Feng, 2016; Suzuki, 2005; Zhao & Zhang, 2007). The Action bridge in England and the Asland bridges in the USA were retrofitted by applying CFRP composite materials to the bottom flange of the girders; stress reduction was observed, resulting in increase the fatigue life (CNR, 2007; Moy, 2002). Several case studies of existing steel railway bridges are presented by (Caglayan, Ozakgul, & Tezer, 2009; Leander, Andersson, & Karoumi, 2010). Monitoring data was used for dynamic response analysis, and fatigue life evaluation.

However, the use of CFRP in flexural strengthening steel beams under monotonic and cyclic loading faces problems such as end-debonding (ED), end-delamination (EDL), and splitting. These problems cause premature failure of strengthened steel beams. Some approaches are suggested to overcome these problems by Kaan (2008) and others (Narmashiri, Jumaat, & Sulong (2010); Rizkalla, Dawood, & Schnerch (2008)), but these methods need to be developed further.

The weakest point in the strengthening system of FRP elements to the steel joints is the bond of the adhesive (Bocciarelli et al., 2009; Buyukozturk, Gunes, & Karaca, 2004; Jones & Civjan, 2003). Some failure modes in CFRP bonded steel techniques are summarized (Zhao & Zhang, 2007): (1) CFRP-adhesive interface failure, (2) adhesive layers failure (cohesive failure), (3) steel-adhesive interface failure, (4) end-delamination CFRP plate, (5) CFRP composite rupture, and (6) steel yielding. The successful implementation of FRP composites on externally bonded strengthening systems is dependent upon the integrity and quality of steel-composite joints and the effectiveness of the epoxy adhesive used (Schnerch et al., 2006).

Generally, the strengthened steel beams using FRP composites suffer from peeling stress and debonding at the end of the plate. Figure 1.1 shows end debonding failure of the CFRP plate of strengthened steel beams. FRP plate debonding in a strengthened steel beams is due to high localized interfacial stresses and peeling stresses in the area of the composite plate end. The intensity of these interfacial shear stresses depend on some factors (Deng & Lee, 2007b; Kambiz & Mohd, 2010; Smith & Teng, 2001; Zhang & Teng, 2010), including bending moment, shear force and cyclic loading effect in the beam at the location of the plate end.



Figure 1.1: CFRP end debonding (Deng & Lee, 2007b)

In a simply-supported beam with three- or four-point bending, ED is more likely to occur when the moment at the plate end is high, but can be delayed when the end of the composite plate is close to the beam support (Deng & Lee, 2007a; Narmashiri, Jumaat, & Sulong, 2012). Besides the location of the plate end, the interfacial shear stresses can also be decreased by other measures in the plate joints: use of spew fillets of epoxy adhesive at the CFRP plate end and softer adhesive near the plate end (Fitton & Broughton, 2005); tapering the plate thickness at the end (Schnerch et al., 2007); and using mechanical anchors or clamps (Narmashiri, Jumaat, & Sulong, 2010; Sen, Liby, & Mullins, 2001). Nevertheless, the application of CFRP end cutting shapes or fabric anchoring to mitigate the end debonding problem may be competent alternatives under monotonic loading and fatigue. In this thesis, the combination of in-plane and tapering CFRP end cutting shapes with spew fillets of adhesive in increasing the monotonic strength is studied. In addition, the effects of lateral bracing and stiffeners on CFRP end debonding are also examined. Finite element (FE) simulations have also been conducted to predict the monotonic and fatigue flexural behavior of CFRP-steel strengthened beams.

1.2 Objectives

To overcome the above mentioned problem statement, five specific objectives are considered, as follows:

1. To examine the strengthened steel beams with different CFRP end cutting shapes in order to increase the monotonic and fatigue strength against end debonding.
2. To study the effects of combined in-plane and tapering CFRP end cutting shapes with spew fillets of adhesive in increasing the monotonic strength.
3. To investigate the effectiveness of a CFRP fabrics' anchoring system in reducing the end problems of strengthened steel beams under monotonic loading and fatigue.
4. To simulate the monotonic behavior of un-strengthened as well as strengthened steel beams with plate debonding.
5. To develop finite element models in order to predict the fatigue life with failure modes of un-strengthened and strengthened steel beams with CFRP composites.

1.3 Scope of work

The scope of this research is the strengthening of steel beams for existing steel structures using only CFRP, particularly for flexural strengthening including monotonic and fatigue. In total, twenty-five beam specimens were experimentally investigated and thirty-four numerical specimens are modelled. In the experimental and numerical investigation, the four-point bending test was used. In the numerical analysis, full 3D simulation modelling and nonlinear analysis were applied to develop the model.

In this research, novel approaches are used to maintain the adhesive bonding between the CFRP and soffit of the wide-flange steel I-beam sections. In flexural strengthening, the

geometry of CFRP tips was researched by cuttings through the thickness of CFRP ith. In this investigation, the effectiveness of end cuttings of CFRP strips in the in-plane direction is researched. One useful method to increase the resistance of externally bonded reinforced (EBR) systems against the CFRP end problem is to anchor the CFRP at the plate tip (Narmashiri, Jumaat, & Sulong, 2010; Rizkalla, Dawood, & Schnerch, 2008; Sallam et al., 2006; Sen, Liby, & Mullins, 2001). In the monotonic and fatigue investigation of this study, the effects of CFRP fabrics anchorage on the whole structural behaviour of the strengthened beams are investigated. Investigations concerning the effects of in-plane and taper CFRP end shape with triangular spew fillets of adhesive on retarding CFRP debonding under monotonic loadings is covered in this work. The effects of lateral bracing and stiffeners on the structure in an EBR system is also investigated.

1.4 Originality and contribution of work

This thesis is based on original research that focuses on mitigation or retardation of CFRP ED failure observed in CFRP strengthened steel I-beams and very effective findings were obtained.

The in-plane CFRP end cutting shape under monotonic loading and fatigue was chosen in order to explore the best end cutting shapes against ED and end delamination. The results show that out of the investigated shapes, the trapezoidal end cutting shape is the best in-plane end shape. To investigate the effects of tapering end shapes with spew fillet of adhesive at plate ends, all structural parameters studied are new. The use of CFRP fabric anchoring at CFRP tips have proven effective for mitigating CFRP end-problems and this too has not been studied before. In addition, the effect of lateral bracing and stiffeners on the failure mode of strengthening plates is also investigated.

The findings of this research have contributed immensely towards a better understanding of CFRP use in monotonic and fatigue flexural strengthening of wide-flange steel I-beams.

1.5 Outline of thesis

This thesis includes five chapters. Each chapter explains the achievements of the research clearly and completely. The chapters of the thesis include: Chapter one - Introduction, Chapter two - Literature Review, Chapter three – Methodology including Experimental Program and Developments of Numerical Models, Chapter four - Results and Discussions, and Chapter five - Conclusions.

In Chapter one, the problem statement and objectives, as well as originality and contribution of this study are introduced.

Chapter two includes a complete literature review on the application of steel in construction, strengthening of steel structures using CFRP, different adhesives for pasting CFRP, various methods for abrasive blasting, and use of CFRP strengthened steel beams for monotonic loads and fatigue.

In Chapter three, a complete description of the research methodology including the preparation of the experimental specimens and testing procedures are explained. The specifications of the specimens and test setup for each objective are explained too. The research methodology for numerical simulation of the specimens using the Finite Element Method (FEM) are also explained in this chapter. A description of the modeling and analysis of the samples using Abaqus software in 3D are included. In addition, the numerical analysis is validated through comparison with the experimental test results.

In Chapter four, the achievements of the experimental test and numerical modelling for the flexural specimens under monotonic loading and fatigue are obtained and discussed based on the objectives. In Chapter five, a summary of the achievements of this research is given with some recommendations for future work to develop the research.

University of Malaya

CHAPTER 2: LITERATURE REVIEW

2.1 Introduction

FRP is being widely applied in strengthening and retrofitting steel structural elements. Fiber-reinforced composite possesses prominent advantages as a structural strengthening material, including high strength, good corrosion resistance, and improved flexural performance which explains why the application of this material has increased considerably. A review of previous research concerning FRP materials, surface preparation, adhesive, flexural strengthening under monotonic loads, and fatigue performance, fatigue crack propagation and failure modes of steel beams are discussed here.

2.2 FRP materials

The application of fiber reinforced materials to retrofit and strengthen steel structures is widely used. In recent years, the search for alternative materials in place of steel for strengthening and maintenance of structures has been a major challenge for civil engineers.

FRP is a composite material that is produced from fibers and resins. It is produced as laminate structure that contains unidirectional woven fabrics or fibers implanted within a thin layer of light polymer matrix material. The fibers are normally created from carbon, glass, aramid or basalt. The matrix is generally made of epoxy, polyester, or nylon. The matrix protects the unidirectional fibers from breaking, as well as transfers stress equally among the fibers. Although FRP exhibits linear behavior and has high tensile strength. Its compressive strength is weak, and it has low shear strength, it has high resistance to corrosion and is low in weight. Normally, the application of FRP composites in civil

engineering can be classified as follows: (1) application in strengthening new structures, (2) retrofitting of existing structures, and (3) architectural applications.

The main types of FRP produced are: (1) carbon fiber reinforced polymer (CFRP), (2) aramid fiber reinforced polymer (AFRP), (3) glass fiber reinforced polymer (GFRP), and (4) basalt fiber reinforced polymer (BFRP).

CFRP materials have been used for marine structures (Allan, Bird, & Clarke, 1988; Grabovac, Bartholomeusz, & Baker, 1993), aerospace parts (Baker, 1987), and so on. CFRP is more commonly used for strengthening of steel structures than other FRP materials because of high strength. In any events, CFRP composite is high tolerant to fatigue damage (Curtis, 1989). It is classified as UHM (Ultra High Modulus), HM (High Modulus), IM (Intermediate Modulus), HT (High Tension) and LM (Low Modulus), SHT (Super High Tension), and HS (High Strength).

Basalt fibers can be created from the basalt rock using single component raw material and drawing and winding fibers from melt. The fiber regarded as a naturally occurring material. Basalt fiber composites show greater strength and modulus of elasticity, and higher chemical stability with similar cost compared to the E-glass FRP (Wu et al., 2010).

GFRP composite is also another type of polymer matrix materials, which is reinforced by using fine glass fibers. It is used for storage tanks, pipes, boat, marine structures, automobile, pressure vassels, aircraft wings, fuselage sections, swimming pools, welding helmets, and roofs. GFRP is classified as E-Glass, S-Glass, S+R-Glass and C-Glass. In addition, AFRP commonly used in strengthening or retrofitting of reinforced concrete (RC) structures. Saadatmanesh & Tannous (1999) tested AFRP tendons and observed very good fatigue and creep performance of the AFRP tendons.

CFRP composite plates or fabrics can be adhesively bonded to fatigue sensitive details in steel structural elements for improving their fatigue life. The higher mechanical properties and excellent fatigue performance of carbon fiber reinforced plate makes them superior candidates to strengthen or retrofit of steel structures with bridges. CFRP composites are made of high strength (in excess of 2000 MPa tensile strength) carbon filaments placed in a resin matrix. They show outstanding mechanical properties with over 1.2 GPa tensile strength and 140 GPa modulus of elasticity. CFRP plates endure more than 1 million cycles fatigue life with a loading range of one-half of the ultimate static capacity (Lorenzo & Hahn, 1986).

2.3 Adhesive

Adhesive is a key requirement for attaching onto the surface of structural elements. Epoxy is a commonly used adhesive in the civil engineering construction industry. Epoxy adhesive has a wide range of structural applications, including fixing of FRP in place. Epoxy adhesives comprise a major part of adhesives that are called “engineering adhesives” or “structural adhesives”. They have also been applied where high bonding strength is required including the construction of automobiles, aircraft, boats and bicycles etc. It can be produced in rigid or flexible, transparent opaque or colored, quick setting or extremely slow setting types. In general, adhesives are one of the necessities when using FRP to strengthen steel structures.

The weakest linkage in plate bonding of the CFRP composites to steel joints is the epoxy adhesive bond (Buyukozturk, Gunes, & Karaca, 2004). The successful strengthening operations are mainly reliant on the effectiveness of the applied adhesive as well as the integrity and quality of the steel-CFRP joints.

Jiao, Mashiri, & Zhao (2012) used Sikadur-330 and Araldite[®] 420 epoxy adhesives to compare the fatigue behaviour of initially cut on the bottom flange in the mid-span of steel beams. The result shown that no significant difference could be observed in the fatigue life for retrofitted beams using the adhesives of Araldite[®] 420 and Sikadur-330(Jiao & Zhao, 2004). Araldite[®] 420 was also used by other researchers (Liu et al., 2009) in applications between the steel surfaces and CFRP plates.

2.4 Cover plate and stiffener

To provide the equivalent of a concrete slab that normally exists in the steel bridges for preventing buckling on the compression flange, Wu et al. (2012) attached a steel cover plate with welding on the surface of the top steel flange of the girders (Figure 2.5). They also welded web stiffeners on the both sides of the steel beam web at supporting and loading points. Web stiffeners assist in preventing web crippling at the mid-span section (Moy & Nikoukar, 2002). In order to provide lateral stability of the steel beams, Kim & Brunell (2011) used stiffeners that were welded at the supporting points. The adhesively bonded steel stiffeners to the flanges and webs on both side of the beam extensively retarded local buckling of the steel beams (Sebastian & Zhang, 2013). Siddique & Damatty (2013) showed that the use of the glass fiber reinforced polymer (GFRP) composites enhances local buckling behaviour of wide flange steel beams, which is effective, especially for the case of slender beams. The application of glass fiber composite plates to the compression flange of a steel beam increases both the load bearing capacity and the deflection at failure. The increment in the load bearing capacity is independent of the web dimensions of the beams for both plastic and slender beams. The study ignored the use of a stiffener. The failure mode of the strengthened slender beams ranges from elastic buckling of the system to GFRP plate rupture when the plate thickness

of the GFRP composites is varied 6.35 mm to 19.00 mm. As the GFRP thickness is significant in their study it could well improve the local buckling.

2.5 Prevention of galvanic corrosion

Even though CFRP composites are non-corrosive substance, when steel in contact with carbon fibers, they can procedure a galvanic cell. To increase the fatigue strength of bridge girders and long-term durability of CFRP reinforcement in a steel structure, the prevention of galvanic corrosion is necessary. Furthermore, to rule out the galvanic corrosion, the flow of corrosion needs to be mitigated. This may be accomplished by insulating the different metals from one another or through preventing a continuous link of the electrolytic solution between the two by coating using a water resistant sealant (Rance & Evans, 1958). It is obvious that if the two different metals are not in contact, galvanic corrosion cannot occur (Brown, 1974). Tavakkolizadeh & Saadatmanesh (2001) examined the corrosion between carbon and steel for various thicknesses of adhesive coating in seawater and de-icing salt solution. The thin coating effect of adhesive with 0.25 mm thickness was found to be substantial as was the sizing used to the carbon fibers. Furthermore, a thicker adhesive between the surfaces of the CFRP and steel was observed to suggestively slow the rate of corrosion of the steel.

Mitigating galvanic corrosion of the CFRP-steel composite can be achieved by the selection of an adhesive with good quality isolation properties (Zhao & Zhang, 2007), or by using a thicker epoxy, water resistant sealant, or non-conductive layer plus a sealant, or bonding a GFRP fabrics' before applying the CFRP layer onto the steel surface (Allan, Bird, & Clarke, 1988; Dawood & Rizkalla, 2007; Dawood, 2005; Yasin, 2008). Hollaway & Cadei (2002) installed a polyester drape veil for providing insulation between the steel

and the carbon for preventing direct contact between them. Fiber glass or an epoxy film was considered to provide effective insulation. In addition, a monitoring program was initiated to detect the cathodic sites so that the galvanic corrosion damage could be mitigated or stopped (Schnerch et al., 2006).

2.6 Surface treatment

The consistency of the bonding joints for the CFRP composite to the surface of the steel structures are highly dependent on the surface treatment processes (Schnerch et al., 2005).

The surface treatment or preparation and the strength of the applied CFRP composite overlay can significantly affect on the monotonic strength and fatigue life of structural elements (Monfared, Soudki, & Walbridge, 2008). For assessing the effect of externally bonded CFRP strengthening approach on fatigue strength, Jiao, Mashiri, & Zhao (2012) used a grinder to remove the corrosion as well as to level the weld area on each steel beam soffit before applying the adhesive. To make a clean, and chemically active surface with rough, Wu et al. (2012) treated the surface of the tension flange using a grinding wheel to reinforce with CFRP for the flexural test. The tension flange of the steel surfaces and the CFRP composites were then washed by acetone.

Tavakkolizadeh & Saadatmanesh (2003) used a sand blaster meticulously with No. 50 glass bids, and washed by saline solution just prior to the application of the composite fabrics' to prevent oxidation. The study by Teng et al. (2011) displayed that the sand blasting process was the most effective surface treatment. Prior to bonding the CFRP strips to the beams, Kim & Harries (2011) used a 40 grit zirconia alumina belt with 1500 sfpm belt sander. This ensured a sound, slightly striated surface to bond the CFRP composite plates. The adhesive layer thickness was approximately 1 mm.

The tips of the FRP plates must be finished smoothly using sandpaper before the attachment of the plate to the steel beams (Deng & Lee (2007a), 2007b)). However, Schnerch et al. (2007) disagreed with Choudhury (2007), as they contended that preparing the surface with a hand grinder followed by sandpapering reduces the bonding ability of the surface. However, a chemically active steel surface that is free from contaminants is essential to enhance the chemical bond between the adhesive and the metallic surface. Brushing, and ultrasonic or vapour degreasing technics are claimed to be the most efficient to remove oil and other potential surface contamination, especially when adequate solvents are used (Hashim, 1999). The contamination may then be removed using the excess solvent, rather than simply re-depositing it on the steel surface as the solvent evaporate.

The most efficient means of achieving a high-energy surface of the steel is by using grit blasting (Hollaway & Cadei, 2002). Grit blasting with angular grit eliminates the inactive oxide and hydroxide deposits by cutting of the base material. The grit size also affects the profile of the steel surfaces. Harris & Beevers (1999) stated that finer particles created a smoother surface than coarser grit particles and smoother surfaces exhibited higher adhesive-steel surface bonding. In addition, the surface profile of the steel was not influenced on the long-term durability (Schnerch et al., 2006). After grit blasting, solvents may be used to wash and clean the steel surface without resulting in poor bonding (Damatty & Abushagur, 2003; Photiou, Hollaway, & Chryssanthopoulos, 2004).

2.7 Basis of flexural design

The ultimate limit state is reached when the strain acting at the extreme fibre of the cross section equals a limit value. For instance, limit values of strains to be considered for a steel beam strengthened in the tension zone are the following:

$$\varepsilon_d^{(t)} = \min\{\varepsilon_{sd}^{(t)}; \varepsilon_{fd}^{(t)} + \varepsilon_0\} \quad (2.1)$$

$$\varepsilon_d^{(c)} = \varepsilon_{sd}^{(c)} \quad (2.2)$$

$\varepsilon_{sd}^{(t)}$ and $\varepsilon_{fd}^{(t)}$ being the design values of the tension strain capacity of the steel and FRP composite, respectively, ε_0 is the initial strain, $\varepsilon_{sd}^{(c)}$ is the design compression strain capacity of steel. $\varepsilon_d^{(t)}$ and $\varepsilon_d^{(c)}$ are the design tensile and compression strain, respectively.

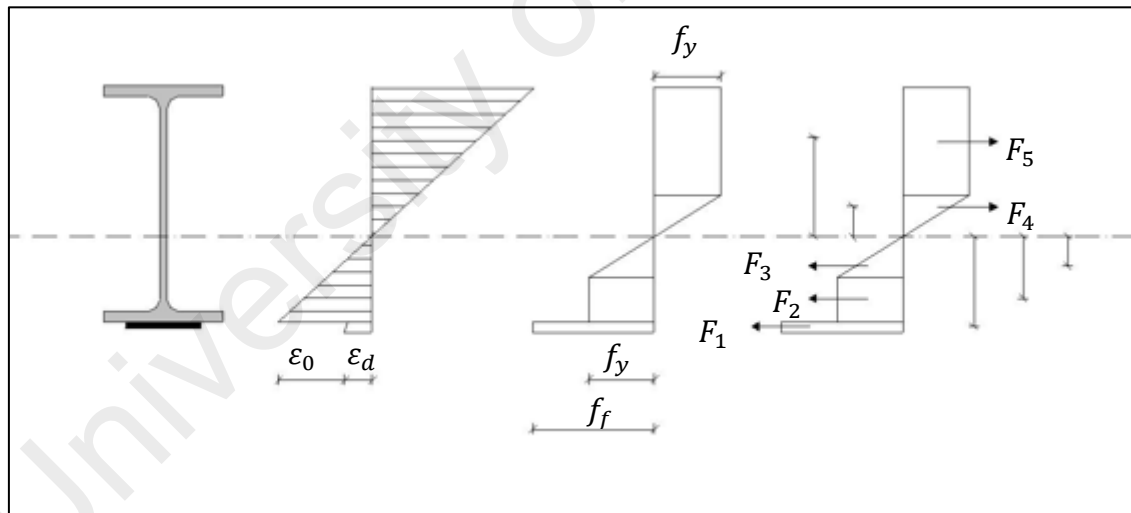


Figure 2.1: Diagram for calculating flexural capacity

The bending moment corresponding to the fulfilment of the equations (2.1) or (2.2) is the flexural capacity of the strengthened beam. The procedure for computing flexural capacity is presented in Figure 2.1. The design flexural capacity, M_{Rd} , can be computed using the following procedure (CNR, 2007):

1. Assume that one of the materials composing the cross section has reached, at the extreme fibre of the cross section, its strain capacity, as specified in equations (2.1) or (2.2);
2. Fix a first value of the neutral axis position; this will fix the whole strain state on the cross section because of the assumption of a linear strain distribution;
3. Evaluate stresses at each fibre of the section, based on the appropriate stress-strain relationship;
4. The equilibrium resultant forces in the direction of the beam axis must be satisfied:

$$F_1 + F_2 + F_3 = F_4 + F_5 \quad (2.3)$$

5. If equation (2.3) is not satisfied then go back to step 1 and repeat steps 2, 3 and 4 with iteration on the neutral axis position, until Equation (2.3) is satisfied;
6. Once determined, the neutral axis position allowing satisfaction of equation (2.3), the design value of the flexural capacity associated to the considered failure mode can be easily computed by the following equation:

$$M_{Rd} = \sum F_i \cdot d_i \quad (2.4)$$

The stress-strain relation for the FRP strengthening system is always linear up to failure. The relevant Young modulus, to be used in the procedure above outlined, is the one measured for the FRP system in the direction parallel to the beam axis. Since the FRP strengthening system is often placed with fibres aligned parallel to the direction of the beam axis, thus maximizing its efficiency, the Young modulus of the FRP strengthening system often coincides with the modulus measured parallel to the fibre direction. The limit values of strain in the steel beam with class 1 or class 2 and in the FRP strengthening system can be set as follows:

$$\varepsilon_d^{(t)} = \varepsilon_{fd}^{(t)} + \varepsilon_0 \quad (2.5)$$

$$\varepsilon_d^{(c)} = \infty \quad (2.6)$$

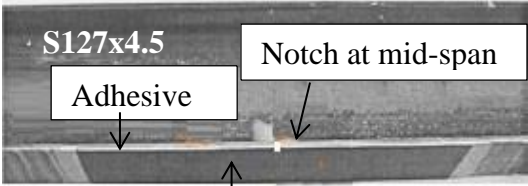
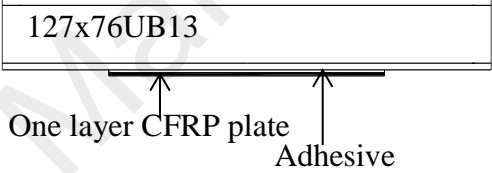
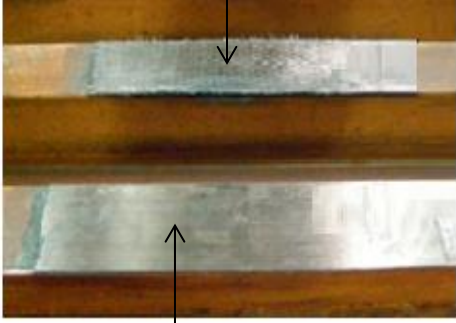
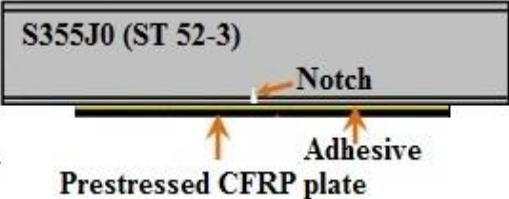
2.8 Flexural strengthening techniques

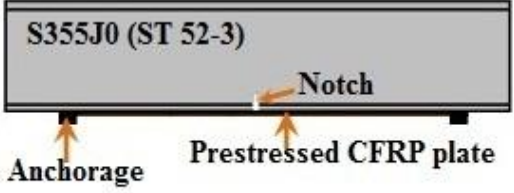
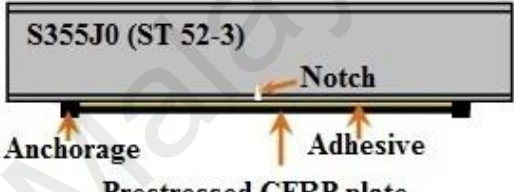
The applications of CFRP to strengthen different steel structural elements have been widely adopted. The following shows some of the applications of CFRP in strengthening steel structures:

1. Upgrading steel I- or W-beam
2. Steel-concrete and bridge girders
3. Tensile elements: joint and steel plate
4. Compressive elements: square, circular, and tube section
5. Cracked elements: fatigue behavior
6. Concrete-filled steel sections
7. Fire-damaged steel sections

Many researches have been carried out in the recent decade; the shape and configuration of FRP composites of an adhesively bonded joint play an important role in respect of the monotonic as well as fatigue strength and lifetime of strengthened steel beams and bridge girders. A number of researchers have investigated reinforced steel beams with different FRP strengthening techniques and compared their fatigue performance. A summary of the reinforcing technique under monotonic and fatigue of steel structures using fiber-reinforced composites is provided in Table 2.1. A details configuration of the end of FRP-adhesive joint, anchoring, plate arrangements and pre-stress FRP plates strengthening systems are described below.

Table 2.1: Strengthening techniques

Specimens reference	Material – dimensions and properties	Figures
<p>S127x4.5 steel beams reinforced with CFRP sheet (Tavakkolizadeh & Saadatmanesh, 2003).</p>	<p>Steel beam: 1.22m long, $f_y = 336.4$ MPa, 330.9 MPa, $E=194.4$ GPa, CFRP: 300 mm x 76 mm x 1.27 mm, $E=144$GPa, $f_u=2137$ MPa Epoxy: 1:1 mixer of resin (bisphenal A based) and hardener (polyethylenepolyamin)</p>	 <p>S127x4.5 Notch at mid-span Adhesive One layer CFRP plate</p>
<p>127x76UB13 Steel beams Strengthened using CFRP plate (Deng & Lee, 2007b).</p>	<p>Steel beam: 1200 mm long, $E=205$ GPa, $f_u = 275$ MPa, FRP: 3 mm thick and 400 mm long Epoxy (Sikadur 31 Normal): $E= 8$ GPa, shear modulus = 2.6 GPa, $f_u = 29.7$ MPa and 0.3 mm thick</p>	 <p>127x76UB13 One layer CFRP plate Adhesive</p>
<p>Grade 400 150UB14 notched steel beams retrofitted with welding, CFRP composites (Jiao, Mashiri, & Zhao, 2012).</p>	<p>Steel beam: L1400xW75xH150 mm, $E= 207.4$ GPa, $f_y= 411.6$ MPa, $f_u = 541.3$ MPa CFRP: 1. Sika®CarboDur M1214 pultruded plates- 1.4 mm thick, $E= 210$ GPa, $F_t= 2.4$ GPa, 2. SikaWrap® Hex-230C woven sheets- 0.13 mm for each ply, $E= 230$ GPa, $f_u = 3.45$ GPa, Epoxy: 1. Sikadur-330 2. AralditeR 420</p>	 <p>SikaWrap® Hex-230C sheet (4 layers) CarDur M1214 plate (1 layer)</p>
<p>S355J0 steel beams bonded with 20% prestressed CFRP plates (Ghafoori, Schumacher, &</p>	<p>Steel beam: 1100x120x65 mm, $E= 210$ GPa, $f_y= 355$ MPa CFRP: 910x50x1.2 mm (S512), $E= 165$ GPa, $f_u = 3.10$ GPa,</p>	 <p>S355J0 (ST 52-3) Notch Adhesive Prestressed CFRP plate</p>

Motavalli, 2012).	Prestressing level 20% of the ultimate CFRP strength= 632 MPa. Araldite 2015 adhesive: E= 1.75 GPa,	
S355J0 (ST 52-3) steel I-beams strengthened using 30% (a) prestressed unbounded and (b) bonded CFRP plates(Ghafoori et al., 2012).	Steel beam: 1100x120x65 mm, E= 210 GPa, $f_y = 355$ MPa CFRP: 910x50x1.2 mm (S512), E= 160 GPa, $f_u = 3.10$ GPa, Prestressing level 30% of the ultimate CFRP strength. Araldite 2015 adhesive: E= 1.75 GPa,	
		

2.8.1 CFRP end shapes

In the monotonic and fatigue flexural strengthening steel beam by using CFRP strips, critical interfacial shear stress and peeling stress occur near the end of the strips of the adhesive joint cause debonding (Deng & Lee, 2007a, 2007b; Narmashiri, Ramli Sulong, & Jumaat, 2012). Some researchers have demonstrated end shapes approaches to overcome the debonding problems of the plate joints (Deng & Lee, 2007a, 2007b; Deng, Lee, & Moy, 2004; Seleem, Sharaky, & Sallam, 2010).

Several researchers have presented considerable structural performance improvements by tapering and reverse tapering the thickness at the end of the CFRP composite materials. The previous research report indicated that significant performance enhancement can be achieved by using this detail for flexural members under monotonic and cyclic loading

conditions (Allan, Bird, & Clarke, 1988; Schnerch et al., 2007). The tapered end shape decreased strain on the adhesive by 38% and reduced the maximum normal stress by about 50%; hence including a taper is a beneficial detail for mitigating debonding of the CFRP plates (Deng, Lee, & Moy, 2004).

Adams, Papiatt, & Coppendale (1978) theoretically obtained the stress distributions from a two-dimensional (2D) finite element idealization in adhesively bonded joints with the taper end of high strength CFRP composites. The use of a tapered CFRP plate was found to be able to reduce the concentration interfacial stresses that occur at the plate ends of the adhesively bonded joints (Bouchikhi et al., 2013). Bendemra, Compston, & Crothers (2015) conducted parametric tests, focusing on six joint design parameters: plate and adhesive thickness, plate tapering angle, stacking sequence, overply layup, and lap length. Results indicated that the tapered scarf joints have a great sensitivity to plate thickness, taper angle, and stacking sequence. Duong (2006) also investigated a tapered bonded joint to predict the adhesive stresses in a bonded line numerically by geometrical nonlinear analysis.

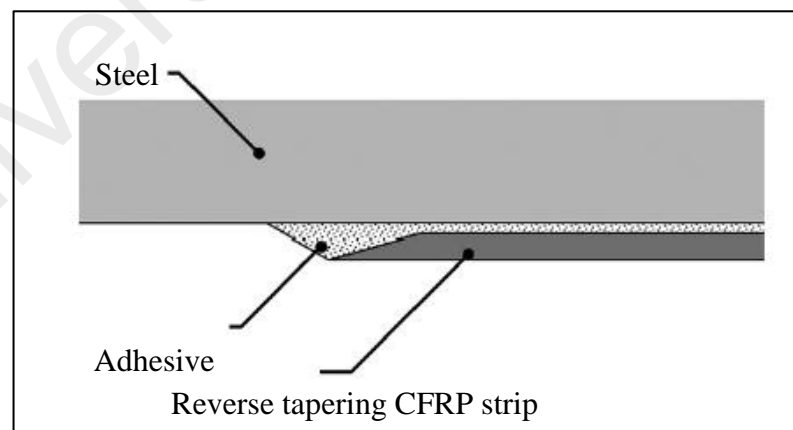


Figure 2.2: Reverse tapering CFRP end (Schnerch et al., 2007)

Schnerch et al. (2007) showed that significant performance increases can be achieved by reverse tapering the thickness at the end of the CFRP composites. Figure 2.2 shows reverse tapering the plate thickness of the fiber composite using adhesive. Even though

the approach reduced the peeling stresses, it did not avoid peeling and plate debonding completely.

Adams & Peppiatt (1974) showed that a 45° triangular spew fillet of adhesive reduces the maximal principal stresses by around 40%. Lang & Mallick (1998) extended the considerations on triangular fillets of adhesive to other arrangements of fillets, and indicated that these relatively simple techniques ensure a much smoother flow of stresses and reduce their intensity. Tsai & Morton (1995) showed, through experimental investigations and numerical analysis, that the concentration of the shear and normal stresses in the adhesive could be considerably reduced by applying adhesive fillet at the end of the overlap in the single-lap joints. They revealed a good agreement between the experiment result and numerical simulation, where a geometrical nonlinear deformation was used in the numerical analysis.

Hildebrand (1994) modeled single lap joint between metal and FRP composite plate by using non-linear finite element approach. Triangular spew fillet of adhesive at the end of the composite plate (Figure 2.3), reverse tapering of the FRP, semi-circular edge and denting are used to improve the joint strength.

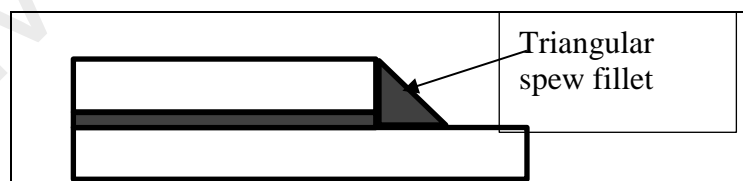


Figure 2.3: Triangular spew fillet of adhesive at the end of the composite plate (Hildebrand, 1994)

2.8.2 End anchoring

End anchoring of the CFRP composite plate can be decreased the effects of debonding and delamination at the composite plate ends for both concrete and steel structural

elements. Generally, L or U shapes CFRP fabrics anchorage are used at the plate ends for concrete or reinforced concrete structures (Jumaat & Alam, 2008). A number of researcher used mechanical anchors or clamps in retrofitting or strengthening steel structures to retard plate end-debonding and end-delamination (Narmashiri, Jumaat, & Sulong, 2010; Sen, Liby, & Mullins, 2001; Sweedan, Alhadid, & El-Sawy, 2016).

The application of a three-piece clamping techniques at the CFRP plate ends for steel and concrete bridge structures enhanced the resistance against debonding and delamination or peeling (Sen, Liby, & Mullins, 2001), however, applying this clamping technique did not increase the load carrying capacity in the beam structures because the failure modes were governed by the holes in the plate composites.

Motavalli & Czaderski (2007) studied the seismic retrofitting by using GFRP fabric and additional CFRP plates of a damaged masonry shear wall that were used anchorage in the concrete with end-anchor plate.

Maaddawy & Soudki (2008) investigated unbonded FRP techniques with mechanical anchorage by using steel plates and bolts in the strengthening of reinforced concrete (RC) slabs. A steel plate with four bolts were consisted in this mechanical anchorage system. The anchor plate was install below the strengthening plate by using steel bolts that were inserted into the predrilled holes through the thickness of the slab at the desired locations. This type of anchoring system damaged the slab, and changed the mode of failure due to the holes in the slab.

Narmashiri, Jumaat, & Sulong (2010) investigated the effectiveness of end-anchorage using steel plates and bolts for strengthened steel I-beams (Figure 2.4); and the effects of arrangement of the bolts in the anchor steel plates. They demonstrated that the spacing of the bolts were more effective in the anchoring system than the dimension of the steel

anchor plate, and end-anchoring of the CFRP plates decreased the deformation and strain of the whole beam including the vertical deflection of the reinforced beams and the tensile strain on the CFRP composite plates. This type of mechanical anchorage was not more effective due to pulling out of the plates.



Figure 2.4: CFRP end anchorage using steel plate and bolts

2.8.3 Plate configurations

Studies on fatigue of double sided reinforcements under tension and full-scale bridge girders rehabilitated with CFRP plates under three-point bending have been conducted at the University of Delaware (Miller et al., 2001). In all the cases, CFRP composite plates remained fully bonded by adhesive to the steel substrate. The results suggested excellent fatigue behaviour of the reinforced elements.

Schnerch et al. (2005) reported that the bonding behaviour of adhesive in the FRP strengthening of steel structures were different than reinforced concrete (RC) structures. They also presented that high bonding stress occurs in steel surfaces to meet the strengthening requirements (Schnerch et al., 2006).

Furthermore, Wu et al. (2012) investigated eight damaged H350 × 175 steel beam specimens, including one un-strengthened and seven strengthened by welded steel, steel wire (SW)-BFRP, high-modulus CFRP (HM-CFRP), and high strength CFRP (HS-CFRP) composite plates using Sikadur-30 Normal epoxy adhesive. The plate configuration of the strengthening technique used by Wu et al. (2012) is shown in Figure 2.5. The elastic modulus, tensile strength, shear strength and ultimate strain of the epoxy were 2.627 GPa, 31.7 MPa, 14.4 MPa, and 1.5%, respectively. An Anchorage system was applied at below the point load and at the end of the reinforced plates. The HM-CFRP has the most excellent strengthening effects and SW-BFRP is the best strengthening composite material in terms of cost-performance ratio (Wu et al., 2012).

Basalt-FRP (BFRP) composites show synthetical advantages in the structural strengthening, seismic rehabilitation, and serving as strengthening structural elements (Wu et al., 2010; Wu, Wang, & Wu, 2011). Nevertheless, the BFRP composite with low modulus may not satisfy the stiffness requirement of some structural materials. Therefore, to obtain higher performance, SW-BFRP can be made from hybridization of BFRP with steel wires or CFRPs (G. Wu et al., 2010; Wu, Wang, & Wu, 2011).

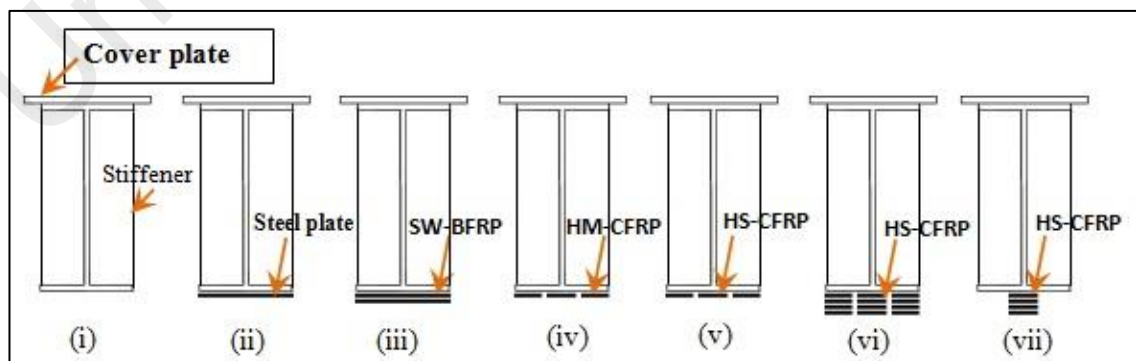


Figure 2.5: Strengthening technique with steel cover plate, stiffener and different CFRP plate configuration (Wu et al., 2012)

The majority of fatigue problems arise from poor detailing or careless fabrication, rather than inaccurate materials selection (James, 1992). Schnerch and others (Schnerch et al., 2005; Zhao & Zhang, 2007) reported that the bonding mechanisms of FRP retrofitted or strengthened steel members are different than reinforced concrete structural members in terms of bonding. High bonding stresses occur in steel members to meet the strengthening requirements (Schnerch et al., 2006). Any violation of fabrication tolerances can unpredictably change the fatigue behaviour and lead to a very scattered fatigue life (Täljsten, Hansen, & Schmidt, 2009).

2.8.4 Pre-stressed FRP plates

A 210ft x 26ft three continuous span rolled steel bridge girder in Guthrie county, Iowa, on state highway 141 was strengthened using externally post-tensioning CFRP rods (Phares et al., 2003). The anchorage systems were bolted to the webs of the steel girders. The proposed prestressed unbounded reinforcement (PUR) system (Ghafoori et al., 2012) can be applied as an alternative to adhesively bonded FRP composite, mainly when there is concern about the effects of water, moisture, high ambient temperature, and high cycle loadings on the glue between the FRP and the steel. Vatandoost (2010) used 14%, 15%, 35%, 0% and 37% prestressed CFRP plates to study the fatigue behaviour of five W310×74 steel beams, in which the 14%, 15% and 35% pre-stressed CFRP plates were bonded to the inner side of the bottom flange, and the 0% and 37% Pre-stressed plates were attached to the cover plate. A pre-stress FRP composite patch is strongly suggested to maximize the effectiveness of the adhesively bonded patch on the steel element

(Colombi, Bassetti, & Nussbaumer, 2003b) and fatigue strengthening (Colombi, Bassetti, & Nussbaumer, 2003a).

Recently, the carbonflex, i.e. carbon-fiber hybrid-polymeric matrix composite (CHMC), strengthening technique was developed by Zhou & Attard (2013), which is a carbon fiber-based composite manufactured using the latest hybrid-matrix technique involving amino-based polymeric composites to provide required damping and high strength sustainability of the carbon fibrous element. Recently, Zhou and others (Zhou & Attard, 2013; Zhou, Attard, Wang, et al., 2013; Zhou, Attard, Zhao, et al., 2013) indicated the enormous potential of carbon-flex as a strengthening substance to subsequently prevent higher damage or catastrophic failure of structures.

2.9 Adhesive curing

If a bridge or long span structure is retrofitted with CFRP strips, it is generally not economic to stop the bridge to traffic during the adhesive curing time, which can take up to 48 hours. During this time, the epoxy adhesive is subject to repeated loading from the traffic. The Concrete Society recommended that the change in the epoxy properties caused by the repeated load during the curing time is expected to be small, perhaps a 10% decrease in the strength of the fully cured structural elements (Society, 2000). Nikouka, Lee, & Moy (2002) studied the improvement in the strength and stiffness of strengthened steel beams with CFRP under repeated loading during the early age curing of the epoxy adhesive. Five pairs of 127 x 76UB13 type steel beams, each 1.2 m long, was strengthened with a 0.98 m long single K13710 ultra-high modulus CFRP plate, attached to the tension flange. A cyclic load was applied to the five specimens with 0.25 Hz frequency and was continued for up to around 48 hours. The study reported that during the curing of the

epoxy, the cyclic loading would affect the final stiffness and failure mode of the strengthened beam when the highest cyclic load was larger than 42 kN. Moreover, the bond would fail to develop if the shear deformation in the epoxy layer during the cure is too large. They also recommended that it was prudent to limit a maximum of 1 MPa shear stress in the epoxy.

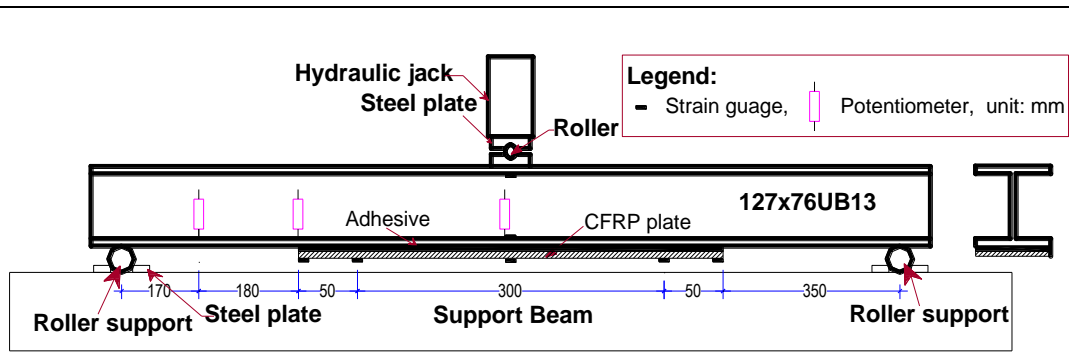
Bourban et al. (1994) indicated a clear advantage at high temperature (about 93°C) from the epoxy adhesive during the initial curing period 10-20 minutes. The resulting adhesive bond is more durable, stronger and tougher when subjected to unfavourable environments (Karbhari & Shulley, 1995). With the intention to open the retrofitting steel bridges to traffic during the curing period of adhesive, Moy (2002) investigated the effect of repeated loadings on the curing of the epoxy. The results confirmed a progressive increment in the stiffness of the reinforced component as the epoxy cured. Furthermore, the beams subjected to higher loadings during the period of curing did not achieve the full adhesive bond. The tests performed showed that cyclic loading at higher load levels reduced the ultimate capacity of the strengthened beams (Moy & Nikoukar, 2002). In addition, The vibration of the traffic during the curing of the adhesive causes a progressive reduction in the fatigue lifetime with increasing strain level (Barnes & Mays, 2001; Moy, 2007).

Zhang et al. (2006) proposed an innovative method involving pre-impregnation (prepreg) advanced composites and a compatible epoxy film for retrofitting steel railway bridges open to traffic during the curing period of the epoxy adhesive. The strengthening system was made from unidirectional HM- and UHM-CFRP pre-impregnations that were cured on site under vacuum assisted pressure. Two cure temperatures were used: 65 °C for 16 hours and 80 °C for 4 hours. A GFRP prepreg layer was placed between the CFRP patch and the steel element. The beams were initially induced by vibration forces and then

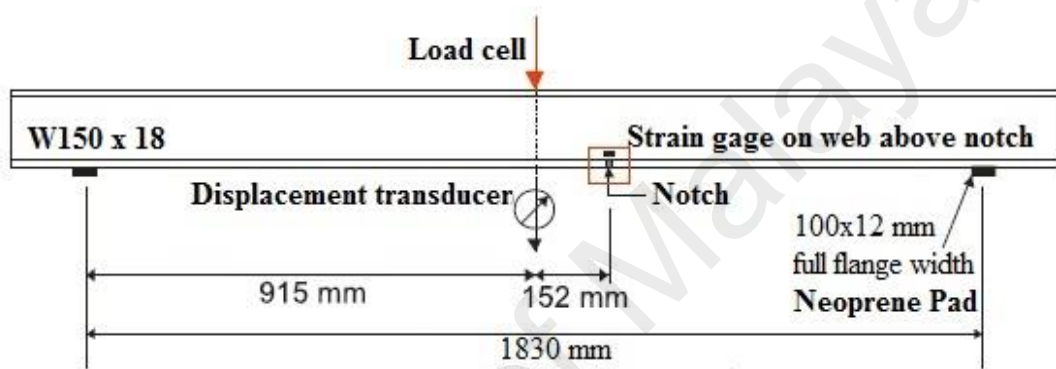
loaded to failure. From the experimental results it was observed that, despite slight damage at the adhesive level, the proposed technique prevented severe brittle failure of the composite beam.

2.10 Support systems and instrumentations

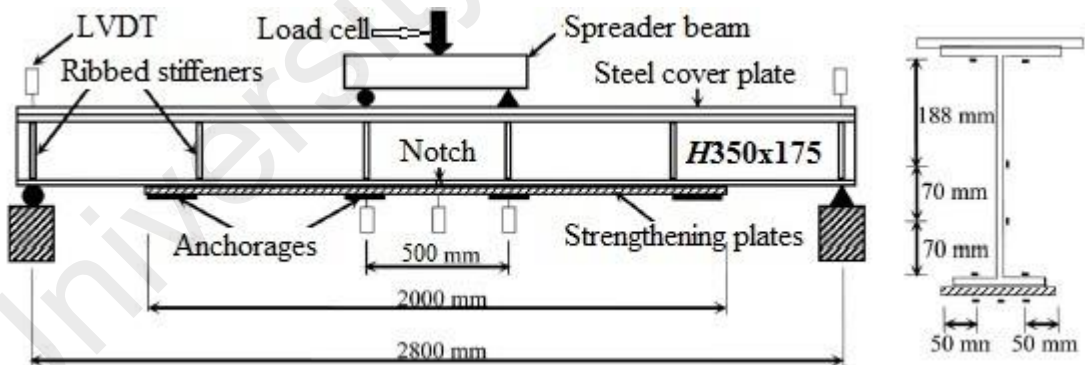
Different support systems have been adopted by different researchers for the monotonic and fatigue test programs of steel beams, as shown in Figure 2.6. Deng & Lee (2007b) tested nine reinforced steel girders by a servo-hydraulic Dennison testing machine, using a three-point bending setup as a simply supported beam (Figure 2.6(a)). The specimens were supported on two rollers, but were restrained from any sideways movement. The loading block had two steel plates, each with a counter seat, and a roller in between. Deflections were measured at three locations by means of potentiometers. Five 2 mm and two 5 mm long strain gauges were used to investigate the crack initiation as well as the effect of crack growth on the stress field in the girder. All the data were recorded using a data logger. Studies on the fatigue of double sided reinforcement subjected to tension and full-scale bridge girders retrofitted with CFRP plates under three-point bending were conducted at the University of Delaware (Miller et al., 2001). Kim & Harries (2011) used a neoprene rubber pad between the support and beam to reduce the concentration of stress, as shown in Figure 2.6(b). In all cases, the CFRP plates remained fully bonded to the steel element. The results suggested excellent fatigue behaviour of the reinforced elements.



(a) (Deng & Lee, 2007b)



(b) (Kim & Harries, 2011)



(c) (Wu et al., 2012)

Wu et al. (2012) tested the strengthened H350 × 175 steel beams under constant amplitude cyclic load using 4 Hz frequency as a simply supported mode and four-point bending, as shown in Figure 2.6(c). The load was measured by the loading cell of a MTS system. To prevent any movement of the specimen during the test, Tavakkolizadeh & Saadatmanesh (2003) used tie down brackets to the roller supports. The loading blocks were designed using a counter seat for the compression flange in order to prevent their movement during the experiments for monotonic loads and fatigue. The loading setup is shown in Figure 2.6(d). The specimens were tested using various constant stresses ranging between 69 and 379 MPa ($R = 0.1$), and a frequency of 5 and 10 Hz. Vertical displacements can be measured by linear variable displacement transducers (LVDT) with a range of ± 50 mm (Wu et al., 2012) and ± 75 mm (Tavakkolizadeh & Saadatmanesh, 2003).

Jiao, Mashiri, & Zhao (2012) conducted fatigue tests under load control with 7 Hz on strengthened steel beams with a 4-point bending rig using a MTS-810 testing machine, which contained the top supporting frame and bottom loading beam as shown in Figure 2.6(e). Two 12 mm thick steel plates were welded to the mid-span of the top supporting frame and the bottom loading beam. Four pin-connected wheels were employed at the supporting and loading points that could freely rotate during the fatigue tests. Two screw-fixed stoppers were used on both sides of the bending rig to prevent the test specimen from changing position during the experiment. The bottom-loading rig was designed using a three-pin system to ensure that the load was distributed between the two loading points. Using SHOWA strip strain gauges, the ultimate load, displacement, number of cycles and corresponding strains of each cycle were recorded using the National Instrument NI 9237 Compact Data Acquisition system.

To fatigue test the reinforced metallic beams using prestressed FRP, Ghafoori et al. (2012) used a pulsator P960 oil hydraulic test machine with a four-point bending setup. The

lubricated rollers of 5 cm diameter at the supports, and a steel plate were employed between the beam and rollers to distribute the load properly (Figure 2.6(f)). Ghafoori, Schumacher, & Motavalli (2012) used a 3-D ICS (image correlation system) to measure the crack length and the corresponding strain deformation at the crack tip area. The measurement window of the ICS was set at 65 mm x 65 mm. The calibration details and the use of the ICS can be found in (Czaderski & Rabinovitch, 2010; Czaderski, Soudki, & Motavalli, 2010; Ghafoori & Motavalli, 2011). The field signature method (FSM) is also effective for detecting and monitoring cracks on steel structures (Kawakam, Kanaji, & Oku, 2011).

2.11 Fatigue performance of reinforced steel beams

A steel structure subjected to repeated load may eventually experience significant fatigue damage during its life. A number of researchers concentrated on fatigue strength and fatigue lifetime prediction of reinforced steel beams and bridge girders. This indicates that there is a need to enhance the fatigue strength and prolong the fatigue lifetime of steel structures with adhesively bonded metal/FRP strengthening techniques. The fatigue behaviour of reinforced steel beams using FRP composite is illustrated below:

2.11.1 Reinforced with fibre polymer composite

Hollaway & Head (2001) indicated that unidirectional continuous fibre polymer composites, which essentially behave linearly up to failure level when loaded parallel to the longitudinal fibers, usually have good fatigue properties. Jiao, Mashiri, & Zhao (2012) compared the behaviour of notched steel beams using the welding method and retrofitted

with CFRP plates and fabrics', respectively, under flexural cyclic loads. In addition, two different epoxy adhesives, i.e. Sikadur-330 and Araldite[®] 420, were used in this test. The observations of the fatigue strength of the specimens reinforced with CFRP composites was extensively longer than that of specimens repaired with the welding method alone. It was observed that the strengthening system with one layer of CFRP plate adhesively bonded could extend the fatigue strength of steel beams about seven times compared to the beams only repaired with the welding method. In addition, the fatigue strength was extended about three times for beams strengthened with four layers of CFRP woven sheets. Mean S–N curves were obtained based on the test data (Figure 2.7), which can be used for predicting the fatigue strength of steel beams strengthened with similar CFRP composite materials.

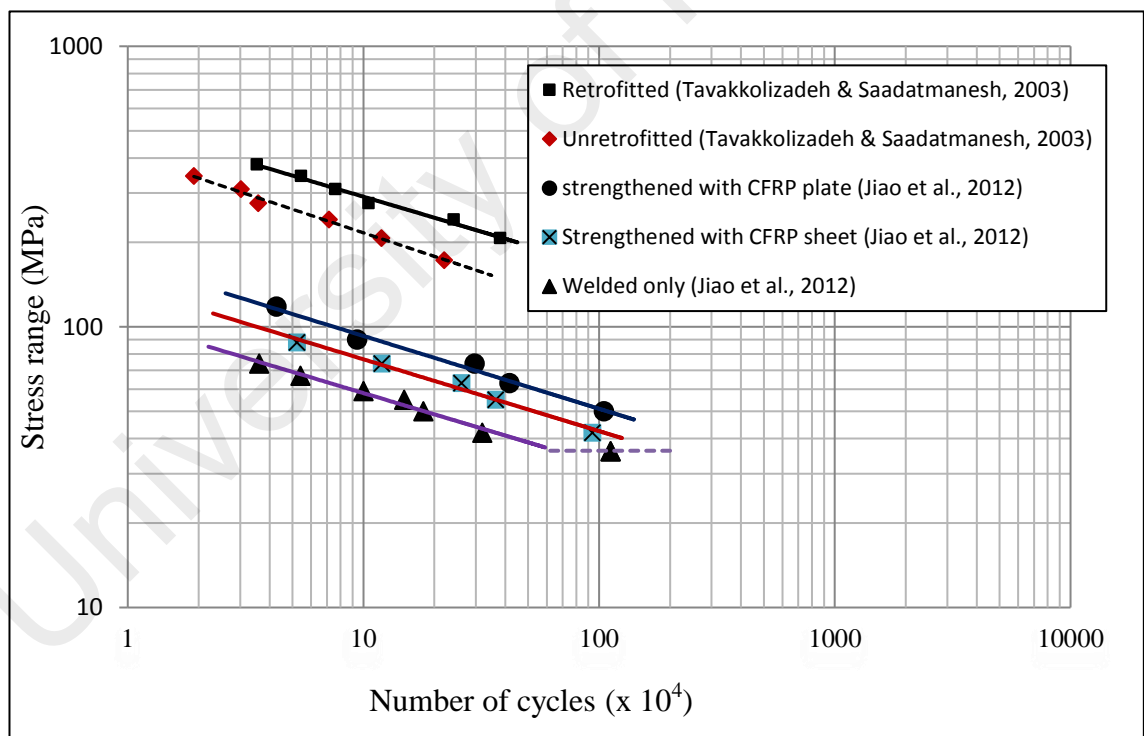


Figure 2.7: S-N curve for steel beam strengthened with non-prestressed CFRP (Jiao, Mashiri, & Zhao, 2012; Tavakkolizadeh & Saadatmanesh, 2003)

Tavakkolizadeh & Saadatmanesh (2003) demonstrated using the S-N curve that the application of CFRP strips could increase the fatigue lifetime of the structural elements more than three times (Figure 2.7). The design S-N curve for unreinforced and reinforced cut specimens were $NS^{3.54} = 1.22 \times 10^{13}$ and $NS^{3.96} = 3.84 \times 10^{14}$, respectively.

The slope of the S-N curves for the specimens (retrofitted and unretrofitted) in a log-log space was slightly smaller than the slope of the AASHTO design curves. They also observed that the CFRP patch not only decreased the crack growth rate, but was also able to carry a few extra cycles even after the tension flange had completely cracked, especially under lower stress ranges (Figure 2.8).

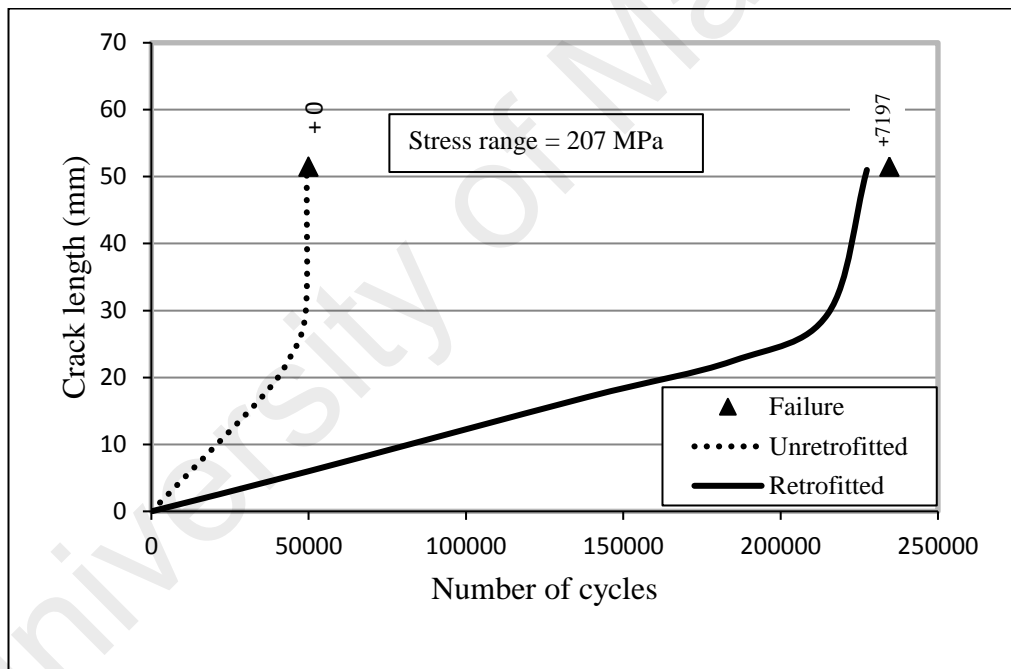


Figure 2.8: Fatigue crack growth curve for unreinforced and reinforced steel beams (Tavakkolizadeh & Saadatmanesh, 2003)

Deng & Lee (2007b) reported the results of an experimental program on small-scale steel beams reinforced by applying CFRP strips. From the tests results an S-N curve was obtained. The fatigue limit, i.e. threshold, of the S-N curve was about 30% of the ultimate

static failure stress, which validates the fatigue limit recommended by the CIRIA Design Guidance (Cadei et al., 2004). To assess the fatigue bond resistance of a steel bridge girder reinforced with CFRP strips, Miller et al. (2001) conducted two test programs. First, they subjected seven small-scale, doubly reinforced specimens to cyclic loads at 82.7 MPa stress for 2.55 million cycles. All CFRP strips were found to remain fully bonded to the steel element without deterioration based on the strain data taken before and after the cyclic loading. Subsequently, two full-scale steel bridge girders retrofitted with CFRP were fatigued for ten million cycles at a constant stress range of 34 MPa. Throughout the tests, the CFRP strips were inspected and monitored for debonding, but none was detected. Therefore, the retrofitting technique was regarded as having good fatigue resistance.

Abed (2012) investigated the effects of temperature on the adhesively bonded steel beams reinforced with CFRP composites. The adhesive materials showed a significant reduction in the fatigue life and failure load of the strengthened structures as the temperature reached the adhesive glass transition temperature (T_g). Furthermore, Keller & Schollmayer (2009) experimentally and numerically investigated the through-thickness performance of adhesively bonded FRP bridge decks and steel girders. They found that no stiffness degradation occurred for cyclic loading of up to 10 million cycles.

For instance, the strengthening or retrofitting of metallic beams, by adhesively bonding a composite plate to the tension flange, enhances the local stiffness when the increment of the global stiffness is marginal (Teng, Yu, & Fernando, 2012; Zhao & Zhang, 2007). The achievement of the local stiffness under cyclic loadings is very significant from the fatigue point of view (Colombi & Fava, 2015). The design criteria (Ghafoori et al., 2015) was released to assist in the design of the FRP elements to strengthen steel structural members.

Wu et al. (2012) investigated the fatigue behaviour of strengthened artificially notched steel beams including the effects of the configuration and the number of layers of HS-CFRP strips, the interface treatment of the SW-BFRP composites, and the type of materials. Compared to the traditional welded steel-plate approach, the experimental results showed that the use of a fiber-reinforced composite strip could not only delay crack initiation, decrease the crack growth rate, and prolong the fatigue life, but also reduce the residual deflection and stiffness decay. The rough surface of the SW-BFRP could extend the fatigue strength of steel beams more effectively than using SW-BFRP with a smooth surface. They also used high modulus CFRP strips as a reinforced material. HM-CFRP demonstrated the best strengthening performance; the fatigue strength of the steel beams could be improved significantly by increasing the number of layers of the strengthening material. Figure 2.9 presents the crack expansion curves for four-layer and one-layer HS-CFRP. When the number of layers was increased from one to four, the crack initiation life and the fatigue lives were considerably enhanced (Figure 2.9). The plate configuration influences the fatigue strength. Colombi & Fava (2016) also examined the fatigue crack propagation of FRP-strengthened steel beams in terms of experimental test and analytical formulation.

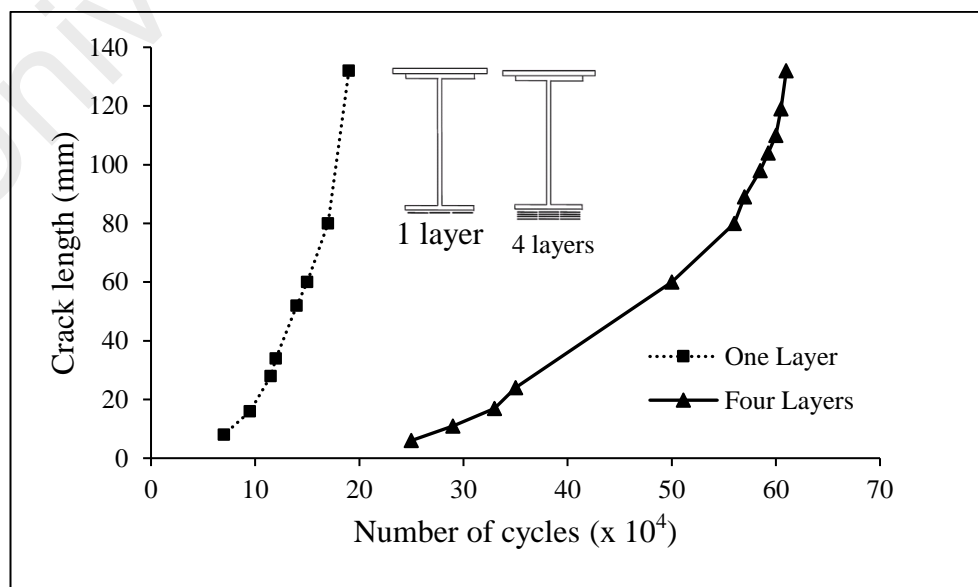


Figure 2.9: Effect of layers of strengthening material (Wu et al., 2012)

To simulate the actual damage caused by corrosion and the expansion of fatigue cracks, several researchers intentionally created notches of different geometry in mid-span or other positions on the tension flange of the beams. In addition, the notch assists like a stress concentrator (Kim & Harries, 2011) in the damage-sensitive regions (Loher et al., 1996; Wu et al., 2012) to commence a vertical crack at the steel web. Figure 2.10 presents the stress characteristics of a strengthened notched steel beam under cyclic loading for incorporation of rectangular notch on both edges (Tavakkolizadeh & Saadatmanesh, 2003), U-shaped notch through the whole tension flange (Kim & Harries, 2011), and Uniform (Jiao, Mashiri, & Zhao, 2012) notches. The S-N curves show that the uniform notch comprising whole flange and web has the least stress compared to other. This clearly demonstrates more fatigue life when the side rectangular notch is incorporated in the flange.

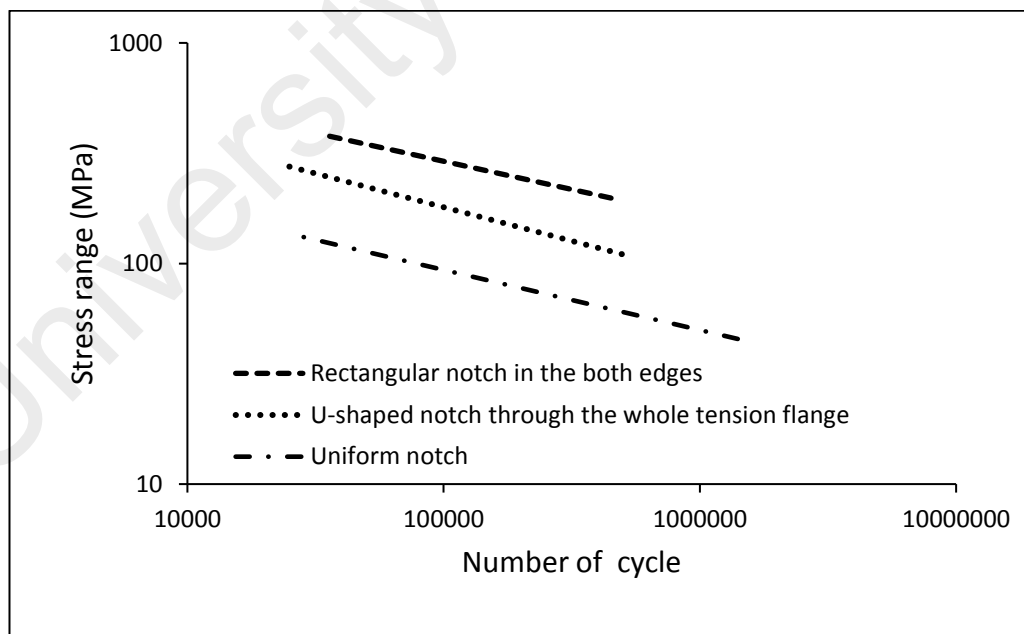


Figure 2.10: Stress behaviour in fatigue for different notch categories

2.11.2 Reinforced with prestressed polymer composite

Although adhesively Bonded FRP flexural strengthening techniques have been found to be an efficient approach to improve the lifetime of fatigued steel structures, there are relatively few studies that have applied prestressed CFRP strips to strengthen against cyclic loadings. Ghafoori et al. (2012) developed a prestressed unbonded reinforcement (PUR) method, and compared the effectiveness and feasibility of the approach with the prestressed bounded reinforcement (PBR) method. It could be used on heritage and historical structures where reversibility is important. The experimental test results for the strengthened beams using the PBR method showed a local strain concentration on the CFRP strip under the cracked section, while the PUR method had a uniform strain distribution along the CFRP strip. In addition, the fatigue performance of the unbonded reinforcement system was better at a high prestressing level of the CFRP without a substantial reduction in ductility.

Ghafoori, Schumacher, & Motavalli (2012) studied the behaviour of notched steel beams reinforced using prestressed and without prestressed bonded CFRP plates under cyclic loading. The experimental results showed that the fatigue strength of a beam reinforced using the prestressed CFRP plate increased more than five times that of an identical beam reinforced using non-prestressed CFRP plate (Figure 2.11). Both specimens were induced by a cyclic load range of 9-90 kN.

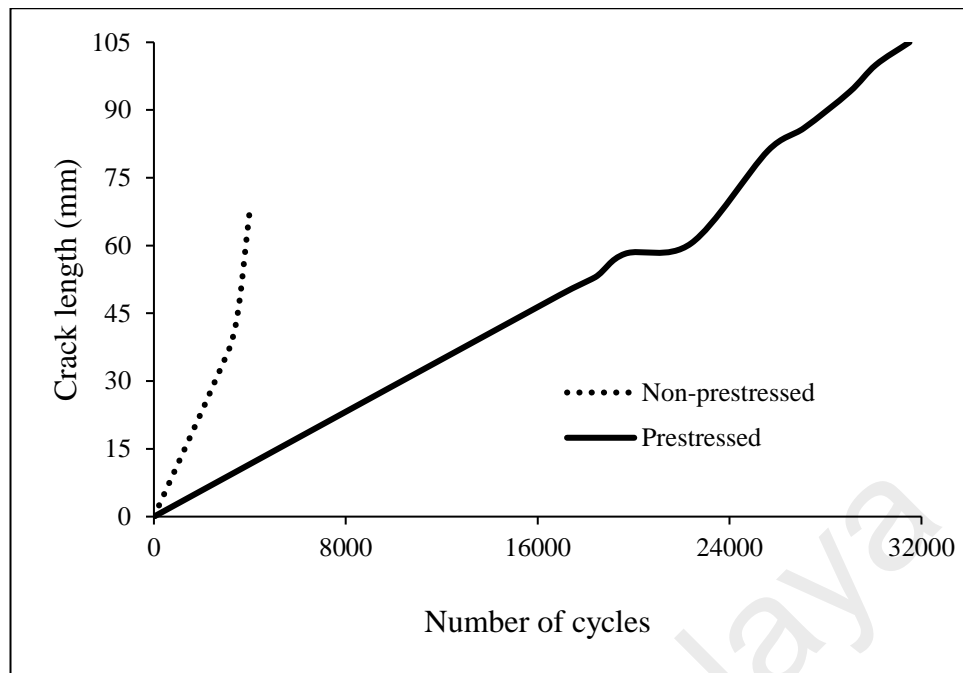


Figure 2.11: FCG curves for strengthened with non-prestressed and prestressed CFRP plates (Ghafoori, Schumacher, & Motavalli, 2012)

Vatandoost (2010) drew deflection range curves for W310×74 steel beam specimens strengthened with 14%, 15%, 35%, 0% and 37% prestressed CFRP plates. The deflection range vs. the number of cycle curves were drawn for the last 45000 cycles. Looking at Figure 2.12, it can be seen that: (1) the highest deflection range belongs to the control beam while the lowest deflection range belongs to specimen 37%-C-M indicating the highest stiffness increase for that specimen. (2) The deflection ranges are dramatically increased at the end of the fatigue life. (3) The lower deflection range for the specimens with CFRP strips on the cover plates confirms the influence of the CFRP strip location on the specimen stiffness. In Figure 2.12, “F” indicates that the strips are bonded to the inner side of the flange, “C” indicates that the strips are attached to the cover plate, and “S and M” indicates the CFRP strip with a standard modulus and moderate modulus, respectively. The beams with reinforcement located on the cover plates showed a greater

fatigue life improvement than those with reinforcement located on the inner side of the flange (Vatandoost, 2010).

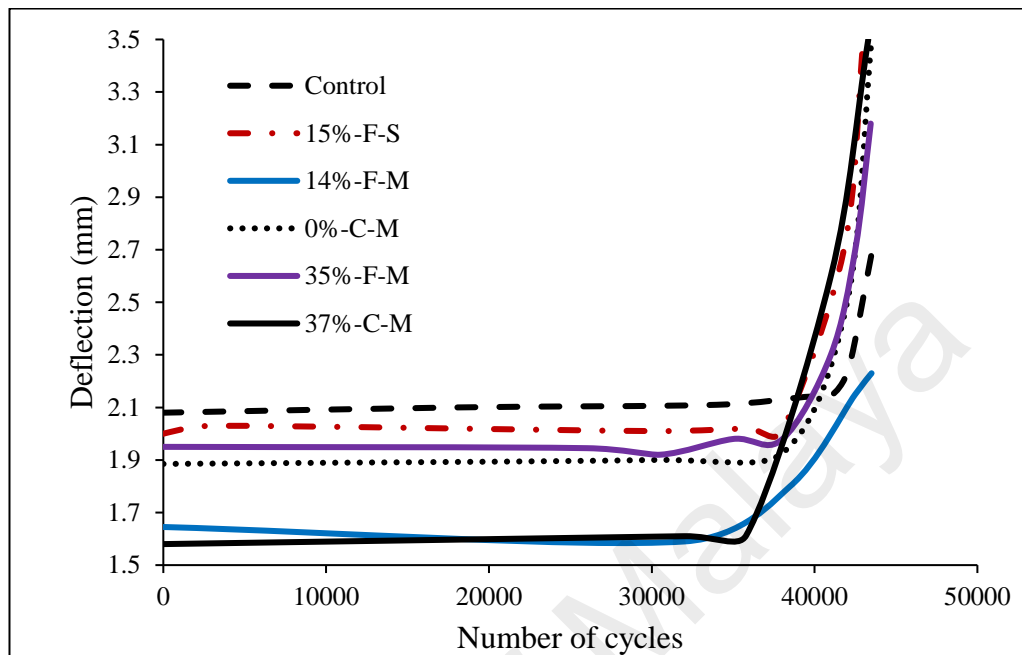


Figure 2.12: Deflection vs. number of cycle curves for strengthened steel beam using 14%, 15%, 35%, 0% and 37% prestressed CFRP plates (Vatandoost, 2010)

2.11.3 Fatigue in hybrid joint and Nano-adhesive

In recent years, fatigue in hybrid adhesive joints, which combine a traditional mechanical joint and a layer of adhesive (bolted/bonded, welded/bonded, and rivet/adhesive), has attracted a considerable number of researchers. This is due to their better fatigue performance compared to only mechanical joints or only bonded joints (Abdel Wahab, 2012; Hoang-Ngoc & Paroissien, 2010; Kelly, 2006; Moroni, Pirondi, & Kleiner, 2010; Sam & Shome, 2010). Furthermore, the use of nano-adhesives (carbon nano-tubes, alumina nano-particles, and quartz nano-particles) is a new field of application to bonded joints and has the potential to improve their fatigue performance (Abdel Wahab, 2012; Yoon & Lee, 2011).

2.12 Failure modes of reinforced steel beams

The deterioration of the steel bridge structural capacity over time may be due to corrosion, impact damage, and/or fatigue cracking (Hollaway & Cadei, 2002; Jones & Civjan, 2003; Liu, Zhao, & Al-Mahaidi, 2005). The crack propagation and failure mode of FRP-strengthened steel structural techniques are normally different than concrete-FRP techniques (Zhao & Zhang, 2007). The difference in failure modes was generally related to the fatigue strength and load-transferring mechanism of the reinforcement material. However, the failure modes depend on the elastic modulus of the FRP and the adhesive thickness (Pipinato, Pellegrino, & Modena, 2012).

Some possible failure modes in a CFRP bonded steel system are summarised (Narmashiri, Ramli Sulong, & Jumaat, 2012; Zhao & Zhang, 2007): (a) debonding, (b) delamination (separation of some carbon fibers from the resin matrix), (c) splitting, and (e) rupture. Debonding may be happened due to steel and adhesive interface failure, Cohesive failure (adhesive layer failure), and CFRP and Adhesive interface failure. The successful implementation of FRP composites of the strengthening systems is dependent upon the quality and integrity of the steel-composite joint and the effectiveness of the epoxy adhesive used (Schnerch et al., 2006). Another premature failure of unrestrained strengthened steel beams due to lateral-torsional-buckling is suggested to investigate by (Narmashiri & Jumaat, 2011).

2.12.1 Debonding failures

However, externally bonded strengthening steel beams with FRP composite plate generally suffers by peeling or delamination and debonding at the end of the composite

plate. FRP-Plate end problems in a strengthened steel beam is due to high peeling stress and interfacial shear stress in the location of the plate end.

Tavakkolizadeh & Saadatmanesh (2003) studied the performance of steel I-beams with an edged notch in the tension flange and reinforced with a bonded CFRP patch under cyclic loading. In Figure 2.13(a), the terms “near” identify the side that the crack started and “far” identify the side that the termination of crack. After reaching the fillet section of web, debonding started at the near edge of the patch. While the crack propagated towards the far edge, the patch debonding at the edge continued to grow. The CFRP debonding remained fairly stable when the crack reached to the far cut end. Then the far edge of the CFRP patch started to debond. The reinforcement failed after around 50 mm of debonding on both sides.

Wu et al. (2012) studied the fatigue behaviour of seven steel beams strengthened by using four different composite strengthening materials. During the experimental test, the fatigue crack started from the notch tip at mid-span in the all specimens as the number of cycles increased due to the high stress concentration in this vicinity. The cracks initiated and propagated slowly along the tension flange, and these cracks extended at a high rate as the load cycled. For the steel beam retrofitted by a welded steel plate, the beam with plate fractured immediately and could not bear any further loading cycles when the crack moved through the tension flange, as shown in Figure 2.13b(i). For specimens reinforced with FRP composite plates, extra number of cycles could still be continued when the crack moved through the tension flange. As the load cycled, the crack extended upwards on the web (Figure 2.13(b)(ii)) until debonding failure (Figure 2.13(b)(iii)). No fatigue rupture was sustained by using the reinforced plate. Hence, the application of a externally bonded reinforced plate can significantly prolong the fatigue life and enhance the failure mode of the strengthened beams compared to the application of a welded steel plate.

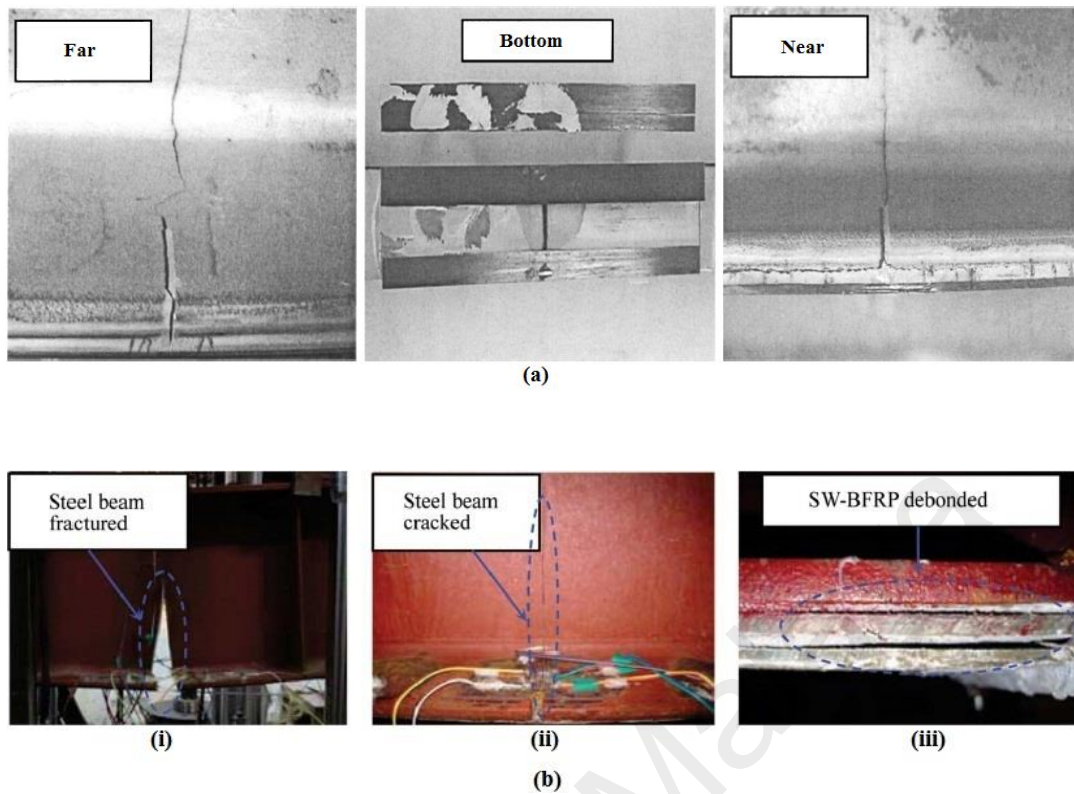


Figure 2.13: Failure modes of retrofitted beams using FRP plates (a) (Tavakkolizadeh & Saadatmanesh, 2003), (b) (Wu et al., 2012)

The FRP reinforcement ends and the regions where geometric discontinuities (cracks) take place are the most sensitive zones to fatigue damage of the adhesive joint, because of the stress concentration (CNR, 2007). Deng & Lee (2007b) found similar crack initiation and propagation in the CFRP reinforced steel beams except one test specimen, which was investigated with a 92.6% load range that caused it to debond immediately at one end after only 30 cycles, Figure 2.14. For the other specimens, the cracks at each end grew quickly, but then almost stopped after one of the two cracks had advanced past the mid-span of the beams. For all the composite plates that had debonded, the cracking initiated at the middle of the adhesive spew fillet and then expanded to the interface of steel surface and glue at a 45° angle.



Figure 2.14: CFRP end debonding due to cyclic loadings

Generally, the FRP end-debonding failure under monotonic loadings occurred as a result of stress from peeling and interracial shear at the plate ends in FRP-strengthening concrete and steel structural elements (Deng & Lee, 2007a; Haghani, Al-Emrani, & Kliger, 2009; Narmashiri & Jumaat, 2011). Figure 2.15 displays CFRP end-debonding failure mode of strengthened steel beams under monotonic loading. Bocciarelli et al. (2016) proposed an energy based analytical method to estimate the strain energy release rate for prediction the end-debonding failure of FRP-retrofitted steel beams. The proposed method was applied in the structural design of strengthened steel beams under static and general loadings configuration. Cornetti et al. (2015) analytically used cohesive damage modelling method to predict FRP end-debonding failure. Deng, Jia, & Zheng (2016) experimentally showed that the strength of the cracked beam by the FRP composite plate strengthening can be enhanced almost twice, whereas the brittle fracture of the strengthened beams caused by the intermediate debonding started from crack region limits the ductility improvement. They also presented an integrated closed form solution

for FRP-strengthened pre-cracked steel beams to obtain the localized interfacial shear and normal stresses by analytical study.



Figure 2.15: End debonding under monotonic loads

Jiao, Mashiri, & Zhao (2012) observed various failure modes for beams strengthened using CFRP plates and fabrics', debonding occurred in the steel surface and epoxy bond interface (Figure 2.16(a)). Again, failure happened between the plies of the fabrics' in the strengthened beams as shown in Figure 2.16(b). The observation also confirmed that the performance of the CFRP plates to resist crack propagation was better than for the CFRP sheets under cyclic loading.

The crack propagation rate depends on the stiffness of the FRP strip, and, largely, on the prestressing force (Täljsten, Hansen, & Schmidt, 2009). Ghafoori et al. (2012) investigated the damaged steel beams reinforced with the PUR and PBR methods and obtained a similar load-carrying capacity, however, the failure modes were different. In the PUR method the CFRP plate slipped in the mechanical anchorage technique at the

onset of the failure, while the CFRP in the PBR method arrived at its tensile strength in the cracked zone, and, finally, plate failure with debonding (Figure 2.17).

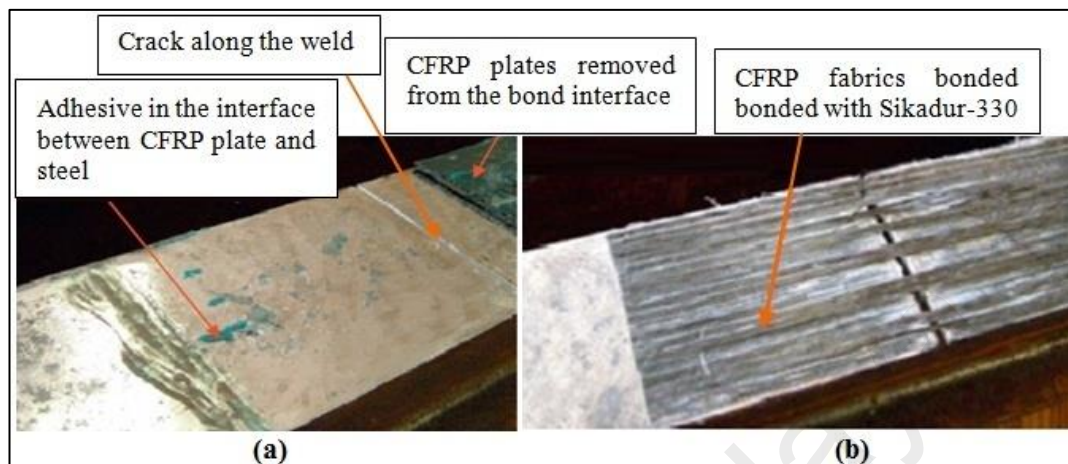


Figure 2.16: Debonding interface of retrofitted beams using (a) CFRP plates; (b) CFRP sheets (Jiao, Mashiri, & Zhao, 2012)

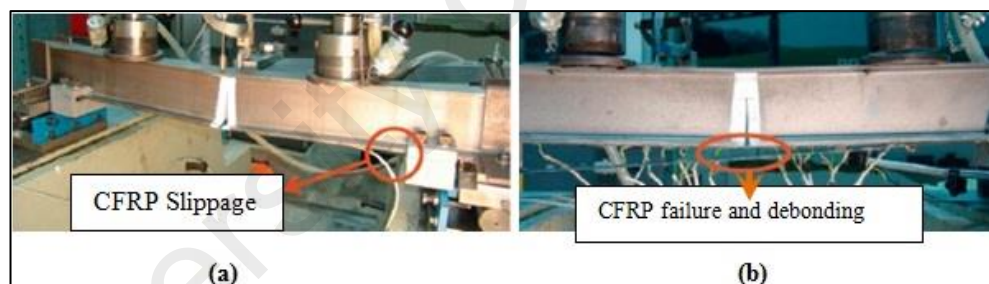


Figure 2.17: The failure modes for (a) PUR technique and (b) PBR technique

The end anchoring technique mitigates the debonding of the FRP strips and maintains the prestressing force, hence also reducing the transfer length (Vatandoost, 2010). Figure 2.18 illustrates the effectiveness of the end anchoring technique in maintaining the CFRP prestress.



Figure 2.18: Performance of end anchorage after failure for steel beam strengthened with prestressed strips to the cover plate (a) Removable end anchor, (b) Fixed end anchor (Vatandoost, 2010)

2.12.2 Lateral torsional buckling

Lateral torsional buckling (LTB) is one of the important factors for instability of unrestrained steel W-beams. The mitigation of instability of strengthened steel beams due to lateral-torsional-buckling is suggested to investigate by (Narmashiri & Jumaat, 2011).

Generally, steel beam experiences global buckling in which the beam is twisted and laterally buckled, when the load acting on the beam reaches to a critical level (Ghafoori & Motavalli, 2015b). The prime factors that influence the LTB of steel W-beams including effective (unsupported) length, boundary conditions of the beam, type and position of the loads, level of load application (stabilizing or destabilizing), material properties, non-prismatic behaviour of the member, magnitude with distribution of residual stress, initial geometric imperfections and loadings eccentricity.

However, LTB occurred on the laterally unrestrained strengthened steel beams which are loaded so as to be under bending about their strong axis. Counting the smallest loading causes LTB of the beam is known as critical LTB loading, which is a tough to mitigate. Specifically, for the steel sections which are under higher warping moments during the

torsion such as W or I sections. Many studies are conducted on un-strengthened steel beams in exploration of this solution (Benyamina et al., 2013; Ozbasaran, 2014).

2.13 Finite Element (FE) simulation

The finite element method (FEM) is an acceptable approach for analysing structures using software. In practice, the FE simulation is developed to validate the monotonic and fatigue strength of the experimental or analytical results.

Based on the surface crack widening energy release rate (Xie, Xu, & Li, 1998) using an elementary material strength theory (Müller, Herrmann, & Gao, 1993) and G^* -integral (Xie & Wang, 2004), an analytical approach was presented by Ghafoori & Motavalli (2011) to estimate the stress intensity factors (SIF) of a pre-cracked steel I-beam. The fatigue rehabilitation of steel structures is usually expected to decrease the value of SIF at the tip of the crack, and, as a result, enhance the post-crack fatigue life (Teng, Yu, & Fernando, 2012). Ghafoori et al. (2012) proposed an analytical method using the experimental test data (the external bending moment, the length of the crack and the corresponding strain applied on the CFRP strip under the cracked segment) and produced the SIF. They used ABAQUS software (version 6.8) to analyse the FE model of the steel beams to validate the results. The geometrical model and more mesh refinement around the loading, anchorage and cracked sections are shown in Figure 2.19. The method was generated to assess the sufficient level of the CFRP prestressing to arrest the fatigue crack growth (FCG). Moreover, the method was employed to study the active, semi-active and passive crack modes with a loaded reinforced beam. Several factors have been considered including crack propagation, excitation frequency and structural damping on the life of the FCG (Wenguang & Guoping, 2010).

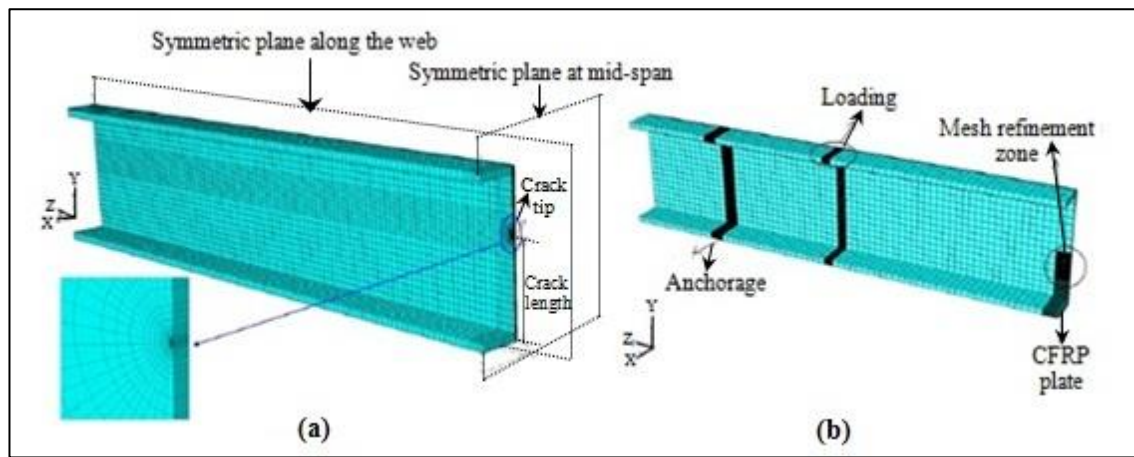


Figure 2.19: (a) A geometrical model using ABAQUS in the FE analysis and (b) the mesh refinement around the loading, anchorage and crack tips (Ghafoori et al., 2012)

Using the concept of fracture, the fatigue crack propagation (FCP) model was proposed by Xiulin & Hirt (1983). This was extended to the FCP of a cracked metallic element retrofitted with adhesively bonded composite patches in the study of Wang and Nussbaumer (Wang & Nussbaumer, 2009). Aljabar et al. (2016) established a mixed mode modification factor for estimation the fatigue life and the crack propagation of CFRP-strengthened tensile steel plates with artificial inclined pre-cracks at different angles.

According to the Paris-Erdogan crack growth law (Paris & Erdogan, 1963), a linear elastic fracture mechanics (LEFM) model was employed to predict the effects of peening treatments on the fatigue performance of welded steel structures (Walbridge, 2008) and to confirm the effectiveness of the prestressed CFRP strips (Vatandoost, 2010). Ghafoori, Schumacher, & Motavalli (2012) introduced a methodology for a pre-cracked beam with a specific crack length under cyclic loadings based on the fracture mechanics (FM) theory to estimate the adequate prestressing level by which the crack expansion is detained. Some strengthened beams were tested under various cyclic load ranges and the investigated test results showed excellent agreement with the developed model. Bennati,

Colonna, & Valvo (2016) modelled strengthened beam with pre-stress composite plate using the theory of classical beam and obtained an increased elastic limit state load for the strengthened steel beam whereas the adhesive was modelled as a cohesive interface.

In fracture mechanics, based on progressive crack modelling methods to predict the fatigue life, the rate of crack growth is related to the SIF (Paris & Erdogan, 1963) or strain energy release rate (Ashcroft, 2004; Erpolat et al., 2004; Johnson & Mall, 1985; Kinloch & Osiyemi, 1993). In the case of adhesively bonded plate joints, a crack shift parameter was proposed to account for the effects of accelerative interaction (Ashcroft, 2004; Erpolat et al., 2004). Important interaction effects were considered where the rate of crack propagation was linked with the mean load changes. However, continuum damage mechanics (CDM) models were developed by Lemaitre & Desmorat (2005) and modified for the damage formation of micro-cracks by (Kattan & Voyiadjis, 2002; Raghavan & Ghosh, 2005). CDM models have been used in a damage evolution law for modelling both pre-crack evolution and crack propagation for constant and variable amplitude fatigue (Bhattacharya & Ellingwood, 1998). For the bonded joints, Wahab et al. (2001) compared both the FM and DM methods to predict the fatigue strength of adhesively bonded CFRP lap joints. They verified that the developed CDM approach compared favourably with a FM method for constant amplitude fatigue (CAF) loadings. The FM and DM based fatigue life prediction of bonded single lap joints (SLJs) subjected to different types of variable amplitude fatigue (VAF) loadings were analysed by Shenoy et al. (2010).

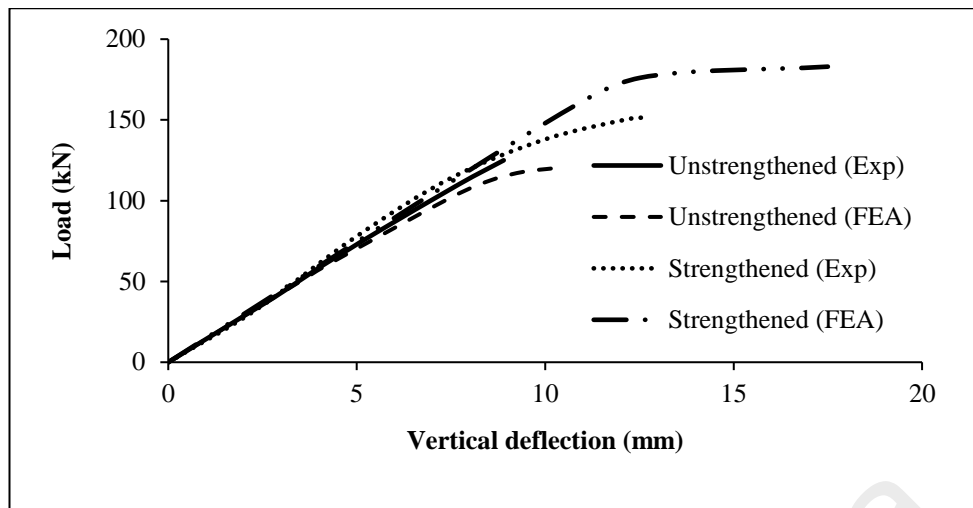


Figure 2.20: Load deflection relationship in experimental and numerical studies (static) (Narmashiri & Jumaat, 2011)

Kim & Harries (2011) developed a three-dimensional (3D) non-linear finite element model for predicting the fatigue strength of notched steel beams using ANSYS software. The steel section was modelled using 3-D structural solid elements (SOLID45); and a linear stress-strain relationship was developed for the CFRP. A non-linear interface element (COMBIN39) with two nodes was applied for modelling the behaviour of the steel-CFRP interface. For the element whose initial relative distance is zero, a bilinear bond-slip relationship was created for them. The study used the strain life method and the concept of Henry's damage theory (Henry, 1953) for the prediction of fatigue life of steel beams. The strain life approach is mainly relevant to a member representing significant plasticity induced by hysteretic loads. The theoretical background of this approach is discussed by Bannantine, Comer, & Handrock (1990). The deflection behaviour of unstrengthened and strengthened beams is shown in Figure 2.20. Furthermore, a typical S-N curve of strengthened steel beam obtained is shown in Figure 2.21, which was compared with category E in the AISC in the study by (ANSI, 2005). The notch provided for the stress concentrating effect is essentially equivalent to a Category E detail. Apart from this, Youssef (2006) developed a model for predicting the linear and non-linear

behaviour including the deflection at mid-span, strains of the steel and FRP, failure mechanism, and failure load of rehabilitated steel beams. The model was founded on the solution of the differential equations governing the behaviour of a strengthened steel beam, which includes representation of the shear and peel behaviour of the epoxy adhesive. To validate the predictions of the model, a steel W-beam strengthened using GFRP sheets was experimentally tested and excellent agreement was found between these results.

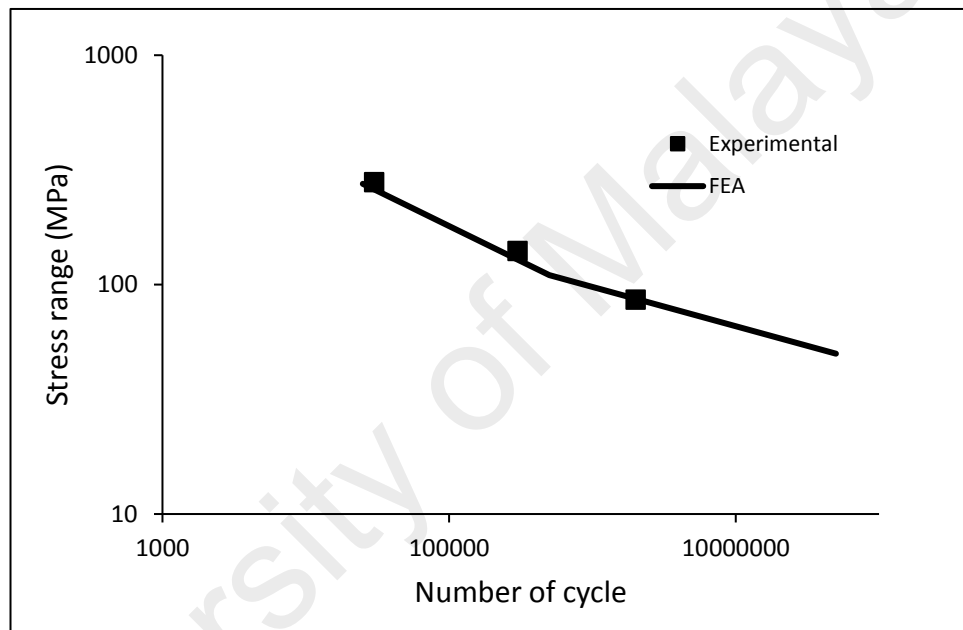


Figure 2.21: S-N curve in experimental and numerical studies (Kim & Harries, 2011)

Zhou et al. (2012) adopted the micro-mechanics based fracture model and the cyclic void growth model (CVGM) for estimating extremely low cycle fatigue (ELCF) fracture of the column-to-beam connections during earthquakes. The model was verified by the experimental results of nine full-scale connection tests. In addition, the refined finite element model was used to simulate the cyclic behaviour of the connection tests, and the CVGM fracture index was calculated using the stress and strain time histories. The number of cycles and the cumulative deformations to ELCF fracture predicted by CVGM

agreed well with the experimental results. The existing methodology also showed reasonable good accuracy for predicting the ELCF fracture of column-to-beam connections under inelastic cyclic loadings.

Pipinato, Pellegrino, & Modena (2011) used a LEFM method in a probabilistic (Cheung & Li, 2003) context to assess the fatigue reliability of steel bridge girders in the presence of seismic loadings. This method could give some new insights to increase the remaining fatigue strength, and could enable for a better understanding of progressive damage phenomena due to fatigue of a large number of steel bridges in seismic regions. Colombi (2005) developed a suitable plasticity based (Chen, Weiss, & Stickler, 1996; KUJAWSKI, 2003) crack retarding model as an extension of the well-known Newman's model (Newman Jr, 1981; Wang & Blom, 1991) for calculating the decrement of crack opening deformation along with the magnification of the crack growth rate retardation of the reinforced notched steel plates.

Teng, Fernando, & Yu (2015) proposed a FE method to predict plate debonding failure of reinforced steel beams. A mixed-mode cohesive law was applied to depict the localized interfacial stresses using bi-linear traction separation model.

From the abovementioned literature, it is revealed that the simulation in the finite element method can be a vital tool to assist in strengthening beam analysis under fatigue. This is because it eventually decreases the experimental cost in finance and time. Good validation of the simulation with practical experiments ensures the advantages of the strengthening techniques. However, the characteristics of strengthened steel beams under fatigue without using notches are still an interesting area to be explored. This interest can be addressed by FE simulation in a consistent manner.

2.14 Literature review summary

In this chapter, detailed reviews on the relevant researches were investigated systematically and carried out in respect of CFRP/steel strengthening techniques under monotonic and cyclic loadings. First, a general introduction was provided. Second, the reinforcing materials were introduced. Then, adhesive selection was reviewed. Significant information and an explanation of the existing research on the monotonic and fatigue behaviour of FRP-strengthened steel structures have been provided. The study also covered the surface preparation techniques, adhesive curing period and support condition under monotonic loading and fatigue, fatigue life, crack initiation and propagation, and failure modes of strengthened steel beams with lateral torsional buckling. Finally, the literatures concerning simulation of monotonic and fatigue strength of strengthened steel beams with FRP were reviewed.

The following research gaps are suggested for research in this area

1. The stress concentration below the point load and lateral torsional buckling of strengthened steel beams need to be prevented for delaying FRP splitting and end-debonding failure mode.
2. The premature failure due to end-debonding and end-delamination of externally bonded FRP strengthened beams under monotonic and cyclic loadings need to be delayed or mitigated.
3. An appropriate rehabilitation method using FRP composites of welded steel structural elements under cyclic loading should be explored to retrofit welded steel bridge girders.
4. The application of nano-adhesives to FRP/steel bonded joints for rehabilitation of steel bridge girders to increase the fatigue life has not been investigated yet.

5. The use of hybrid joints to strengthen steel structural elements with FRP requires further study.

University of Malaya

CHAPTER 3: METHODOLOGY

3.1 Introduction

The methodology applied in this research work is divided into two parts, experimental test and numerical simulation. Flow chart of the methods are presented in Figure 3.1. The aim of current study is to improve the CFRP end problems on structural strengthening system under monotonic loadings and fatigue. Therefore, appropriate geomantic end cutting shapes of the plates and adhesive at the tip of the bonding are essential for improvement on the structural behaviour of externally bonded strengthened steel beams with FRP composites. Hence, this research focuses on the effects of geometric in-plane (namely rectangle, semi-circular, semi-ellipse and trapezoidal) end cutting shapes of CFRP plates, and combination with tapering plate end on structural behavior of strengthened wide-flange steel beams such as CFRP failure modes, load carrying capacity, deformations, strain and stress distribution in different regions using numerical simulation and experimental test. Another feature of study is to identify the geometrical configuration using triangular spew fillets of adhesive at the tip of the plate that minimises the stress peaks at the CFRP plate tips of strengthened beams. The effect of stiffeners at below loading points, and lateral bracing on CFRP end-debonding and buckling failures of steel beams under monotonic loads are also examined. Section 3.2 describes the experimental test investigation including the design, materials used, preparation and strengthening procedure of the specimens, instrumentation of the specimens and the test set-up. The simulation of the numerical analysis is discussed in Section 3.3 to provide an accurate prediction of the behaviour of beams strengthening system.

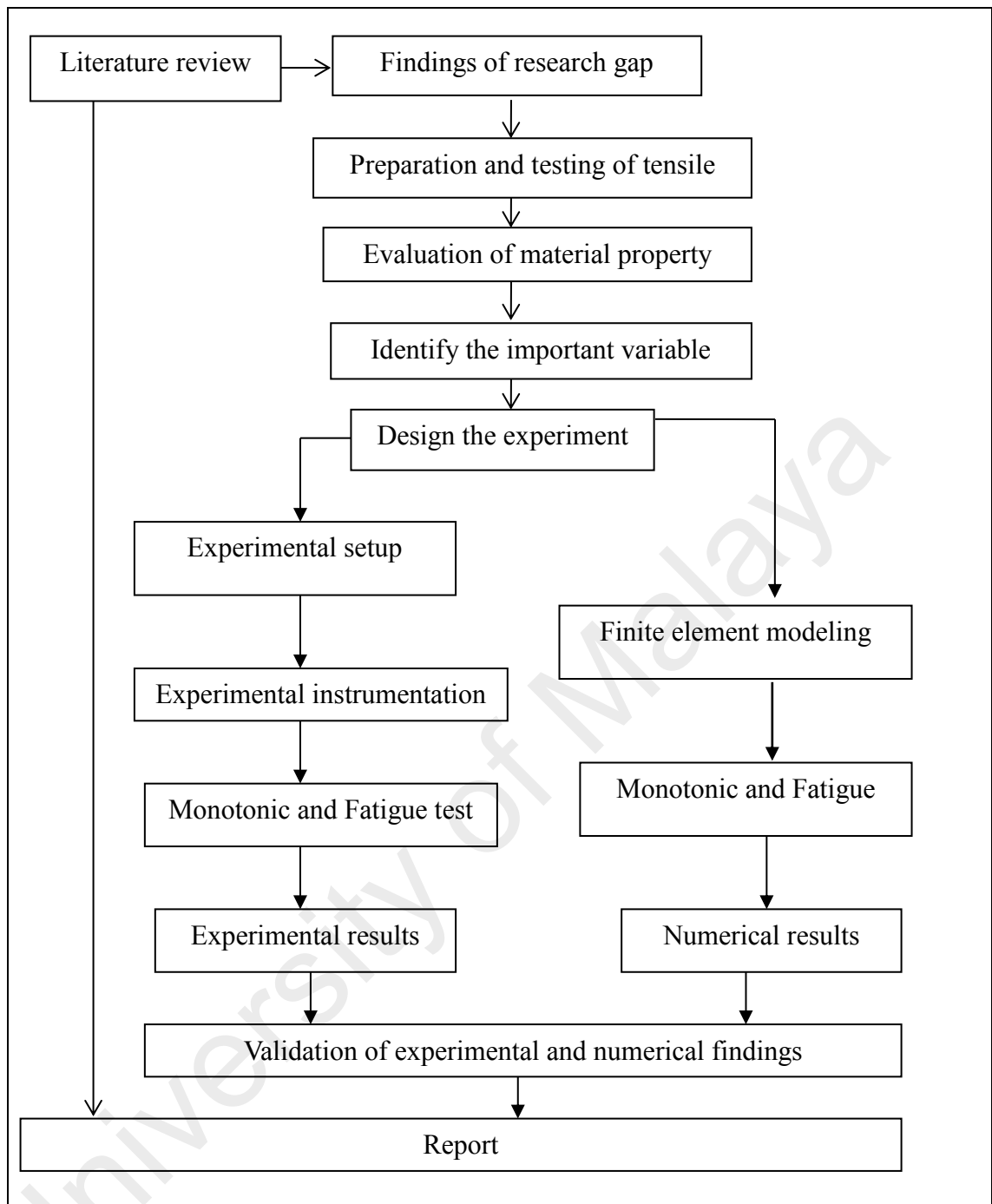


Figure 3.1: Flow chart of the methods

3.2 Experimental program

One of the most important and effective approach for investigating the behavior of structural elements is experimental testing. An experimental research program was conducted to investigate the performance of steel beams strengthened using carbon fiber

reinforced polymer (CFRP) plates subjected to flexure monotonic and cyclic loads. The program consisted of twenty-five steel beams: eighteen specimens for monotonic and seven for fatigue investigations.

3.2.1 Materials

The CFRP strengthened wide-flange steel I-beams comprised a combination of three materials in this research: mild steel (W-beam sections and steel plates), CFRP (plates and wrappings) and adhesive. In the following sections, the properties of these materials are explained in detail.

3.2.1.1 Wide-flange steel I-beam (W-section)

In this research, A6-ASTM mild steel W 150x100x24 sections were used. The mild steel material has low amount of carbon (0.16-0.29%) and is more ductile than carbon steel (Narmashiri, 2011). The flexibility of mild steel allows large deformation before failure of structures. In this study, wide-flange steel I-beam (W-beam) section with the mild steel property are chosen to strengthen in both monotonic and fatigue investigations. Table 3.1 shows the material properties with dimensions of the selected wide-flange steel I-sections. Tensile test coupons are prepared and tested to check the mechanical properties of the wide-flange steel I-beams section. Details in Appendix A.

(a) Tensile coupon

To achieve the material parameters such as yield strength, ultimate strength, % elongation, % area of reduction and young's modulus of selected steel beam, a uniaxial

standard tensile coupon test was conducted. According ASTM A370, the tensile test specimens were prepared. Dimensions of the specimens are shown in Figure 3.2. Both ends of the specimens were 75 mm length and a surface condition such that they are firmly gripped the coupon during testing. The gauge length of all coupon was 200 mm. Nine specimens were prepared from different beam sections, i.e. six flanges and three webs. Sample cutting and preparation of the tensile coupon are illustrated in Figure 3.3(a and b). One strain gauge was fixed at middle of the specimens to measure the elongation as shown in Figure 3.3(c).

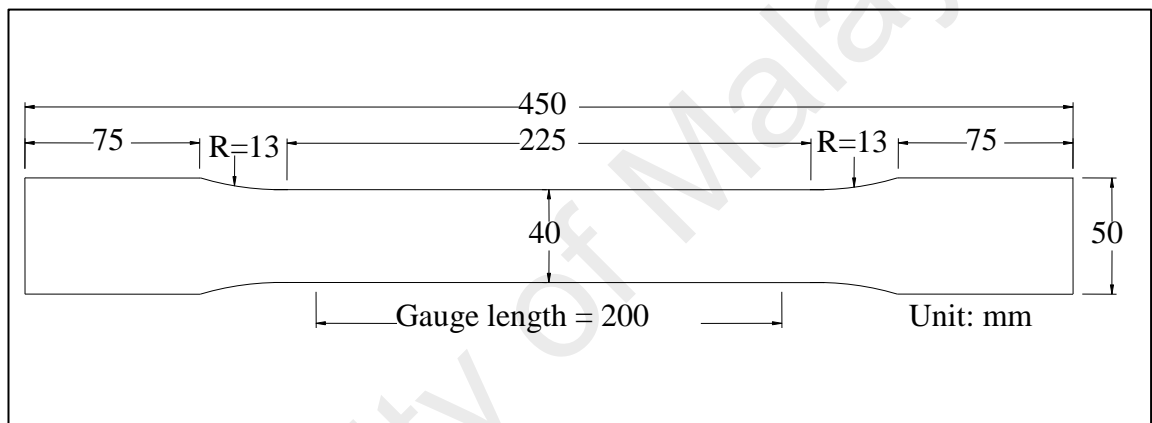


Figure 3.2: Dimensions of the tensile test specimens

A universal tensile testing machine with hydraulic gripping system was employed in the test. The machine was linked with a computer-controlled system in which the load and extension was graphically exhibited together with the calculations of stress and strain data. The applied tensile load and extension also were recorded by a data logger during the test. The tensile coupon testing was carried out by applying axial load with 1.25 mm/min speed to till failure of the specimens. Tensile coupon test setup is shown in Figure 3.4(a). The failure modes were observed cup and cone fracture as presented in Figure 3.4(b).

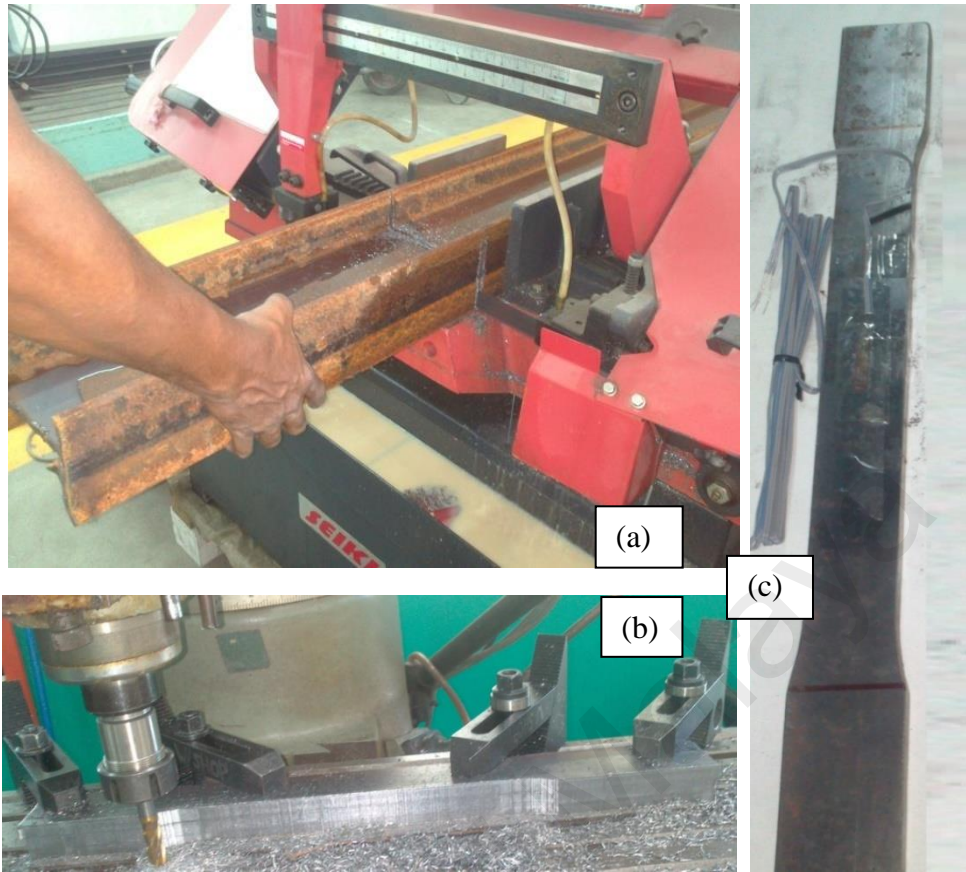


Figure 3.3: Tensile test coupon (a) Sample cutting, (b) Preparation and (c) Coupon with strain gauge

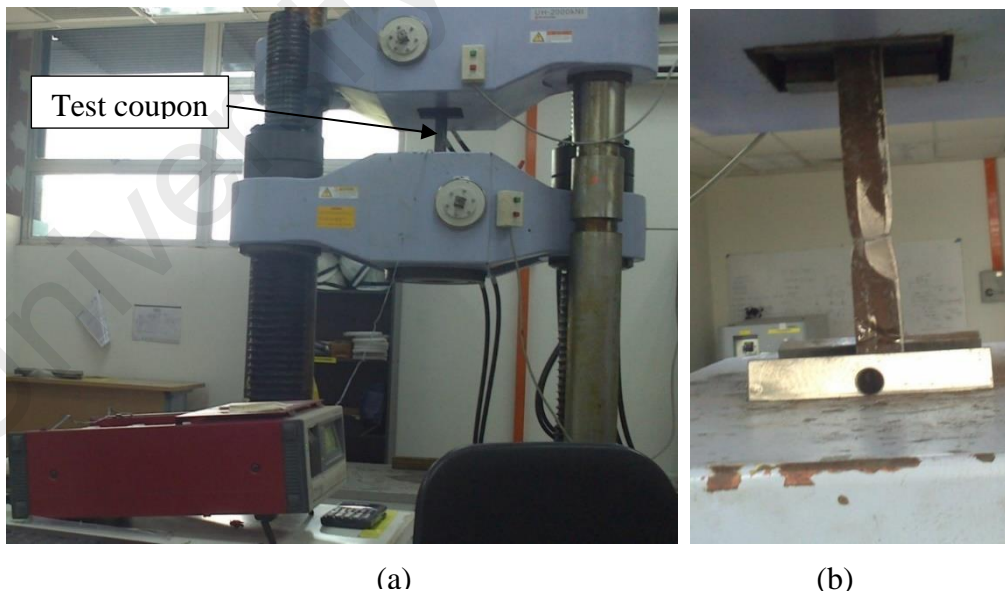


Figure 3.4: (a) Tensile coupon test set-up, (b) Failure mode

3.2.1.2 CFRP

Carbon fiber reinforced polymer composites have high tensile strength and can significantly enhance the structural performance as reinforcement. Typically, CFRP composites are produced in the form of a plate (strip) and fabrics (sheet). In this research, both types of CFRP materials were used, Sika CarboDur® S1014 pultruded plates and SikaWrap®-301 C woven carbon fiber fabrics (Figure 3.5). Normally, the fibers in CFRP are unidirectional.

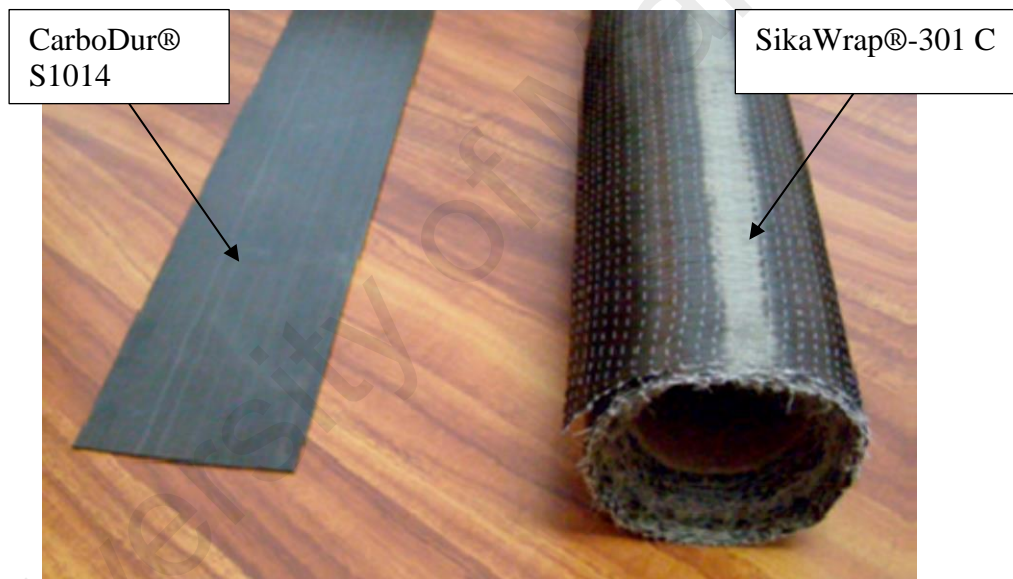


Figure 3.5: Carbon fiber reinforced polymer (CFRP) materials

In this research, CFRP strips and fabrics are applied. The CFRP strip is Sika CarboDur® S1014. The dimensions and material properties of this CFRP are shown in Table 3.2 (given by manufacturer). The CFRP fabrics is SikaWrap® -301 C woven carbon fiber fabrics. SikaWrap® -301 C is flexible and 0.13 mm thick each ply, and can be applied via wet layup to curved the structural surfaces. The fiber fabrics are used as an anchorage.

The specification of this kind of CFRP is shown in Table 3.3 (given by manufacturer). Detailed study will be carried out on monotonic and fatigue flexural behavior of strengthened wide-flange steel I-beams using externally bonded CFRP strips.

3.2.1.3 Adhesive

In this research, Sikadur[®]-30 and Sikadur[®]-330 epoxy are applied for bonding CFRP strips and fabrics. The structural epoxy adhesive used to install the CFRP strips on the steel surface of the structural elements must be strong enough to transfer the interfacial shear stress between the surfaces (Schnerch et al., 2006; Schnerch et al., 2005). Adhesive Sikadur[®]-30 (Sika Canada, 2009) is chosen to be applied as it is widely used (Bocciarelli et al., 2009; Narmashiri, Jumaat, & Sulong, 2010). This is essentially a thixotropic adhesive mortar based on a two solvent components free epoxy resin. Adhesive Sikadur[®] -30 is a part of resin and hardener with 3:1 proportions that must be mixed using 1% in weight of ballotini (1 mm diameter) to make a uniform thickness of the bonded length. Table 3.4 shows the material properties with dimensions of the used adhesive (given by manufacturer). The Sikadur[®]-30 epoxy resin has an elongation at failure (1%), which is less than the ultimate elongation (1.9%) of the fiber composite plate.

Sikadur[®]-330 adhesive is a two part (4:1), thixotropic epoxy based impregnating resin. The impregnation resins are applied for bonding SikaWrap[®] fabric/sheet reinforcement. A trowel and impregnation roller are used to apply the adhesive properly. Table 3.5 shows the dimensions with material properties of the Sikadur[®]-330 epoxy (given by manufacturer).

3.2.1.4 Steel stiffener plates

Steel plate stiffeners with a dimension of 47.7×12 mm were welded to the flanges and web on both sides of the beam below the loading point in specimens M1, M2, M4-M17, and F1-F7. Web stiffeners assist in preventing web crippling at the mid-span section (Moy & Nikoukar, 2002). In order to provide lateral stability of the steel beams, Kim & Brunell (2011) used stiffeners that were welded at the supporting points. The steel beams were stiffened using welded steel plates at below the point load of the steel beams reduce the effects of load on the flange (Narmashiri, 2011). The properties of the steel stiffener plates are the same as the wide-flange steel I-beams (Table 3.1).

University of Malaya

Table 3.1: Dimensions and material properties of wide-flange steel I-beams (W-beam)

Steel- Mild steel A6-ASTM									
Length	Steel I-section Dimensions (mm)				E-Modulus (MPa)	Stress (MPa)		Strain (%)	
	Width	Height	Flange Thick.	Web Thick.	Mean Value	Yielding (F _y)	Ultimate (F _u)	Yielding (ε _y)	Ultimate (ε _u)
2300	102	160	10.2	6.6	200000	306	457	0.12	13.5

Table 3.2: Dimensions and material properties of CFRP plates Sika CarboDur® S1014 (Sika@CarboDurPlates, 2013)

Dimensions (mm)		E- Modulus* (MPa)				Tensile Strength* (MPa)				Strain (%)
Width	Thickness	Mean Value	Min. Value	5% Fracture value	95% Fracture value	Mean Value	Min. Value	5% Fracture Value	95% Fracture Value	Strain at break
100	1.4	165000	>160000	162000	180000	3100	>2800	3000	3600	1.7 [±0.01]

* Mechanical values obtained from longitudinal direction of fibers.

Table 3.3: Dimensions and material properties of CFRP fabrics SikaWrap®-301 C

Dimensions (mm)		Areal Weight	Fiber Density	Consumption	E- Modulus* (Nominal)	Tensile Strength* (Nominal)	Strain (%)
Width	Thickness	g/m ²	(g/cm ³)	Kg/m ²	MPa	MPa	Strain at break
100	0.17	300 (±5%)	1.80	0.5 – 1.0	230000	4900	2.1 (±0.01)

* Mechanical values obtained from longitudinal direction of fibers.

Table 3.4: Dimensions and material properties of adhesive: SikaDur® 30

Thickness (mm)	Compressive Strength (MPa)		Tensile Strength (MPa)		Shear Strength (MPa)	Bond Strength on Steel (MPa)	
	E-Modulus	Strength 7 Days	E-Modulus	Strength 7 Days	Strength 7 days	Mean Value	Min. Value
1	9600	70-95	11200	24-31	14-19	>30	>21

Table 3.5: Dimensions and material properties of Sikadur®-330 epoxy

Thickness (mm)	E-Modulus 7 days (MPa)		Tensile Strength 7 days	Viscosity (mPas)		Elongation at break	Bond Strength on steel
	Flexural	Tensile	(MPa)	+23°C	+35°C	%	(MPa)
1	3800	4500	30	6000	5000	0.9	> 4

3.2.2 Test specimens

In this research, twenty-five experimental specimens are prepared based on the test matrix are given in Table 3.6. There are two categories in terms of loading, i.e. flexural monotonic and fatigue specimens (18 specimens for monotonic loading and 7 specimens for cyclic loading).

Table 3.6: Test matrix of the experimental program

Group	ID	Description	End cutting shapes	Loading	
A	M0	Unstrengthened beam (effect of lateral bracing and stiffeners)	-	Monotonic	
	M1			Monotonic	
	M2			Monotonic	
B	M3	Strengthened beam (effect of lateral bracing and stiffeners)	Rectangular	Monotonic	
	M4		Rectangular	Monotonic	
	M5		Rectangular	Monotonic	
C	M5	Strengthened with different CFRP end cutting shape	Rectangular	Monotonic	
	M6		Semi-ellipse	Monotonic	
	M7		Semi-circular	Monotonic	
	M8		Trapezoidal	Monotonic	
D	M9	CFRP in-plane end cutting shape with triangular spew fillet of adhesive	Rectangular	Monotonic	
	M10		Trapezoidal	Monotonic	
E	M11	Combination of the best CFRP end cutting shape with	Tapering	Rectangular	Monotonic
	M12			Trapezoidal	Monotonic
	M13		Tapering and spew fillet of adhesive	Rectangular	Monotonic
	M14			Trapezoidal	Monotonic
	M15		Reverse tapering	Rectangular	Monotonic
	M16			Trapezoidal	Monotonic
F	M17	Anchorage using CFRP fabrics	Rectangular	Monotonic	
G	F1	Unstrengthened Beam	-	Cyclic	
	F2			Cyclic	
H	F3	Strengthened with different CFRP end cutting shapes	Rectangular	Cyclic	
	F4		Semi-ellipse	Cyclic	
	F5		Semi-circular	Cyclic	
	F6		Trapezoidal	Cyclic	
I	F7	Anchorage using CFRP fabrics	Rectangular	Cyclic	

The experimental specimens were divided into nine groups (Table 3.6). Groups A and G are the control beams for monotonic and fatigue specimens, where the beams were left unstrengthened. The specimens of group B were tested to investigate the effect of lateral bracing and stiffeners on the failure mode of the strengthening plate. Different in-plane CFRP end cutting shapes were applied to strengthen the specimens of groups C and H under monotonic loads and fatigue. A combined in-plane and taper CFRP end shape with a triangular spew fillet of adhesive was applied for groups D and E. The strengthened specimens of groups F and I were anchored using CFRP wrapping.

Thirty-four beams were modelled (including twenty-five specimens) to simulate the structural behavior of the experimental unstrengthened and strengthened steel beams. Nine specimens were modelled to optimize the end anchorage using CFRP fabrics in terms of parametric studies, under monotonic loading and fatigue. Table 3.7 illustrates a detailed specification of the monotonic specimens tested and analysed in this research. Table 3.8 presents the anchored specimens under monotonic loading that were modelled for parametric study using finite element analysis. A detailed specification of the specimens for fatigue investigation is given in Table 3.9.

Flexural strengthening under monotonic loading and fatigue of structures using CFRP composite plates is a common application. High tensile stress and strain occur at the bottom of section due to flexure. Consequently, to flexurally strengthen the steel beams, CFRP plates were installed on the tensile (bottom) flange (Figure 3.6 and Figure 3.7). The best region to install CFRP is the tensile region because (CNR, 2007): (1) this region is the furthest from the neutral axis and can increase the moment of inertia appropriately, and (2) CFRP materials have high tensile strength.

A key problem to be faced when managing FRP strengthened beams is the possible premature failure due to debonding and delamination. The CFRP ED and EDL cause

premature failure, which is an essential issue that needs to be resolved. Narmashiri (2011) investigated the effects of different CFRP lengths (600 mm, 1000 mm, 1500 mm, 1700 mm, and 1800mm) on the failure modes of strengthened steel I-beams. The result shows that the strengthened beam with a 1000 mm length CFRP plate underwent CFRP failure by ED and EDL. This research highlights various approaches to provide solutions for the end problems of strengthened wide-flange steel I-beams using 100000 mm² CFRP plate area with 1000 mm to 1025 mm plate length. The width and the bonded area of the CFRP plates are constant in this research. The length of the plate is varied because of different in-plane CFRP end cutting shapes. In the following sections, the test specimens are explained in detail according to the objectives of this research.

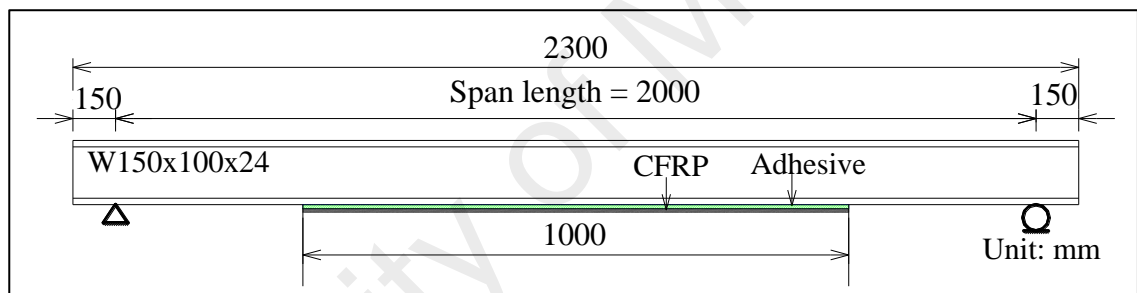


Figure 3.6: Elevation projection of the specimens

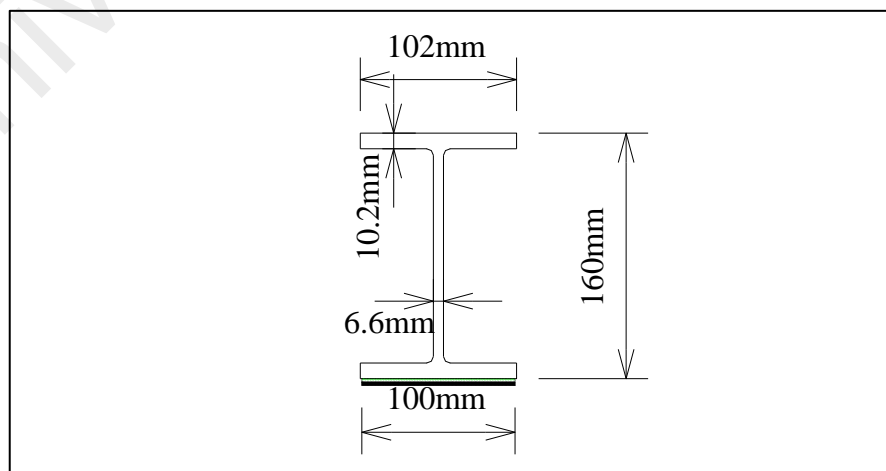


Figure 3.7: Cross section of the specimens

Table 3.7: Specifications of the monotonic specimens

No.	Specimens	Stiffeners below loads	Lateral bracing	Specification of CFRP plates				Triangular fillet adhesive at ends	Anchorage at plate end	Method	
				L_{CFRP} (mm)	Plate area (mm ²)	CFRP end shapes				Exp.	FE
						In-plane	Tapering				
1	M0	N/A	N/A	N/A	N/A	N/A	N/A	N/A	N/A	√	√
2	M1	√	N/A	N/A	N/A	N/A	N/A	N/A	N/A	√	√
3	M2	√	√	N/A	N/A	N/A	N/A	N/A	N/A	√	√
4	M3	N/A	N/A	1000.00	100000	Rectangular	N/A	N/A	N/A	√	√
5	M4	√	N/A	1000.00	100000	Rectangular	N/A	N/A	N/A	√	√
6	M5	√	√	1000.00	100000	Rectangular	N/A	N/A	N/A	√	√
7	M6	√	√	1010.75	100000	Semi-ellipse	N/A	N/A	N/A	√	√
8	M7	√	√	1021.50	100000	Semi-circular	N/A	N/A	N/A	√	√
9	M8	√	√	1025.00	100000	Trapezoidal	N/A	N/A	N/A	√	√
10	M9	√	√	1000.00	100000	Rectangular	N/A	√	N/A	√	√
11	M10	√	√	1025.00	100000	Trapezoidal	N/A	√	N/A	√	√
12	M11	√	√	1000.00	100000	Rectangular	Tapering	N/A	N/A	√	√
13	M12	√	√	1025.00	100000	Trapezoidal	Tapering	N/A	N/A	√	√
14	M13	√	√	1000.00	100000	Rectangular	Tapering	√	N/A	√	√
15	M14	√	√	1025.00	100000	Trapezoidal	Tapering	√	N/A	√	√
16	M15	√	√	1000.00	100000	Rectangular	Reverse tapering	√	N/A	√	√
17	M16	√	√	1025.00	100000	Trapezoidal	Reverse tapering	√	N/A	√	√
18	M17	√	√	1000.00	100000	Rectangular	N/A	N/A	√	√	√

Table 3.8: Specifications of the anchored specimens under monotonic loading for parametric studies using numerical modeling

No.	Specimens	Stiffeners below loads	Lateral bracing	Specification of CFRP plates			End anchorage using CFRP fabrics (wrapping)			Method	
				L_{CFRP} (mm)	Plate area (mm ²)	CFRP end shapes	Layer	Length (mm)	Width (mm)	Exp.	FE
						In-plane					
1	M18	√	√	1000.00	100000	Rectangular	1	220	175	N/A	√
2	M19	√	√	1000.00	100000	Rectangular	2	220	175	N/A	√
3	M20	√	√	1000.00	100000	Rectangular	4	220	175	N/A	√
4	M21	√	√	1000.00	100000	Rectangular	3	170	175	N/A	√
5	M22	√	√	1000.00	100000	Rectangular	3	220	125	N/A	√
6	M23	√	√	1025.00	100000	Trapezoidal	3	220	175	N/A	√

Table 3.9: Specifications of the fatigue specimens

No.	Specimens	Specification of CFRP plates			End anchorage using CFRP fabrics (wrapping)	Method	
		L_{CFRP} (mm)	Plate area (mm ²)	CFRP end shapes		Exp.	Numerical
				In-plane			
1	F1 (UB)	N/A	N/A	N/A	N/A	√	√
2	F2 (CB)	N/A	N/A	N/A	N/A	√	√
3	F3	1000.00	100000	Rectangular	N/A	√	√
4	F4	1010.75	100000	Semi-ellipse	N/A	√	√
5	F5	1021.50	100000	Semi-circular	N/A	√	√
6	F6	1025.00	100000	Trapezoidal	N/A	√	√
7	F7	1000.00	100000	Rectangular	√ (3 layers)	√	√
8	F8	1000.00	100000	Rectangular	√ (1 layers)	N/A	√
9	F9	1000.00	100000	Rectangular	√ (2 layers)	N/A	√
10	F10	1025.00	100000	Trapezoidal	√ (3 layers)	N/A	√

UB: Un-strengthened beam; CB: Control beam

3.2.2.1 Effect of lateral bracing and stiffeners

The experimental program involved strengthening and testing a total of six beam specimens to investigate lateral bracing and stiffeners. Three specimens were considered as reference beams (M0, M1 and M2), while the other three specimens were strengthened with CFRP strips (M3, M4 and M5). The strengthened specimens were bonded with 1,000 mm long CFRP strips. Table 3.7 presents the specifications of the beams used in this research. Steel plate stiffeners with a dimension of 47.7 mm × 12 mm were welded to the flanges and web on both sides of the beam below the loading point in specimens M1, M2, M4, and M5.

3.2.2.2 In-plane end cutting shapes

Normally, CFRP flexural strengthened structures suffer two modes of failure at the end of the plate, which are called delamination and debonding. To increase the strength of the structures against these problems, application of different tapered end cutting shapes can be done (Deng & Lee, 2007a, 2007b; Deng, Lee, & Moy, 2004; Linghoff, Haghani, & Al-Emrani, 2009; Rizkalla, Dawood, & Schnerch, 2008; Schnerch et al., 2007). Application of this kind of end cutting shape is very difficult for thin plates. Hence, in-plane end cutting shapes are proposed to increase the bonding at the end of the plate.

The normal in-plane end cutting shape for CFRP plates is rectangular (straight). In order to investigate the effects of different in-plane CFRP end cutting shapes, four shapes are chosen (Figure 3.8): (1) rectangular, (2) semi-ellipse, (3) semi-circular (rounded) and (4) trapezoidal. The in-plane shapes can be easily fabricated using a mechanical sander as shown in Figure 3.9.

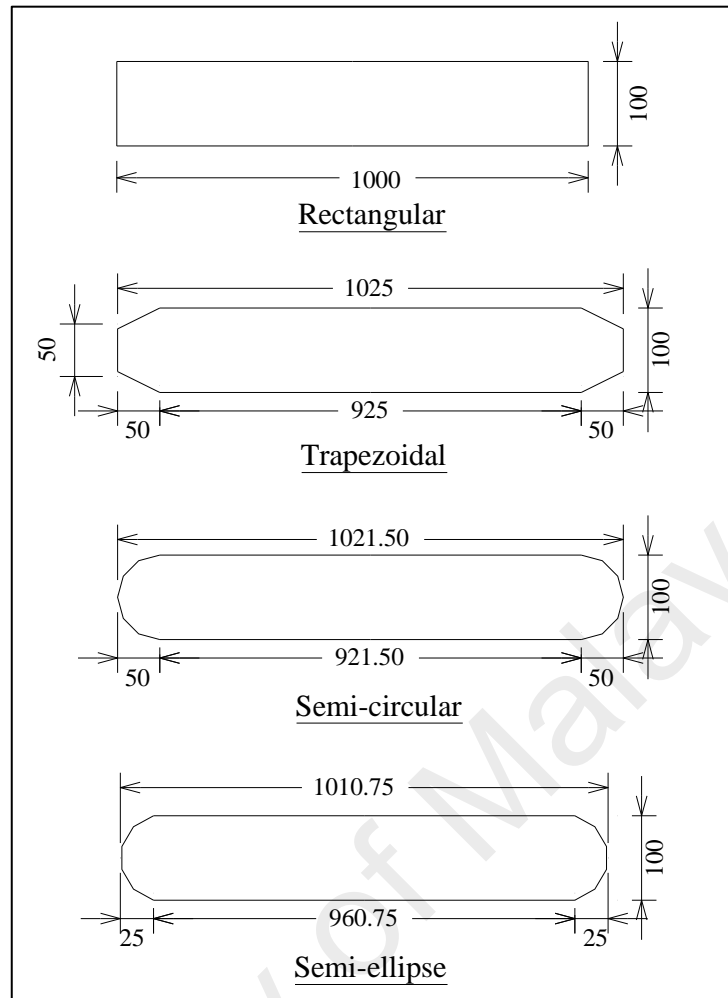


Figure 3.8: Different in-plane end cutting shapes with measurements: (a) rectangular, (b) trapezoidal, (c) semi-circular, (d) semi-ellipse

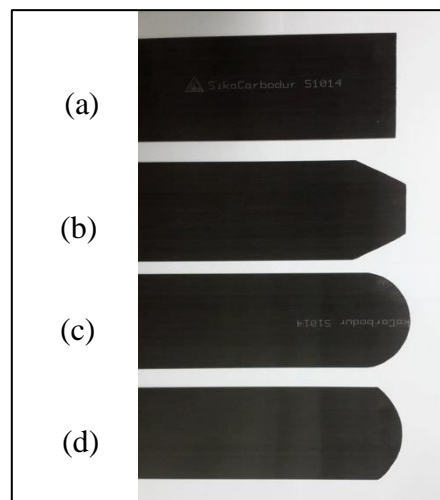


Figure 3.9: (a) rectangular, (b) trapezoidal, (c) semi-circular and (d) semi-ellipse in-plane CFRP end cutting shapes

If the same length of CFRP strip is chosen, then for the specimens with different CFRP end cutting shapes, the sectional areas of the pasted CFRP to steel would be different. This may affect the strength of the strengthened specimens. In this research, the CFRP plate's length is different for each specimen, however, the sectional areas for the pasted CFRP to steel surface for all specimens are the same. In this case, the plate's length for the specimen's rectangular, trapezoidal, semi-circular, semi-ellipse are 1000 mm, 1025 mm and 1021.50 mm, and 1010.75 mm, respectively. The sectional area of the CFRP pasted to the steel beams for all strengthened specimens was 100000 mm².

3.2.2.3 In-plane and tapering combined end shape with spew fillet

In this research, the effects of the combination of in-plane and tapering CFRP end cutting shapes with triangular spew fillets of adhesive at the end of specimen plates will be investigated to retard the CFRP end problems on monotonic and fatigue flexural specimens. Figure 3.10 presents a strengthened specimen with a tapered plate. A taper can be easily fabricated in the direction of the fiber by using a mechanical sander, as shown in Figure 3.11.

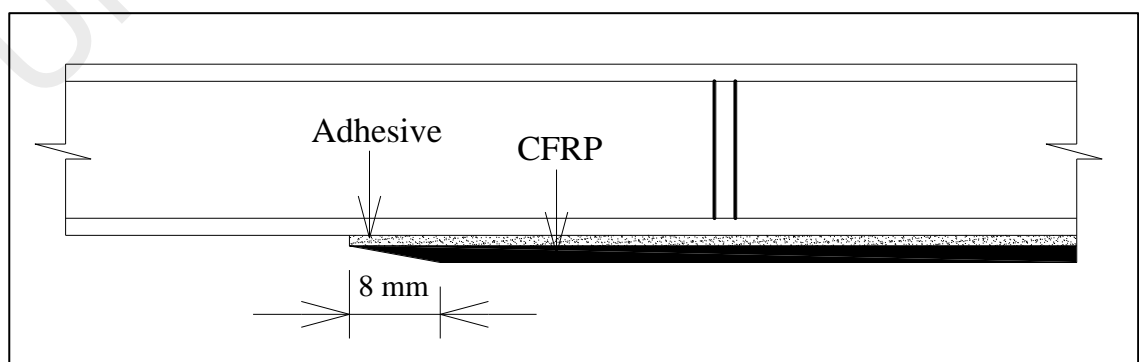


Figure 3.10: Specimen with a tapered CFRP end shape

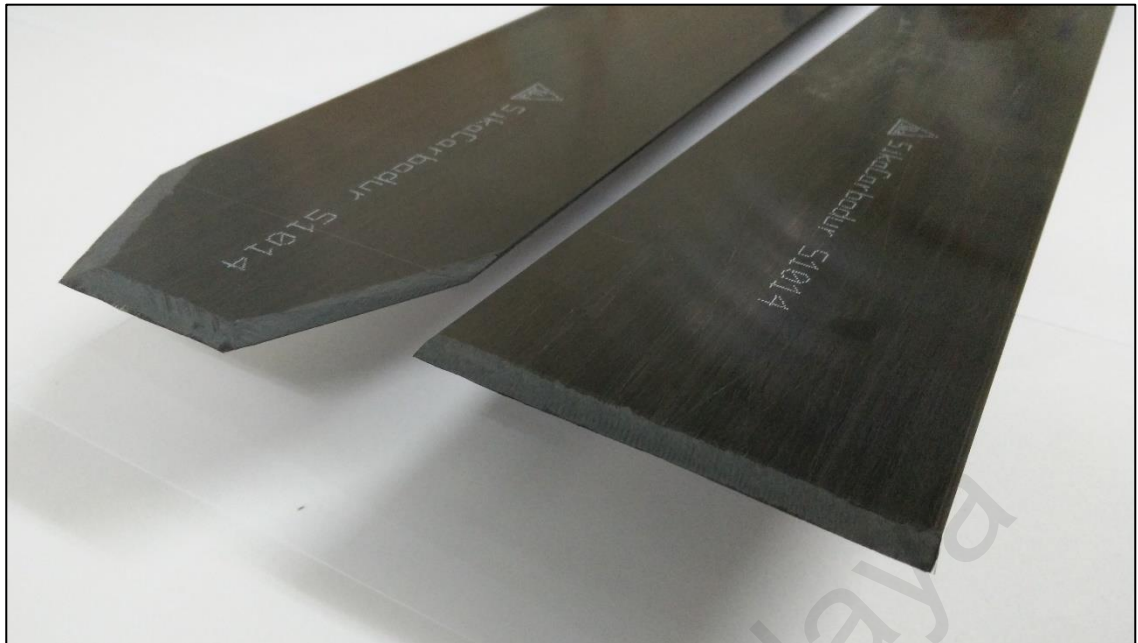


Figure 3.11: Tapered end shapes

The strengthened specimens with triangular spew fillets of adhesive at the end of the CFRP plates are shown in Figure 3.12 to Figure 3.14. In the previous section, the in-plane CFRP end shapes were described in detail. The CFRP composite plates should be cut to length and have their end cutting detailed in accordance with the design of the adhesive bond joints.

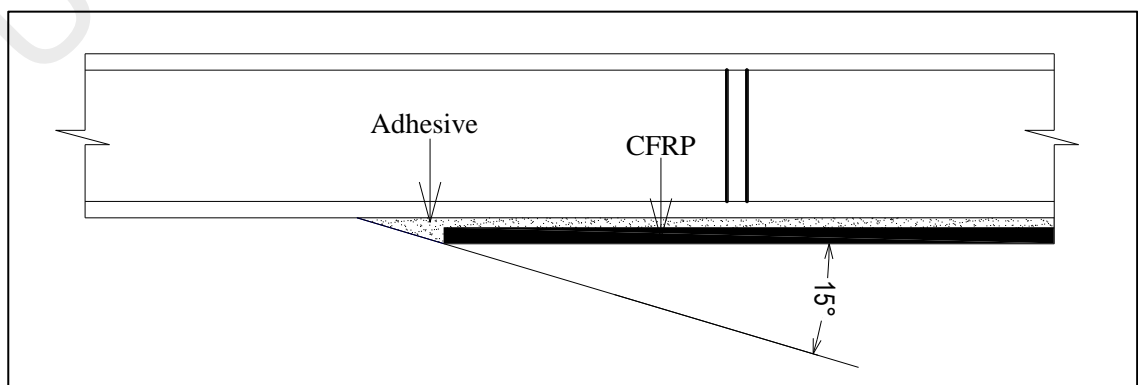


Figure 3.12: In-plane CFRP end cutting shapes with triangular adhesive fillets

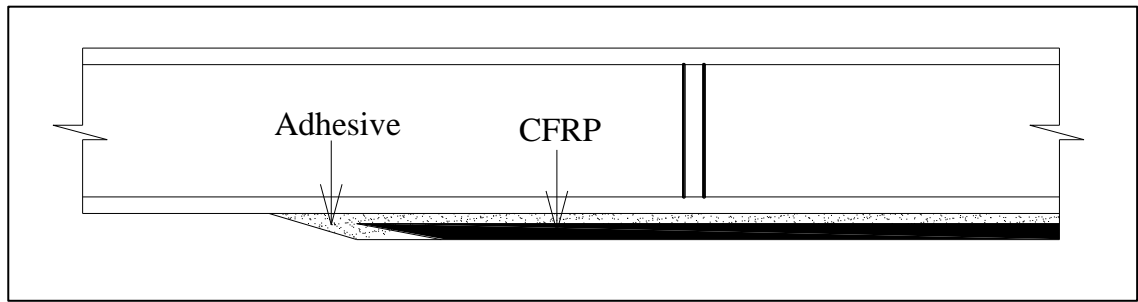


Figure 3.13: CFRP tapered ends with triangular adhesive fillets

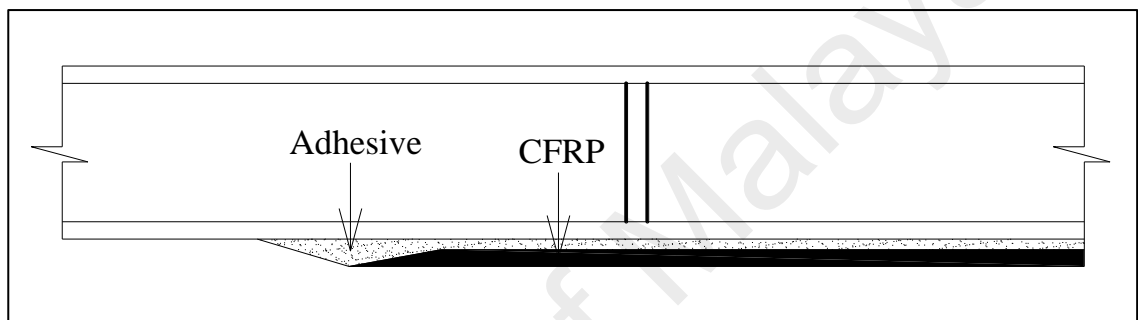


Figure 3.14: Reverse tapered CFRP end with a triangular adhesive fillet

3.2.2.4 CFRP fabrics anchoring

According to previous studies, two modes of failure can occur at the tip of a CFRP-adhesive bond joint for CFRP flexural strengthened steel beams (Narmashiri, Ramli Sulong, & Jumaat, 2012), namely ED and EDL.

The peeling stress and debonding at the tip of the CFRP plates are the main problems that occur during CFRP flexural strengthening of steel elements using monotonic and cyclic loading. This is commonly attributed to the much high stresses and strains concentration that occurs at the tips of the composite plate (Ghafoori & Motavalli, 2015a; Haghani, Al-Emrani, & Kligler, 2009; Narmashiri, Jumaat, & Sulong, 2010; Seleem, Sharaky, & Sallam, 2010; Sen, Liby, & Mullins, 2001). One of the methods to overcome

these problems is the application of some additional materials to cover by anchorage or clamp the end of the CFRP strips. Application of a clamping technique at the end of the CFRP composite plates for steel and reinforced concrete (RC) bridges was proposed by (Sen, Liby, & Mullins, 2001). Nevertheless, using this clamping technique did not enhance the load bearing capacity of the whole beam structure because the holes in the CFRP caused the strip to fail. Mechanical fastening was investigated under monotonic loads using metallic plates and bolts as end-anchorage to address end debonding problems (Narmashiri, Jumaat, & Sulong, 2010). In this type of mechanical anchorage, pulling out of the CFRP plate from the metallic plate resulted in a considerable drop in strength.

The critical regions in which failure of the CFRP may occur include the end of the CFRP plate. However, the application of CFRP fabrics using adhesive as an anchoring material can be easier and more convenient than mechanical anchoring systems in these areas which increase the bonding strength. In this research, the effects of applying CFRP fabrics to anchoring systems using adhesive on CFRP end problems in strengthening wide-flange steel I-beams (W-beam) for monotonic and fatigue flexural will be investigated. The length of the CFRP fabrics is 220 mm as cover the round of bottom flange. Figure 3.15 displays the length and width of CFRP fabrics. A triple layered C-shape anchor was used at the end of the CFRP plate using CFRP fabrics with a width of 175 mm (Figure 3.16). Figure 3.17 shows the installation of CFRP fabrics.

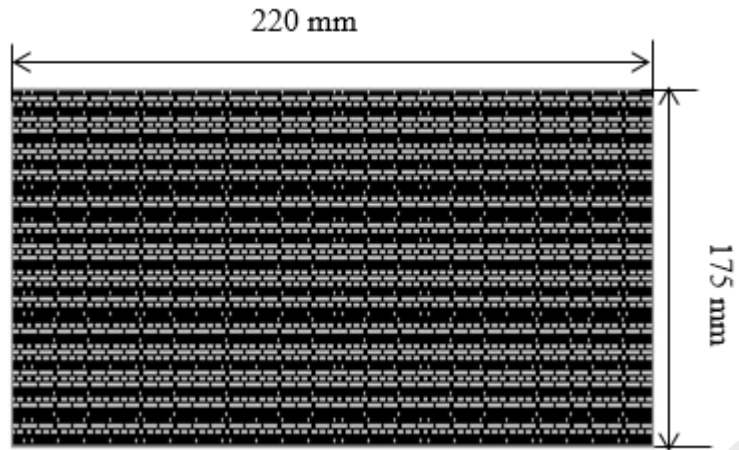


Figure 3.15: Length and width of the CFRP fabrics

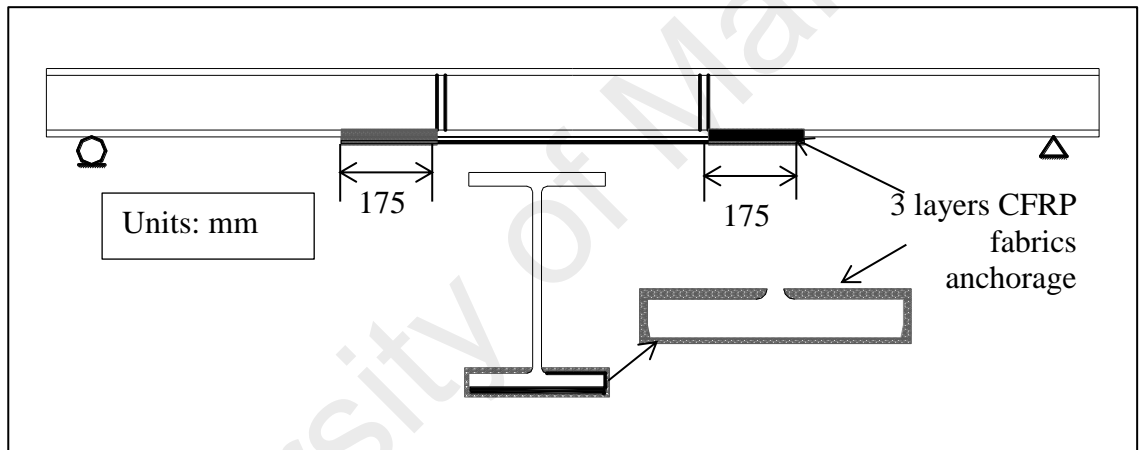


Figure 3.16: Dimensions and positions of end-anchorage using CFRP fabrics



Figure 3.17: Attachment of CFRP fabrics to specimens for anchorage using adhesive

3.2.3 Preparation of the specimens

Before starting the experiment tests, the specimens must be prepared including surface preparation with sand blasting of the beams, cutting and cleaning CFRP reinforced plates, mixing adhesive properly, applying adhesive on the steel surface and installing CFRP plates. In this section the procedure for preparing the monotonic and fatigue flexural specimens are explained in detail. However, preparations of the strengthening specimens for monotonic and fatigue investigation are similar.

The first step for preparation of the specimens is the cutting of the steel W-beam sections to suitable lengths. Normally, steel beams are 12000 mm in length. Tensile coupons with 500 mm length were collected from each full beam for testing to check the properties of the selected steel beam sections. The steel beams are cut as follows:

$$5 \times 2300 \text{ mm (specimens)} + 500 \text{ mm (tensile coupon)} = 12000 \text{ mm.}$$

Consequently, using these lengths no wastage results from the cutting of the steel beams. To increase the accuracy of cutting, a horizontal band saw blade is used to cut the wide-flange steel I-beams.

The second process to prepare the specimens is welding the steel stiffener with 12 mm thickness on the web and flange. The steel stiffeners are welded to the steel beams below the point load by using the carbon welding method. The weld dimension is 6 mm in all region.

The third process is sand blasting of the steel surfaces to which the CFRP strips are expected to be installed. Normally, steel surfaces are oxidized because of the weather or manufacturing processes or polluted by oil, color, or dust. The best method to remove these pollutions is through sandblasting until a white and clean surface is seen (Schnerch

et al., 2007; Schnerch et al., 2005). To remove the rust on the surface of the bottom tension flange was treated of each specimen by using a grinding wheel. And the surfaces were cleaned and washed with acetone. According to Sika® product information, for strengthening monotonic and fatigue specimens, the tensile flanges are sand blasted in S.A. 2.5. Figure 3.18 shows the sand blasted surface of the steel beams. All strengthened beams are sand blasted at the bottom of the tensile flange.

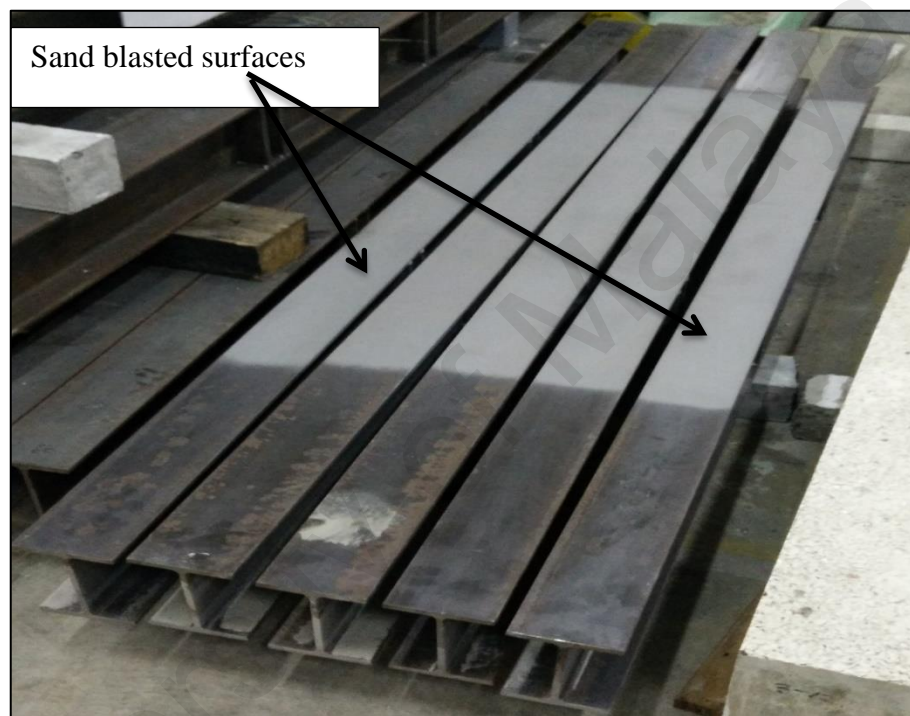


Figure 3.18: Sand blasted steel beams

The fourth step is the mixing of the adhesives. Adhesive Sikadur® -30 was chosen to make bonding between the CFRP plates and the surface of the steel beams (Bocciarelli et al., 2009; Narmashiri, Ramli Sulong, & Jumaat, 2012). Adhesive Sikadur® -30 is a 6 kg two-part epoxy resin. It includes part A, which is white in colour (resin), and part B, which is black in colour (hardener). They must be mixed in the weight ratio of 3:1 (Sikadur®-30, 2014). Sikadur®-330 adhesive is also two part, but ratio 4:1 resin and hardener. The epoxy adhesive are applied for bonding SikaWrap® fabric reinforcement. First, each set must be mixed separately. Then, the hardener set of adhesive is added to

the resin set, and they are mixed together appropriately to produce a light grey colour mixture. Before mixing and applying the adhesive on the surfaces everything must be carefully prepared. The mixture is applied on the CFRP and steel surface quickly within a few minutes. It is better to mix the adhesive in small quantities to suit the rate of work. In order to avoid wastage of the adhesive only a suitable quantity of the adhesive that can be used within the requisite time frame should be mixed at any one time.

Before application of the epoxy adhesive, the CFRP strips are carefully cleaned. They must be free from any extra material such as dust and oil. Acetone is used on the cotton to clean the CFRP strips.

The next step is the application of the adhesive on the sand blasted steel surfaces (Figure 3.19). Then, the CFRP reinforced plates were installed to the bottom tension flange of the strengthened specimens and clamped properly to make bond between the CFRP plates and surface of the steel beams. Clamping using fastening clamps prevents air holes forming between the plates and the steel surfaces. Placing of the CFRP plates and clamping of beams with adhesively bonded CFRP plates are displayed in Figure 3.20 and Figure 3.21, respectively. The average thickness of the adhesive layers was kept to 1 mm. The period of the adhesive curing lasted more than seven days.



Figure 3.19: Applying adhesive on the surface of the beam flange



Figure 3.20: Placing of the CFRP plate



Figure 3.21: Clamping the strengthened beams using fastening clamps

For the anchored specimens with CFRP fabrics, the following additional processes must be completed. Two layers of the CFRP fabrics are applied to cover the bottom flange as an anchorage. The anchored regions are covered by using Sikadur®-330 adhesive for each layer. The length of the covered region is the same as the round of bottom flange. Three layers C-shape anchor is used at the end of the CFRP plate with 175 mm width CFRP fabrics.

3.2.4 Test setup

In this section, the instrumentation to test strengthened wide-flange steel I-beams for monotonic and fatigue flexural specimens are explained in detail.

The beams had a total length of 2,300 mm. All specimens were tested using simply supported under four-point bending at a span of 2,000 mm. The test program was conducted by an Instron universal testing machine that had a loading capacity of 1000 kN. The monotonic and cyclic loadings was transferred from the actuator to the beam specimen by using a spreader beam. The distance between two point loads applied by a spreader beam was 600 mm. The spreader beam was positioned on the top of each specimen to confirm two-point loading. One hinge and one roller supports, carried the reactions, therefore, the loading state was four points incremental bending loads. A schematic four-point bending setup without and with lateral bracing are shown in Figure 3.22. Figure 3.23 shows the test setup for experimental studies.

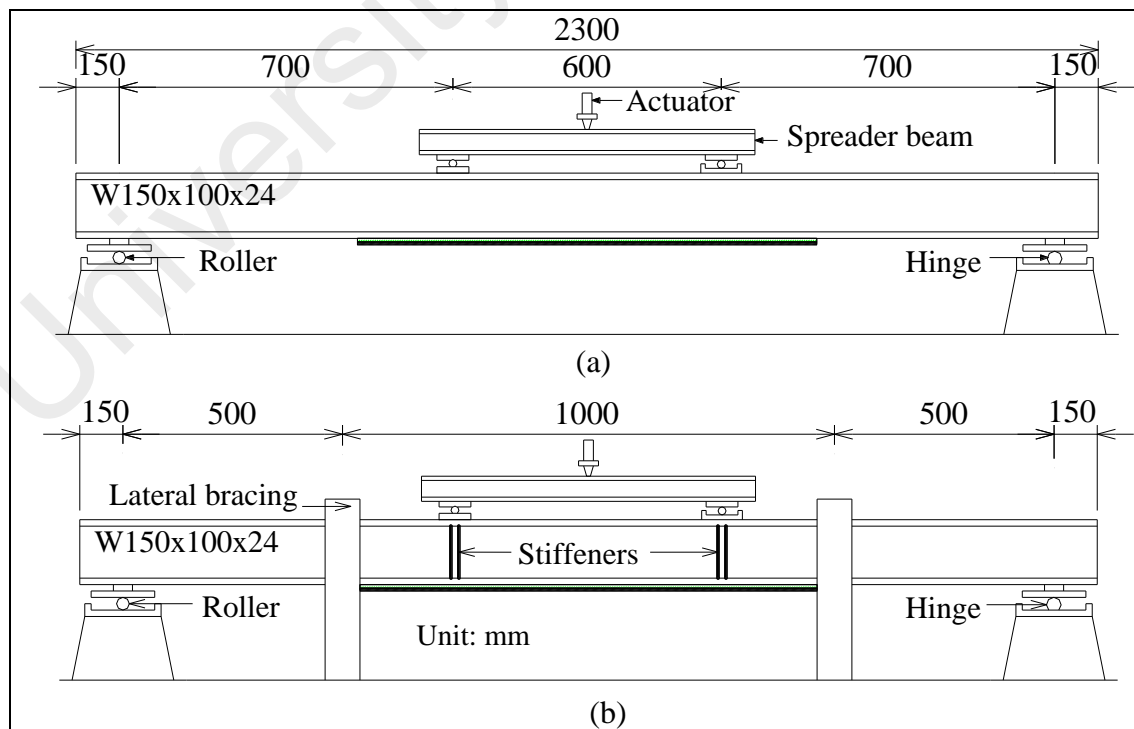


Figure 3.22: Schematic four-point bending setup (a) without and (b) with lateral bracing

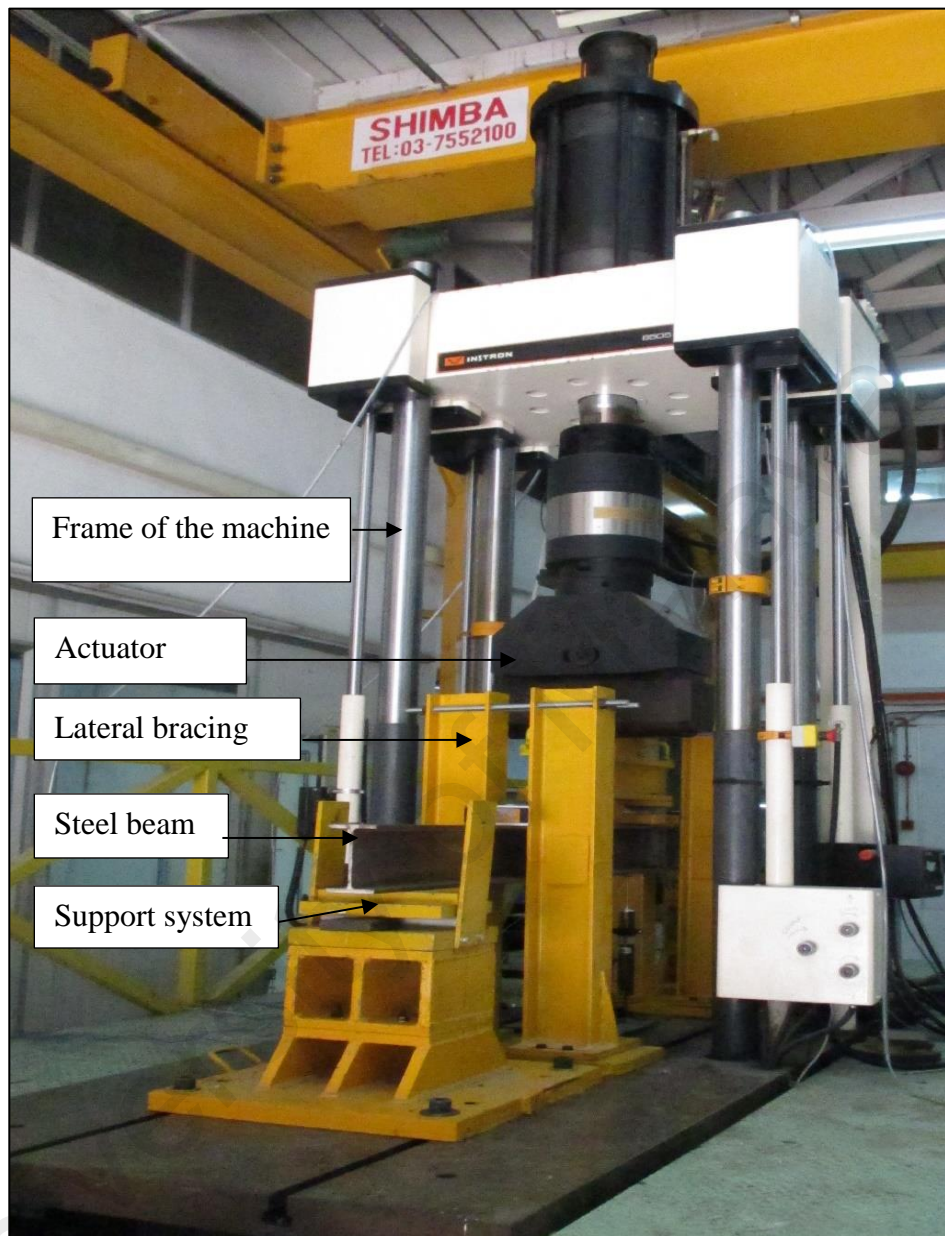


Figure 3.23: Test set-up

Unrestrained beams were loaded in stiffer planes and were allowed to undergo LTB. When a laterally unsupported beam was not adequately supported against LTB, the design bending strength was governed by buckling strength. Wide-flange Steel I-beams were found to be relatively weak in resistance to bending and torsion about the minor axis, and if not held in line by floor construction, lateral bracing could become unstable under load (Narmashiri & Jumaat, 2011). Gaylord, Gaylord, & Stallmeyer (2007)

suggested that the spacing of the lateral bracing should be $L_c = \frac{1900b_f}{\sqrt{F_y}}$ mm. Lateral bracing against lateral instability was used in specimens M2 and M5 to M17 as shown in Figure 3.22(b). Specimens M0, M1, M3 and M4 were tested without lateral bracing in this study Figure 3.22(a).

Mid-span vertical and horizontal deflections were measured by linear variable displacement transducers (LVDT). Strain readings were monitored by strain gauges attached to different locations of the mid-span, at the loading point and at the tip of the CFRP. All the LVDTs and strain gauges were connected to the data logger. After calibrating the data logger, the spreader beam was placed on the specimen. The data of the tested specimen was recorded from the data logger.

For cyclic loadings, a closed-loop system program was used to deliver a waveform sinusoidal load at a frequency of 3 Hz. The load set point, load range, frequency and number of cycles were controlled by an electronic controller (MTS® 407 Controller). The sinusoidal waveform was checked using a conventional oscilloscope. Loading was monitored using a fatigue-resistant load cell. A dynamic data logger was used to measure the data in the experimental investigation of fatigue specimens.

3.2.5 Test equipment

In this research, all tests are conducted by Instron-8805 universal testing machine for investigating monotonic and fatigue flexural behaviour on strengthened steel beams with a four-point bending and simply supported manner. Lateral support are used as a lateral bracing to prevent lateral displacement.

The longitudinal strains along the steel girder and CFRP plates were measured using 5 mm long 120Ω electrical resistance strain gauges. Five gauges were attached on the steel surface at mid-span, as demonstrated in Figure 3.24 and Figure 3.25. Several strain gauges were attached to the CFRP strips, and are spaced as shown schematically in Figure 3.24. In addition, two LVDTs were positioned at mid-span to measure the vertical deflection and horizontal displacements. The data measured by the strain gauges, LVDTs, loads and were recorded using a data logger. Whereas the dynamic data logger was used to measure the data of strain gauges, laser displacement transducer (LDT), loads and number of cycles for fatigue specimens.

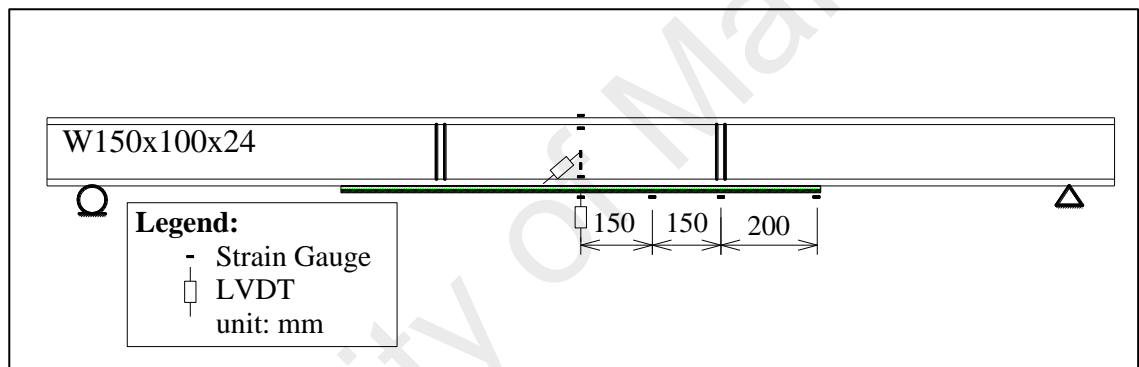


Figure 3.24: Position of the strain gauges

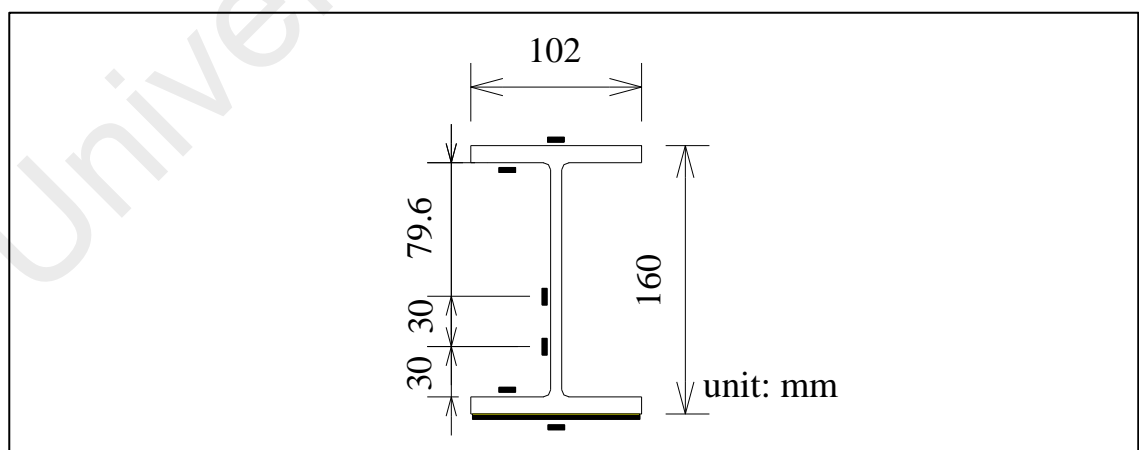


Figure 3.25: Strain gauges at mid-span

The instrumentation in this research using the Instron universal testing machine, support system, spreader beam, lateral support, LVDT, strain gauges, and data logger are explained below.

3.2.5.1 Instron-8505 universal testing machine

In the research, all specimens under monotonic and cyclic loading are performed by Instron 8505 universal testing machine with a maximum loading capacity of 1000 kN. The amount of the transferred load between the hydraulic actuator and the spreader beam are measured by using the load cell. For application of the manual load, the actuator and the speed of the loading are controlled by the computer using Instron software.

3.2.5.2 Support system

To test the monotonic and fatigue flexural strengthened steel beams, a simply supported manner with four-point bending are employed using Instron-8505 testing machine in this research. One roller and one hinge are contained in the support system. Steel plate are used in the both support between the beam and rollers to distribute the load properly and that could freely rotate during the fatigue tests.

3.2.5.3 Spreader beam

The flexural tests are based on the four-point bending. The four-point bending state means that the load is applied to the beam in two points, and two other point load are the supports. In order to apply the load of the hydraulic jack to the beam in two points, the

spreader beam is used (Figure 3.26). The spreader beam, which is used in this research, is strong enough to transfer the load without failure. It has a length of 600 mm and one hinge and one roller supports (Figure 3.27). The load of the hydraulic jack is applied at the center of the load cell, which is positioned at the middle of the spreader beam. Then, the two symmetrical point loads are applied to the main beam. As mentioned, in the two-point loading case, the loads are applied as points. In fact, the loads are not point load, but they are designated as such because they are applied on a small surface area of the structure as points. Normally, applying point load causes high stress concentrated below the loading points steel structures. In order to reduce the stress concentration below the loading points on the flanges, in the region of the point load steel stiffeners are installed.

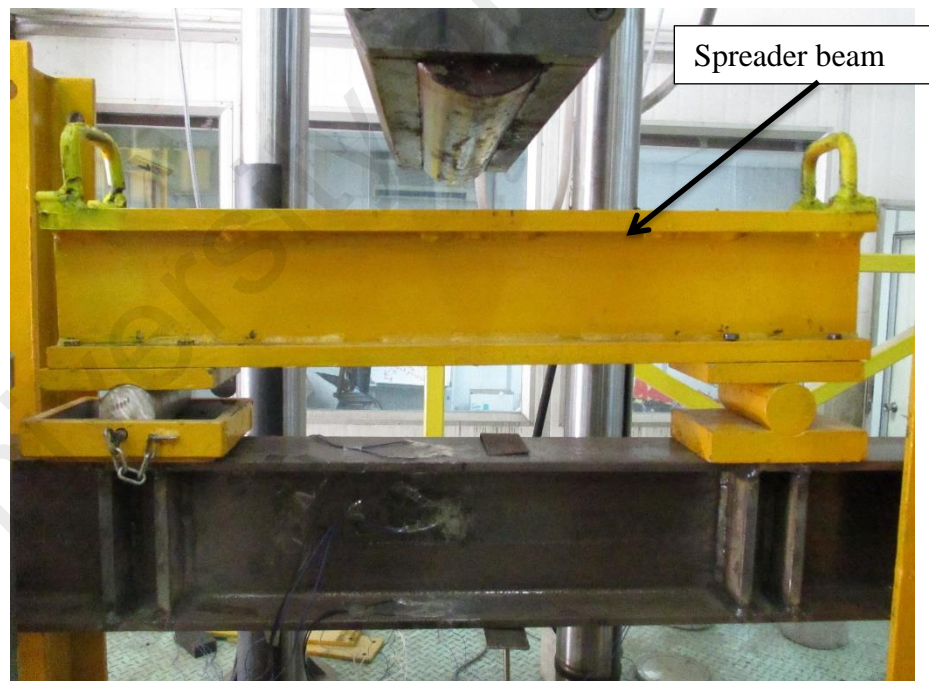


Figure 3.26: Spreader beam

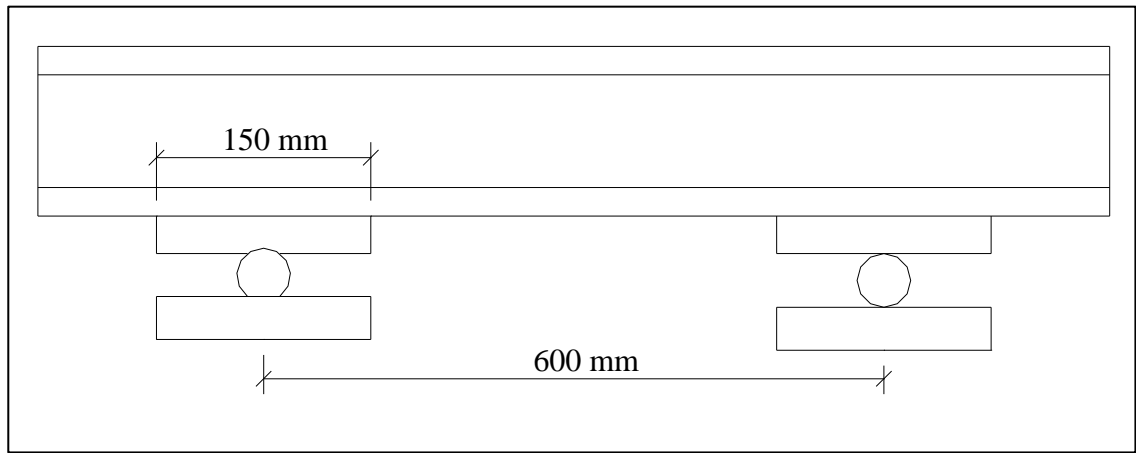


Figure 3.27: Span length of the spreader beam

3.2.5.4 Strain gauge

Normally, strain gauges are used for the actual and laboratory structures to measure the strain in different region. Generally, the direction of installation of the strain gauges depends on the kind of strain. For instance, for the measurement of normal stress in the beam, the strain gauge is installed parallel to the beam axis. Otherwise, if any possibility to occur of lateral buckling in the beam, then the strain gauge is installed in a perpendicular direction (transverse) to the beam axis.



Figure 3.28: Strain gauge

In this research, the strain gauges are installed in parallel directions to the beam axis to measure strain in the different regions. Only one strain gauge is installed in the web with transverse direction to check the transverse strain which is produced due to LTB. The strain gauges used in this research are kyowa type KFG-5-120-C1-11 with a length of 5 mm (Figure 3.28).

3.2.5.5 Linear Variable Displacement Transducers (LVDTs)

Normally, Linear Variable Deformation Transducer (LDVT) is used to measure deflection in different regions under monotonic loadings. In this research two LVDT's are used. One LVDT (200 mm) is located vertically at the mid-span to measure the vertical deflection (Figure 3.29). The other LVDT (50 mm) is located at the mid-span horizontally to measure the lateral deformation.



Figure 3.29: Linear Variable Deformation Transducer (LVDT)

3.2.5.6 Data logger

A data logger is used to record and monitor the data that is measured by the load cell, strain gauges, and LVDT's. In this research, one data loggers are used to record the amount of load via the load cell, vertical mid-span deflection via the vertical LVDT, lateral deformation at the mid-span via the horizontal LVDT, and strain gauges. A dynamic data logger was used to measure the experimental data of fatigue specimens (Figure 3.30).

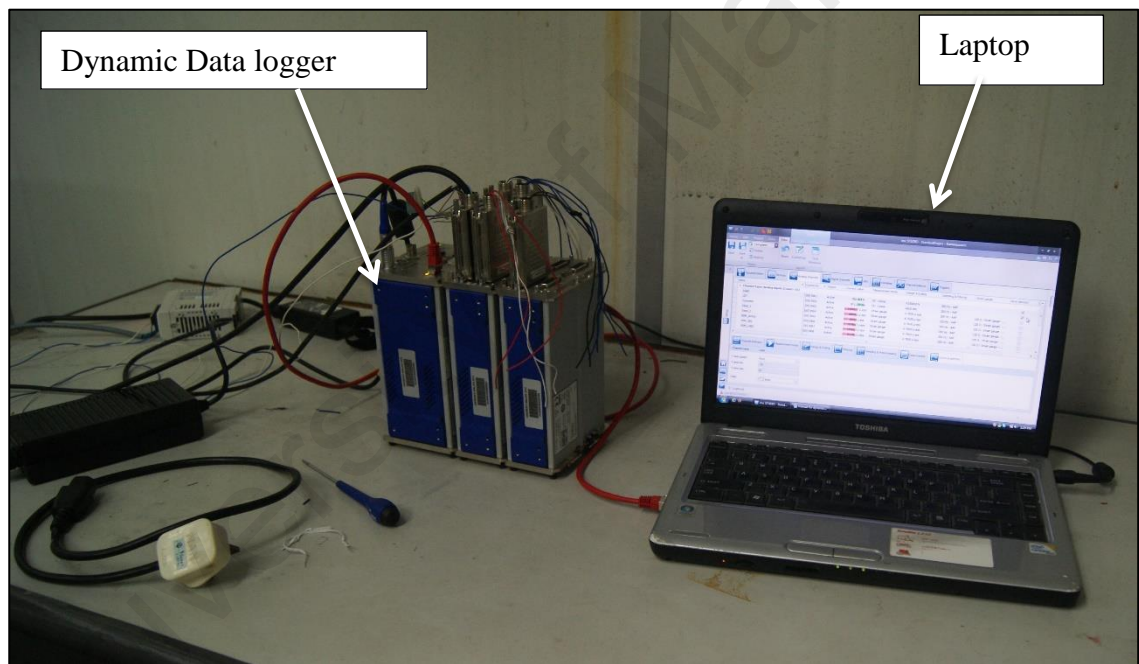


Figure 3.30: Dynamic data logger connected with laptop

3.2.6 Test procedures

In this section, the test procedures of experimental investigation for both monotonic and fatigue flexural specimens are described in detail.

3.2.6.1 Monotonic

The following test procedures were carried out for monotonic investigation.

First of all, the strain gauges were installed. According to the objectives, 9 gauges were installed on the critical region of each specimen (Figure 3.24). For each beam, two strain gauges are installed on the compressive (top) flange at the mid-span; one in the longitudinal direction in the outer side and another one in the inner side to record the axial strain. One strain gauge is installed in the web with transverse direction to measure the transverse strain which is produced due to LTB. Another one is fixed in the web with longitudinal direction. One strain gauge is installed in the inner side of the bottom flange (tensile) at the mid-span longitudinally. Another, four strain gauges are installed on the CFRP plate longitudinally to record the axial strain distribution along the CFRP plate.

To install the strain gauges, the selected surfaces were cleaned by using a grinder. Then, the surfaces were re-blasted by using rough sand-paper and then by using the smooth sandpaper. Subsequently, the surfaces were cleaned by using cotton that was submerged in acetone. Finally, the strain gauges were installed on the surfaces by using the glue.

In order to measure deflection, one LVDT was placed horizontally on the web at mid-span for measuring the lateral deformation, and one LVDT was placed vertically on the bottom flange of the beam at middle for vertical deflection.

An incremental monotonic load was employed by a hydraulic actuator through a load cell of 1000 kN capacity. The load was applied with displacement control at a constant rate of 0.75 mm per minute. The specimens were loaded until failure while the strain and deflection were recorded in the critical regions.

3.2.6.2 Fatigue

A similar procedure of monotonic specimens was followed for the preparation of the fatigue specimens.

The specimens were tested in flexure in a four-point bending configuration with a span of 2000 mm between the centerline of the supports. The distance between the two applied loads is 600 mm. The loads were applied using a steel spreader beam. The two point loads were applied over two transverse steel plates, which covered the entire width of the specimen. A schematic test setup is shown in Figure 3.22(a). One steel roller and one hinge were placed in the two side of the spreader beam. The specimen was supported on a roller support at one end and a hinged support at the other end.

The tests were conducted using a closed-loop hydraulic Instron universal testing machine. The maximum loading capacity of the machine is 1000 kN. For cyclic loadings, a closed-loop system was used to deliver a sinusoidal waveform load at a frequency of 3 Hz. The sinusoidal cyclic load are applied with a load ratio of $R = 0.1$. The maximum loads are applied 50% and 80% of the static capacity of the control specimens. The cyclic loading parameters are shown in Figure 3.31. The parameter, loads can be replaced with stress, moment, torque, strain, deflection, or stress intensity factors. The frequency of the cyclic loadings is set at 3 Hz (Ghafoori, Schumacher, & Motavalli, 2012) in the fatigue investigation for strengthened wide-flange steel I-beams. The specimens were loaded under constant amplitude control, based on the reported in (Wu et al., 2012). Figure 3.32 presents the cyclic loading patterns of all fatigue specimens for load range 10% -80%.

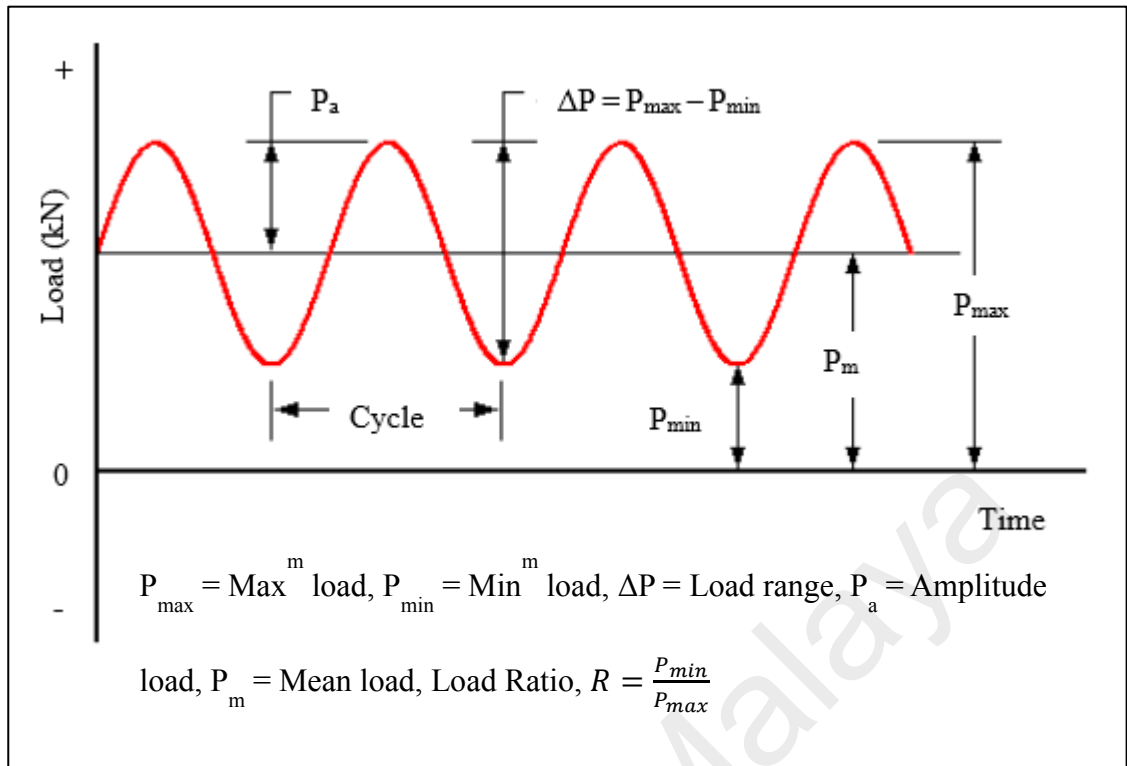


Figure 3.31: Cyclic loading parameters

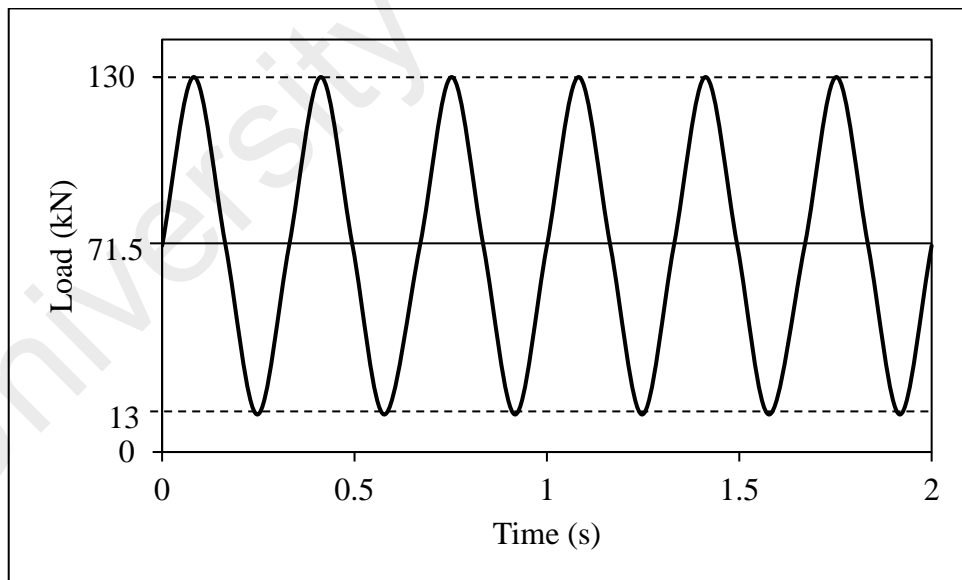


Figure 3.32: Fatigue cyclic loading

The load range, load set point, and preset number of cycles with frequency were controlled by MTS[®] 407 Controller. A conventional oscilloscope was used to check the

loading of the sinusoidal waveform. Loading was monitored using a fatigue-resistant load cell.

3.3 Numerical simulation

One of the suitable approaches to study the effects of strengthening the existing structural elements is numerical simulation using software. The finite element method (FEM) has been adopted in most of the structural analysis software.

The FEM can be applied to obtain solutions of a variety of problems in structural engineering by following a numerical procedure. In the early 1900s during the beginning of the modern finite element method's use, some researchers approximated or modelled elastic continua using discontinuous equivalent elastic bars. Courant has been credited with being the first person for developing the finite element method (Motavalli & Czaderski, 2007).

Retrofitted or strengthened steel structural elements can be simulated in either 2D or 3D (Deng, Lee, & Moy, 2004; Narmashiri & Jumaat, 2011; Seleem, Sharaky, & Sallam, 2010). Generally, 3D shell and solid elements and 2D planar shells are used to simulate the 3D and 2D models. The application of an appropriate meshing method with meshing size helps to ensure the accuracy of structural modeling. In addition, selecting a suitable boundary condition including the loading and support system can increase the consistency of simulation modelling. Normally, structures can be analyzed using linear or non-linear approaches. In this section, the approaches of numerical simulation will be introduced. Furthermore, the results of some simulated specimens in 3D are compared to the experimental test results for selection of the best modelling and analyzing approaches having the highest simulation accuracy.

3.3.1 Finite element simulation

In this research, the Abaqus finite element program ("ABAQUS/CAE. 6.12 User's manual;," 2014) was used to develop the finite element simulation of the strengthened wide-flange steel I-beams with CFRP composite plates. An extensive number of numerical models were generated to compare the results of experimental work with several structural parameters, thereby making the study more economic. Nevertheless, as some parameters (such as the magnitude of stress and strain on steel-CFRP interface) were not assessable by experimental investigation, utilization of software was required to simulate the specimen's behavior.

Abaqus is capable of simulating several structural engineering problems. This software is suitable of performing monotonic, cyclic, fluid flow, heat transfer, and electromagnetism analyses. A model can be created with standard/explicit, CFD, and electromagnetic database.

Abaqus is capable of simulating strengthened steel beams with a CFRP composite plate (Ghafoori et al., 2012). In this research, Abaqus is used to investigate monotonic and fatigue flexural parameters of strengthened wide flange steel I-beams. For this aim, the Abaqus FEA (version 6.14) software was used for the FE modelling of the beams ("ABAQUS/CAE. 6.12 User's manual;," 2014).

3.3.2 Modelling method

The simulation of the CFRP strengthened wide-flange steel I-beams can be modelled either in 2D (Colombi, 2006), which may reduce the running duration, or in 3D (Bocciarelli & Colombi, 2013; Seleem, Sharaky, & Sallam, 2010). To reduce the running

time, a quarter of the steel beam (Linghoff & Al-Emrani, 2010) or half of the beam (Haghani, Al-Emrani, & Kliger, 2009) can be simulated. Nevertheless, a full length beam can also be modelled for simulation (Bocciarelli & Colombi, 2013; Seleem, Sharaky, & Sallam, 2010).

In this study, all the beam specimens are simulated in 3D modelling using Abaqus CAE. In addition, all beams are simulated in the 3D solid modelling cases in order to select the modelling method, and the results of various structural parameters in the modelling cases are compared to the experimental test results.

3.3.2.1 3D Modelling

A 3D nonlinear FE model was developed to investigate the monotonic and fatigue flexural specimens of strengthened steel beam with CFRP strips.

All the strengthening elements with steel beams were generated as a 3D solid. All parts in the 3D solid elements had the dimensions set in all directions. For fatigue investigation in the 3D solid case, the main problems are a higher duration of running time due to assembly of several elements and the large amount of equations. In the application of the non-linear approach, the problem of the large running time is more significant. Figure 3.33 and Figure 3.34 show part of the wide-flange steel I-beam and CFRP in the 3D solid modelling case, respectively. The steel beam is assembled with stiffeners at loading points (Figure 3.33). The material property assignment of the all parts was done systematically. All created parts were assembled together using an assemble module (Figure 3.35).

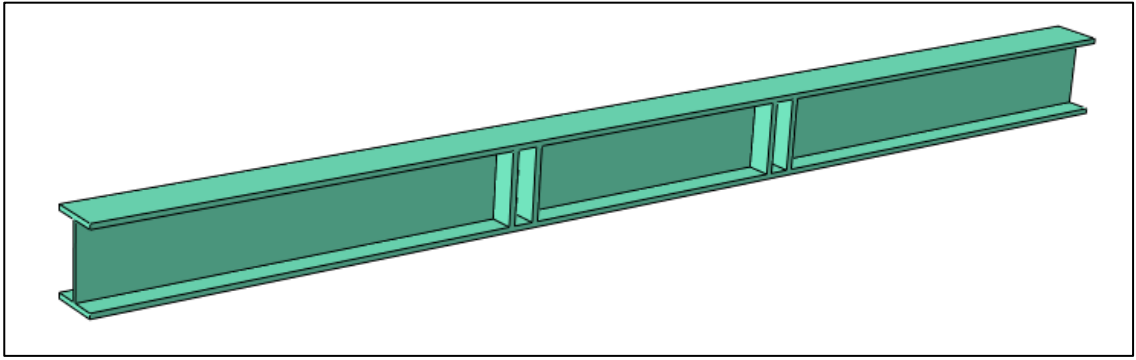


Figure 3.33: Part of the steel beam

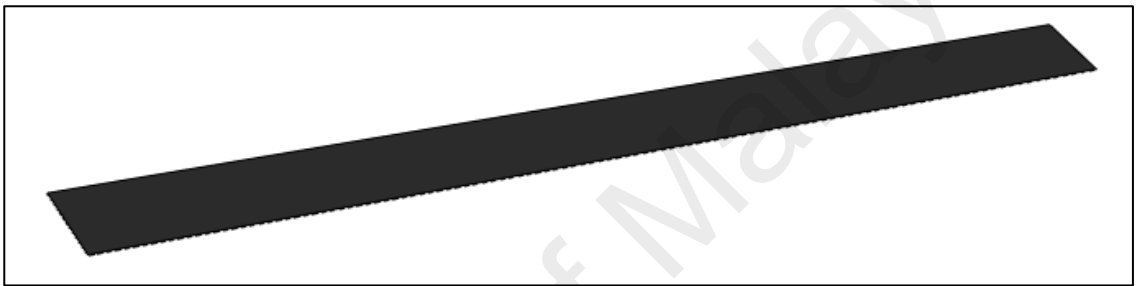


Figure 3.34: Part of the CFRP strip

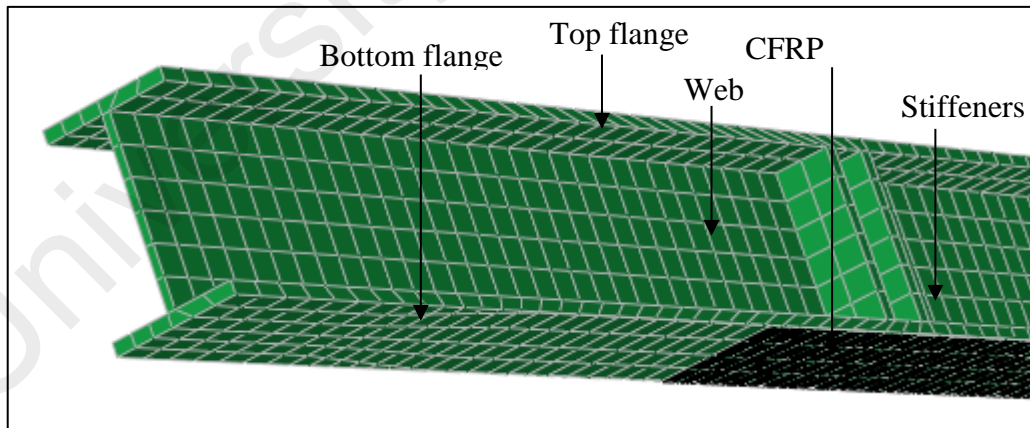


Figure 3.35: Assembly of different parts

3.3.3 Element selection

Appropriate selection of the elements is one of the most significant points in FE simulation. For the appropriate element selection in 3D modelling, material properties, structural characteristics and boundary conditions are important. Elastic, plastic, and linear or nonlinear properties must be provided in the material property module correctly. The structural characteristics such as structural element, shell, mass, axisymmetric, plane stress and strain are an important part of element selection. Static, dynamic, heat transfer, and electromagnetism loading parameters with support constraints were considered. For unconstrained steel beams, one of the most significant characteristics was lateral torsional buckling (LTB). The plane-stress or plane-strain element were not chosen in the unconstrained beams to achieve out-plane deformations appropriately.

In FE modelling of the wide flange I-beam sections, steel stiffeners and CFRP strips, an 8-node linear brick, reduced integration, and hourglass control (C3D8R) were used with exclusive hexahedral elements. For modelling of the adhesive to achieve the cohesive behaviour and the surface-based cohesive behaviour, the cohesive surface technique was conducted. This is an easy and simplified way to model a cohesive connection by means of the traction-separation interface behaviour. Two surfaces are created using a partition at the top surface of the top flange to apply the load and at the soffit of the bottom flange for boundary conditions of the steel beams. For steel, the linear-isotropic and nonlinear-elastic material property was defined.

3.3.4 Materials property

The property of materials must be clearly defined to make the software able to calculate initial forces and displacements. All materials' properties defined in the software were

given by the manufacturer and were similar to the experimental materials' data (as given in Section 3.2).

Steel and CFRP material properties are defined in the software. An elastic and plastic material property with stress–strain relationship was used to model the steel. Also, for steel, the elastic-isotropic and plastic-isotropic material property were defined.

Tensile coupon tests were performed to define the mechanical properties of the wide-flange steel I-beams. The mechanical steel properties beams were obtained in accordance with ASTM A370. Figure 3.36 shows the stress-strain graph for the steel beams used in this research. The fiber composites have linear properties and they are unidirectional materials. The epoxy adhesive was defined as a cohesive material.

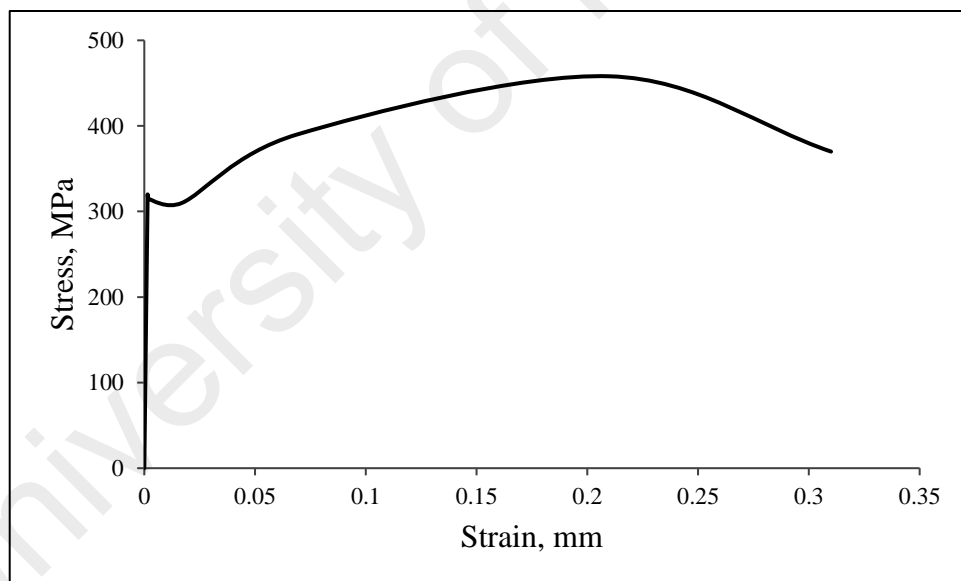


Figure 3.36: Stress-strain diagram

The CFRP composites were modelled as linear elastic orthotropic materials. Engineering properties were defined to model the unidirectional CFRP composite material. For unidirectional material model, the elastic modulus (E_3) was set to 165 GPa based on a nominal thickness of 1.4 mm, $\vartheta_{13} = \vartheta_{23} = 0.0058$. The elastic modulus in the other two

directions (i.e. $E_1 = E_2$), the Poisson's ratio and the shear moduli were assumed the following values respectively based on the values reported in (Piggott, 2002): $E_1 = E_2 = 9.65$ GPa and $G_{13} = G_{23} = 5.2$ GPa. ν_{12} and G_{12} were set to 0.3 and 3.7 GPa, respectively.

The geometric non-linearity was defined to include the non-linear effects of large structural deformations and displacements in the numerical simulation.

3.3.5 Boundary conditions with lateral bracing against buckling instability

The beams were modelled in a four-point bending scheme, where all beams were simply supported with hinged support on one side and roller support on the other. The load was applied as the pressure over a certain area corresponding to the load application region in the experimental lab tests. Figure 3.37 shows a render model as a wireframe of the supporting and loading position for simulation of strengthened steel beams under monotonic loading and fatigue. Lateral bracing was used in specimens M2 and M5 to M17 as a lateral constraint against lateral instability in this study. The load was applied as incremental static load following an automatic load control scheme. The modified standard/static general method was adopted.

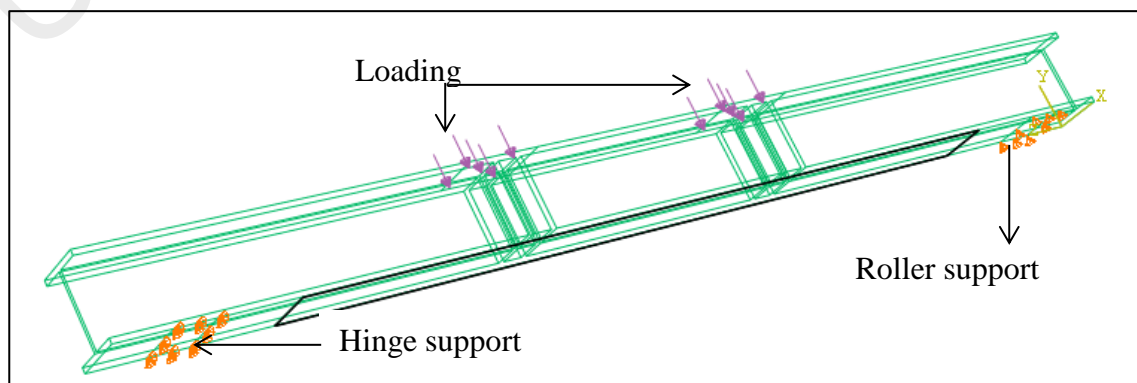


Figure 3.37: support and loading condition position of strengthened steel beams

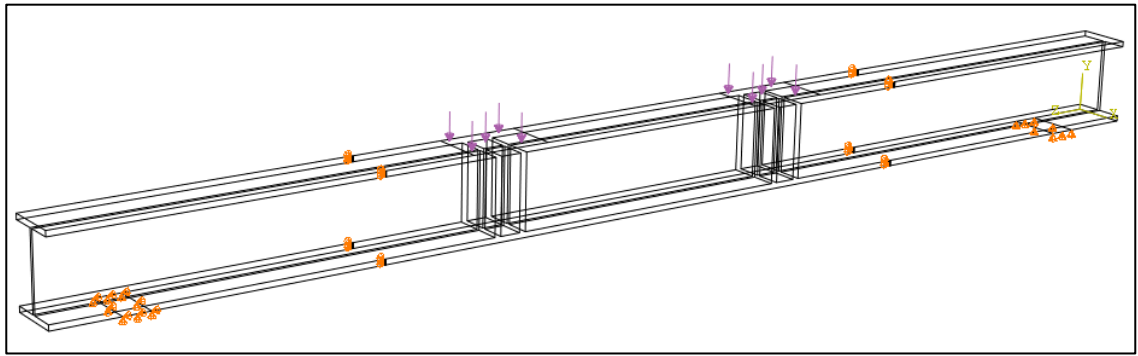


Figure 3.38: Boundary condition with lateral constraint

3.3.6 Meshing method

The selection of the appropriate meshing technique and mesh size enhances the accuracy of the numerical simulations. Figure 3.39 shows the mesh of the strengthened steel beams. Meshing of the strengthened specimen using CFRP fabrics' anchorage is exhibited in Figure 3.40. Based on a mesh convergence study, 4 mm x 4 mm square elements were selected for the steel beam and the CFRP plate in the steel-plate bonded area using bottom-up meshing. A partition was generated in the bonded area of the steel beam. In FE modelling of the wide flange I-beam sections, steel stiffeners and CFRP strips, an 8-node linear brick, reduced integration, and hourglass control (C3D8R) were used with exclusive hexahedral elements. The meshing method with a hexahedral shape also reported in (Teng, Fernando, & Yu, 2015).

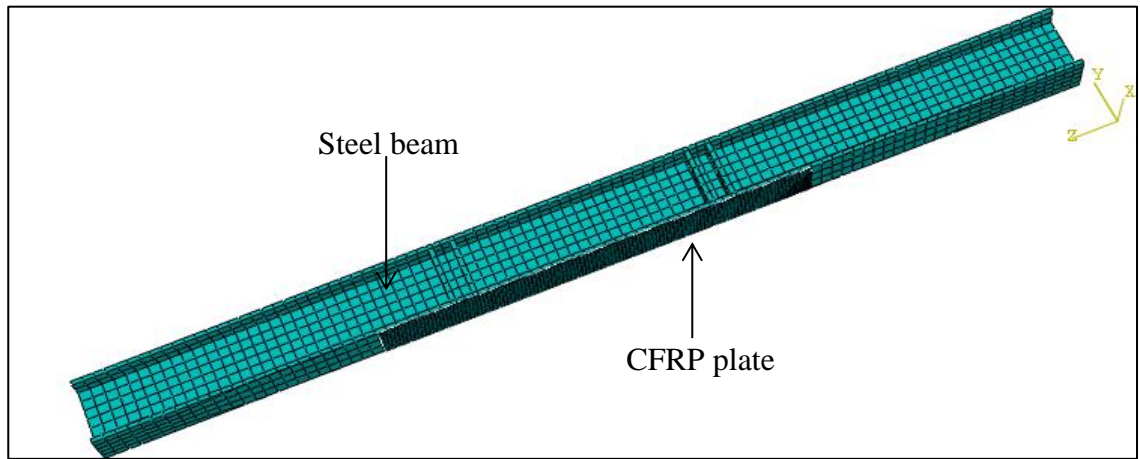


Figure 3.39: Meshing of the strengthened beams

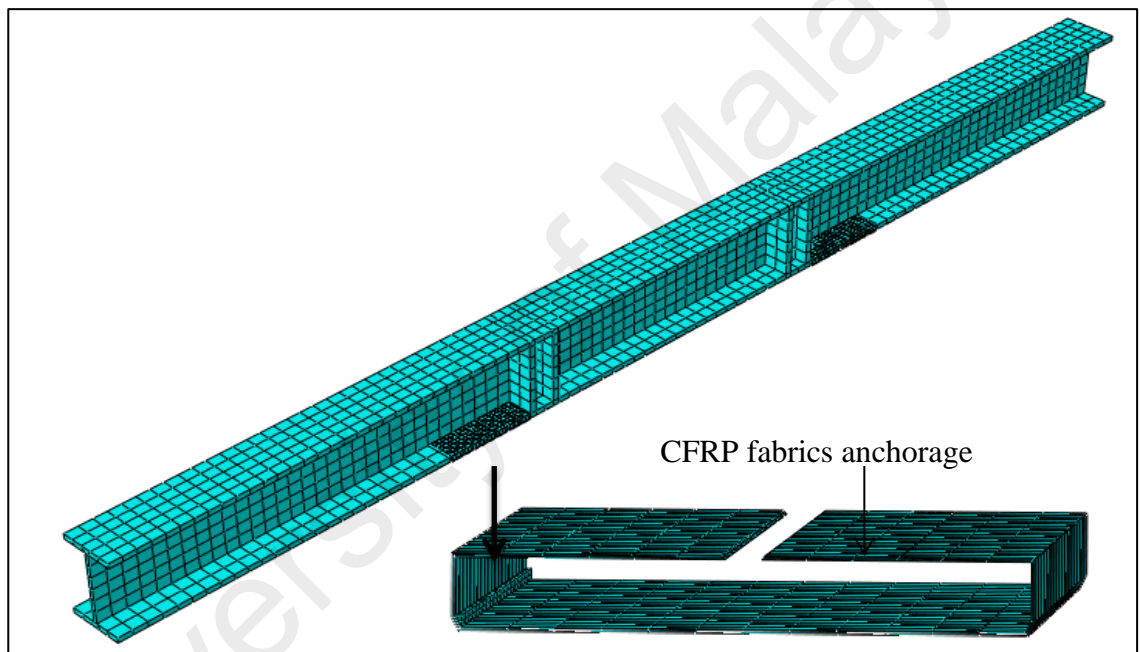


Figure 3.40: Meshing of anchored specimen with CFRP fabrics

3.3.7 CFRP–steel interface and debonding modelling

To create an interface between steel beams and CFRP, surface-based cohesive behaviour using traction-separation law was adopted. Figure 3.41 presents a graphic interpretation of a simple bilinear traction–separation law in terms of effective traction stress (T) and effective opening displacement (δ). Traction–separation laws were represented by linear

relationships at each loading step (Yang & Thouless, 2001), while one or more steps were defined in different ways for a more accurate representation of material behaviour.

The cohesive was described by the shape of a triangle. G_c , T_{ult} and δ_f were the critical release energy, effective ultimate nominal stress and failure separation, respectively.

Debonding occurred when $\delta > \delta_0$.

The initial stiffness per unit area of the material (load per unit displacement per unit area) was $K_{eff} = \frac{T_{ult}}{\delta_f}$, and critical release energy, $G_c = \frac{T_{ult}\delta_f}{2}$ where, effective elastic modulus of the cohesive materials was $E_{eff} = K_{eff}h_{eff}$, and h_{eff} was the initial effective constitutive thickness of the cohesive section.

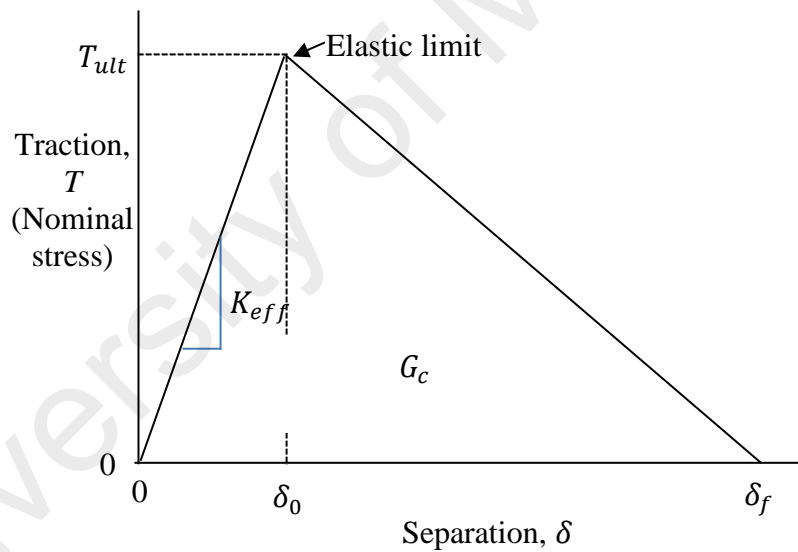


Figure 3.41: ABAQUS traction-separation cohesive material law

Cohesive behaviour adopted a linear elastic traction-separation law prior to debonding. Failure of the cohesive bond was considered by the progressive degradation of the stiffness of the bond, for which it was essential to define a debonding propagation. Nominal traction stress (T) contained one normal traction (T_n) and two shear tractions

(T_s and T_t). δ_n , δ_s and δ_t represented the corresponding separations. The tractions in all three directions are expressed by:

$$T_n = K_{nn}\delta_n \quad (3.1)$$

$$T_s = K_{ss}\delta_s \quad (3.2)$$

$$T_t = K_{tt}\delta_t \quad (3.3)$$

Where, K_{nn} , K_{ss} , K_{tt} are the stiffness values of the normal and the two shear directions respectively.

3.3.8 Proposed anchorage design

To develop a design process that can be used to achieve the same results obtained in the experimental investigation, a shear friction mechanism has been considered to develop a simplified model. This model calculates the maximum possible tensile force in the middle of the CFRP plate corresponding to the typical failure mode of FRP rupture (Rasheed et al., 2015). This force needs to be developed along the plate shear span by providing distributed CFRP fabric anchors across the debonding plane. Accordingly, the transverse CFRP area required along the shear span is that which produces enough tension to control the shear friction. The summary of the proposed design procedures are as follows:

maximum CFRP tensile force at the level of failure is shown in Equation (3.4).

$$\text{CFRP rupture, } T_{f(\text{CFRP plate})} = E_f A_f \varepsilon_f \quad (3.4)$$

Horizontal shear force per unit length of shear span is shown in Equation (3.5).

$$V_{sf} = \frac{T_{f(\text{CFRP plate})}}{L_{af}} \quad (3.5)$$

where V_{sf} is the factored shear force per unit shear span of the plate, L_{af} is the length of the shear span of the plate, and ε_f is the effective FRP transverse strain.

Anchoring tension force per unit length in the direction of transverse CFRP using the shear friction expression is shown in Equation (3.6).

$$T_{sf(anchor)} = \frac{V_{sf}}{\mu} \quad (3.6)$$

Anchoring tension force per unit length in the direction of transverse CFRP,

$$T_{sf(anchor)} = \phi A_{vf} E_f \varepsilon_f \quad (3.7)$$

$$A_{vf} = \frac{T_{sf(anchor)}}{\phi E_f \varepsilon_f} = \frac{V_{sf}}{\phi(\mu) E_f \varepsilon_f} \quad (3.8)$$

Capacity reduction factor, $\phi = 0.85$

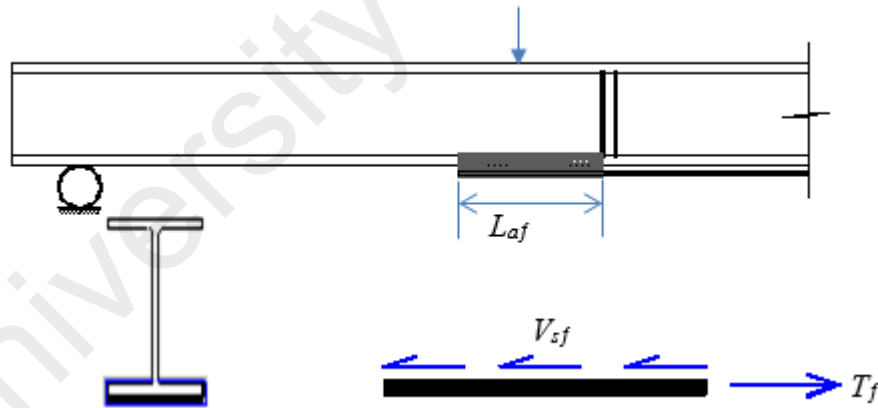


Figure 3.42: Shear friction mechanism in the transverse CFRP

Width (w_f), thickness (t_f) and the number of layers (n) for the transverse CFRP,

$$A_{vf} = 2t_f w_f = \frac{V_{sf}}{0.85 E_f \varepsilon_f(\mu)} \quad (3.9)$$

$$w_f = 0.59 \frac{V_{sf}}{E_f t_f \varepsilon_f(\mu)} \quad (3.10)$$

$$w_{f(total)} = w_f * L_{af} \quad (3.11)$$

$$n = w_{f(total)} / w_{(used)} \quad (3.12)$$

3.3.9 Monotonic loading model

A monotonic incremental load was modeled for the simulation of the beams until failure occurred. The failure mode of the beams was modelled to the point at which the steel element showed significant plasticity or when debonding of the CFRP composite was predicted for the strengthened steel beams. The load was simulated in the first step as uniform pressure applied at the top of the beam. However, failure of the unidirectional CFRP plate was expressed by the maximum stress failure criterion. Kim & Harries (2011) provided details of the model for the monotonic load.

3.3.10 Fatigue loading model

The model for fatigue investigation of the test specimens was more complicated than the monotonic due to the necessary change of the constituent properties for increased number of fatigue cycles. A sinusoidal cyclic load was applied with a load ratio of $R = 0.1$. The maximum loads applied were 50% and 80% of the yield load of the static unstrengthened specimens. Loads could be replaced with stress, moment, torque, strain, deflection, or stress intensity factors. In order to incorporate ramp and cyclic loadings in the finite element (FE) model, two steps were defined in the FE simulation. The ramp was simulated in the first step as uniform pressure using static and general procedures. The cyclic loading was modelled using dynamic and implicit procedures with amplitude control applied at the top of the beam. The frequency of the cyclic loadings was set at 3

Hz in the fatigue investigation for unstrengthened and strengthened wide-flange steel I-beams.

3.3.11 Specification of the simulated models

Numerical models for specimens under monotonic loading and fatigue flexural studies were generated. A total of thirty-four specimens were simulated and investigated: twenty-four flexural monotonic and ten fatigue models.

For the flexural monotonic investigations, twenty-four beam models were developed. In order to examine the effects of stiffeners and lateral bracing, in-plane CFRP end cutting shapes, combined in-plane and taper CFRP end shapes, and spew fillets of adhesive on the structural behavior including the failure mode of the CFRP composite plate of wide-flange steel I-beams, the same specimens as the experimental studies were simulated. To optimize the end anchorage using CFRP fabrics, seven specimens were modelled with different layers, lengths and widths of the CFRP fabrics in Abaqus. The specifications of the monotonic specimens are illustrated in Table 3.7 and Table 3.8.

For the fatigue flexural study, to investigate the effect of in-plane CFRP end cutting shapes on the fatigue behavior of strengthened specimens, the same end shapes (rectangular, semi-ellipse, semicircular, and trapezoidal) were chosen in the experimental and numerical investigation. To investigate the effects of end anchorage using CFRP fabrics, four specimens were modelled with different layers of the fabrics. A detailed specification of the specimens for fatigue investigation are given in Table 3.9.

CHAPTER 4: RESULTS AND DISCUSSIONS

4.1 Introduction

The flexural behavior of wide-flange steel I-beams strengthened with CFRP strips, including the monotonic and fatigue responses are addressed in this research. The mitigation of the debonding problem of strengthened beams is the main purpose of this research. In this chapter, the achievements of the experimental and numerical studies are investigated and described. For flexural strengthening, the effects of applying different in-plane CFRP end cutting shapes, combinations of CFRP in-plane and tapering end shapes with triangular fillets, and CFRP fabrics anchoring at tip of the CFRP plate to retard the CFRP end debonding on strengthened beams related to load bearing capacity, failure mode, fatigue life, strain and deformation were discussed and detailed accordingly. A finite element (FE) modeling approach to predict the monotonic and fatigue behavior of CFRP-steel strengthened beams was also discussed.

4.2 Monotonic flexural strengthening

The CFRP strips were installed on the bottom flange of steel beam to improve the flexural behaviour. Since CFRP materials do not have sufficient compressive strength, thus their usage in the compressive (top) flange is not useful.

However, flexurally strengthened steel beams experience problems such as CFRP plate ED and EDL (Deng & Lee, 2007b; Narmashiri, Ramli Sulong, & Jumaat, 2012). The CFRP ED and EDL cause premature failure, which is an essential issue that needs to be resolved. This research highlights various approaches to reduce these end problems of strengthened wide-flange steel I-beams. Also, the effects of these approaches on the

whole I-beam's structural behavior are studied. In the monotonic specimens, the objectives include:

1. Study of the effect of stiffeners and lateral bracing.
2. Investigation of the effects of different in-plane CFRP end cutting shapes.
3. Examination of the effects of the combination of CFRP in-plane and tapering end shapes with triangular spew fillets of adhesive at the tips of the plate.
4. Investigation of the effects of using CFRP fabrics for anchoring externally bonded CFRP plates.

The extensive results obtained from the experimental investigation under monotonic loading are presented in this section. See Appendix B for more results of the monotonic investigation.

4.2.1 Effect of lateral bracing and stiffeners

4.2.1.1 Load-deflection relationship and failure mode

Figure 4.1 shows the load-deflection relationships of un-strengthened specimens M0, M1 and M2. The figure shows that specimen M0 had the lowest load carrying capacity, when compared with M1 and M2. The difference in load carrying capacity among the specimens was mainly related to the type of failure mode. Specimen M0 failed as a result of stress concentration and the compression flange buckling below the loading plate, which in turn to LTB. The load carrying capacity of specimen M0 was mainly controlled by stress concentration and local buckling failure at below the loading plate (Figure 4.2). The presence of the stiffeners in specimen M1 prevented stress concentration failure and hence increased the load carrying capacity up to 13.8% over specimen M0. LTB contributed to premature failure in specimens M0 and M1, which was due to the absence

of lateral support for the effective length of the beam. In addition, the use of stiffeners and lateral bracing in specimen M2 results in an increase of load carrying capacity up to 15.8% over specimen M0. Table 4.1 presents a summary of test results.

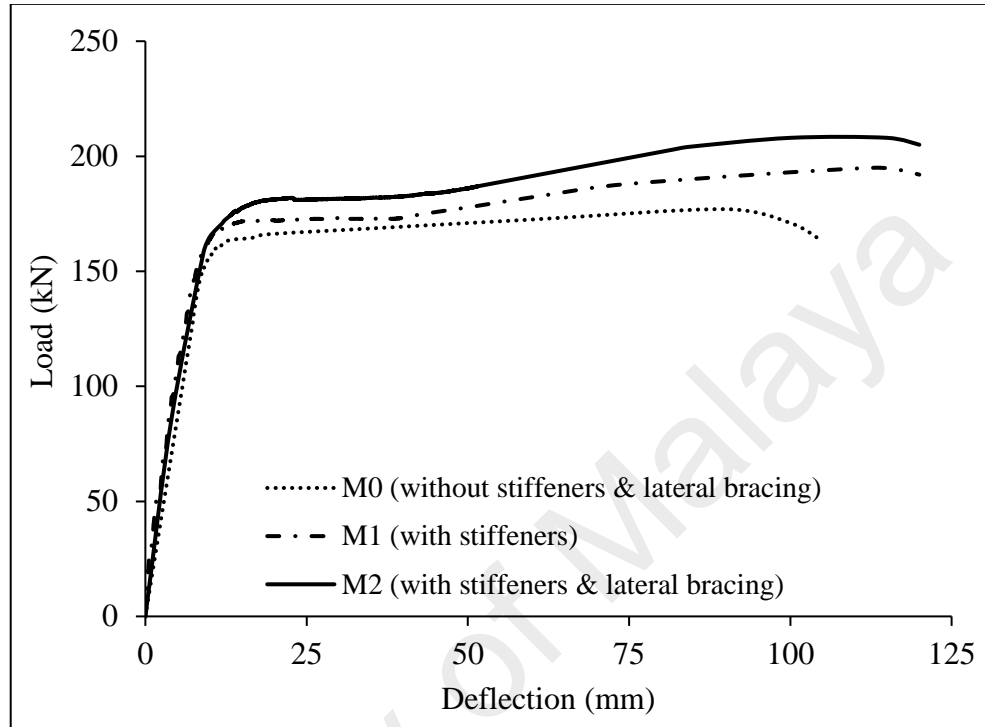


Figure 4.1: Load-deflection diagram of un-strengthened specimens

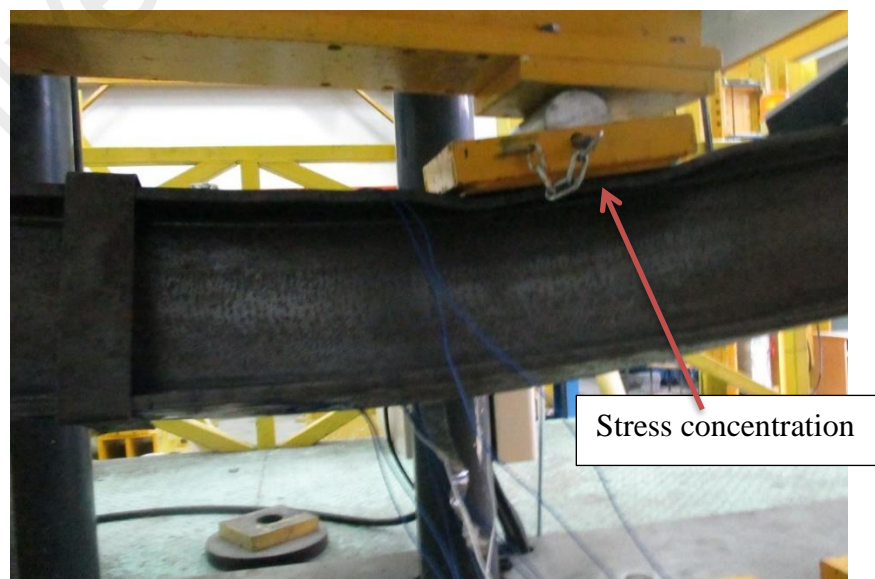


Figure 4.2: Stress concentration and local buckling failure below the loading plate

Table 4.1: Monotonic strength with ductility and failure modes (effect of stiffeners and lateral bracing related specimens)

Test unit	Stiffeners below point loads	Lateral bracing	Strengthening CFRP plates	Ductility index								Load carrying capacity		CFRP Failure mode
				Peak				Failure				Load	Increment	
				μ_{dp}	Ratio to UB	μ_{Ep}	Ratio to UB	μ_{df}	Ratio to UB	μ_{Ef}	Ratio to UB	kN	%	
M0	N/A	N/A	N/A	10.30	1	22.20	1	11.4	1	24.7	1	174	-	
M3	N/A	N/A	√	3.45	0.34	6.90	0.31	10.6	0.93	22.4	0.91	198	13.80%	S-ED
M1	√	N/A	N/A	12.20	1	26.60	1	13.6	1	26.6	1	193.50	11.20%	
M4	√	N/A	√	4.40	0.37	8.65	0.33	12.8	0.94	26.5	0.99	206	18.30%	S-ED
M2	√	√	N/A	12.60	1	27.93	1	13.5	1	30.1	1	201.50	15.8%	
M5	√	√	√	5.40	0.43	11.0	0.40	13.0	0.97	30.5	1.02	215.29	23.70%	ED

S: Splitting, ED: End debonding, UB: Un-strengthened beam (M0, M1, M2); μ_{dp} : Displacement ductility index at peak load; μ_{df} : Displacement ductility index at failure load; μ_{Ep} : Energy ductility index at peak load; μ_{Ef} : Energy ductility index at failure load.

The sequence of CFRP failure modes was generally dominated by LTB and stress concentration below loading points. Figure 4.3 shows a comparison of load-deflection diagrams of strengthened specimens M3, M4 and M5. The strength of specimen M5 was about 9% and 7% larger than strengthened specimens M3 and M4 respectively, which showed that bracing could increase the strength but only slightly in this case due to debonding problems.

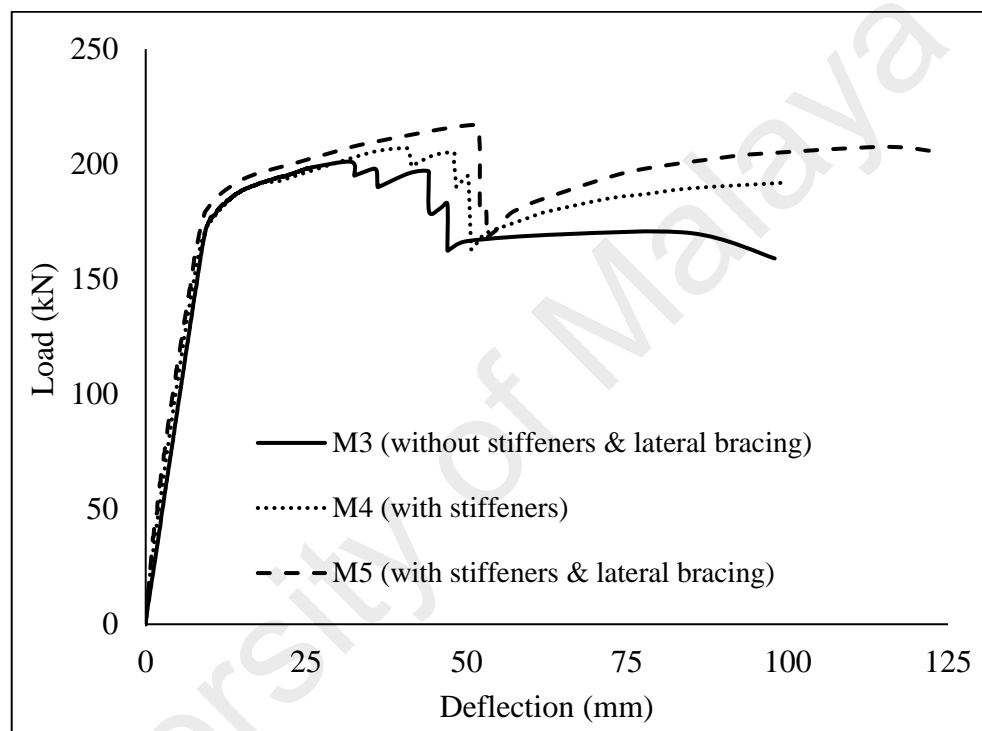


Figure 4.3: Load-deflection diagram of strengthened beams

The load-deflection diagram also indicated that the load dropped when the CFRP strips split and debonded from the steel beams. Specimens M3, M4 and M5 showed that the strengthened CFRP plates failed at deflection 34%, 37% and 43% compared to their corresponding un-strengthened beams. Figure 4.4 shows the deflection at peak load in the strengthened beams before the failure of CFRP by debonding. The failure of strengthened specimens M3 and M4 was initiated by CFRP splitting. The splitting of the CFRP plate as a result of LTB; this was in line with findings by Narmashiri, Ramli Sulong, & Jumaat (2012). Figure 4.5 shows the splitting of the CFRP plate. Specimen

M3 was also affected by stress concentration below the point load that caused premature failure through the earlier splitting of the CFRP plate. The lateral bracing in specimen M5 almost prevented the splitting below point load of the plate and initiated debonding at 48.9 mm vertical deflection. It also increased the load bearing capacity to 16.42% more than M2, at the same level of deflection.

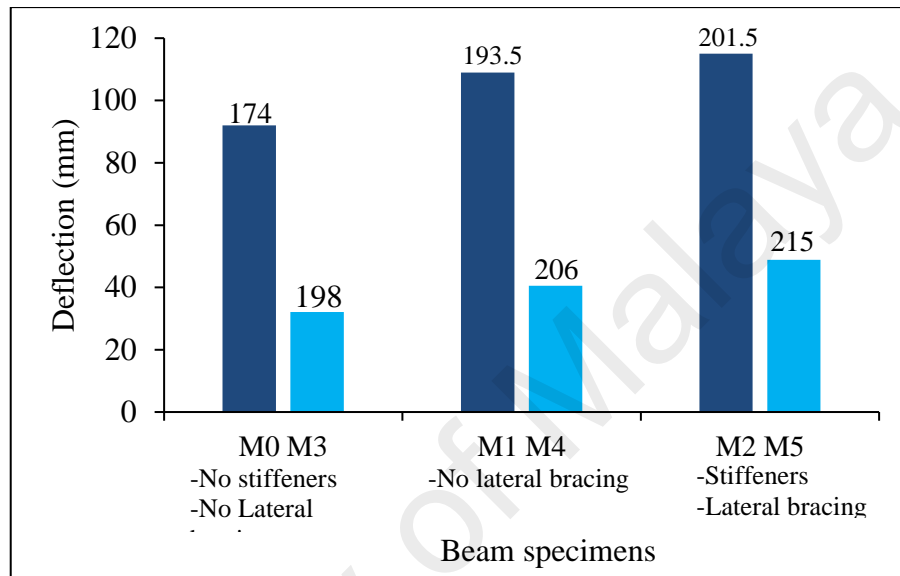


Figure 4.4: Variation of deflection values of un-strengthened (M0, M1 and M2) and strengthened beams (M2, M3, M4) at peak load (kN)



Figure 4.5: Splitting failure mode of CFRP plate (specimen M3)

The majority of the cross-section stiffness came from the stiffener preventing stress concentration and local buckling below the point load. Lateral bracing also significantly increased stiffness by preventing the buckling. Therefore, the use of a proper system of stiffeners and lateral bracing could lead to remarkable enhancement in bending stiffness and load bearing capacity.

4.2.1.2 Lateral displacement

Figure 4.6 shows load-lateral displacement relationships at the mid-span of strengthened beams. It illustrates that after initiation of splitting of the CFRP strip on specimen M3, the movement changed to the opposite direction. The splitting of the whole CFRP strip was followed by the lateral movement returning to the original direction until debonded. The horizontal movement of the specimen changed due to stress concentration below the point load and LTB. The horizontal deflection of the specimen M4 was in one direction and was followed by the occurrence of LTB. Lateral bracing increases buckling strength by restraining the lateral displacement of the beam.

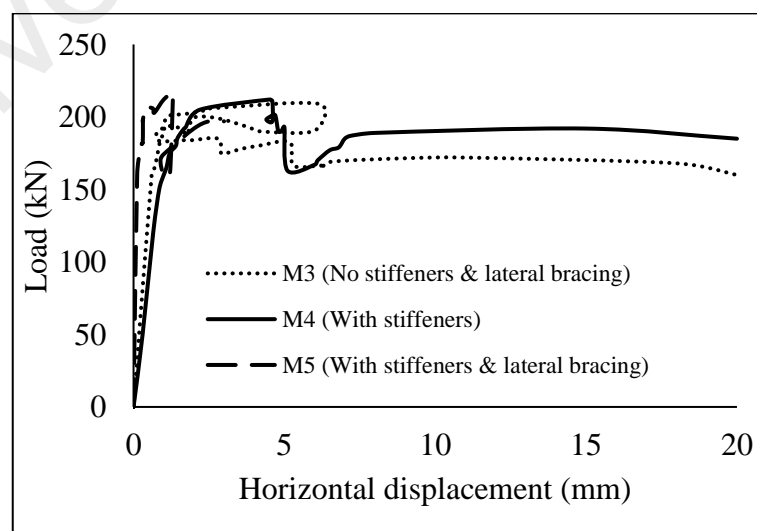


Figure 4.6: Load-lateral displacement relationships of strengthened beams

Therefore, it can be concluded that applying lateral bracing to strengthened steel I-beams can prevent the instability of the beams as a result of LTB failure. In addition, the use of steel plate stiffeners can be effective in preventing stress concentration below the point load. Lateral bracing increases buckling strength by significantly reducing the influence of LTB.

4.2.1.3 Ductility

The ductility of a strengthened steel beam ensures the capability of a structure to endure considerable plastic deformation without substantial loss of strength. In this research, the ductility indices of strengthened beams were obtained based on displacement (μ_d) and energy (μ_E) ratios (Hawileh et al., 2014). The displacement ductility index at peak load (μ_{dp}) and at failure load (μ_{df}) are expressed as follows:

$$\mu_{dp} = \frac{\Delta_p}{\Delta_y}, \text{ and } \mu_{df} = \frac{\Delta_f}{\Delta_y} \quad (4.1)$$

Where Δ_y , Δ_p and Δ_f are displacements at yield, peak and failure loads, respectively.

The energy ductility index (μ_E) at peak load (μ_{Ep}) and at failure load (μ_{Ef}) are expressed as follows:

$$\mu_{Ep} = \frac{E_p}{E_y}, \text{ and } \mu_{Ef} = \frac{E_f}{E_y} \quad (4.2)$$

Where E_y , E_p and E_f are energy at yield, peak and failure loads, respectively.

The calculated ductility indices of all beams in related to the effect of lateral bracing and stiffeners objectives are presented in Table 4.1. The ratio of the ductility indices for displacement of specimens M3, M4 and M5 were 0.34, 0.37 and 0.43; while that for

energy were 0.30, 0.33 and 0.40, respectively, which corresponded to control specimens at peak loads. This indicated that strengthened beams with the CFRP plate suffered from the loss in ductility.

Several researchers have reported that the ductility of strengthened beams could be reduced as a result of reinforcements by externally bonded FRP plates (Morsy et al., 2014; Rasheed et al., 2010), which could be attributed to the brittle behaviour of the CFRP plate. FRP materials also have a linear stress–strain relationship up to the point of failure. It was observed that the ductility ratio for strengthened specimens M3, M4 and M5 at failure load increased for the displacement ductility by 0.93, 0.94 and 0.97; while that for energy ductility increased by 0.91, 0.99 and 1.02, mainly as a result of the ductile properties of steel beams. The ductility of specimen M3 was less than specimens M4 and M5 due to stress concentration and LTB failure. The effect of stiffeners and lateral bracing on beam behaviour indicated an increase in ductility, caused by a delay in the debonding of the reinforcing plate from the surface of steel beams. Therefore, stiffeners prevented stress concentration below the loading points. Lateral bracing retarded the CFRP splitting failure by preventing LTB, consequently increasing displacement and energy ductility of the strengthened beams.

4.2.2 Different in-plane end cutting shapes

Figure 3.8 exhibits the dimensions of the selected end cutting shapes. In order to investigate the effects of different in-plane CFRP end cutting shapes, rectangular (M5), semi-ellipse (M6), semi-circular or rounded (M7) and trapezoidal (M8) shapes were chosen. The effects of applying different end cutting shapes on the whole structural characteristics i.e. failure mode, load bearing capacity, strain on adhesive, and

deformations were studied. In addition, the effect of spew fillets of adhesive at the tips of the CFRP in-plane end cutting shapes were also investigated.

4.2.2.1 Failure mode

The sequences of CFRP failure modes are indicated in Table 4.2. It shows that debonding of the CFRP plates was observed as the primary failure mode followed by ED. All specimens were simply supported and failed by debonding. The initiation of ED failure of all strengthened specimens with in-plane end cutting shapes start in the hinge side of the simply supported beams and result in debonding of the whole plates. Figure 4.7 shows a steel beam surface where the CFRP plate failed by ED. A CFRP plate with ED is illustrated in Figure 4.8. The debonding occurred between the epoxy adhesive and steel surface.



Figure 4.7: CFRP end debonded steel surface



Figure 4.8: CFRP plate with ED

The presence of high interfacial stress near the tips of the FRP plate, which normally initiates failure in the bonding system, is considered one of the main problems in strengthened steel beams (Haghani, Al-Emrani, & Kliger, 2009). Figure 4.9 shows debonding of the CFRP plate in externally bonded strengthening specimens. Failure here was due to loss of the bond between the adhesive and CFRP, which resulted in the separation of the CFRP plate from the bottom flange. Previous studies have explained that failure of this type occurred as a result of stress from peeling and interfacial shear at the FRP tips in concrete and steel structures that have been strengthened using CFRP plates (Deng & Lee, 2007a; Haghani, Al-Emrani, & Kliger, 2009; Narmashiri & Jumaat, 2011). Application of the trapezoidal in-plane CFRP end cutting shape is strongly recommended because the debonding failure mode was found to be delayed compared to other end cutting shapes including rectangular, semi-ellipse and semi-circular under monotonic loads.

Table 4.2: Specifications, load carrying capacity and failure modes of strengthened specimens with different CFRP in-plane end shapes

No.	Specimens	Specification of CFRP plates			Triangular fillet adhesive at ends	Load carrying capacity		Deflections at peak load mm	Failure modes (Sequential)
		L_{CFRP} (mm)	Plate area (mm ²)	CFRP end shapes In-plane		Load	Increment		
						(kN)	(%)		
1	M2 (Control)	N/A	N/A	N/A	N/A	201.50	-	115	
2	M5	1000.00	100000	Rectangular	N/A	215.29	6.85%	48.9	ED-D
3	M6	1010.75	100000	Semi-ellipse	N/A	218.15	8.3%	53	ED-D
4	M7	1021.50	100000	Semi-circular	N/A	228.22	13.26%	57	ED-D
5	M8	1025.00	100000	Trapezoidal	N/A	231.97	15.12%	62	ED-D
6	M9	1000.00	100000	Rectangular	√	224.50	11.42%	52.5	ED-D
7	M10	1025.00	100000	Trapezoidal	√	239.85	19.05%	66	ED-D

ED: End debonding; D: Debonding; L_{CFRP} : CFRP plate length



Figure 4.9: CFRP debonding failure mode of a strengthened specimen

The trapezoidal shape with a spew fillet of adhesive at the plate tips also exhibited ED CFRP failure mode. The effect of spew fillet on beam behaviour was an increase in ductility, caused by a delay in the debonding of the reinforcing plate from the surface of the steel beams.

4.2.2.2 Load-deflection relationship

Figure 4.10 shows the load-deflection behaviour of the strengthened beams using different CFRP in-plane end cutting shapes compared to the unstrengthened control beam

(M2). Overall, the trapezoidal shape (M8) showed in the highest increment on the load bearing capacity at 15.12% and initiated debonding at 59.8 mm vertical deflection. The rectangular end shape did not increase the load bearing capacity as much as the semi-ellipse and semi-circular end cutting shapes. The use of spew fillets of adhesive at the tips of the CFRP in-plane rectangular (M9) and trapezoidal (M10) end cutting shapes in strengthening steel specimens are effective. Figure 4.10 also illustrates that the use triangular spew fillet of adhesive increases 19.05% the load carrying capacity of specimen M10 before debonding of the CFRP plate, as compared to the un-strengthened beam (M2).

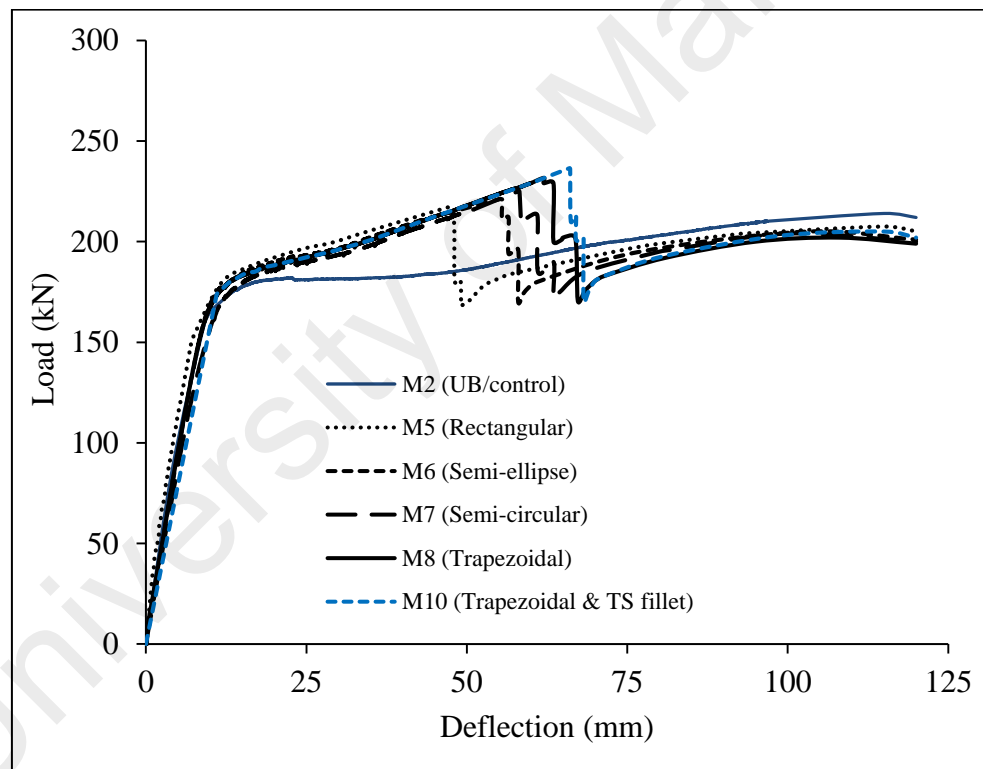


Figure 4.10: Load deflection diagrams of strengthened beams using different CFRP end shapes

Figure 4.11 shows the deflection at peak load in the strengthened beams before the failure of CFRP by debonding. The strengthened specimens using rectangular, semi-ellipse, semi-circular and trapezoidal in-plane end cutting shapes showed that the CFRP plates

failed compared to their corresponding unstrengthened beams at deflections of 43%, 45%, 50% and 52%, respectively.

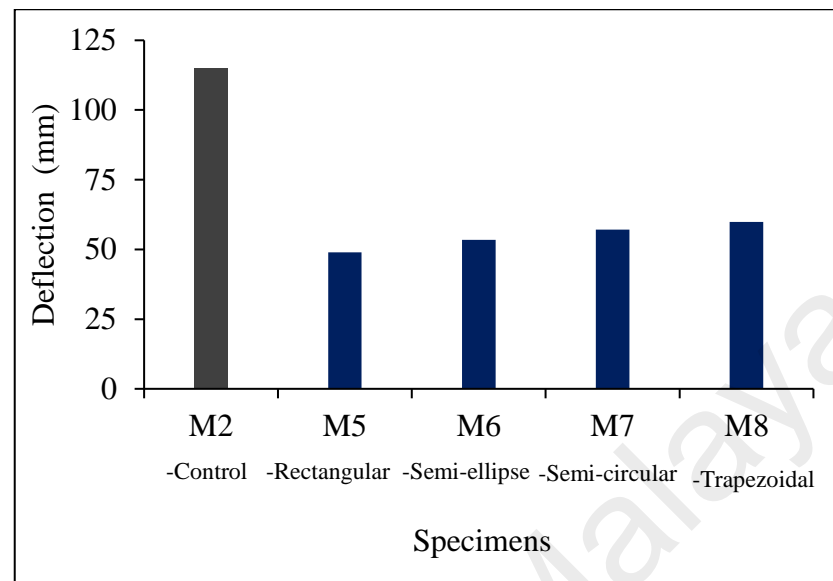


Figure 4.11: Variation of deflection values of the control beam and strengthened beams using different CFRP in-plane end cutting shapes at peak load

It can be concluded that the best increment in load bearing capacity was obtained by the application of the trapezoidal shape followed by the rectangular, semi-ellipse and semi-circular.

4.2.2.3 Ductility

The displacement and energy ductility indices of strengthened beams with different CFRP in-plane end shapes are presented in Table 4.3. The ratio of the ductility indices for displacement of specimens with rectangular (M5), semi-ellipse (M6), semi-circular (M7) and trapezoidal (M8) CFRP in-plane end cutting shapes were 0.44, 0.48, 0.49 and 0.56, respectively; while that for energy were 0.41, 0.46, 0.47 and 0.57, respectively, which corresponded to control specimens at peak or debonding loads. The trapezoidal CFRP in-plane end shows better ductile behavior than other end cutting shapes. The result indicated that the ductility of strengthened beams is reduced due to debonding of

externally bonded FRP plates. The ductility of the flexural specimens decreased with increased numbers of externally bonded strengthening plates due to the non-ductile behaviour of CFRP plates (Rasheed et al., 2010). It was observed that the ductility ratio at failure load for specimens with different in-plane end shapes was not increased, and remained close to 1.0 due to immediately dropping the load after debonding of strengthening plates.

At peak load or debonding load, the ratio of the displacement and energy ductility index for the strengthened specimen M10, with a trapezoidal end cutting shape using a spew fillet of adhesive, was 0.60 and 0.62, respectively, compared to the unstrengthened specimens.

Table 4.3: Ductility indices of specimens with in-plane CFRP end cutting shapes

Test unit	Displacement ductility index				Energy ductility index			
	μ_{dp}	Ratio to CB	μ_{df}	Ratio to CB	μ_{Ep}	Ratio to CB	μ_{Ef}	Ratio to CB
M2 (CB)	11.79	1.00	12.31	1.00	26.09	1.00	27.23	1.00
M5	5.20	0.44	13.05	1.06	10.68	0.41	27.56	1.01
M6	5.71	0.48	13.04	1.06	12.05	0.46	28.15	1.03
M7	5.79	0.49	12.63	1.03	12.44	0.47	27.60	1.01
M8	6.60	0.56	12.56	1.02	14.54	0.56	27.68	1.02
M9	5.80	0.49	13.04	1.06	14.04	0.54	29.80	1.10
M10	7.12	0.60	12.90	1.05	16.08	0.62	28.75	1.06

μ_{dp} : displacement ductility index at peak load; μ_{df} : displacement ductility index at failure load; μ_{Ep} : energy ductility index at peak load; μ_{Ef} : energy ductility index at failure load

The variation of the displacement and energy ductility indices of the strengthened beams with different CFRP in-plane end cutting shapes are shown in Figure 4.12. The figure shows that strengthened specimens using different in-plane end shapes increase the ductility indices for displacement by 10% to 27% and energy from 13% to 36%,

compared to using the common rectangular end cutting shape. The specimen with the trapezoidal end shape had the highest ductility. The difference in ductility indices among the specimens was mostly related to the debonding load.

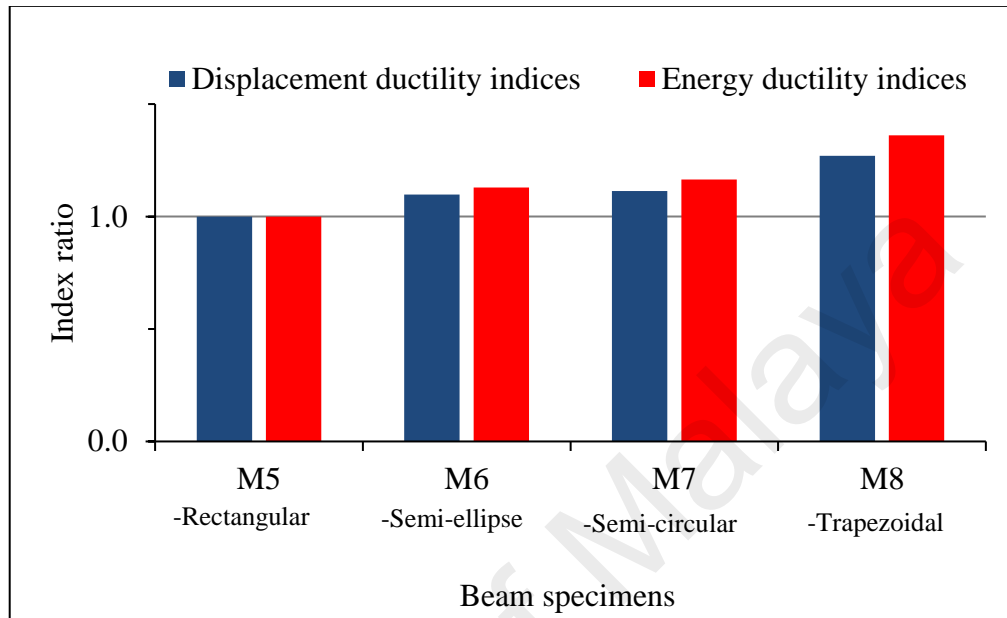


Figure 4.12: Variation of ductility indices of strengthened specimens with different CFRP in-plane end shapes at debonding load

The trapezoidal end cutting shape and the spew fillet delayed the failure of the CFRP plate by increasing the debonding load, and consequently increasing displacement and energy ductility of the strengthened specimens.

4.2.2.4 Measured strains

Investigation of the effects of different in-plane CFRP end cutting shapes on strains along the plates were measured with strain gauges placed at the mid span, below the point load, between the mid span and point load, and end of the plate under monotonic loading. Figure 4.13 shows the distribution of strain along the CFRP plate at a load level of 175 kN and 215 kN for specimens with rectangular (M5), semi-ellipse (M6), semi-circular (M7) and trapezoidal (M8) in-plane CFRP end shapes. All end-cutting shapes exhibit

almost similar strain between the mid span and below the point load. Beyond the point load, strain decreased gradually towards the CFRP end. Also, strain intensity was observed at the CFRP tip. The different strain values observed among the specimens related to various in-plane CFRP end shapes. At the load level of 175kN, the strain for specimen M5 was high, and showed a higher rate of increase of strain with increasing load as compared to other in-plane end cutting shapes. Figure 4.13 also shows the specimens with trapezoidal and semi-circular in-plane shapes (M7 and M8) had lower strain at the tips of the CFRP plates.

Therefore, it can be concluded that by applying trapezoidal and semi-circular in-plane CFRP end cutting shapes, the end debonding problems are delayed due to decreasing strain at the end of the plate.

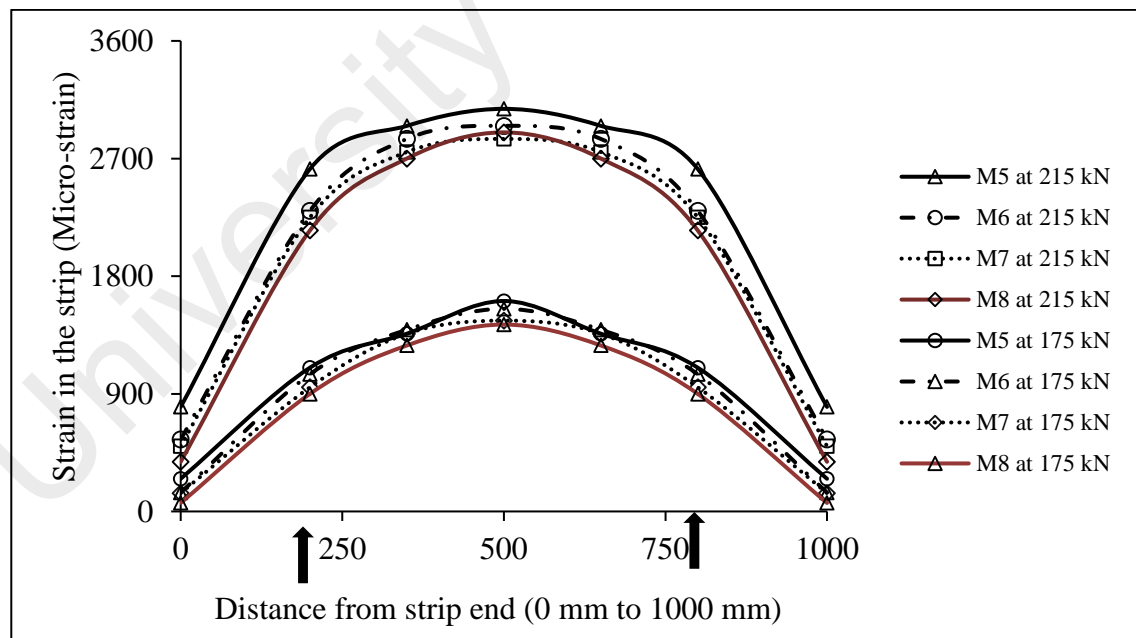


Figure 4.13: Strain distribution along the CFRP plate for specimens with different in-plane end shapes

4.2.3 Tapering end shape with spew fillet of adhesive

One of the objectives of this thesis is to investigate the effects of applying the combination of in-plane and tapering end shape with spew fillets of adhesive at the tips of the CFRP plates on the structural behaviour of strengthened wide-flange steel I-beams. For this purpose, rectangular (M11, M13 and M15) and trapezoidal (M12, M14 and M16) end cutting shapes combined with tapering and reverse tapering CFRP were used. A triangular spew fillet of adhesive was also applied to strengthen specimens M13, M14, M15 and M16 to investigate the effectiveness on monotonic structural performance.

The following characteristics are considered to investigate the effects of tapering CFRP end cutting shapes and triangular spew fillets of adhesive: (1) CFRP failure modes, (2) load-deflection behaviour, (3) ductility indices, and (4) strain on CFRP. Specifications, load bearing capacities, and failure modes of the specimens with taper end cutting shapes and spew fillets of adhesive are shown in Table 4.4.

4.2.3.1 Failure mode

With regards to failure modes, the following failure modes were observed for specimens M11 to M16, strengthened with taper CFRP plates and spew fillets of adhesive: (1) EDL, (2) ED and (3) debonding whole plate.

EDL is another premature CFRP failure mode observed in this research. Delamination failure means the separation of CFRP plate into individual layers in the longitudinal direction. Figure 4.14 shows the failure mode which was initiated by EDL. Delamination or interlaminar CFRP failure occurs due to high normal (peeling) stress concentration at the CFRP tips (Deng, Lee, & Moy, 2004). This type of failure occurs

for both steel and concrete structures. FRP plate configuration with tapering that uses spew fillets of adhesive shows improvement in the bond properties of the adhesively bonded joints (Deng & Lee, 2007b; Schnerch et al., 2007).

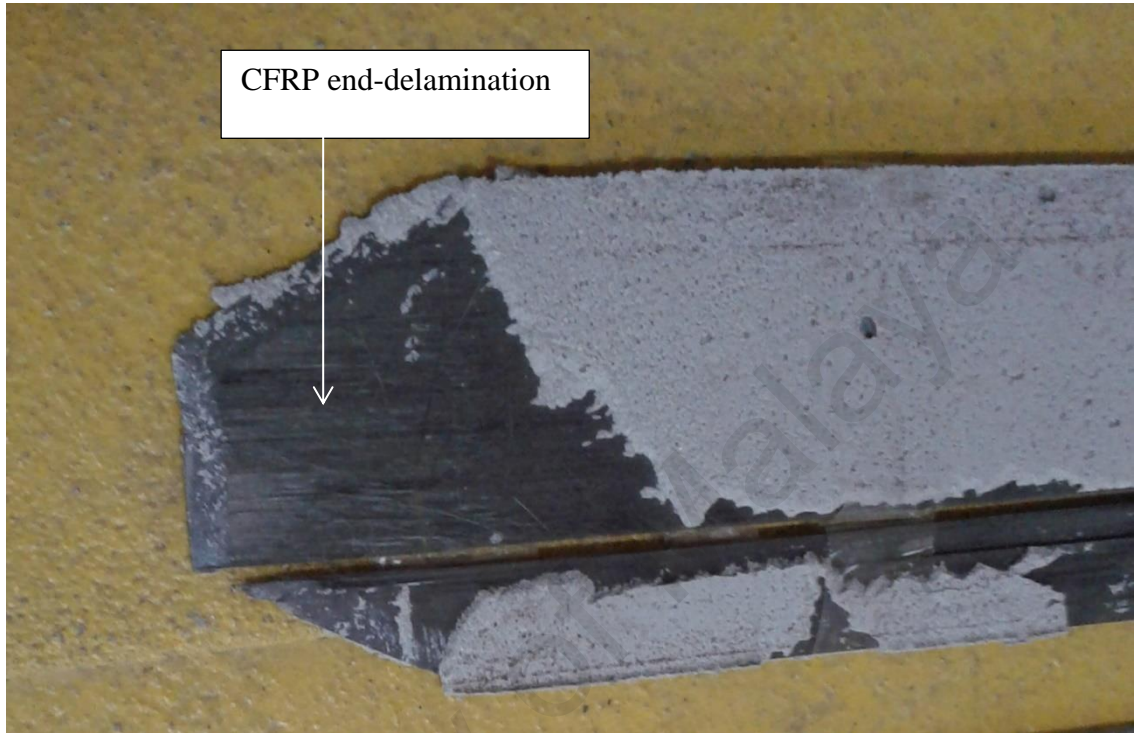


Figure 4.14: End delamination failure mode of a reverse taper CFRP plate

Table 4.4: Specifications, load carrying capacity and failure modes of strengthened specimens with tapered CFRP end shapes and spew fillets.

No.	Specimens	Specification of CFRP plates				Triangular fillet adhesive at ends	Load bearing capacity		Failure modes (Sequential)
		L_{CFRP} (mm)	Plate area (mm ²)	CFRP end shapes			Experimental		
				In-plane	Tapering		Load (kN)	Increment (%)	
1	M2 (Control)	N/A	N/A	N/A	N/A	N/A	201.50	-	
2	M5	1000.00	100000	Rectangular	N/A	N/A	215.29	6.85%	ED-D
3	M11	1000.00	100000	Rectangular	Tapering	N/A	216.23	7.31%	EDL-ED-D
4	M13	1000.00	100000	Rectangular	Tapering	√	227.50	12.9%	EDL-ED-D
5	M15	1000.00	100000	Rectangular	Reverse tapering	√	225.95	12.2%	EDL-ED-D
6	M8	1025.00	100000	Trapezoidal	N/A	N/A	231.97	15.12%	ED-D
7	M10	1025.00	100000	Trapezoidal	N/A	√	239.85	19.05%	ED-D
8	M12	1025.00	100000	Trapezoidal	Tapering	N/A	225.40	11.86%	EDL-ED-D
9	M14	1025.00	100000	Trapezoidal	Tapering	√	241.95	20.07%	EDL-ED-D
10	M16	1025.00	100000	Trapezoidal	Reverse tapering	√	241.30	19.75%	EDL-ED-D

ED: End debonding; EDL: End delamination; D: Debonding; L_{CFRP} : CFRP plate length

4.2.3.2 Load deflection relationship

The load bearing capacities of the specimens in relation to the tapered CFRP plate ends and spew fillet objectives are presented in Table 4.4.

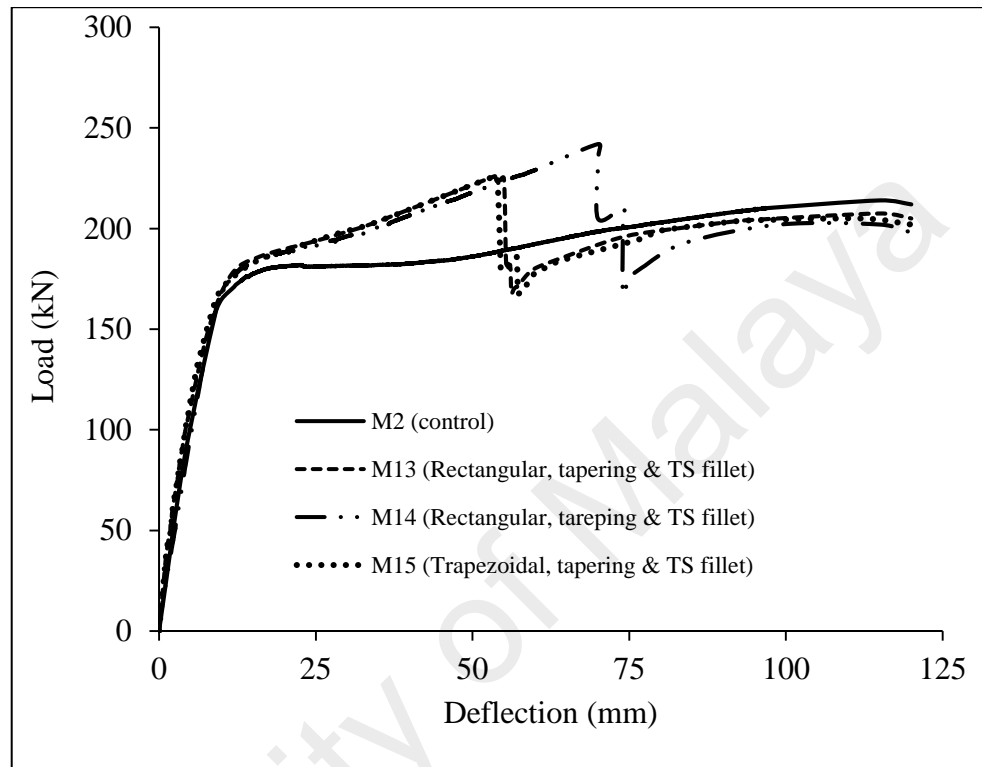


Figure 4.15: Load-deflection plots of specimens M13, M14 and M15 are compared with control beam

The load versus displacement plots of specimen M13, strengthened with a tapered-rectangular CFRP plate, and M14; strengthened with tapered-trapezoidal CFRP plate, and M15, strengthened with reverse tapered-rectangular are compared with the control beam (M2) in Figure 4.15. In addition, the spew fillets of adhesive at the end of all four strengthened specimens (M13 to M16) were applied. Two aspects are noted from Figure 4.15. Firstly, the strengthened beams showed about 13% to 20% strength enhancement over the plain control beam, and the strength enhancement increased by the trapezoidal end cutting shape with triangular fillet of adhesive. Secondly, EDL

was observed as the primary failure mode followed by ED of all the strengthened beams and after attaining a peak, the load dropped suddenly and the load-deflection curve then followed the response of the control unstrengthened beam closely.

Figure 4.16 shows the load-deflection curves of strengthened beams (M8, M10, M12, M14 and M16) using trapezoidal CFRP in-plane end cutting shape with and without tapered plates or spew fillets of adhesive compared to the unstrengthened control beam (M2). The strength of specimen M12, which was only strengthened with a tapered CFRP plate, is about 7 kN less than that of M8, which was only strengthened with an in-plane end cutting shape. In addition, the strength of M12 was 14 kN lower than that of M10, which was strengthened with spew fillets of adhesive. Tapered and reverse tapered plates with spew fillets show significant increments of loads as compared to plates that are only tapered. The use of spew fillet with a tapered (M14) and reverse tapered (M16) plate increased the load carrying capacity to about 20.07% and 19.75%, respectively, compared to the control beam (M2). It is clearly seen that the strength of specimens using spew fillets (M10, M14 and M16) is significantly higher than that of the specimen which was only strengthened with tapering (M12). In other words, spew fillets at plate ends delay the debonding, because it leads to reduced stress concentrations at the plate end.

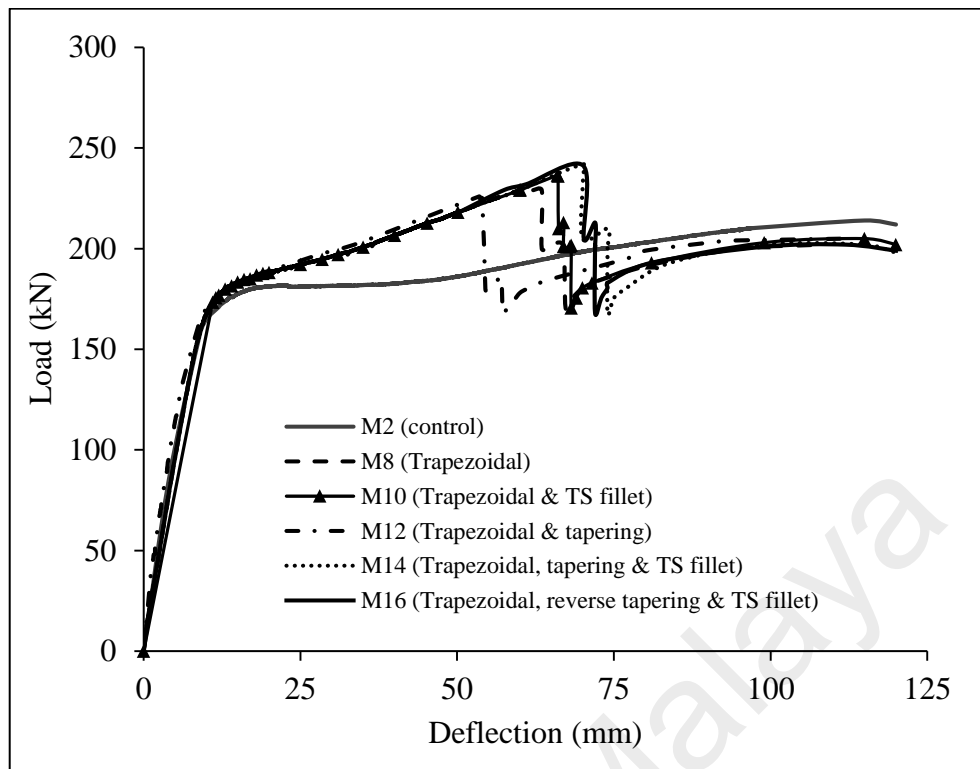


Figure 4.16: Load- deflection curve for specimens with and without of taper CFRP plates or spew fillet of adhesive

Figure 4.17 shows the variation of deflection values at peak loads of the control beam and strengthened specimens with and without tapered CFRP composite plates or spew fillets of adhesive before the failure of CFRP by debonding. In addition, a trapezoidal in-plane end cutting shape was used in all strengthened specimens (M10, M12, M14 and M16). The strengthened specimen M10, using only spew fillets at plate ends, M12, with only tapered CFRP plate, M14, with tapered plate and spew fillet, and M16, with reverse tapered plate and spew fillet showed that the CFRP plates failed compared to their corresponding un-strengthened specimen at deflection about 57.5%, 47%, 60% and 60%, respectively. The tapered and reverse tapered plate with spew fillets shows a significant delay of EDL and ED of CFRP plates. The use of spew fillet with tapered (M14) and reverse tapered (M16) plates increased the load carrying capacity to about 20.07% and 19.75% higher than the control beam (M2). It is also seen that the spew

fillet at the plate end of M10 is more effective in delaying the debonding of the CFRP plate than that of the specimen that was only strengthened with tapering (M12).

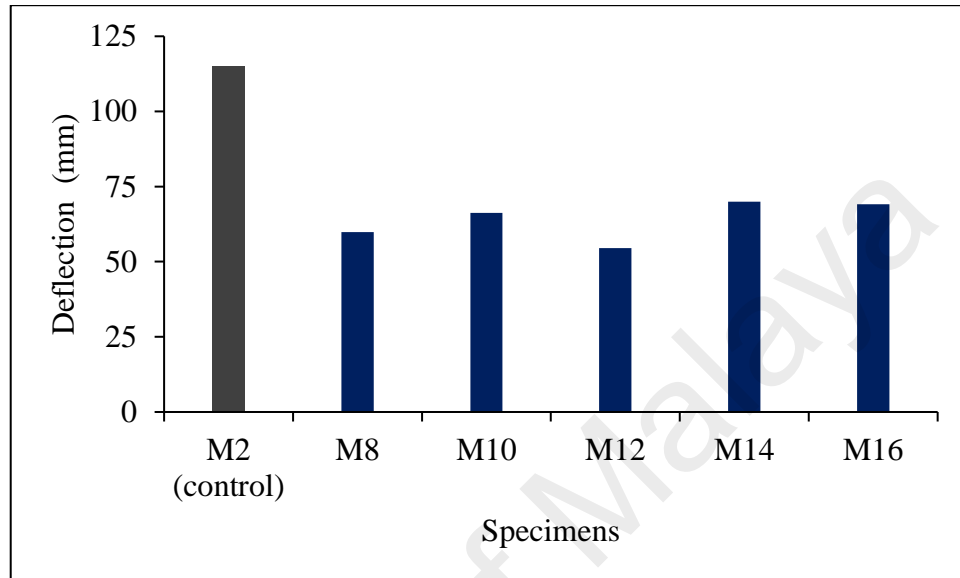


Figure 4.17: Variation of deflection values at peak loads of control beam and strengthened specimens with and without of taper CFRP plates or spew fillet of adhesive

4.2.3.3 Ductility

The ductility indices of strengthened specimens using trapezoidal CFRP in-plane end cutting shape with and without tapered plates or spew fillets of adhesive are presented in Table 4.5. The ratio of the ductility indices for displacement of strengthened specimens M8, with only in-plane end shape, M10, using spew fillet, M12, with tapered CFRP plate, M14, with tapered plate and spew fillet, and M16, with reverse tapered plate and spew fillet, at peak or debonding loads were 0.56, 0.60, 0.5, 0.63 and 0.63; while that for energy were 0.56, 0.62, 0.48, 0.66 and 0.66, respectively, which compared to unstrengthened specimens. It indicated that the strengthened beam M12, with the combination of in-plane and tapered end cutting shape, had the lowest ductility

among the strengthened specimens. At failure loads, the displacement and energy ductility ratio for strengthened specimens with and without tapered CFRP plates or spew fillets of adhesive were observed. It was found that the values were almost similar to the unstrengthened specimen due to the sudden dropped load after immediate debonding.

Table 4.5: Ductility indices of specimens with tapered CFRP plate ends and spew fillets

Test unit	Displacement ductility index				Energy ductility index			
	μ_{dp}	Ratio to CB	μ_{df}	Ratio to CB	μ_{Ep}	Ratio to CB	μ_{Ef}	Ratio to CB
M2 (CB)	11.80	1.00	12.31	1.00	26.10	1.00	27.23	1.00
M8	6.60	0.56	12.57	1.02	14.55	0.56	27.68	1.02
M10	7.11	0.60	12.90	1.05	16.08	0.62	28.75	1.06
M12	5.80	0.50	12.76	1.03	12.49	0.48	25.85	0.95
M14	7.45	0.63	12.77	1.03	17.26	0.66	28.92	1.06
M16	7.46	0.63	12.77	1.04	17.19	0.66	28.69	1.05

μ_{dp} : displacement ductility index at peak load; μ_{df} : displacement ductility index at failure load; μ_{Ep} : energy ductility index at peak load; μ_{Ef} : energy ductility index at failure load

The variation of the ductility indices for displacement and energy of the strengthened beams with and without tapered CFRP plates or spew fillets of adhesive compared to the normal strengthened beams with trapezoidal in-plane end shapes are shown in Figure 4.18. The figure shows that strengthened specimens with tapered plates and spew fillets have higher ductility indices for displacement by 8% to 13%. Similarly, strengthened specimens have higher energy values which are 11% to 18% higher than trapezoidal in-plane end cutting shape. The use of a tapered plate without additional strengthening decreases the displacement and energy ductility to about 12% and 14%, respectively, due to early fail of the tapered CFRP plate. The difference in ductility indices among the specimens was mostly related to the debonding load.

The tapered and reverse tapered CFRP plates with spew fillets of adhesive at plate ends increased the displacement as well as energy ductility of the strengthened specimens by delaying the failure of CFRP.

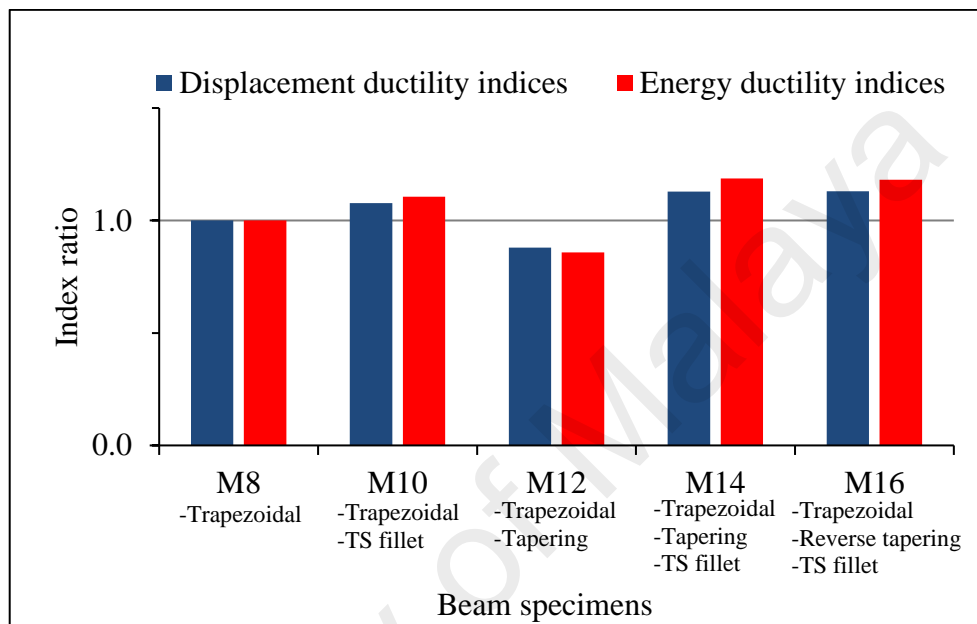


Figure 4.18: Variation of the ductility indices at debonding loads of strengthened specimens with and without tapered CFRP plates or spew fillets of adhesive

4.2.3.4 Measured strains

In order to investigate the effectiveness of tapered CFRP plates and triangular spew fillets of adhesive at the tips, the tensile strain along the CFRP plates was also measured by strain gauges. The distribution of strain along the CFRP plate at load levels of 175 kN and 225 kN are presented in Figure 4.19, showing strengthened specimens M8, with an in-plane shape, M12, with a tapered plate, and M14, with a tapered plate and spew fillets of adhesive. All CFRP plates had a trapezoidal end shape. The strain readings at load levels of 175 kN and 215 kN show that the specimen M14 had lower strain than

specimens M8 and M12 due to spew fillets of adhesive. Also, strengthened specimens M12, with a tapered plate, had a higher strain intensity at the end of the CFRP plate, which initiated the EDL and led to debonding of the plate.

Therefore, it can be concluded that the use of spew fillets of adhesive at the plate end can not only delay the EDL and end-bonding failure modes, but it can also significantly reduce the strain intensity at the tip of the CFRP plate.

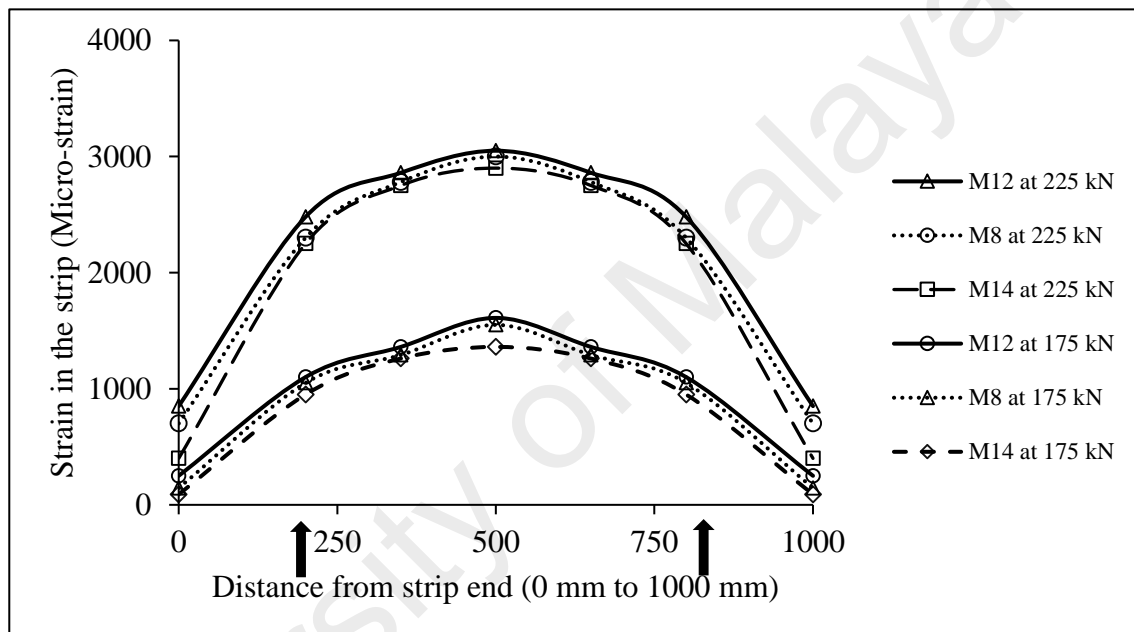


Figure 4.19: Strain distribution along the CFRP plate for specimens with and without tapered CFRP plates or spew fillets of adhesive

4.2.4 CFRP fabrics anchoring

One of the most effective ways for improving the flexural strength of steel beams consists of bonding FRP plates at their bottom flange in order to upgrade the existing tensile strength. However, a key problem to be faced when managing FRP strengthened beams is the possible premature failure due to debonding between the adhesive layer and steel surface. In this section, it is seen that the end of CFRP plates suffer from EDL and ED, identified in the critical regions. The effects of the anchoring system on the structural

behaviour of beams were investigated. Table 4.6 shows the specifications, load bearing capacities, and failure modes of the specimens for the anchoring objective.

To investigate the effects of CFRP fabrics anchoring, a specimen was anchored at the end of the CFRP plate with CFRP sheets. A C-shaped anchor using CFRP fabrics was applied to investigate effectiveness against ED or EDL in steel beams externally strengthened with FRP strips. A triple-layered, C-shaped anchor was used at the end of the CFRP plate with 175 mm width CFRP fabrics.

4.2.4.1 Failure mode

The failure modes of the CFRP before and after anchoring were not the same. Before anchoring, the sequence of failure mode for CFRP composite strengthened steel I-beam was: EDL, ED, debonding of the whole plate. In this study, the behavior of the FRP-strengthened steel beams was investigated experimentally and numerically to analyse the application of CFRP fabrics at the end of the plates.

CFRP fabrics' anchoring was more effective on the delamination and debonding at the end of the externally bonded CFRP plates because the ends of the plates were suitably wrapped using the composite fabrics. Debonding was observed in the whole plate length of the anchored specimen except the portion which was wrapped by the CFRP composite fabrics. High interfacial shear stresses in the CFRP-steel interface was induced below the loading point. When the incrementally applied monotonic loading increased further, the interfacial shear stresses in the CFRP-steel interface and the tensile stresses in the composite plate also increased more. When the both stresses reached critical, intermediate crack debonding (ICD) started below the loading point on the side of the hinge support, and this to propagated to another side.

Table 4.6: Specifications, load carrying capacity and failure modes of specimens with and without anchorage

No.	Specimens	Specification of CFRP plates				Triangular fillet adhesive at ends	Anchorage	Load bearing capacity		Failure modes (Sequential)
		L_{CFRP} (mm)	Plate area (mm ²)	CFRP end shapes				Experimental		
				In-plane	Tapering			Load (kN)	Increment (%)	
1	M2 (Control)	N/A	N/A	N/A	N/A	N/A	N/A	201.50	-	-
2	M5	1000.00	100000	Rectangular	N/A	N/A	N/A	215.29	6.85%	ED-D
3	M13	1000.00	100000	Rectangular	Tapering	√	N/A	227.50	12.9%	ED-EDL-D
4	M14	1025.00	100000	Trapezoidal	Tapering	√	N/A	241.95	20.07%	ED-EDL-D
5	M17	1000.00	100000	Rectangular	N/A	N/A	√	249.76	23.95%	ICD

ED: End debonding, EDL: End delamination, ICD: Intermediate crack debonding; D: Debonding; L_{CFRP} : CFRP plate length

With CFRP fabrics' anchoring, the failure modes of the CFRP plates changed to intermediate crack induced debonding (Figure 4.20). IC debonding failure in FRP-strengthened beams is due to the development of high interfacial stresses at locations of the bonding area. Many researchers have assumed that the FRP/beam interface is subjected to a pure Mode II loading (in-plane shear) condition when IC debonding failure occurs (Fang, 2002; Lu et al., 2007). The intermediate debonding initiates at a critical section in the high moment region and propagates to whole plate. ICD is commonly initiated under below the loading point of FRP strengthened beams. In this case, CFRP fabrics' anchoring system was ineffective due to IC debonding. The failure mode of the CFRP ED is prevented.



Figure 4.20: IC debonding failure mode of CFRP fabrics anchored specimens under monotonic loadings

4.2.4.2 Load deflection relationship

The load deflection curves for the anchored specimen M17, with CFRP fabrics, and unstrengthened specimen are given in Figure 4.21. The curves show that by using CFRP fabrics anchorage, the load bearing capacity was enhanced up to 23.95%. This indicates that by using CFRP fabrics' anchoring, the load bearing capacity increased significantly. After achieving a peak, the load suddenly dropped due to the intermediate plate debonding and the load-deflection curve then followed the response of the control beam closely.

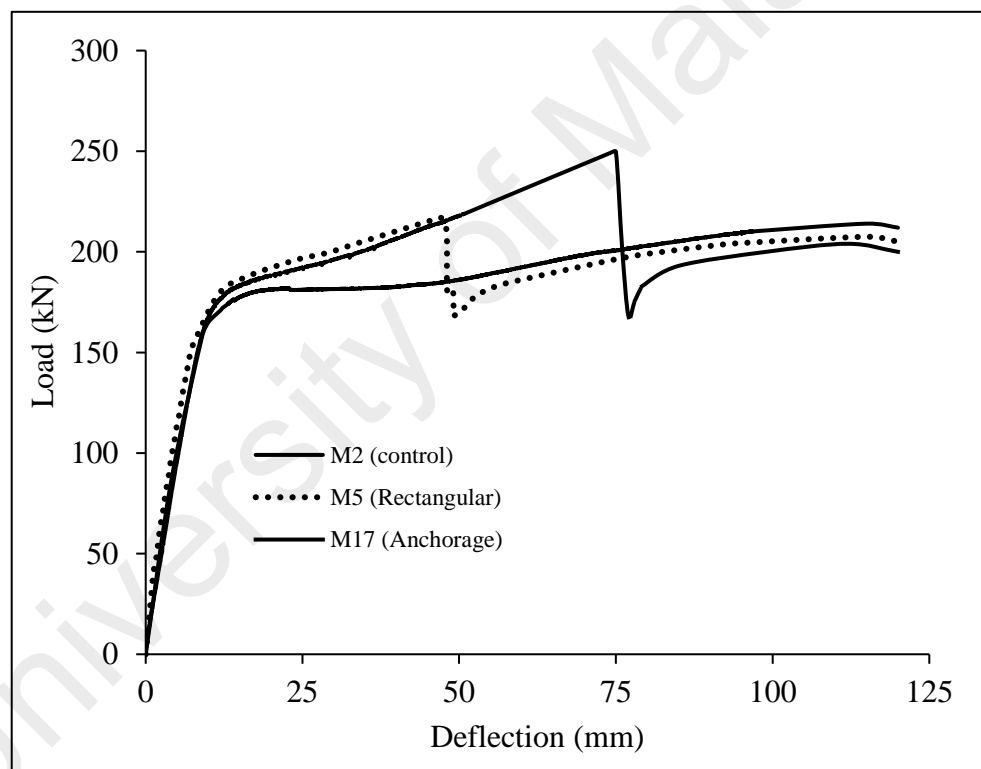


Figure 4.21: Load-deflection curve of control beam and strengthened anchored specimens

The variation of mid span deflection values at peak loads of the control beam and strengthened specimens with and without anchoring are presented in Figure 4.22. It shows that the CFRP plates of anchored specimens failed at deflection of about 61%,

as compared to the control beam. The deflection at the peak loads of the strengthened specimen M5 was 48.9 mm, while the anchored specimen reached up to 69 mm deflection.

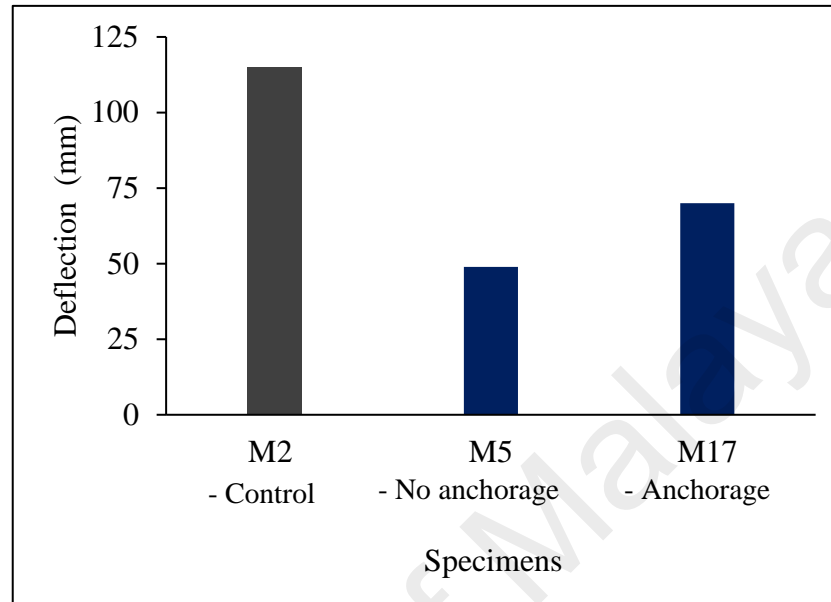


Figure 4.22: Variation of deflection at peak loads of control beam and strengthened specimens with and without anchoring

Table 4.6 shows the specification in strengthening schemes, load bearing capacity and failure modes for different specimens. As can be observed, all beams strengthened with CFRP plates, with or without the anchor, achieved higher loads compared to the control unstrengthened beams. However, the important characteristic of the beams with anchors is the absence of a relatively steep drop in load after initiation of partial IC debonding and the ability of the beams with anchor to maintain their ductile response until the failure of the CFRP. Note that the maximum deflection reached in the control beam before failure is approximately 115 mm, while the FRP strengthened beams reached up to 69 mm at peak load before debonding of the strengthening plates. The drop in load in the CFRP strengthened beam indicates the initiation of IC debonding. It can be noted that beams with anchors have higher loads and greater deflections at failure than other strengthened beams without anchors.

Test results showed that beams with an anchor had generally up to 16% higher debonding and failure load, and they reached higher deflection at failure than the other strengthened beams without anchors. Finally, a significant outcome of the study is that anchors are effective in mitigating end debonding and contributing to the flexural stiffness of the beam.

4.2.4.3 Ductility

Table 4.7 shows the displacement and energy ductility of strengthened specimens with and without anchorage using CFRP fabrics. The ratio of the ductility indices for displacement of strengthened specimens M5, with rectangular in-plane end shape, M17, with rectangular shape using end anchorage, at peak or debonding loads were 0.44 and 0.67; while that for energy were 0.41 and 0.72, respectively, which compared to un-strengthened control beam. At failure loads, the displacement and energy ductility ratio for strengthened specimens with CFRP anchorage was increased a little, 1.04 and 1.08, respectively, than the control specimen due to an extreme drop in load after immediate debonding.

Table 4.7: Ductility indices of specimens with and without anchorage.

Test unit	Displacement ductility index				Energy ductility index			
	μ_{dp}	Ratio to CB	μ_{df}	Ratio to CB	μ_{Ep}	Ratio to CB	μ_{Ef}	Ratio to CB
M2 (CB)	11.80	1.00	12.30	1.0	26.09	1.00	27.23	1.00
M5	5.20	0.44	13.00	1.06	10.68	0.41	27.56	1.01
M13	5.79	0.49	12.63	1.02	12.48	0.48	27.45	1.01
M15	5.63	0.48	12.63	1.03	12.04	0.46	27.33	1.00
M17	7.96	0.67	12.90	1.04	18.85	0.72	29.53	1.08

μ_{dp} : displacement ductility index at peak load; μ_{df} : displacement ductility index at failure load; μ_{Ep} : energy ductility index at peak load; μ_{Ef} : energy ductility index at failure load

The difference of the ductility indices for displacement and energy among the strengthened specimens with and without anchorage are shown in Figure 4.23. It shows that strengthened specimens using anchorage increase the ductility index for displacement from 42% to 53% and energy from 64% to 76% as compared to other strengthened beams with same end shape (rectangular) using with or without taper plates or spew fillets.

It indicated that the anchorage using CFRP fabrics increases the ductility of the strengthened structural specimens by prevention of end problems before IC debonding of the CFRP plates.

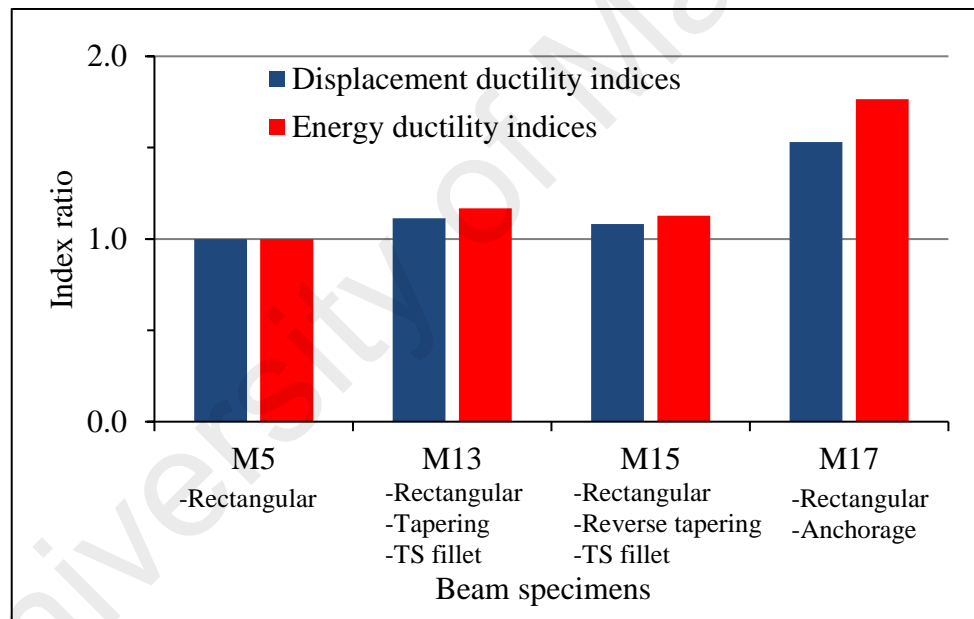


Figure 4.23: Effect of CFRP fabrics anchorage on ductility indices

4.2.4.4 Measured strains

The effects of CFRP end-anchoring on strain along the CFRP plate at a load of 215 kN are shown in Figure 4.24. The anchored specimens show considerable reduction in strain on CFRP at the end and mid span of CFRP plates compared to non-anchored specimens.

Figure 4.25 illustrates the variation of strain on the tension flange in the mid span versus applied load by experimental tests. It shows that specimens using anchorage considerably increase the stiffness by decreasing strain in the mid span tension flange before failure of the CFRP plate of the strengthened wide-flange steel I-beams. The maximum tensile strain at peak load or before failure of CFRP plate by IC debonding for anchored specimen was about 3330 $\mu\epsilon$. The strain in the mid span tension flange before debonding failure of the strengthened beams M5 (with an in-plane end shape) and M14 (with a tapered plate and spew fillet) was reached at 3080 and 3150 $\mu\epsilon$, respectively. This indicates the high strain capacity of the beams, with a low rate of increment due to anchorage of the strengthened beams.

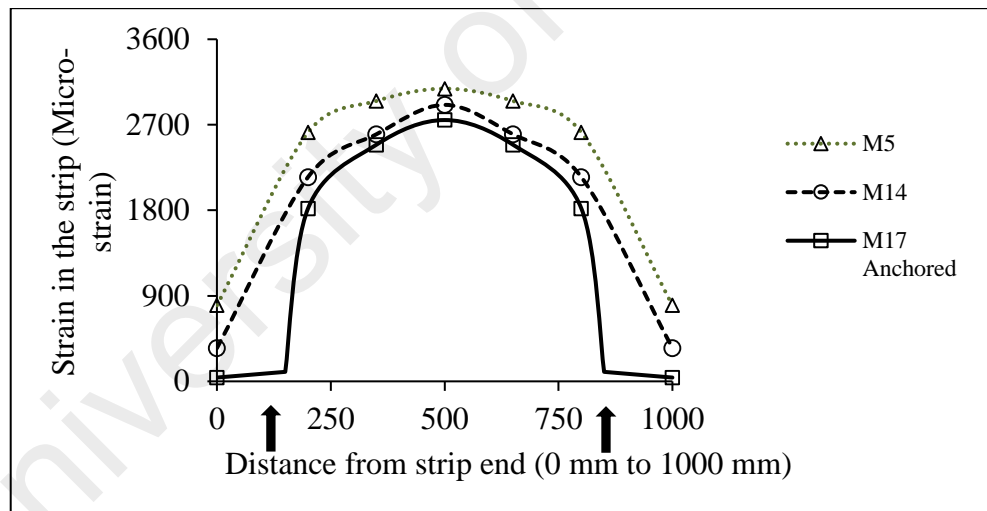


Figure 4.24: Strain distribution along the CFRP composite plate for specimens with and without CFRP fabrics anchorage at a 215 kN load

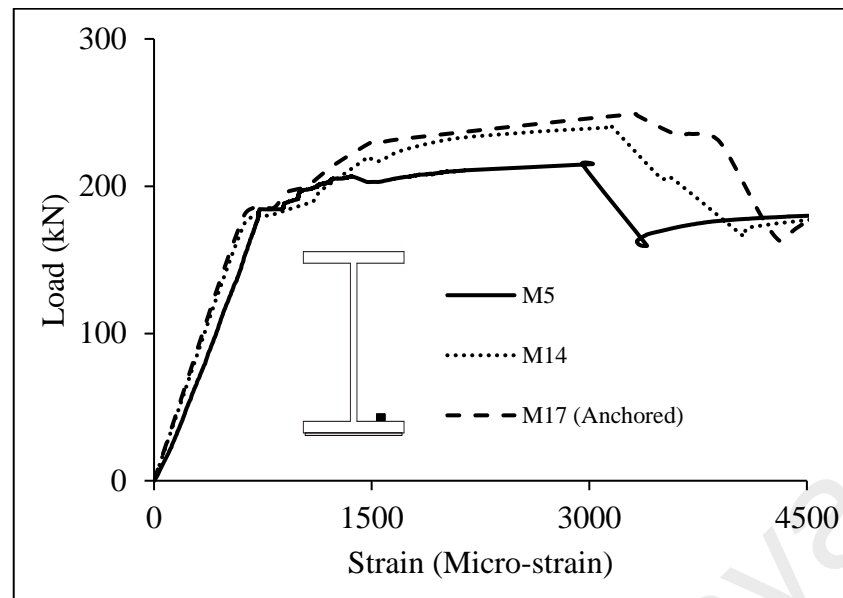


Figure 4.25: Strains in the mid-span tension flange versus applied load

It can be concluded that the application of end anchorage using CFRP fabrics decreased the rate of strain. Also, the CFRP fabrics' anchoring not only increased the stiffness and load bearing capacity, it also increased the strain capacity at the mid span of the strengthened wide flange steel I-beams.

4.2.5 Numerical simulation

A 3D nonlinear FEM was developed to investigate the monotonic flexural specimens of non-strengthened and strengthened wide-flange steel I-beams with CFRP plates. The comparison between FE numerical and experimental test results for the steel beam specimens in terms of yield load and peak load is summarized in Table 4.8. As shown in Table 4.8, there is a good agreement between the simulated load carrying capacities and the experiment result of most of the test specimens.

Table 4.8: Comparison of yield load and peak load between numerical and experimental results of monotonic specimens

No.	Specimens ID	Yield load (kN)		Peak load (kN)	
		Num.	Exp.	Num.	Exp.
1	M0	149.50	148.30	172.00	174.00
2	M1	158.50	160.00	191.50	193.50
3	M2	162.00	163.50	199.00	201.50
4	M3	165.00	163.00	194.50	198.00
5	M4	166.50	168.50	203.00	206.00
6	M5	169.00	171.50	211.50	215.00
7	M6	169.00	171.00	217.00	221.00
8	M7	169.20	171.00	221.50	225.00
9	M8	169.50	171.30	224.50	229.00
10	M9	169.50	171.00	220.00	224.00
11	M10	170.00	171.50	231.00	236.50
12	M11	169.00	171.00	218.00	213.00
13	M12	169.10	171.50	229.00	225.75
14	M13	169.50	171.50	233.50	227.00
15	M14	169.90	171.60	245.50	241.95
16	M15	169.50	171.00	228.00	225.50
17	M16	169.80	171.50	244.50	241.30
18	M17	175.00	171.80	256.00	249.75

Five types of failure mode have been observed. These are the stress concentration and local buckling at below point load, lateral torsional buckling, plate ED and intermediate crack debonding failure mode in the CFRP-steel interface obtained from FE numerical analysis.

The simulation of stress concentration below the loading point combined with local buckling and LTB is shown in Figure 4.26. The stress concentration of the compression flange in the beams without steel plate stiffeners increases greatly during loading and causes local buckling failure below the loading point of the beam and initiates early ED. The LTB failure mode also observed in specimen UB2 (Figure 4.27). The influence of LTB and failure of the compression flange at mid span of the simulated and tested strengthened beams are shown in Figure 4.28(a) and (b). They illustrate that web stiffeners below the point load prevent failure because of stress concentration below the

loading plate. This is a common failure in unrestrained strengthened and unstrengthened steel structures (Narmashiri, 2011).

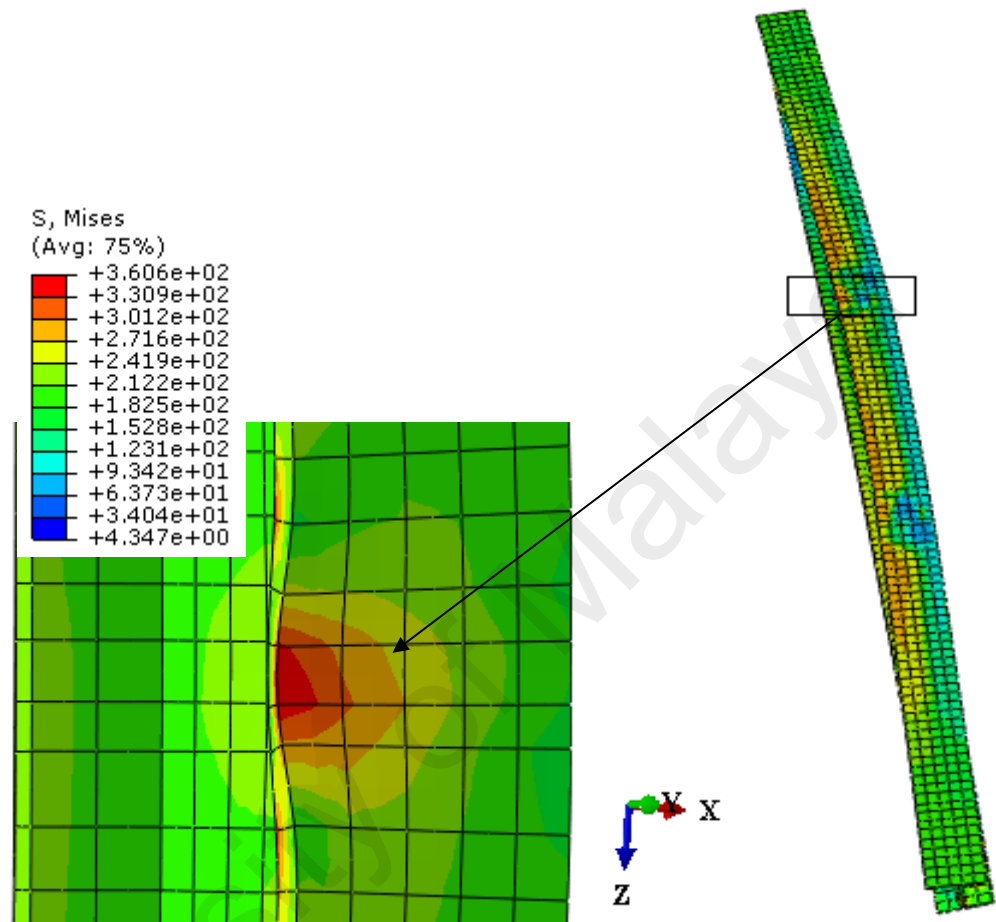


Figure 4.26: (a) Stress concentration and local buckling at below the loading point and (b) Lateral torsional buckling of specimen M0

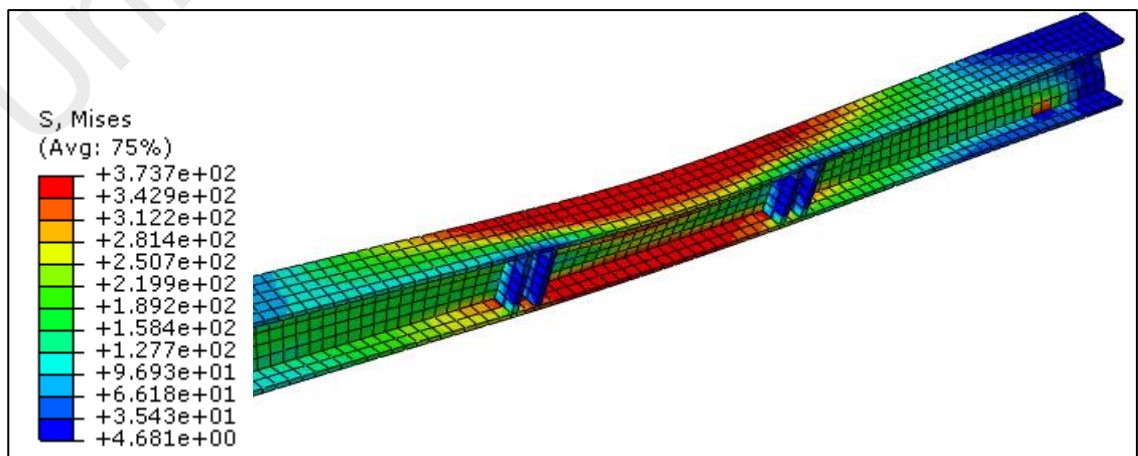


Figure 4.27: Lateral torsional buckling failure mode of specimen M1

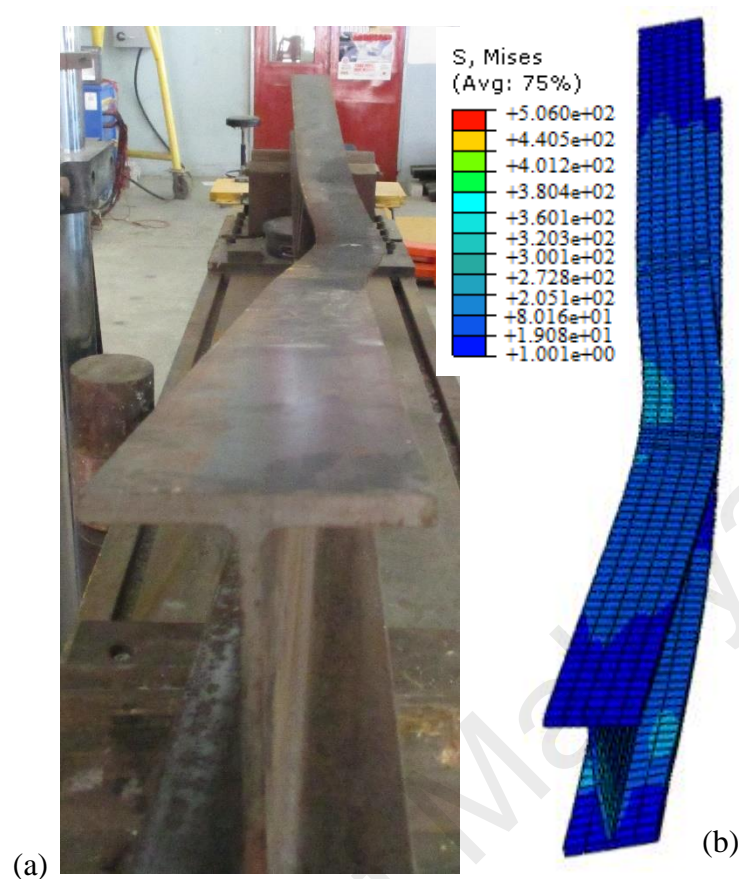


Figure 4.28: Lateral torsional buckling in specimen M4: (a) experimental, (b) FE

Unrestrained beams were loaded in stiffer planes and were allowed to undergo LTB. When a laterally unsupported beam was not adequately supported against LTB, the design bending strength was governed by buckling strength. Wide flange steel I-beams were found to be relatively weak in resistance to bending and torsion about the minor axis, and if not held in line by floor construction, bracing or lateral support could become unstable under load (Narmashiri & Jumaat, 2011). Thus, a lateral constraint was used against lateral instability in numerical non-linear modelling as lateral bracing in monotonic specimens M2 and M5 to M17 in this study. The effectiveness of lateral bracing for a strengthened wide-flange steel I-beam is shown in Figure 4.29. In addition, the use of steel plate stiffeners can be effective in preventing the stress concentration below the point load and delaying the ED failure mode (Figure 4.29). The initiation of ED for a simulated strengthened beam is presented in Figure 4.29.

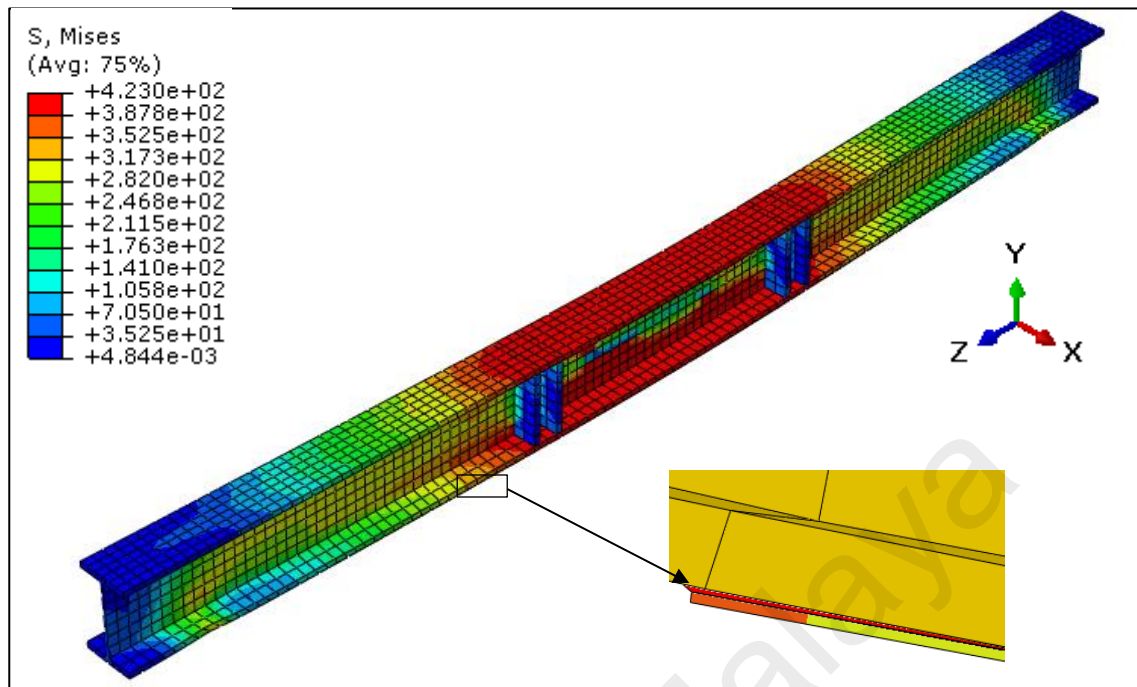


Figure 4.29: Effect of stiffeners and lateral bracing with ED initiation of the CFRP plate in specimen M5

One key limitation of strengthened steel W- or I-beams is the presence of high interfacial stress at the tip of the FRP composite strip, and strain intensity on the adhesive near the end of the strip (Narmashiri, Ramli Sulong, & Jumaat, 2012), which typically governs ED failure. High strain intensity occurred on the adhesive at the CFRP tip and caused end debonding, which is shown in Figure 4.30 for a simulated beam of a strengthened specimen. The failure of all specimens including those strengthened with: in-plane and tapered CFRP end shapes and spew fillets of adhesive was initiated by ED except anchored specimens which failed by IC debonding (Figure 4.31) in the CFRP-steel interface.

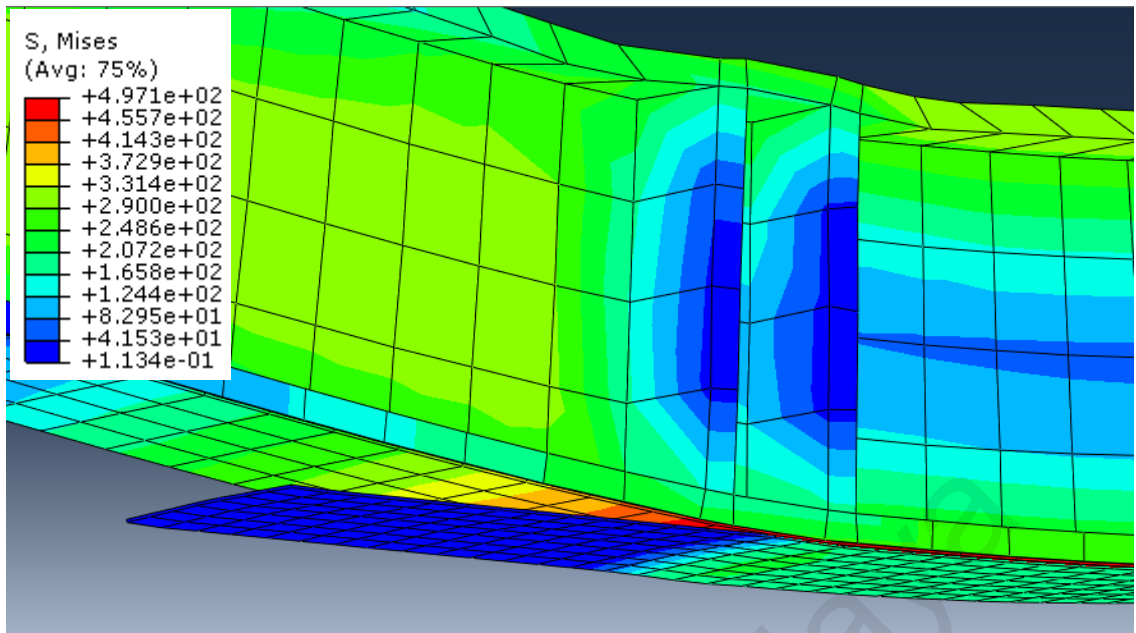


Figure 4.30: End debonding failure mode (FEM)

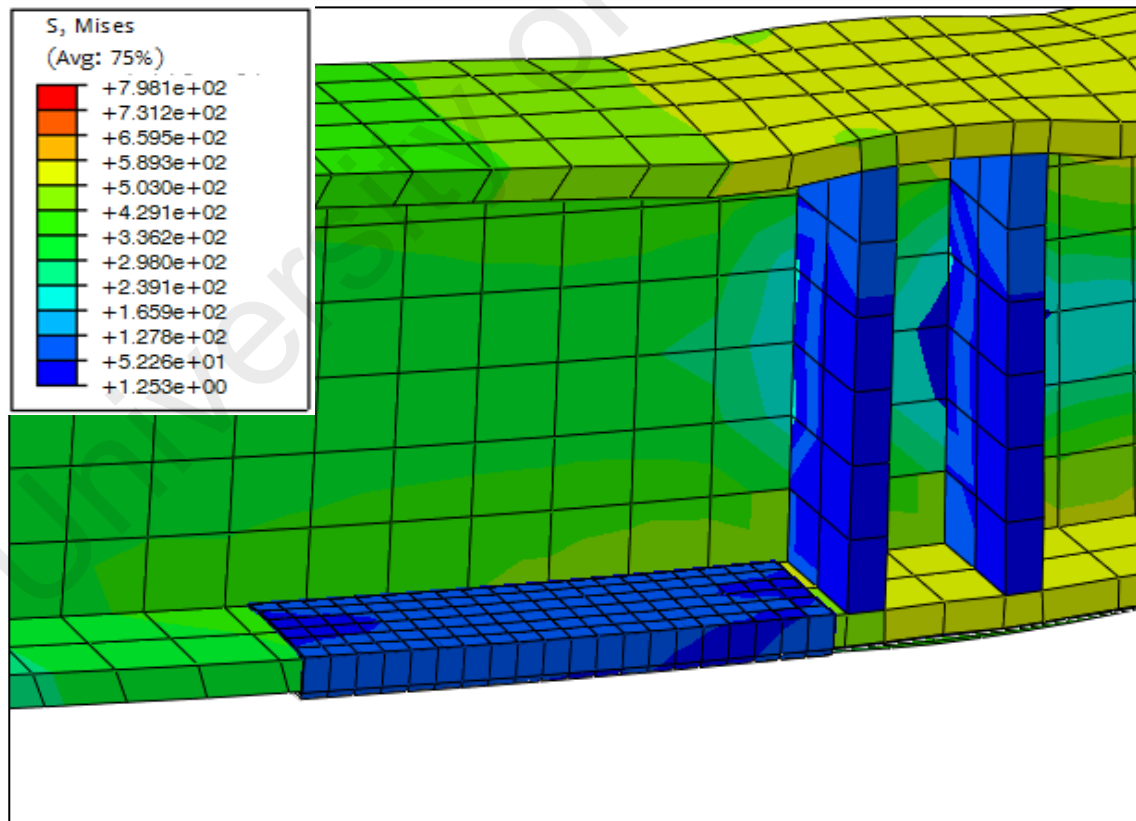


Figure 4.31: Simulation of the IC debonding (anchored specimen, M17)

In verifying the model, the result of a published works are also used (Deng & Lee, 2007a) (Figure 4.32). A load deflection diagram for unstrengthened specimens are presented in Figure 4.33. Figure 4.34 compares the load-deflection behaviour of the FE model with the experimental measurements of strengthened specimens M3 to M5. The dotted and solid lines represent the curve of the numerical and experimental results, respectively. The displacement increases linearly with the load and the slopes of the curves are similar. The load drops at a certain displacement when the failure occurs between the CFRP and steel interface. The maximum load carrying capacity of the strengthened specimen M5 from the experimental test and the numerical simulation was 215kN and 217.6 kN, respectively. The predicted peak load of all monotonic specimens are in reasonable agreement with the experimental results. From the general static analysis, good agreement was achieved in both the experimental and numerical simulation. See Appendix B for more results.

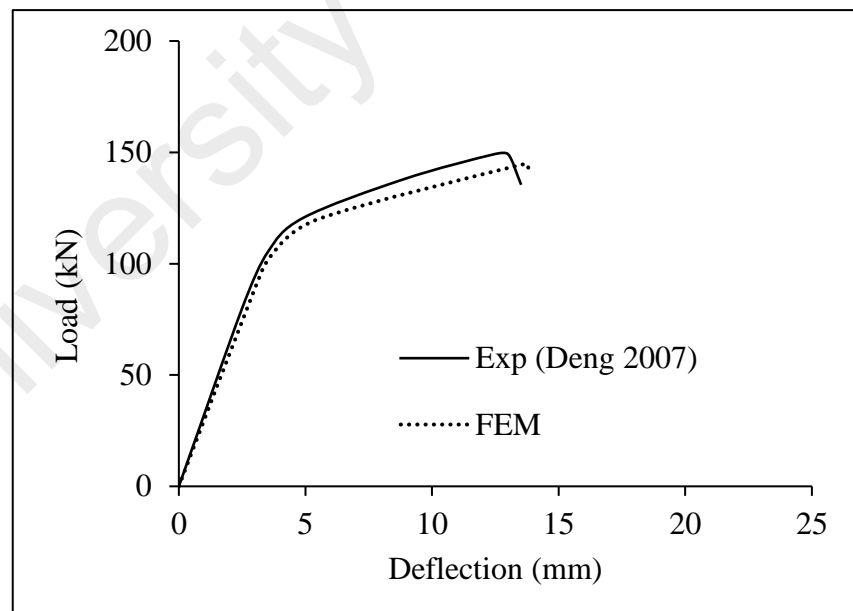


Figure 4.32: Load-deflection diagram between experimental (Deng & Lee, 2007a) and FEM

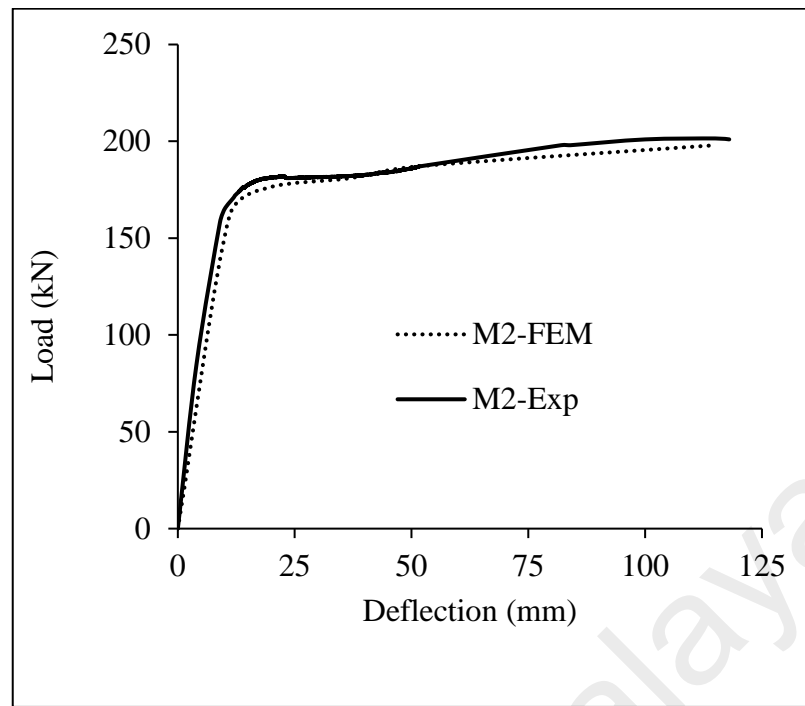


Figure 4.33: Load-deflection diagram of un-strengthened specimen

University of Malaya

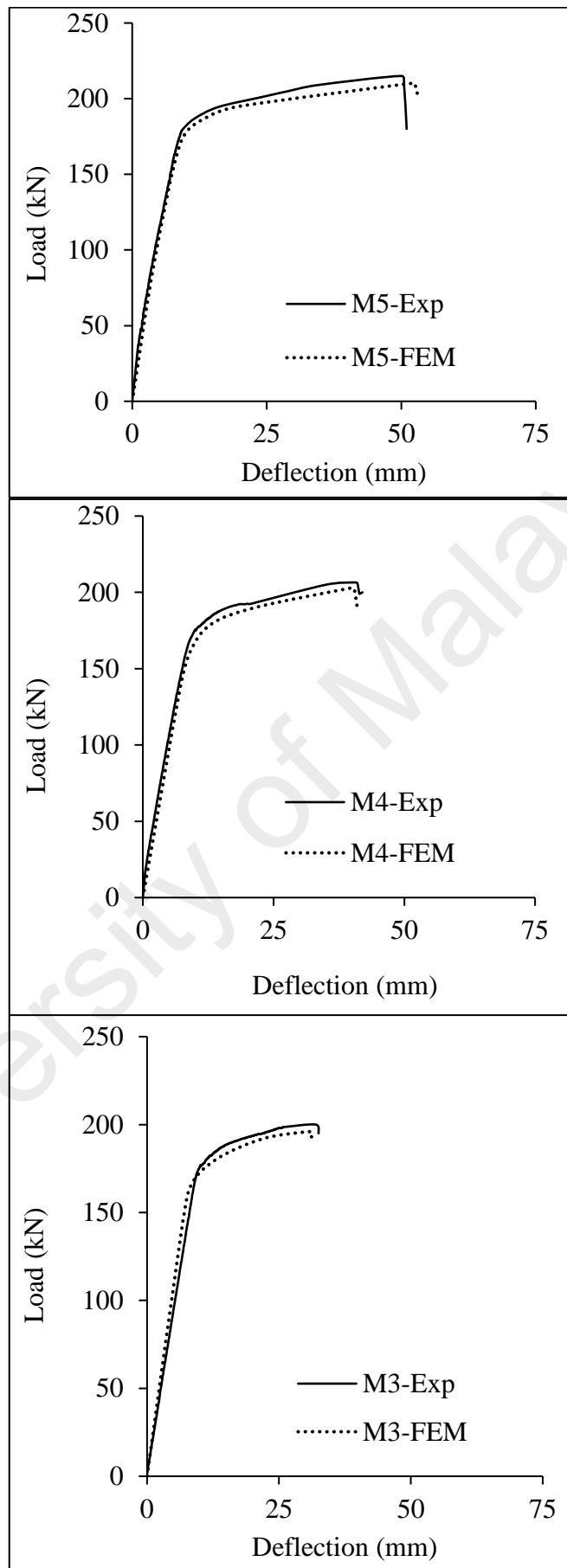


Figure 4.34: FEM and experimental load-deflection diagram of strengthened specimens

4.2.6 Parametric study using FE modelling

The effect of the layer, length and width of CFRP fabrics on the end anchoring of the externally bonded CFRP plate in terms of failure load and failure mode using FEM are presented in Table 4.9. The following failure modes were predicted for anchored specimens using CFRP fabrics/wrapping at the plate end under monotonic loadings: (1) wrapping fracture, (2) wrapping debonding, and (3) IC debonding of the CFRP plate.

Table 4.9: Failure load and failure mode of anchored specimens (FEM)

Specimens ID	CFRP plate end shape	CFRP fabrics/wrapping			Failure load	Failure mode
		Layer	Length (mm)	Width (mm)		
M18	Rectangular	1	220	175	239.00	Wrapping fracture
M19	Rectangular	2	220	175	247.80	Wrapping fracture
M17	Rectangular	3	220	175	256.00	ICD (plate)
M20	Rectangular	4	220	175	258.60	ICD (plate)
M21	Rectangular	3	170	175	243.10	Wrapping debonding
M22	Rectangular	3	220	125	243.10	Wrapping debonding
M23	Trapezoidal	3	220	175	257.70	ICD (plate)

The specimens M18 and M19 were modelled for end anchorage using one layer and two layers with a 220 mm length and a 175 mm width CFRP fabrics/wrapping, failed by wrapping fracture. A simulated wrapping fracture of the anchored specimen is displayed in Figure 4.35. No fracture was observed in the specimens M17, M20, M21, M22 and M23, which used at least three layers fabrics. Specimens M17, M20 and M23 failed due to intermediate crack debonding of the CFRP plate, whereas anchored specimens M21 and M22 failed earlier by debonding in the layer of the CFRP wrapping due to a shorter length and width. The fracture and debonding of the CFRP wrappings indicate the ED of the CFRP plates.

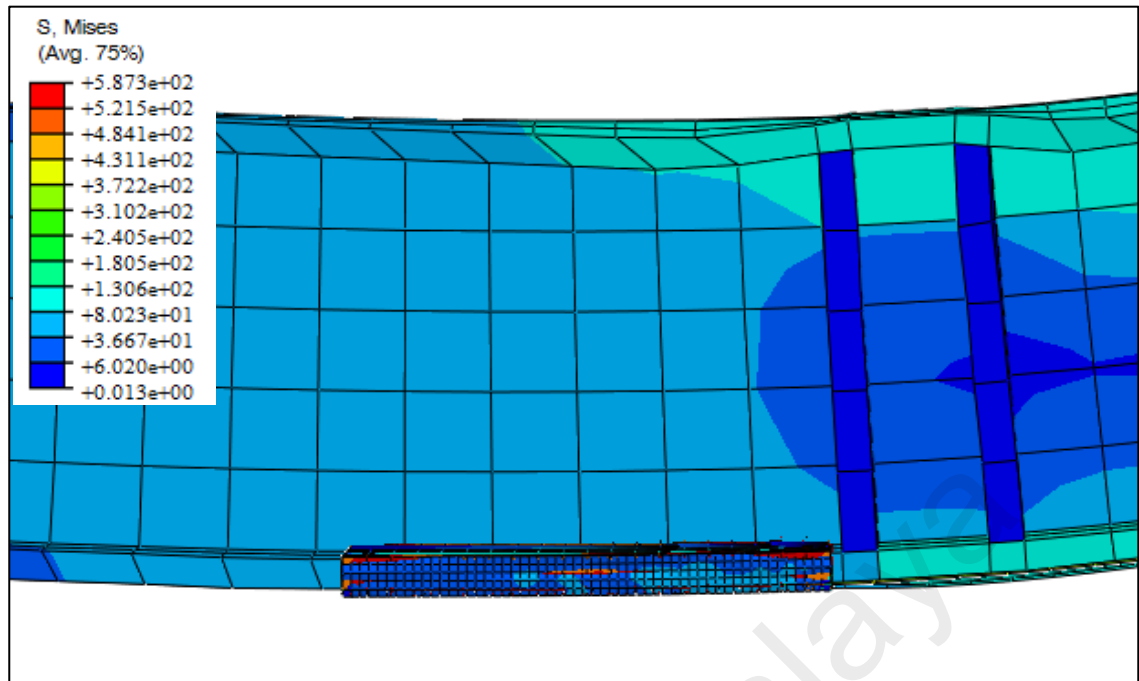


Figure 4.35: Fracture of the wrapping failure mode (FEM)

Therefore, the proposed end anchorage using three layers of CFRP fabrics with a 220 mm length and a 175 mm width can prevent end debonding failure mode of the strengthened wide-flange steel I-beams.

4.3 Fatigue Performance

The experimental test of fatigue specimens was conducted to study the fatigue performance of wide-flange steel I-beams strengthened by using CFRP composite plate under cyclic loadings with constant amplitude. The maximum load that was applied was 80% of the static yield load of the unstrengthened specimens. Only one unstrengthened fatigue specimen was tested with a 10% - 50% load range. The frequency of the cyclic loading was set at 3 Hz in the fatigue investigation.

To study the presence of the shear-lag phenomenon at the CFRP-steel interface for strengthened specimens, strain gauges were fixed at mid span along the height of the

steel specimens. The strain profiles with the position of the strain gauges (SG) at mid span for strengthened specimen F3 are presented in Figure 4.36. The measured strain profiles of each specimen indicate similar values as that of F3.

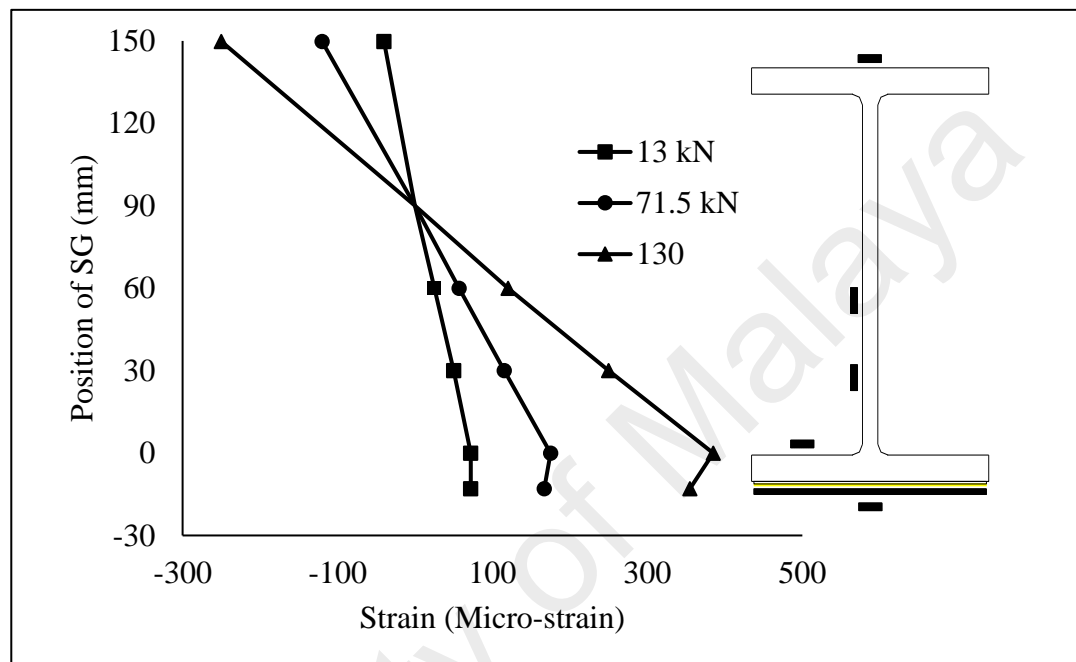


Figure 4.36: Strain profile at mid-span of strengthened specimen F3

According to Figure 4.36, the strain distribution within the cross section of the steel beam was linear but exhibited discontinuity on the CFRP-steel interface. The figure shows that the cross section of steel beam agreed with the statement that plane section remains plane, but the shear-lag phenomenon was clearly indicated at the interface between the CFRP composite plate and the surface of the steel tension flange. The shear-lag phenomenon become more serious for strengthened specimens as the loading was increased.

This section presents and discusses the results of the fatigue test specimens of strengthened wide-flange steel I-beams with different in-plane CFRP end cutting shapes and CFRP fabrics' anchorage. The fatigue life, failure initiation life, observations of ED of the CFRP plates, plate debonding at different stages and fracture of the steel beams during testing are presented. The profile for the deflection versus the number of cycles is discussed and is related to the cyclic behaviour of the constituent materials used in the beam specimens (steel beams and CFRP). The deformation of each strengthened specimen under cyclic loading is presented in terms of the measured strain versus the number of cycles of fatigue life. See Appendix C for more results regarding the fatigue investigation.

4.3.1 Different in-plane end cutting shapes

The experimental results of the fatigue test strengthened specimens with different in-plane CFRP end cutting shapes are presented in Table 4.10. Fatigue life, failure modes with CFRP plate debonding, deflection versus number of cycles, strains versus number of cycles, and observed effects of CFRP end shapes under cyclic loadings are presented below.

4.3.1.1 Failure mode

The sequences of CFRP failure modes are indicated in Table 4.10. The following failure modes were observed for the strengthened specimen with rectangular (F3), semi-ellipse (F4), semi-circular (F5) and trapezoidal (F6) CFRP end cutting shape under fatigue: (1) ED, (2) plate debonding, and (3) steel beam fracture (SBF).

Table 4.10: Fatigue test result of strengthened specimens with in-plane CFRP end cutting shapes

No.	Specimens ID	Specification of CFRP plates			% of loading	ED initiation (No. of cycles)	Plate debonding at mid-span (No. of cycles)	Fatigue life (No. of cycles)	Increments (%)	Failure mode
		L_{CFRP} (mm)	Plate area (mm ²)	End shapes						
1	F2 (Control)	N/A	N/A	N/A	80%	-	-	241181	-	SBF
2	F3	1000.00	100000	Rectangular	80%	279587	296170	298893	23.93%	ED-SBF
3	F4	1010.75	100000	Semi-ellipse	80%	302029	326000	328364	36.15%	ED-SBF
4	F5	1021.50	100000	Semi-circular	80%	329656	353050	355866	47.56%	ED-SBF
5	F6	1025.00	100000	Trapezoidal	80%	351209	367440	370493	53.62%	ED-SBF

ED: End debonding; SBF: Steel beam fractured

Figure 4.37 shows the ED failure mode under cyclic loading. The initiation of ED failure of all strengthened specimens with in-plane CFRP end cutting shapes started on the hinge side of the simply supported beams and was propagated towards mid span of the beams. The steel beam fracture occurred on the same side of plate debonding below the loading point of the beams in all cases. Beams F3, F4, F5 and F6 failed after 298893, 328364, 355866 and 370493 cycles, respectively.



Figure 4.37: ED of the CFRP plate

Figure 4.38 shows the failure modes of fatigue specimens with different in-plane CFRP end cutting shapes. The retrofitted beam subjected to a high cyclic loading was shown to exhibit a large brittle fracture. The form of brittle fracture being addressed had been termed “constraint-induced fracture” and could occur without any noticeable fatigue crack growth, and, more importantly, without any warning. The fracture occurred less than 1% of fatigue life after CFRP debonding in all cases of specimens with in-plane CFRP end shapes. Fracture of the steel beams occurred beside the stiffeners, which is connected by welding to the flange and web at below the point load. High residual stress influences fracture failures due to welding. The catastrophic fatigue failure shown in

Figure 4.38 was the result of fracture crack growth from the bottom flange through the web in just a few cycles. The control beam also fails by fracture below the point load under cyclic loading (Appendix C).



Figure 4.38: Failure mode of fatigue strengthened specimens with different in-plane CFRP end cutting shapes under fatigue

The end cutting shapes of the bonded CFRP plates had a significant impact on the effectiveness of the reinforcement. The application of the trapezoidal in-plane CFRP end cutting shapes delay the end debonding failure mode compared to the other end cutting shapes including rectangular, semi-ellipse and semi-circular under cyclic loads.

4.3.1.2 Fatigue life and failure initiation life

The fatigue lives for strengthened specimens with different in-plane end cutting shapes are illustrated in Table 4.10. The fatigue life is determined as the number of cycles corresponding to the point when a fracture propagates from the beam flange to the web-flange region. Beyond this point, brittle fracture occurred, with the fracture propagating to the middle of the web in a few cycles for all specimens. When the CFRP end debonding propagates towards the mid span of the beams, and the steel beam fracture propagates to a visible size, the number of cycles of the fatigue load is defined as the ED initiation life and steel beam fracture initiation life, respectively. Table 4.11 presents the fatigue failure initiation life of strengthened specimens with different in-plane CFRP end cutting shapes and that of an unstrengthened specimen.

Table 4.10 shows that the fatigue life improvement varied with different in-plane CFRP end cutting shapes but that the trapezoidal CFRP plate significantly increased the fatigue life of strengthened steel beams compare to the other in-plane CFRP end cutting shapes. It illustrates that the fatigue life of strengthened specimens with rectangular (F3), semi-ellipse (F4), semi-circular (F5) and trapezoidal (F6) end shapes was increased by about 24%, 36%, 47.50% and 53.50%, respectively, as compared to the unstrengthened beam (F2). Thus, the use of a trapezoidal CFRP plate could extend the fatigue life of

strengthened wide-flange steel I-beams more successfully than other in-plane CFRP end cutting shapes.

It is well known that a higher applied load level results in a lower fatigue life for steel structures. Hence, for the strengthened steel beams, the use of composite CFRP plate, which reduces the load range, would unquestionably extend the fatigue life as well as failure initiation life. With respect to the CFRP end debonding initiation life, Table 4.11 shows that strengthened specimens with different CFRP end shapes could reach 279587 – 351209 cycles. However, the debonding initiation life of the CFRP plate of specimen F6, with a trapezoidal end cutting shape, was higher than those of the strengthened specimens with other in-plane end cutting shapes.

In general, ED initiation occurred at above 92% fatigue life of each strengthened beam and was related to the end cutting shapes. Figure 4.39 shows the comparison of ED initiation life and fatigue life of strengthened specimens with different in-plane shapes.

The increased rate of fracture initiation life of strengthened specimens with different end shapes is shown in Table 4.11. The SBF initiation life of the unstrengthened beam F2 was 241052 cycles, whereas the strengthened beam F3, with a rectangular CFRP end shape, had a fracture initiation life of 298774 cycles, which was 1.24 times that of F2. The fracture initiation life of strengthened beams F4 and F5, with semi-ellipse and semi-circular CFRP plates, were 1.36 and 1.48 times that of F2, respectively, whereas the SBF initiation life of beam F6, strengthened by a trapezoidal CFRP end shape, was 1.54 times that of the unstrengthened beam.

Table 4.11: Failure initiation life of specimens with different CFRP end shapes

Specimens ID	CFRP end shape	ED initiation life (No. of cycles)	SBF_{il} (No. of cycles)	$\alpha_i = \frac{SBF_{il}(specimens)}{SBF_{il}(CB)}$
F2 (CB)	-	-	241052	1.00
F3	Rectangular	279587	298774	1.24
F4	Semi-ellipse	302029	328260	1.36
F5	Semi-circular	329,656	355772	1.48
F6	Trapezoidal	351209	370415	1.54

α_i : increase rate of steel beam fracture (SBF) initiation life, SBF_{il} : SBF initiation life

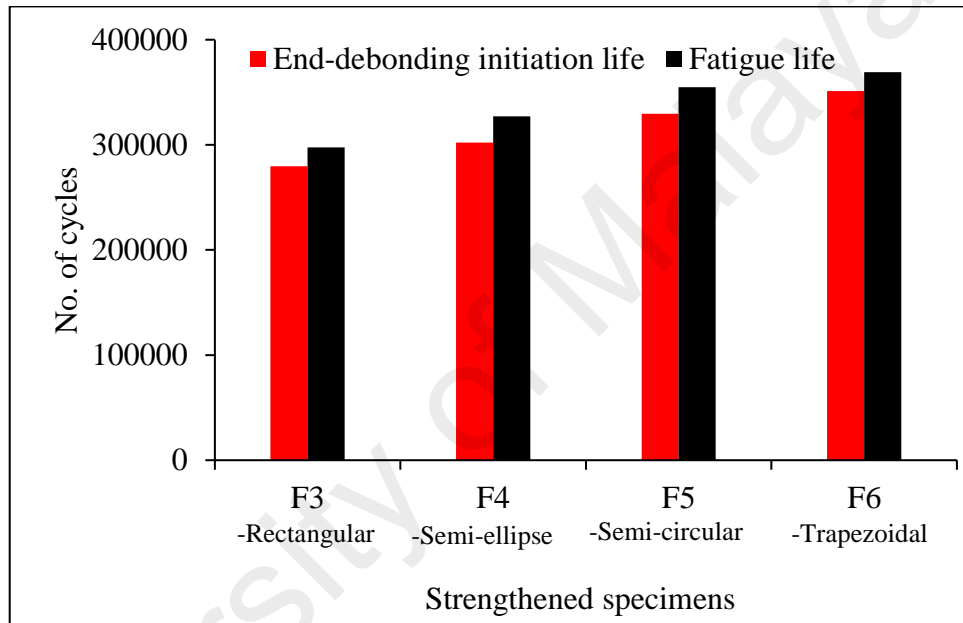
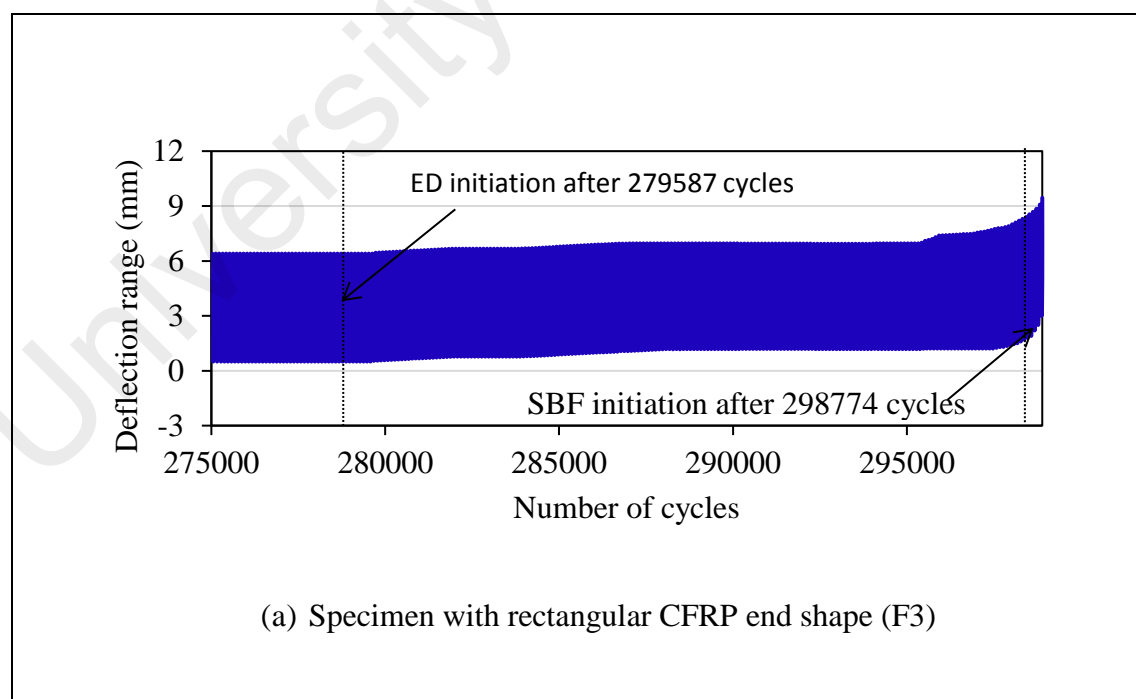


Figure 4.39: Comparison of ED initiation life and fatigue life of strengthened specimens with CFRP end shapes

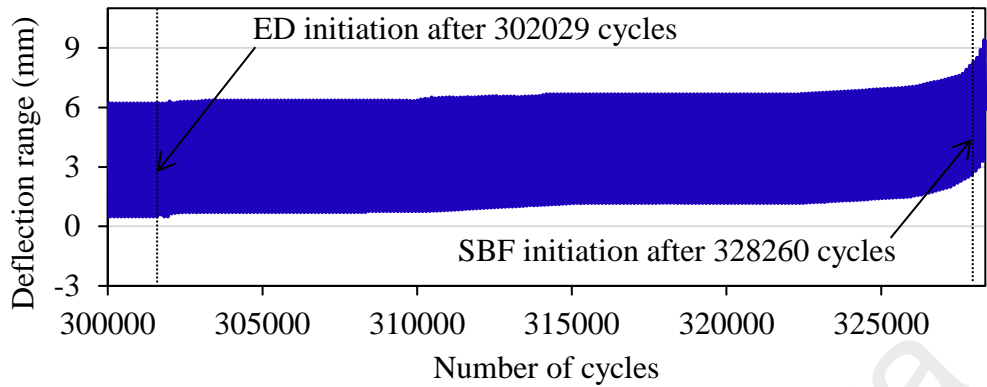
The in-plane CFRP end cutting shapes considerably increase the number of cycles under repeated loadings. In addition, the trapezoidal end shape of the bonded CFRP plates experienced the highest failure initiation life as well as fatigue life followed by specimens with other in-plane CFRP end cutting shapes. Hence, when compared to rectangular, trapezoidal, semi-ellipse and semi-circular end shapes; the trapezoidal in-plane CFRP end cutting shape showed better performance under cyclic loading, which indicates that the trapezoidal shape was more consistent in fatigue resistance.

4.3.1.3 Deflection versus number of cycles

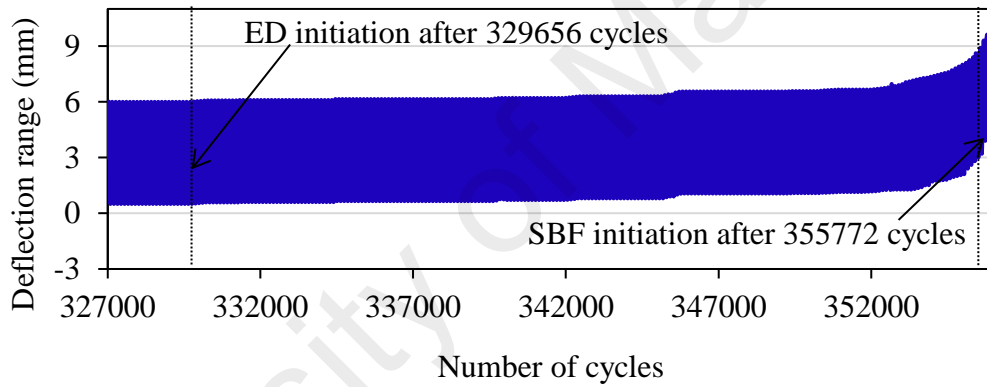
The deflection ranges versus number of cycles for all tested specimens strengthened by different CFRP plate end cutting shapes are shown in Figure 4.40(a) - (d). The deflection ranges were measured at mid span by laser displacement transducer (LDT) during fatigue testing under sinusoidal cyclic loading. These figures document critical steps for all specimens in terms of ED and steel beam fracture of the steel beams. A similar trend for deflection versus number of cycles is observed for each strengthened specimen. The deflection slowly increases after ED initiation. The deflection increments are more rapid when CFRP plate debonding occurs below the point load, followed by a sudden increase in deflection after the steel beam fracture initiation occurs below the point load for all specimens. Meanwhile, an upward move in the deflection was observed for all the strengthened beams after fracture initiation (Figure 4.40).



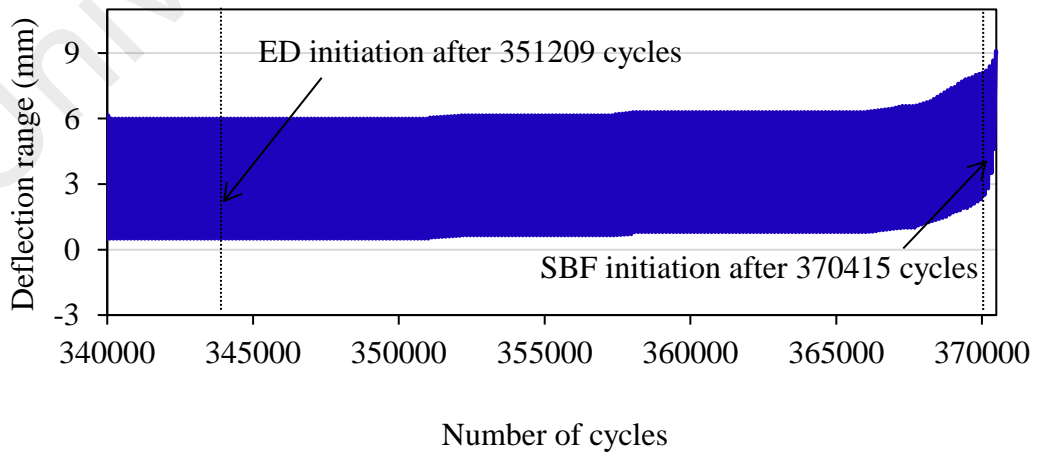
'Figure 4.40, continued'



(b) Specimen with semi-ellipse CFRP end shape (F4)



(c) Specimen with semi-circular CFRP end shape (F5)



(d) Specimen with trapezoidal CFRP end shape (F6)

Figure 4.40: Deflection versus number of cycles.

The variation of maximum deflection versus fatigue life for specimens with different in-plane CFRP end cutting shapes is presented in Figure 4.41. The deflection values were lower for specimen F6, strengthened by a trapezoidal CFRP end cutting shape, as compared to other end shapes in the deflection curve. In Figure 4.41, the highest deflection belongs to the unstrengthened beam (F2), while a lower deflection range for specimens with semi-circular (F5) and trapezoidal (F6) CFRP end plates indicate the influence of the shapes on the CFRP plate end on the specimen's stiffness. A low deflection value due to the in-plane CFRP end cutting shapes shows the high fatigue life. The deflection values are dramatically increased at the end of the fatigue life due to brittle fracture of the steel beams.

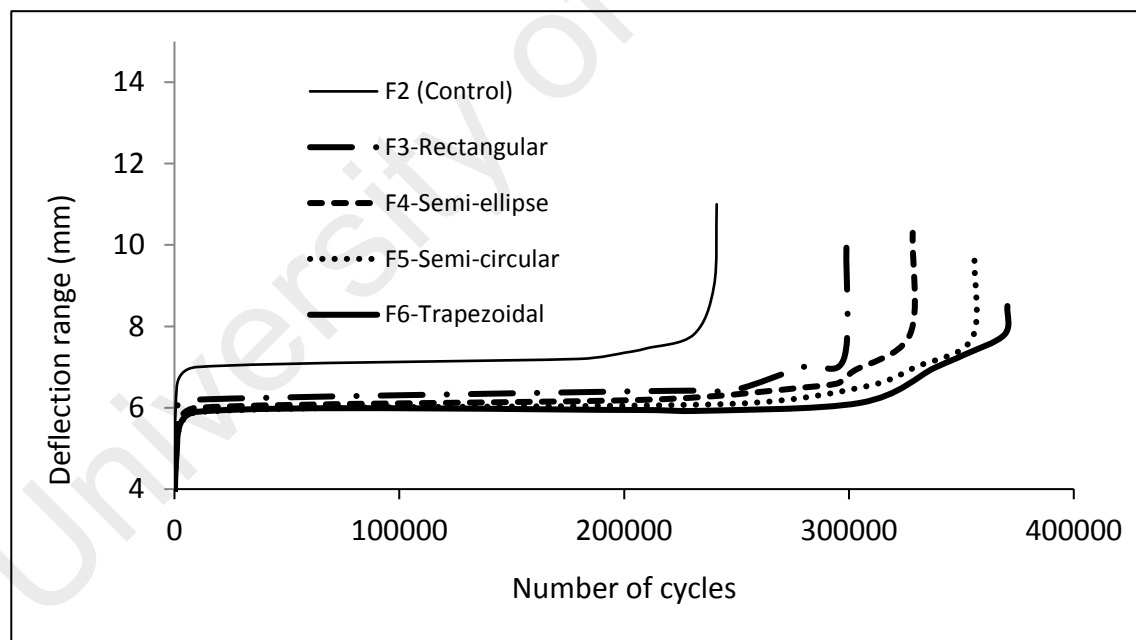


Figure 4.41: Maximum deflection versus number of cycles for strengthened beams with different CFRP end shapes

4.3.1.4 Strain versus life

The strain ranges versus number of cycles in the tension CFRP plates at the middle, below point load and at the plate end for specimens with different in-plane CFRP end cutting shapes are presented in Figure 4.42 to Figure 4.45. The measured strains during ED initiation, plate debonding and steel beam fracture are presented in detail. All strengthened specimens with in-plane CFRP end cutting shapes were fractured below the point load in the hinge side of the simply supported beams.

(a) Specimen F3

Figure 4.42(a) - (c) shows the strain ranges versus number of cycles curved for all strain gauges on the CFRP plate in the tensile flange. The strain diagram was plotted for cycles 275000 to 298893. These figures show that the slope of the strain curves changed as the number of cycles increased. Looking at Figure 4.42(b) and (c), the strain ranges and strain values dramatically increase after debonding of the plate. The end debonding was initiated after 279587 cycles (93.6% of fatigue life) and propagated towards the point load and mid span after 294290 and 296170 cycles, respectively. The steel beam fracture initiated below the point load after 298774 cycles (99.94% of fatigue life). The strengthened beam, F3, failed by fracture of the steel beam after 298893 cycles. Looking at Figure 4.42(a), (b) and (c), the strain ranges and strain values dramatically increased after debonding of the plate.

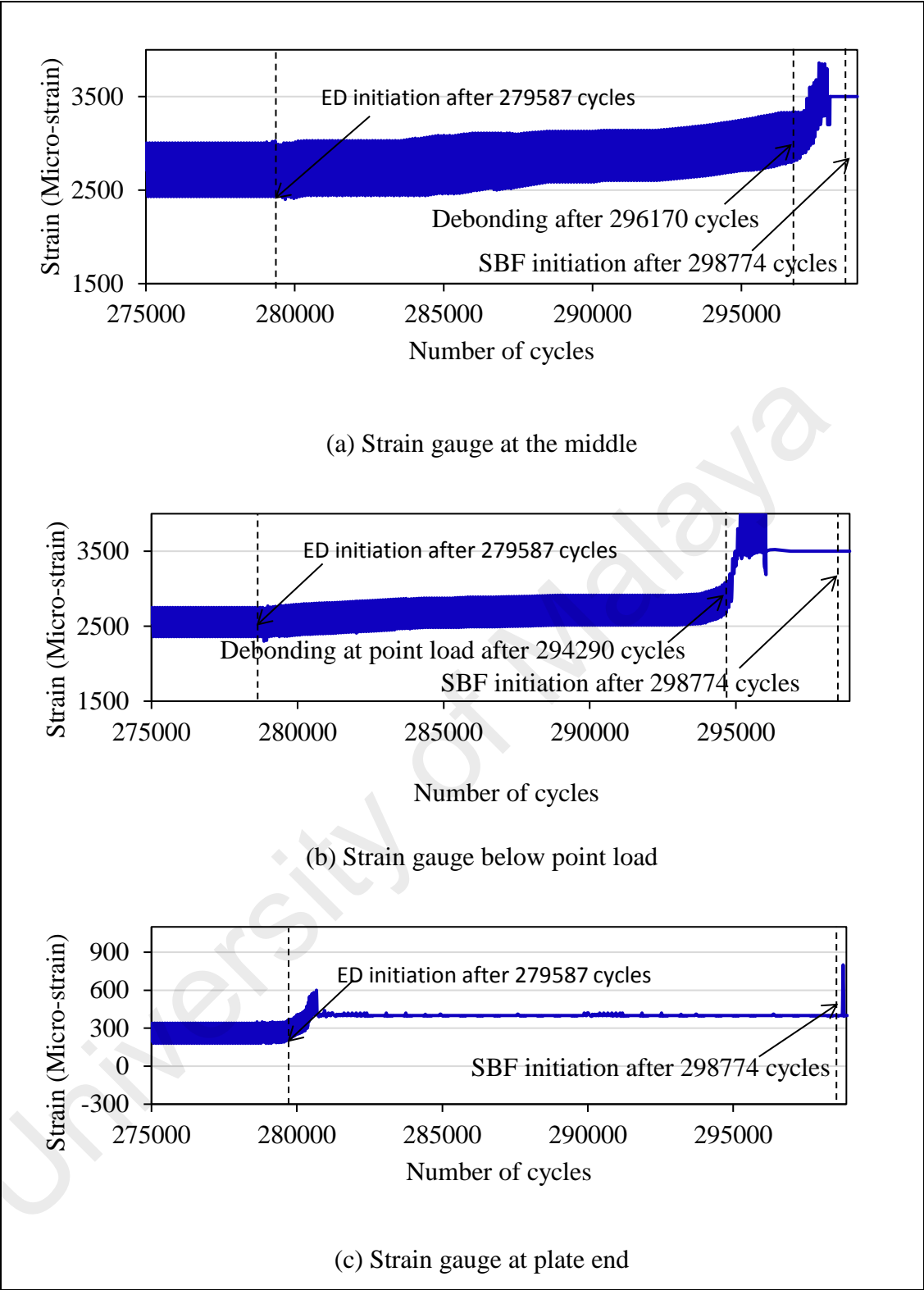


Figure 4.42: Strain in the tension plate versus number of cycles for specimen with a rectangular shape (F3)

(b) Specimen F4

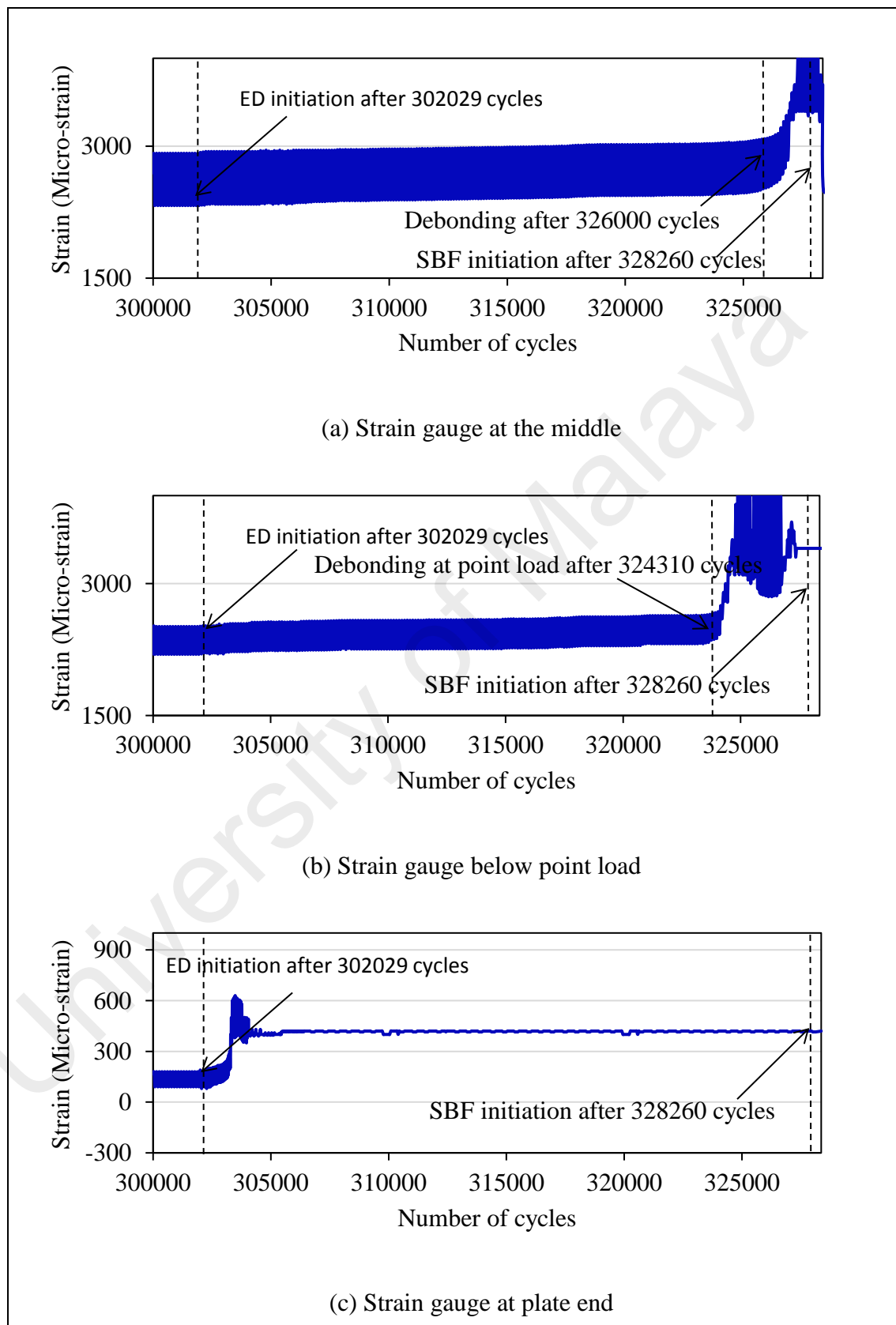
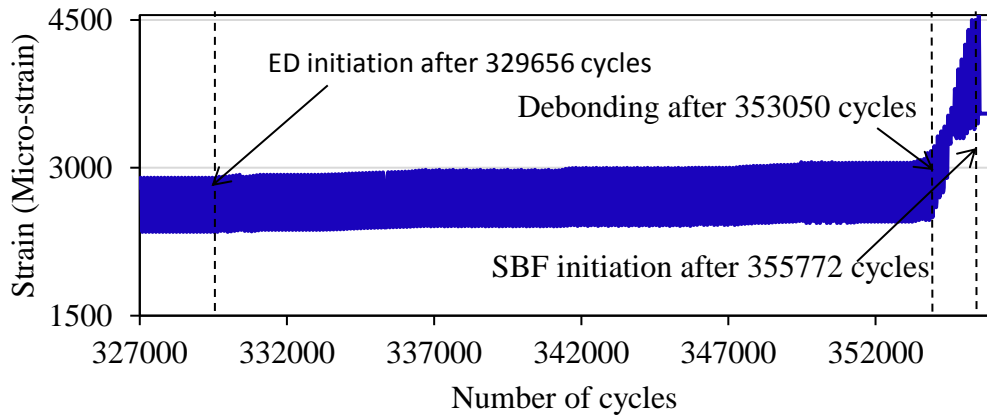


Figure 4.43: Strain in the tension plate versus number of cycles for specimen with a semi-ellipse end shape (F4)

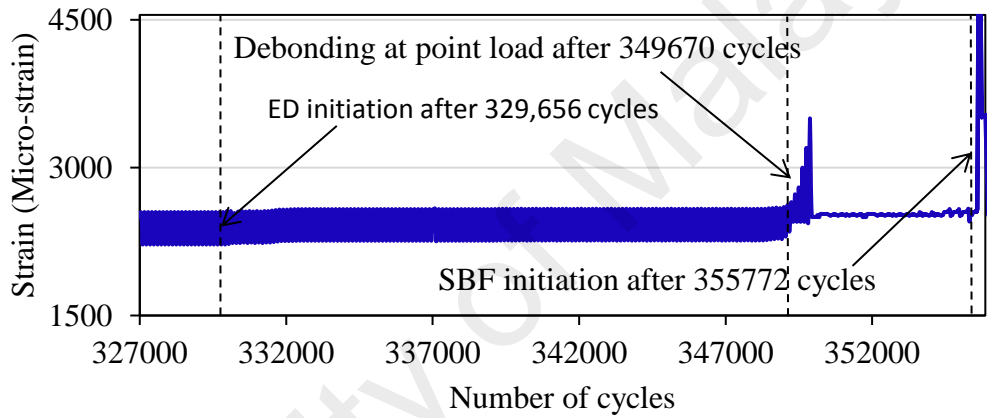
The debonding of the plate for specimen F4, strengthened with semi-ellipse CFRP end cutting shape, was initiated by ED at 302029 cycles. CFRP plate debonding occurred below point load after 324310 cycles and propagated to the mid span of the beam after 326000 cycles. The fracture of the steel beam started below point load after plate debonding at 328260 cycles, followed by the specimen failure at 328364 cycles. The plots of strain variation versus life at mid span, below point load and plate end on the tension CFRP plate for specimen F4 are presented in Figure 4.43(a) - (c). For this specimen, strain data for only three gauges are plotted on the CFRP plate. The strain range versus number of cycles was stable until plate debonding occurred and was accompanied by a sharp increase in strain gauges at the middle and below point loads. Strain gauge at the plate end exhibited a rapid increase in strain after ED of the plate.

(c) Specimen F5

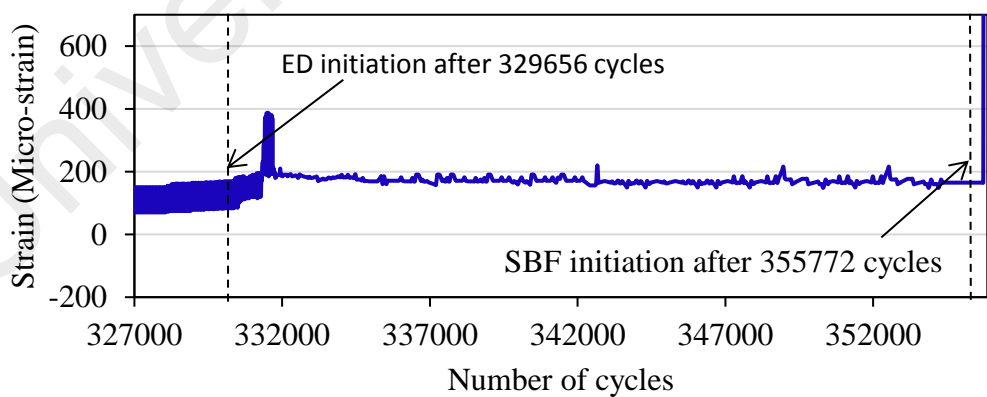
Plate debonding initiation in specimen F5, strengthened with a semi-circular end shape was observed at the end of the CFRP plate after 329656 cycles. After 354712 cycles, the CFRP plate was debonded at point load level followed by plate debonding at the middle after 3380 cycles. The strengthened specimen failed by steel beam fracture after 355866 cycles. Figure 4.44(a) - (c) shows the variation of strain gauge data in the CFRP plate with a semi-circular end shape for the specimen F5. Looking at Figure 4.44, the strain ranges and strain values dramatically increase after debonding of the plate. Looking at the strain profiles and strain values along the strips, it can be seen that the profiles of strain are generally higher at the middle of the plate. Debonding of the CFRP plates caused abrupt increase in tensile strain.



(a) Strain gauge at the middle



(b) Strain gauge below point load



(a) Strain gauge at plate end

Figure 4.44: Strain in the tension plate versus number of cycles for specimen with a semi-circular end shape (F5)

(d) Specimen F6

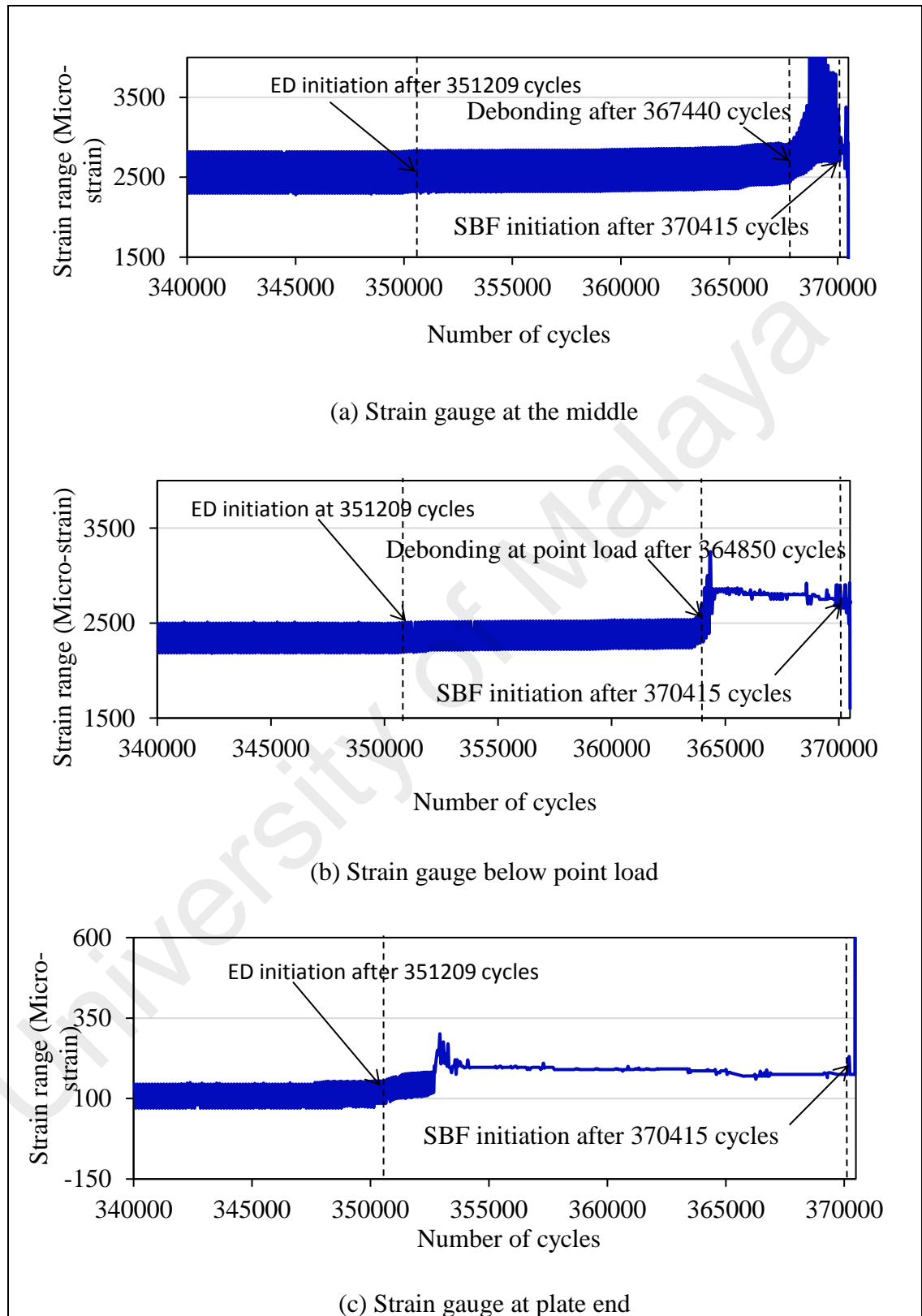


Figure 4.45: Strain in the tension plate versus number of cycles for specimen with a trapezoidal shape (F6)

End debonding initiation in the specimen F6, with a trapezoidal CFEP in-plane end cutting shape was observed at 351209 cycles (94% of fatigue life). Plate debonding below the point load occurred at 364850 cycles and propagated to the mid span after 367440 cycles. The specimen failed by brittle fracture of the steel beam at 370493 cycles. Fracture was initiated below the point load after 370415 cycles (99.96% of fatigue life) and grew through the bottom flange thickness to the web. Figure 4.45(a) - (b) presents the strain-life variation in the tension CFRP plate with a trapezoidal end shape for the strengthened specimen F6. The strain curves are displayed for cycles 340000 to 370493. A similar strain amplitude was measured for all strain gauges until debonding of the plate occurred during the fatigue test under cyclic loading. A strain fluctuation of the strain profile is presented in Figure 4.42 to Figure 4.45, and indicates failure of adhesive bonding. Compared the strain data from the strain gauge located at the plate end in Figure 4.42(c) to Figure 4.45(c), it can be seen that the CFRP plate using a trapezoidal end shape contributes to decreased strain than other plate end shapes.

Figure 4.46 indicates the normal strain along the CFRP plate for all specimens with different CFRP end shapes at the fatigue life of 279500 cycles. It illustrates that the maximum strain along the plate occurred for the rectangular end cutting shape. For all other shapes, strain values between the mid span and point load was almost similar. After point load, the strain reduced toward the CFRP plate tip. The highest reduction in strain was achieved by the trapezoidal end cutting shape. This shows that the CFRP in-plane end cutting shape is effective as well as the tapered cutting shape.

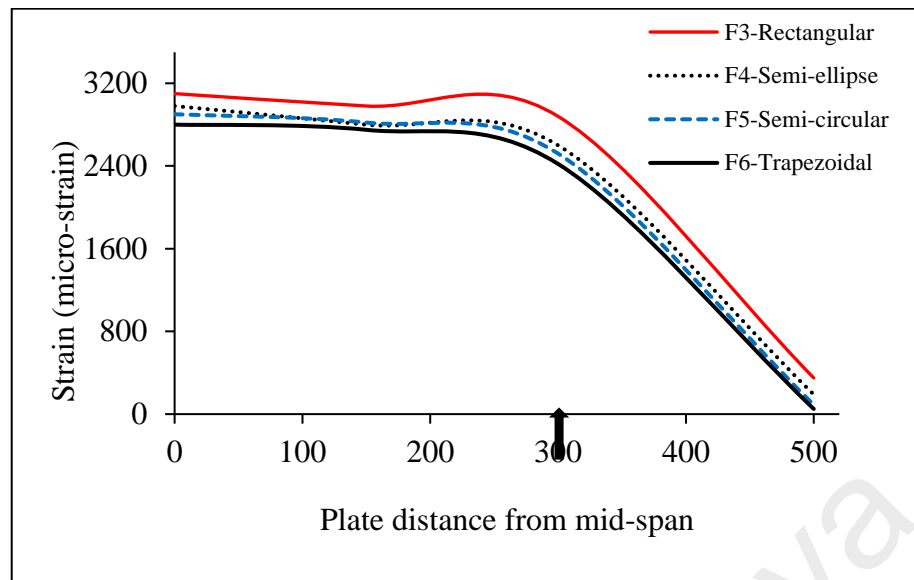


Figure 4.46: Strain on CFRP plate for different in-plane CFRP end shapes at the level of 279500 cycles

Therefore, it can be concluded that the application of trapezoidal in-plane CFRP end cutting shapes is more effective in delaying end debonding initiation by decreasing strain at the end of the plate. It also increases the fatigue life of strengthened wide-flange steel I-beams.

4.3.2 CFRP fabrics anchoring

The experimental result with specifications, fatigue life, and failure modes of the strengthened specimens using CFRP fabrics anchorage are presented in Table 4.12.

The effects of the fabrics anchoring system on the structural behaviour of wide-flange steel I-beams under cyclic loading were investigated.

Table 4.12: Fatigue test result of specimens with and without anchorage

No.	Specimens ID	Specification of CFRP plates			Anchorage	% of loading	Debonding initiation (No. of cycles)	Plate debonding at mid-span (No. of cycles)	Fatigue life (No. of cycles)	Increments (%)	Failure mode
		L_{CFRP} (mm)	Plate area (mm ²)	End shapes							
1	F2 (CB)	N/A	N/A	N/A	N/A	80%	-	-	241181	-	SBF
2	F3	1000	100000	Rectangular	N/A	80%	279587	296170	298893	23.93%	ED-SBF
3	F6	1025	100000	Trapezoidal	N/A	80%	351209	367440	370493	53.62%	ED-SBF
4	F7	1000	100000	Rectangular	√	80%	518685	569650	575401	138.60%	ICD-SBF

ED: End-debonding; ICD: Intermediate crack debonding; SBF: Steel beam fractured

4.3.2.1 Failure mode

Table 4.12 indicates the sequences of failure modes of anchored specimens (F7) under fatigue. It shows that the failure in strengthened specimens F7, with CFRP fabrics' anchorage, was initiated by intermediate debonding (IC debonding) below the point load and propagated to the mid span. The beam failed by fracture of the steel beams on the same side of plate debonding after 575401 cycles. Steel beam fracture was initiated beside the stiffener below the point load at 99.91% of fatigue life and grew through the thickness of the tension flange to the web.



Figure 4.47: Failure mode of anchored specimen with CFRP fabrics (F7) under fatigue

Figure 4.47 shows the failure mode of the strengthened specimen with anchorage under cyclic loading. It indicates that IC debonding occurred between the steel surface and the CFRP plate in the adhesive bonding. When normal stress and local interfacial stresses between the plate and steel surface reach critical values, intermediate debonding initiates below the loading point on the side of the hinge

support and propagates to the mid span of the beam. No debonding was observed at end of the plate section which was covered by the CFRP fabrics' anchorage.

Figure 4.47 also shows the brittle fracture of the steel beam below the point load under fatigue. The anchored specimen subjected to a high cyclic loading exhibited a large brittle fracture. The form of brittle fracture being addressed had been termed "constraint-induced fracture". Fracture of the steel beams occurred beside the stiffeners, which are connected by welding to the flange and web below the point load. High residual stress influence to fracture failures due to welding between stiffeners and steel beams below point load. The fracture occurred at 9.8% of fatigue life after the initiation of intermediate debonding below point load in the anchored specimen. The catastrophic fatigue fracture shown in Figure 4.47 was the result of fracture growth from the bottom flange through the web at beside the stiffener in a few cycles.

The CFRP fabrics' anchoring was more effective to mitigate ED problems under cyclic loading. This type of anchoring was not capable of preventing intermediate debonding between the steel surface and CFRP plate.

4.3.2.2 Fatigue life and failure initiation life

The variation of fatigue life for strengthened specimens with and without anchorage is presented in Table 4.12. It illustrates that the fatigue life of specimens F7, with CFRP fabrics anchorage, increased by 92.50%, and 138.60% compared to the strengthened specimen with a rectangular end shape (F3) and unstrengthened beam (F2), respectively. The increment of fatigue life in the anchored specimen was 55.30% of the specimen with the best in-plane CFRP end cutting shape (trapezoidal) in this research.

Table 4.13: Failure initiation life of specimens with and without anchorage

Specimens ID	CFRP end shape	Anchor	ED initiation n life (No. of cycles)	SBF_{il} (No. of cycles)	$\alpha_i = \frac{SBF_{il}(specimens)}{SBF_{il}(CB)}$
F2 (CB)	-		-	241002	1.00
F3	Rectangular	without	279587	298774	1.24
F6	Trapezoidal	Without	351209	370415	1.54
F7	Rectangular	with	518685	574880	2.40

α_i : increase rate of steel beam fracture (SBF) initiation life, SBF_{il} : SBF initiation life

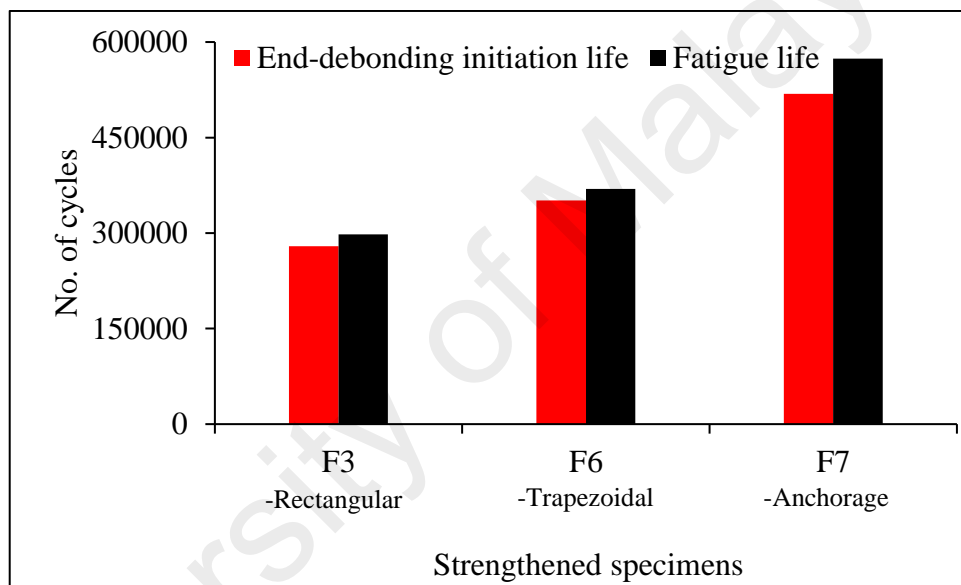


Figure 4.48: Comparison of ED initiation life and fatigue life of specimens with and without anchorage

Table 4.13 presents the debonding initiation life and steel beam fracture initiation life of anchored specimen compared to unanchored specimens. The initiation of intermediate debonding in specimen with fabrics anchorage at below the point load occurred after 518685 cycles (90.4% of fatigue life). The increment of debonding initiation life in the anchored specimen was 48% to 85.50% of the strengthened specimen without an anchor. Figure 4.48 shows the comparison between the debonding initiation life and fatigue life for strengthened specimens with and without anchoring.

The increased rate of fracture initiation life of strengthened specimens with and without anchorage is exposed in Table 4.13. The SBF initiation life (574880 cycles) of anchored specimen F7 was 2.40 times that of unstrengthened specimen F2, whereas strengthened specimens without anchorage were 1.24 - 1.54 times that of F2.

The application of CFRP fabrics' anchorage in strengthened wide-flange steel I-beams with bonded composite CFRP plates significantly increase the fatigue life and the failure initiation life.

4.3.2.3 Deflection versus number of cycles

The deflection ranges versus the number of cycles graph for anchored specimen F7, strengthened by an externally bonded composite CFRP plate, is presented in Figure 4.49. The deflection ranges were measured at mid span during fatigue testing under sinusoidal repeated loading. The figure documents the critical stages for the specimen in terms of intermediate debonding at the plate end and mid span, and steel beam fracture of the beams. A similar trend for deflection versus number of cycles is observed for each strengthened specimen. The deflection slowly increases after the initiation of IC debonding at point load after 518685 cycles until propagation of plate debonding to mid span of the beam. The increments of the deflection are more rapid when CFRP plate debonding occurs at mid span, followed by a sudden increase in deflection after the fracture initiation of the beam below the point load after 574880 cycles and grew through the bottom flange thickness towards the web.

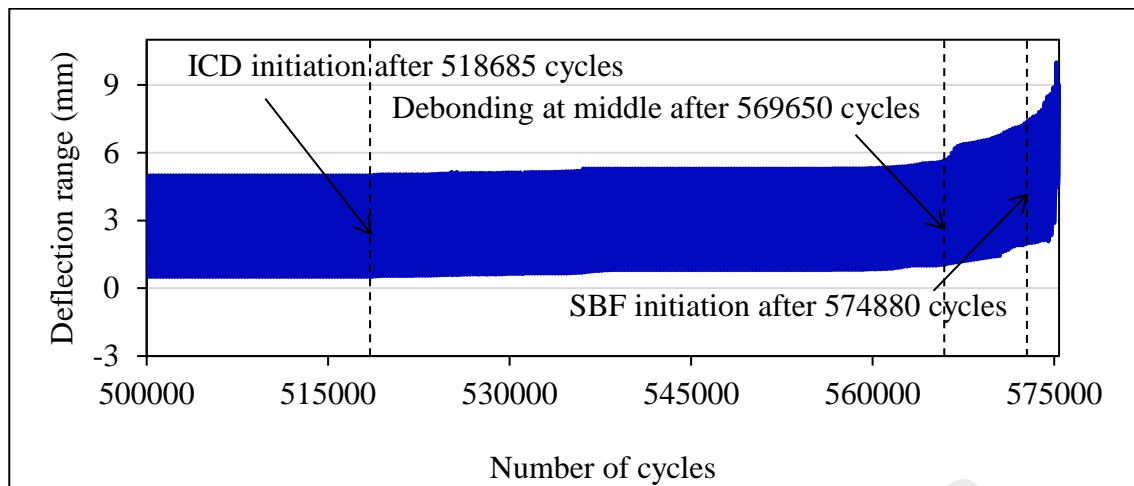


Figure 4.49: Deflection ranges versus number of cycles of an anchored specimen (F7)

Figure 4.50 presents the variation of deflection versus life for strengthened specimens with and without anchorage. The maximum deflection curves have been drawn for the whole fatigue life of the specimens. Looking at Figure 4.50, it can be indicated that: (1) the highest deflection belongs to the unstrengthened bare beam (F2), while the lowest deflection belongs to anchored strengthened specimen presenting the uppermost stiffness increase for that specimen F7; (2) the deflection values are intensely increased at the end of fatigue life due to sudden catastrophic failure through the tension flange to the web of the steel beams; and (3) the low deflection value in the specimen with anchorage shows the high fatigue life and indicates the influence of CFRP fabrics' anchoring system on the specimen stiffness.

The application of anchorage at the end of the fiber composite plate significantly improves the stiffness and fatigue life due to reduction of deflection values.

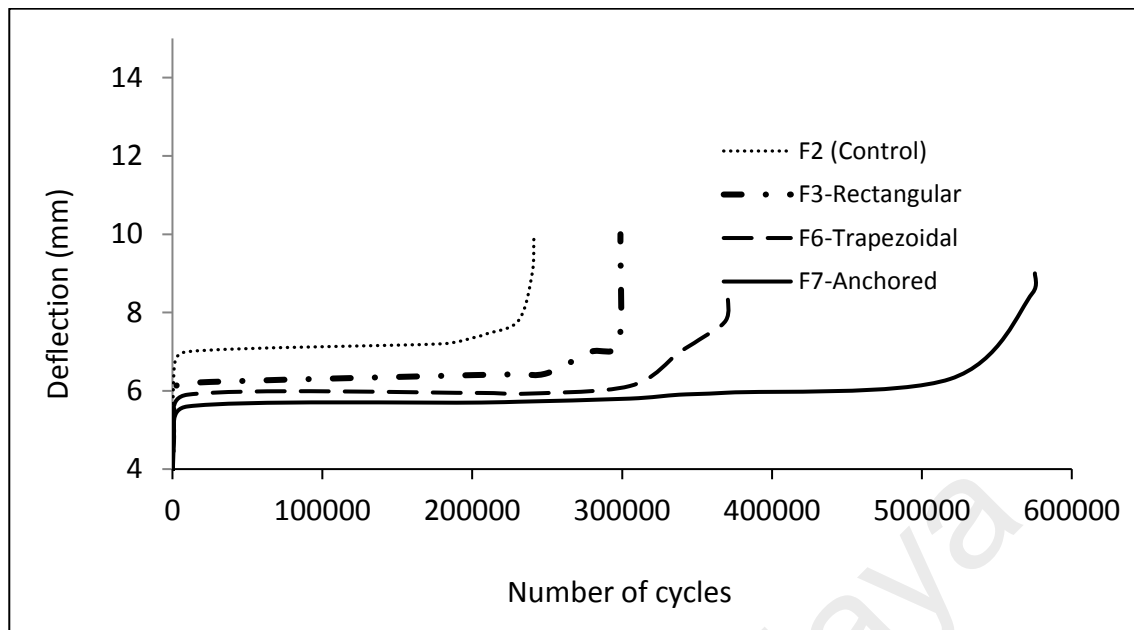
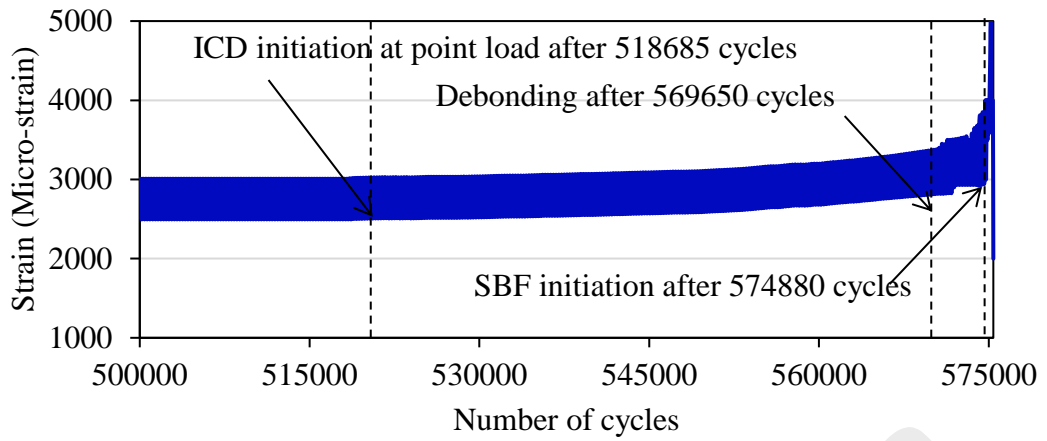


Figure 4.50: Maximum deflection versus number of cycles curve for strengthened specimens with and without anchorage

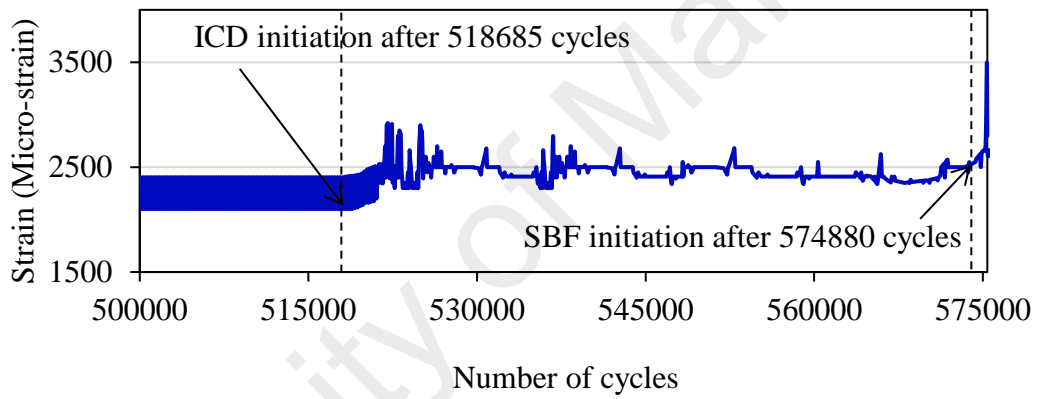
4.3.2.4 Strain versus life

The strain ranges versus number of cycles at debonding and steel beam fracture initiation for anchored specimens is shown in Figure 4.51(a) - (c). The measured strains on the CFRP plate at the middle, below point load and at the plate end are presented in detail. The strain curves are plotted for cycles 500000 to 575401. The figure shows that the slope of the strain curves changes as the number of cycles increases.

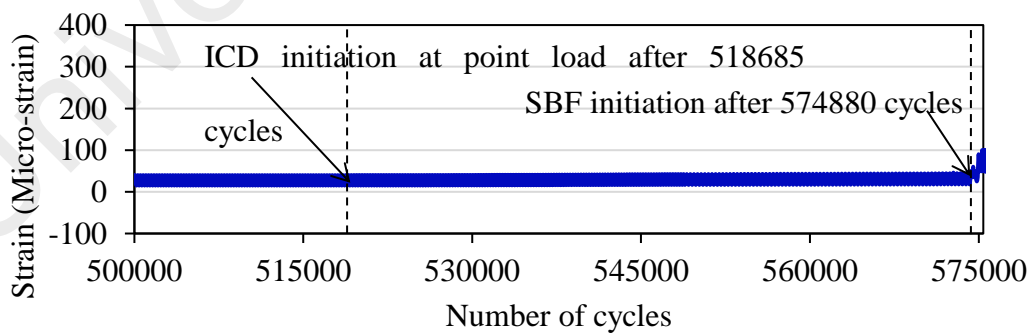
The strain values in the anchored beams were stable until the initiation of intermediate debonding (IC debonding) between the composite plate and steel surface. IC debonding was initiated below point load after 518685 cycles (90.2% of fatigue life) and propagated towards the mid span after 569650 cycles. The anchored specimen failed by brittle fracture of the beam at 575401 cycles.



(a) Strain gauge at the middle



(b) Strain gauge below point load



(c) Strain gauge at plate end on the wrapping

Figure 4.51: Strain in the tension plate versus number of cycles for an anchored specimen (F7)

In the strain gauge at the plate end, a constant strain profile is observed until specimen fracture occurs, indicating no ED, shown in Figure 4.51(c). The strain gauge below point load was stopped after intermediate debonding of the CFRP plate (Figure 4.51(b)). The strain values increased progressively for the strain gauge located at the middle of the composite plate (Figure 4.51(a)). However, the strain ranges increased more rapidly as the number of cycles increased. Crack growth into the web and plate debonding and fracture growth through the bottom flange to the beam web was conveyed by a substantial increase in strain of the CFRP plate prior to failure.

Figure 4.52 shows the maximum normal strain along the tension composite plate for specimens with and without anchorage at the cycle 279500. It illustrates that the maximum strain along the plate was higher for the externally bonded strengthened plate without anchorage. The slope of the strain curve followed a similar trend in the plate for all specimens, except the anchored region of Specimen F7. A significant reduction in strain was achieved by anchorage at the plate end, which was covered using CFRP fabrics. This is a promising discovery which contributes to the mitigation of end problems.

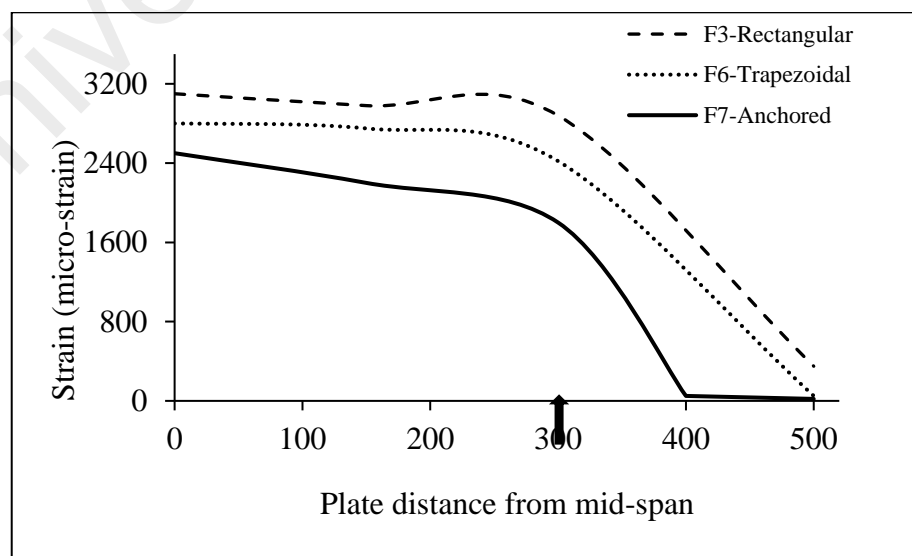


Figure 4.52: Maximum strain on CFRP plates for specimens with and without anchorage at 279500 cycles

Therefore, it can be concluded that application of end-anchoring using CFRP fabrics is effective against delamination and debonding at the end of externally bonded CFRP plates, and this application strengthens wide-flange steel I-beams under fatigue.

4.3.3 Comparison of predicted and experimental fatigue data

To validate the fatigue strength of the experimental results of strengthened wide flange steel I-beams, a FE simulation was used. A sinusoidal cyclic load was applied with a load ratio of $R = 0.1$. A maximum load for the fatigue test of 80% of the static capacity of the control specimens was applied. The frequency of the cyclic loading was set at 3 Hz in the fatigue investigation.

FEMs were employed with the same dimensions and geometry as the experimentally tested strengthened and unstrengthened specimens for prediction of fatigue behaviour. A comparison of predicted fatigue life using finite element analysis with experimental test results for the steel beam specimens is given in Table 4.14.

Table 4.14: Comparison of predicted fatigue life with experimental result

No.	Specimens ID	Specification		Fatigue life (Number of cycles)	
		CFRP end shapes	Anchorage by CFRP fabrics	Numerical	Experimental
1	F1 (UB)	-	-	2000000	2000000
2	F2 (CB)	-	-	242045	241181
3	F3	Rectangular	-	305524	298893
4	F4	Semi-ellipse	-	339275	328364
5	F5	Semi-circular	-	353920	355866
6	F6	Trapezoidal	-	377876	370493
7	F7	Rectangular	With (3 layers)	587570	575401

A catastrophic fatigue fracture below the point load was observed in all the steel beams after debonding of the CFRP plate at a load range of 10% - 80%. To evaluate the validity of the experimental results, a non-linear interface element was applied for modelling the behaviour of the steel-CFRP interface. The fatigue fracture below the point load and plate debonding of simulated strengthened steel specimens is presented in Figure 4.53. The failure of all strengthened specimens with in-plane CFRP end cutting shapes was initiated by ED.

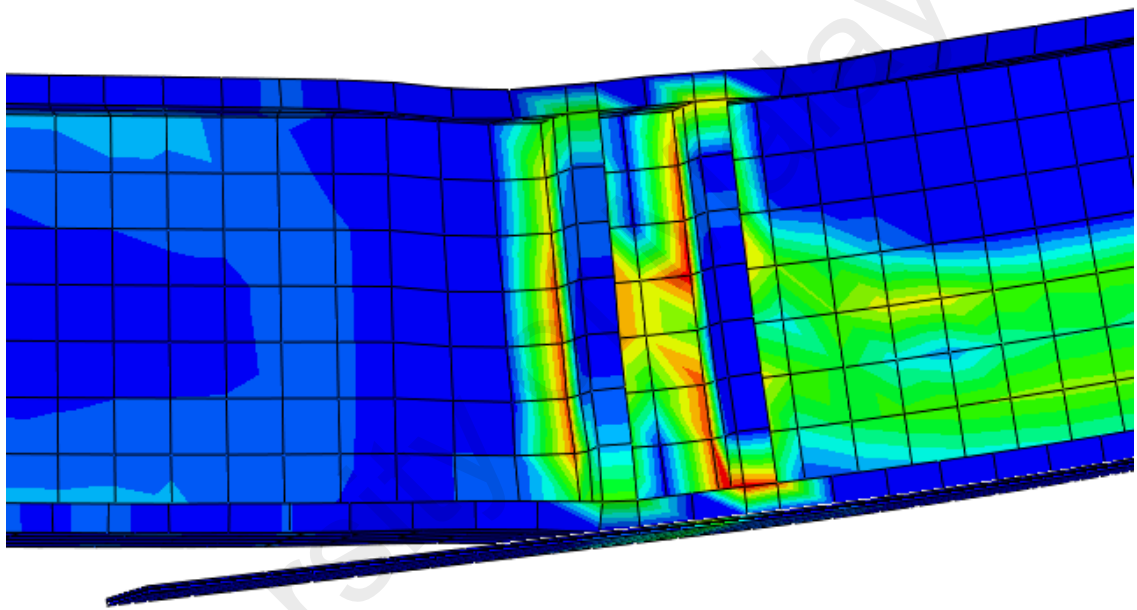


Figure 4.53: End-debonding and steel beam fracture initiation at below point load under fatigue (FEM)

Anchored specimens F7, F8, F9 and F10, using different layers of CFRP fabrics/wrapping with lengths of 220 mm and 175 mm were modelled to predict the fatigue life and failure mode (Table 4.15). The failure of the model F7 and F10, anchored with 3 layers of CFRP fabrics, was initiated by IC debonding in the plate-steel interface below the point load whereas specimen F8, anchored using one layer, and F9, anchored using two layer fabrics/wrapping, failed by a wrapping fracture. The fracture of the CFRP wrapping indicates CFRP plate ED. Hence, the proposed

end anchorage using three layers of CFRP fabrics/wrapping can mitigate end debonding of the plate for the strengthened wide-flange steel I-beams. A simulated failure mode with IC debonding of the CFRP plate of anchored specimen is presented in Figure 4.54. The fatigue life of the anchored specimen F7 from the experimental investigation and the numerical simulation was 575401 and 587570 cycles, respectively. In addition, validations were accomplished by comparing the load-deflection diagram of the strengthened specimens obtained from the experimental and numerical data at 100000 cycles and 360000 cycles (Figure 4.55). The finite element modelling of tested beams was found to provide accurate prediction of the fatigue behaviour of strengthened and unstrengthened beams.

Table 4.15: Predicted fatigue life and failure mode of anchored beams (FEM)

Specimens ID	CFRP plate end shape	Layer of CFRP fabrics	Fatigue life (No. of cycles)	Failed
F8	Rectangular	1	390482	CFRP fabrics fracture
F9	Rectangular	2	547655	CFRP fabrics fracture
F7	Rectangular	3	587570	CFRP plate (ICD)
F10	Trapezoidal	3	589685	CFRP plate (ICD)

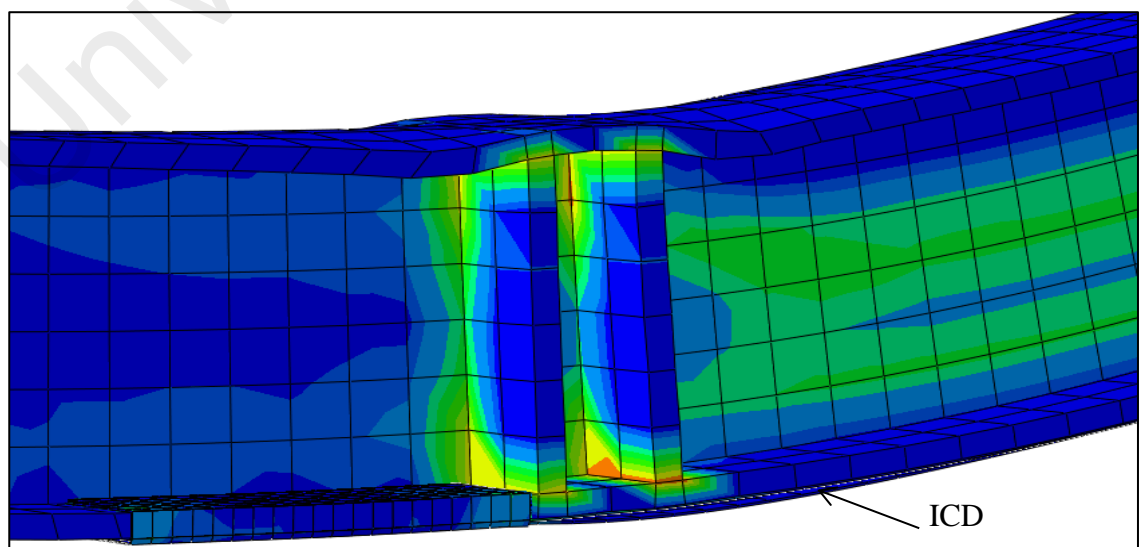


Figure 4.54: Fatigue failure of anchored specimen, F7 (FEM)

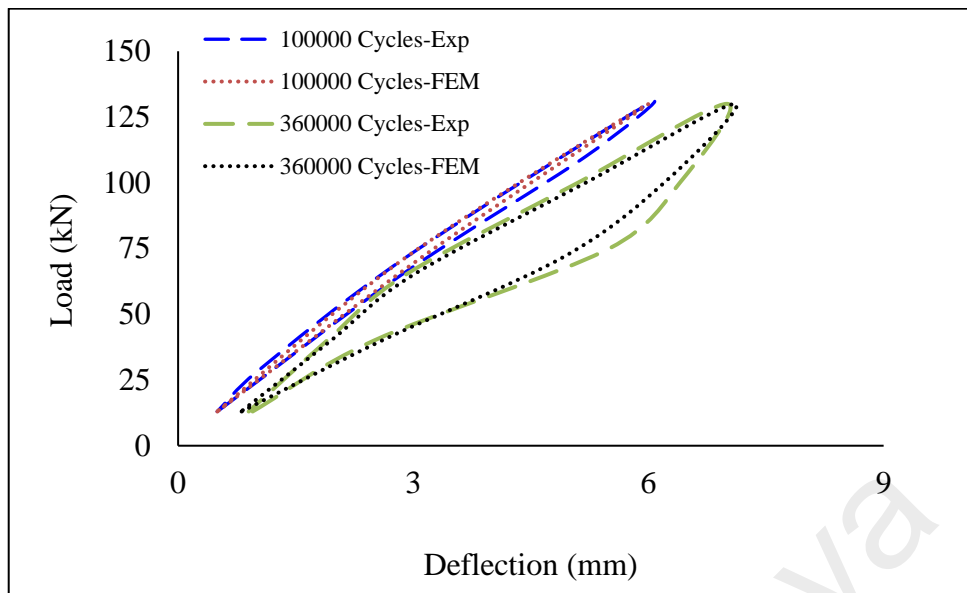


Figure 4.55: Load versus deflection for strengthened beam with in-plane end cutting shape (specimen F6)

University of Malaya

CHAPTER 5: CONCLUSIONS

The conclusion in terms of the monotonic strength and fatigue performance are presented in this chapter. The correlation between the results of the experiment and finite element modelling showed satisfactory agreement and successfully captured the failure mode of the strengthened wide-flange steel I-beams under monotonic and fatigue investigations.

5.1 Monotonic strength

1. The use of steel plate stiffeners does not only prevent stress concentration below the point load, but it can also help to delay the plate debonding of the externally bonded CFRP plate. The use of lateral bracing also contributes to retard the failure of the CFRP plate by preventing LTB.
2. To investigate the effects of end cutting shapes, four different in-plane CFRP end cutting shapes were considered. The strain on adhesive at the CFRP tip for trapezoidal in-plane CFRP end cutting shape decreased significantly. The trapezoidal end was the best of the investigated in-plane CFRP end cutting shapes in delaying ED initiation. Specimens strengthened with trapezoidal plate end showed significant increases in both in-plane flexural strength and stiffness.
3. The use of combined in-plane and tapered plate with spew fillets of adhesive resulted in an increment in the load bearing capacity of the beam. The use of spew fillets of adhesive at the tips of the CFRP plate significantly delayed the EDL and ED failure modes.
4. The application of CFRP fabrics' anchoring greatly increased the load bearing capacity (24%) and ductility due to prevention of ED and EDL. It also

significantly decreased the rate of strain in the tension CFRP composite plate before IC debonding of the plate. The anchored specimen failed by intermediate debonding in the steel-plate interface. Future research should focus on different measures for preventing the IC debonding problem, which can lead to safer design and enhanced utilization of the strength of beams. The nonlinear numerical analysis showed that the plate end anchorage using three layers with 220 x 175 mm CFRP fabrics can mitigate end debonding failure mode of the strengthened wide-flange steel I-beams. The simulation of the flexural behavior with plate debonding of monotonic specimens were in good agreement with the experimental results.

5.2 Fatigue performance

1. The fatigue performance of wide-flange steel I-beams can be enhanced significantly by applying in-plane CFRP end cutting shapes. The use of in-plane CFRP end cutting shapes increased the fatigue life to about 24% - 54%. The higher improvement of fatigue life was achieved in the strengthened specimen with a trapezoidal end shape. Hence, a CFRP plate with a trapezoidal end shape can prolong the fatigue life of the beam more effectively than other in-plane CFRP end cutting shapes.
2. The application of anchorage using three layers CFRP fabrics greatly improves the fatigue life (139%) of externally bonded strengthened beams.
3. For beams tested at a high load range of fatigue (10% - 80%), all strengthened and unstrengthened beams failed by steel beam fracture below point load. In the strengthened beams with different in-plane end cutting shapes, the failure was initiated by ED. On the other hand, failure of the anchored specimen involved

fracture through the bottom flange and into the web, followed by intermediate debonding between steel surface and plate. The finite element modelling of tested beams was found to provide accurate prediction of the behaviour of beams. The results also revealed the importance of mitigating ED initiation, which indicates that the anchorage using CFRP fabrics is consistent in fatigue resistance for externally bonded, strengthened wide flange steel I-beams.

5.3 Recommendations for future work

The following recommendations are suggested for future research in this area:

1. An effective surface treatment technique that can retard failure at the adhesive/steel interface under cyclic loading needs to be developed for use in practice.
2. The effects of the thickness of the adhesive on the EBR system requires more investigation. In addition, the optimum adhesive thickness should be studied to slow down delamination and debonding.
3. The mitigation of IC debonding should be explored for monotonic and cyclic loading.
4. A better estimation of the ductility of FRP strengthened wide-flange steel I-beams should be studied.
5. The fatigue behavior of pre-stressed wide-flange steel I-beams strengthened with FRP should be examined.
6. The optimum size of welding for stiffeners connected with steel beams below the point load should be investigated under cyclic loading.

REFERENCES

- ABAQUS/CAE. 6.12 User's manual;. (2014).
- Abdel Wahab, M. (2012). Fatigue in Adhesively Bonded Joints: A Review. *ISRN Materials Science*, 2012.
- Abed, G. (2012). *Effects of temperature on the adhesive bonding in steel beams reinforced with CFRP composites*. University of Southampton.
- Adams, R., Papiatt, N., and Coppedale, J. (1978). Prediction of strength of joints between composite materials. *Jointing in fibre reinforced plastics*, 64-78.
- Adams, R., and Peppiatt, N. (1974). Stress analysis of adhesive-bonded lap joints. *The Journal of Strain Analysis for Engineering Design*, 9(3), 185-196.
- Aljabar, N., Zhao, X., Al-Mahaidi, R., Ghafoori, E., Motavalli, M., and Powers, N. (2016). Effect of crack orientation on fatigue behavior of CFRP-strengthened steel plates. *Composite Structures*, 152, 295-305.
- Allan, R., Bird, J., and Clarke, J. (1988). Use of adhesives in repair of cracks in ship structures. *Materials science and technology*, 4(10), 853-859.
- ANSI, B. (2005). AISC 360-05-Specification for Structural Steel Buildings. *Chicago~AISC*.
- Ashcroft, I. (2004). A simple model to predict crack growth in bonded joints and laminates under variable-amplitude fatigue. *The Journal of Strain Analysis for Engineering Design*, 39(6), 707-716.
- Baker, A. (1987). *Fibre Composite Repair of Cracked Metallic Aircraft Components*. Paper presented at the 1987 Australian Aviation Symposium: 'Innovate or Enervate'; Preprints of Papers, The, c.
- Bannantine, J. A., Comer, J. J., and Handrock, J. L. (1990). *Fundamentals of metal fatigue analysis* (Vol. 90): Prentice Hall Englewood Cliffs, NJ.
- Barnes, R., and Mays, G. C. (2001). The effect of traffic vibration on adhesive curing during installation of bonded external reinforcement. *Proceedings of the ICE-Structures and Buildings*, 146(4), 403-410.
- Bendemra, H., Compston, P., and Crothers, P. J. (2015). Optimisation study of tapered scarf and stepped-lap joints in composite repair patches. *Composite Structures*, 130, 1-8.
- Bennati, S., Colonna, D., and Valvo, P. S. (2016). A cohesive-zone model for steel beams strengthened with pre-stressed laminates. *Procedia Structural Integrity*, 2, 2682-2689.

- Benyamina, A. B., Meftah, S. A., Mohri, F., and Daya, E. M. (2013). Analytical solutions attempt for lateral torsional buckling of doubly symmetric web-tapered I-beams. *Engineering Structures*, 56, 1207-1219.
- Bhattacharya, B., and Ellingwood, B. (1998). Continuum damage mechanics analysis of fatigue crack initiation. *International Journal of Fatigue*, 20(9), 631-639.
- Bocciarelli, M., and Colombi, P. (2013). On the elasto-plastic behavior of continuous steel beams reinforced by bonded CFRP lamina. *Engineering Structures*, 49, 756-766.
- Bocciarelli, M., Colombi, P., Fava, G., and Poggi, C. (2009). Fatigue performance of tensile steel members strengthened with CFRP plates. *Composite Structures*, 87(4), 334-343.
- Bocciarelli, M., Colombi, P., Fava, G., and Sonzogni, L. (2016). Energy-Based Analytical Formulation for the Prediction of End Debonding in Strengthened Steel Beams. *Composite Structures*.
- Bouchikhi, A., Megueni, A., Gouasmi, S., and Boukoulou, F. (2013). Effect of mixed adhesive joints and tapered plate on stresses in retrofitted beams bonded with a fiber-reinforced polymer plate. *Materials & Design*, 50, 893-904.
- Bourban, P. E., McKnight, S. H., Shulley, S. B., Karbhari, V. M., and Gillespie, J. W. (1994). *Durability of steel/composites bonds for rehabilitation of structural components*. Paper presented at the Infrastructure@ sNew Materials and Methods of Repair.
- Brown, A. (1974). *The corrosion of CFRP-to-metal couples in saline environments*. Paper presented at the Proceedings of the 2nd International Conference on Carbon Fibres.
- Buyukozturk, O., Gunes, O., and Karaca, E. (2004). Progress on understanding debonding problems in reinforced concrete and steel members strengthened using FRP composites. *Construction and Building Materials*, 18(1), 9-19.
- Cadei, J., Stratford, T., Hollaway, L., and Dcukett, W. (2004). *Strengthening metallic structures using externally bonded fibre-reinforced polymers* (Vol. 595): CIRIA.
- Caglayan, B., Ozakgul, K., and Tezer, O. (2009). Fatigue life evaluation of a through-girder steel railway bridge. *Engineering Failure Analysis*, 16(3), 765-774.
- Chen, D., Weiss, B., and Stickler, R. (1996). A model for crack closure. *Engineering Fracture Mechanics*, 53(4), 493-509.
- Cheung, M., and Li, W. (2003). Probabilistic fatigue and fracture analyses of steel bridges. *Structural safety*, 25(3), 245-262.
- Choudhury, S. (2007). *Effects of a debonding flew size and location on the flexural performance of FRP retrofitted steel sections*. (master of Science), The University of Texas, Arlington.

- CNR, D. (2007). 202/2005. Guidelines for the design and construction of externally bonded FRP systems for strengthening existing structures – Metallic structures – Preliminary study. National Research Council, Rome.
- Colombi, P. (2005). Plasticity induced fatigue crack growth retardation model for steel elements reinforced by composite patch. *Theoretical and Applied Fracture Mechanics*, 43(1), 63-76.
- Colombi, P. (2006). Reinforcement delamination of metallic beams strengthened by FRP strips: fracture mechanics based approach. *Engineering Fracture Mechanics*, 73(14), 1980-1995.
- Colombi, P., Bassetti, A., and Nussbaumer, A. (2003a). Analysis of cracked steel members reinforced by pre-stress composite patch. *Fatigue & Fracture of Engineering Materials & Structures*, 26(1), 59-66.
- Colombi, P., Bassetti, A., and Nussbaumer, A. (2003b). Delamination effects on cracked steel members reinforced by prestressed composite patch. *Theoretical and Applied Fracture Mechanics*, 39(1), 61-71.
- Colombi, P., and Fava, G. (2015). Experimental study on the fatigue behaviour of cracked steel beams repaired with CFRP plates. *Engineering Fracture Mechanics*, 145, 128-142.
- Colombi, P., and Fava, G. (2016). Fatigue crack growth in steel beams strengthened by CFRP strips. *Theoretical and Applied Fracture Mechanics*.
- Cornetti, P., Corrado, M., De Lorenzis, L., and Carpinteri, A. (2015). An analytical cohesive crack modeling approach to the edge debonding failure of FRP-plated beams. *International Journal of Solids and Structures*, 53, 92-106.
- Curtis, P. (1989). The fatigue behaviour of fibrous composite materials. *The Journal of Strain Analysis for Engineering Design*, 24(4), 235-244.
- Czaderski, C., and Rabinovitch, O. (2010). Structural behavior and inter-layer displacements in CFRP plated steel beams—optical measurements, analysis, and comparative verification. *Composites Part B: Engineering*, 41(4), 276-286.
- Czaderski, C., Soudki, K., and Motavalli, M. (2010). Front and side view image correlation measurements on FRP to concrete pull-off bond tests. *Journal of Composites for Construction*, 14(4), 451-463.
- Damatty, A., and Abushagur, M. (2003). Testing and modeling of shear and peel behavior for bonded steel/FRP connections. *Thin-Walled Structures*, 41(11), 987-1003.
- Dawood, M., and Rizkalla, S. (2007). *Bond and splice behavior of CFRP laminates for strengthening steel beams*. Paper presented at the International conference on advanced composites in construction. United Kingdom: University of Bath.

- Dawood, M. M. R. (2005). Fundamental behavior of steel-concrete composite beams strengthened with high modulus carbon fiber reinforced polymer (CFRP) materials.
- Deng, J., Jia, Y., and Zheng, H. (2016). Theoretical and experimental study on notched steel beams strengthened with CFRP plate. *Composite Structures*, 136, 450-459.
- Deng, J., and Lee, M. M. (2007a). Behaviour under static loading of metallic beams reinforced with a bonded CFRP plate. *Composite Structures*, 78(2), 232-242.
- Deng, J., and Lee, M. M. (2007b). Fatigue performance of metallic beam strengthened with a bonded CFRP plate. *Composite Structures*, 78(2), 222-231.
- Deng, J., Lee, M. M., and Moy, S. S. (2004). Stress analysis of steel beams reinforced with a bonded CFRP plate. *Composite Structures*, 65(2), 205-215.
- Duong, C. (2006). A unified approach to geometrically nonlinear analysis of tapered bonded joints and doublers. *International Journal of Solids and Structures*, 43(11), 3498-3526.
- Erpolat, S., Ashcroft, I., Crocombe, A., and Abdel-Wahab, M. (2004). Fatigue crack growth acceleration due to intermittent overstressing in adhesively bonded CFRP joints. *Composites Part A: Applied Science and Manufacturing*, 35(10), 1175-1183.
- Fang, T. (2002). Study on U-shaped sheet behavior of anti-debonding in the concrete beam reinforced flexurally with FRP. *master's thesis, Tsingua University, China*.
- Fitton, M., and Broughton, J. (2005). Variable modulus adhesives: an approach to optimised joint performance. *International journal of adhesion and adhesives*, 25(4), 329-336.
- Gaylord, E. H., Gaylord, C. N., and Stallmeyer, J. E. (2007). Design of steel structures, Third edition.
- Ghafoori, E., and Motavalli, M. (2011). Analytical calculation of stress intensity factor of cracked steel I-beams with experimental analysis and 3D digital image correlation measurements. *Engineering Fracture Mechanics*, 78(18), 3226-3242.
- Ghafoori, E., and Motavalli, M. (2015a). Lateral-torsional buckling of steel I-beams retrofitted by bonded and un-bonded CFRP laminates with different pre-stress levels: Experimental and numerical study. *Construction and Building Materials*, 76, 194-206.
- Ghafoori, E., and Motavalli, M. (2015b). Normal, high and ultra-high modulus carbon fiber-reinforced polymer laminates for bonded and un-bonded strengthening of steel beams. *Materials & Design*, 67, 232-243.
- Ghafoori, E., Motavalli, M., Botsis, J., Herwig, A., and Galli, M. (2012). Fatigue strengthening of damaged metallic beams using prestressed unbonded and bonded CFRP plates. *International Journal of Fatigue*.

- Ghafoori, E., Motavalli, M., Nussbaumer, A., Herwig, A., Prinz, G., and Fontana, M. (2015). Design criterion for fatigue strengthening of riveted beams in a 120-year-old railway metallic bridge using pre-stressed CFRP plates. *Composites Part B: Engineering*, 68, 1-13.
- Ghafoori, E., Schumacher, A., and Motavalli, M. (2012). Fatigue behavior of notched steel beams reinforced with bonded CFRP plates: Determination of prestressing level for crack arrest. *Engineering Structures*, 45, 270-283.
- Grabovac, I., Bartholomeusz, R., and Baker, A. (1993). Composite reinforcement of a ship superstructure—project overview. *Composites*, 24(6), 501-509.
- Haghani, R., Al-Emrani, M., and Kligler, R. (2009). Interfacial stress analysis of geometrically modified adhesive joints in steel beams strengthened with FRP laminates. *Construction and Building Materials*, 23(3), 1413-1422.
- Harries, K. A., Varma, A., El-Tawil, S., Liu, J., Xiao, Y., Moy, S., . . . Hollaway, L. (2011). *Steel-FRP Composite Structural Systems*. Paper presented at the Composite Construction in Steel and Concrete VI.
- Harris, A., and Beevers, A. (1999). The effects of grit-blasting on surface properties for adhesion. *International journal of adhesion and adhesives*, 19(6), 445-452.
- Hashim, S. (1999). Adhesive bonding of thick steel adherends for marine structures. *Marine structures*, 12(6), 405-423.
- Hawileh, R. A., Rasheed, H. A., Abdalla, J. A., and Al-Tamimi, A. K. (2014). Behavior of reinforced concrete beams strengthened with externally bonded hybrid fiber reinforced polymer systems. *Materials & Design*, 53, 972-982.
- Henry, D. L. (1953). *A theory of fatigue damage accumulation in steel*. Ohio State University.
- Hildebrand, M. (1994). Non-linear analysis and optimization of adhesively bonded single lap joints between fibre-reinforced plastics and metals. *International journal of adhesion and adhesives*, 14(4), 261-267.
- Hoang-Ngoc, C.-T., and Paroissien, E. (2010). Simulation of single-lap bonded and hybrid (bolted/bonded) joints with flexible adhesive. *International journal of adhesion and adhesives*, 30(3), 117-129.
- Hollaway, L., and Cadei, J. (2002). Progress in the technique of upgrading metallic structures with advanced polymer composites. *Progress in Structural Engineering and Materials*, 4(2), 131-148.
- Hollaway, L. C., and Head, P. R. (2001). *Advanced polymer composites and polymers in the civil infrastructure*: Elsevier Science.
- Hu, L. L., Zhao, X. L., and Feng, P. (2016). Fatigue Behavior of Cracked High-Strength Steel Plates Strengthened by CFRP Sheets. *Journal of Composites for Construction*, 20(6), 04016043.

- James, M. (1992). Optimising the fatigue resistance of materials.
- Jiao, H., Mashiri, F., and Zhao, X.-L. (2012). A comparative study on fatigue behaviour of steel beams retrofitted with welding, pultruded CFRP plates and wet layup CFRP sheets. *Thin-Walled Structures*, 59, 144-152.
- Jiao, H., and Zhao, X.-L. (2004). CFRP strengthened butt-welded very high strength (VHS) circular steel tubes. *Thin-Walled Structures*, 42(7), 963-978.
- Johnson, W., and Mall, S. (1985). A fracture mechanics approach for designing adhesively bonded joints. *ASTM STP*, 876, 189-199.
- Jones, S. C., and Civjan, S. A. (2003). Application of fiber reinforced polymer overlays to extend steel fatigue life. *Journal of Composites for Construction*, 7(4), 331-338.
- Jumaat, M. Z., and Alam, M. A. (2008). Behaviour of U and L shaped end anchored steel plate strengthened reinforced concrete beams. *European Journal of Scientific Research*, 22(2), 184-196.
- Kambiz, N., and Mohd, Z. J. (2010). Shear strengthening of steel I-beams by using CFRP strips. *Scientific Research and Essays*, 5(16), 2155-2168.
- Karbhari, V., and Shulley, S. (1995). Use of composites for rehabilitation of steel structures-determination of bond durability. *Journal of Materials in Civil Engineering*, 7(4), 239-245.
- Kattan, P. I., and Voyiadjis, G. Z. (2002). *Damage mechanics with finite elements: practical applications with computer tools* (Vol. 1): Springer.
- Kawakam, Y., Kanaji, H., and Oku, K. (2011). Study on application of field signature method (FSM) to fatigue crack monitoring on steel bridges. *Procedia Engineering*, 14, 1059-1064.
- Keller, T., and Schollmayer, M. (2009). Through-thickness performance of adhesive joints between FRP bridge decks and steel girders. *Composite Structures*, 87(3), 232-241.
- Kelly, G. (2006). Quasi-static strength and fatigue life of hybrid (bonded/bolted) composite single-lap joints. *Composite Structures*, 72(1), 119-129.
- Kim, Y. J., and Brunell, G. (2011). Interaction between CFRP-repair and initial damage of wide-flange steel beams subjected to three-point bending. *Composite Structures*, 93(8), 1986-1996.
- Kim, Y. J., and Harries, K. A. (2011). Fatigue behavior of damaged steel beams repaired with CFRP strips. *Engineering Structures*, 33(5), 1491-1502.
- Kim, Y. J., and Heffernan, P. J. (2008). Fatigue behavior of externally strengthened concrete beams with fiber-reinforced polymers: State of the art. *Journal of Composites for Construction*, 12(3), 246-256.

- Kinloch, A., and Osiyemi, S. (1993). Predicting the fatigue life of adhesively-bonded joints. *The Journal of adhesion*, 43(1-2), 79-90.
- KUJAWSKI, D. (2003). Methods for crack opening load and crack tip shielding determination: a review. *Fatigue & Fracture of Engineering Materials & Structures*, 26(11), 1053-1067.
- Lang, T., and Mallick, P. (1998). Effect of spew geometry on stresses in single lap adhesive joints. *International journal of adhesion and adhesives*, 18(3), 167-177.
- Leander, J., Andersson, A., and Karoumi, R. (2010). Monitoring and enhanced fatigue evaluation of a steel railway bridge. *Engineering Structures*, 32(3), 854-863.
- Lemaitre, J., and Desmorat, R. (2005). *Engineering damage mechanics: ductile, creep, fatigue and brittle failures*: Springer.
- Linghoff, D., and Al-Emrani, M. (2010). Performance of steel beams strengthened with CFRP laminate—Part 2: FE analyses. *Composites Part B: Engineering*, 41(7), 516-522.
- Linghoff, D., Haghani, R., and Al-Emrani, M. (2009). Carbon-fibre composites for strengthening steel structures. *Thin-Walled Structures*, 47(10), 1048-1058.
- Liu, H., Xiao, Z., Zhao, X.-L., and Al-Mahaidi, R. (2009). Prediction of fatigue life for CFRP-strengthened steel plates. *Thin-Walled Structures*, 47(10), 1069-1077.
- Liu, H., Zhao, X., and Al-Mahaidi, R. (2005). *The effect of fatigue loading on bond strength of CFRP bonded steel plate joints*. Paper presented at the International symposium on bond. Proceedings of the International Symposium on Bond Behaviour of FRP in Structures (BBFS 2005).
- Loher, U., Mueller, B., Leutwiler, R., and Esslinger, V. (1996). *CFRP-strengthened aluminum structures*. Paper presented at the 17th int. SAMPE Europe conference on success of materials by combination, Basel.
- Lorenzo, L., and Hahn, H. T. (1986). Fatigue failure mechanisms in unidirectional composites. *Composite materials: fatigue and fracture, ASTM STP*, 907, 210-232.
- Lu, X., Teng, J., Ye, L., and Jiang, J. (2007). Intermediate crack debonding in FRP-strengthened RC beams: FE analysis and strength model. *Journal of Composites for Construction*, 11(2), 161-174.
- Maaddawy, T. E., and Soudki, K. (2008). Strengthening of reinforced concrete slabs with mechanically-anchored unbonded FRP system. *Construction and Building Materials*, 22(4), 444-455.
- Miller, T. C., Chajes, M. J., Mertz, D. R., and Hastings, J. N. (2001). Strengthening of a steel bridge girder using CFRP plates. *Journal of Bridge Engineering*, 6(6), 514-522.

- Monfared, A., Soudki, K., and Walbridge, S. (2008). *CFRP reinforcing to extend the fatigue lives of steel structures*. Paper presented at the Fourth International Conference on FRP Composites in Civil Engineering (CICE2008), Zurich, Switzerland.
- Moroni, F., Pironi, A., and Kleiner, F. (2010). Experimental analysis and comparison of the strength of simple and hybrid structural joints. *International journal of adhesion and adhesives*, 30(5), 367-379.
- Morsy, A. M., Helmy, K. M., El-Ashkar, N. H., and Nada, M. (2014). Flexural strengthening for RC beams using CFRP sheets with different bonding schemes. *Concrete Solutions 2014*, 313.
- Motavalli, M., and Czaderski, C. (2007). *FRP composites for retrofitting of existing civil structures in Europe: state-of-the-art review*. Paper presented at the International Conference of Composites & Polycon., American Composites Manufacturers Association. Tampa, FL, USA.
- Moy, S. (2002). *Early age curing under cyclic loading-an investigation into stiffness development in carbon fibre reinforced steel beams*. Paper presented at the Advanced Polymer Composites for Structural Applications in Construction: Proceedings of the First International Conference, Held at Southampton University, Uk, on 15-17 April 2002.
- Moy, S. (2007). *CFRP reinforcement of steel beams adhesive cure under cyclic load*. Paper presented at the Proc. 1st Asia-Pac. Conf. FRP in Struct.
- Moy, S., and Nikoukar, F. (2002). *Flexural behaviour of steel beams reinforced with carbon fibre reinforced polymer composite*. Paper presented at the Advanced Polymer Composites for Structural Applications in Construction: Proceedings of the First International Conference, Held at Southampton University, Uk, on 15-17 April 2002.
- Müller, W., Herrmann, G., and Gao, H. (1993). Elementary strength theory of cracked beams. *Theoretical and Applied Fracture Mechanics*, 18(2), 163-177.
- Narmashiri, K. (2011). *Carbon Fibre Reinforced Polymer Strips for Flexural and Shear Strengthening of Steel I-beams*. (PhD Thesis), University of Malaya.
- Narmashiri, K., and Jumaat, M. Z. (2011). Reinforced steel I-beams: A comparison between 2D and 3D simulation. *Simulation Modelling Practice and Theory*, 19(1), 564-585.
- Narmashiri, K., Jumaat, M. Z., and Sulong, N. H. R. (2012). Strengthening of steel I-beams using CFRP strips: an investigation on CFRP bond length. *Advances in Structural Engineering*, 15(12), 2191-2204.
- Narmashiri, K., Jumaat, M. Z., and Sulong, N. R. (2010). Investigation on end anchoring of CFRP strengthened steel I-beams. *International Journal of the Physical Sciences*, 5(9), 1360-1371.

- Narmashiri, K., Ramli Sulong, N., and Jumaat, M. Z. (2012). Failure analysis and structural behaviour of CFRP strengthened steel I-beams. *Construction and Building Materials*, 30, 1-9.
- Newman Jr, J. C. (1981). A crack-closure model for predicting fatigue crack growth under aircraft spectrum loading. *ASTM STP*, 748, 53-84.
- Nikouka, F., Lee, M., and Moy, S. (2002). *Strengthening of metallic structures using carbon fibre composites*. Paper presented at the IABSE Symposium Report.
- Ozbasaran, H. (2014). A Parametric Study on Lateral Torsional Buckling of European IPN and IPE Cantilevers.
- Paris, P., and Erdogan, F. (1963). A critical analysis of crack propagation laws. *Journal of Basic Engineering*, 85, 528.
- Phares, B. M., Wipf, T. J., Klaiber, F. W., Abu-Hawash, A., and Lee, Y.-S. (2003). *Strengthening of steel girder bridges using FRP*. Paper presented at the Proc., 2003 Mid-Continent Transportation Research Symp.
- Photiou, N., Hollaway, L., and Chryssanthopoulos, M. (2004). *An ultra-high modulus carbon/glass fibre composite system for structural upgrading of steel members*. Paper presented at the Proceedings of the 2nd International Conference on FRP Composites in Civil Engineering–CICE 2004.
- Piggott, M. R. (2002). *Load bearing fibre composites*: Springer.
- Pipinato, A., Pellegrino, C., and Modena, C. (2011). Fatigue assessment of highway steel bridges in presence of seismic loading. *Engineering Structures*, 33(1), 202-209.
- Pipinato, A., Pellegrino, C., and Modena, C. (2012). Fatigue Behaviour of Steel Bridge Joints Strengthened with FRP Laminates. *Modern Applied Science*, 6(10), p1.
- Raghavan, P., and Ghosh, S. (2005). A continuum damage mechanics model for unidirectional composites undergoing interfacial debonding. *Mechanics of materials*, 37(9), 955-979.
- Rance, V., and Evans, U. (1958). Corrosion and its Prevention at Bimetallic Contacts. *HM Stationary Office, London*, 1.91-91.94.
- Rasheed, H. A., Decker, B. R., Esmaily, A., Peterman, R. J., and Melhem, H. G. (2015). The Influence of CFRP Anchorage on Achieving Sectional Flexural Capacity of Strengthened Concrete Beams. *Fibers*, 3(4), 539-559.
- Rasheed, H. A., Harrison, R. R., Peterman, R. J., and Alkhrdaji, T. (2010). Ductile strengthening using externally bonded and near surface mounted composite systems. *Composite Structures*, 92(10), 2379-2390.
- Rizkalla, S., Dawood, M., and Schnerch, D. (2008). Development of a carbon fiber reinforced polymer system for strengthening steel structures. *Composites Part A: Applied Science and Manufacturing*, 39(2), 388-397.

- Saadatmanesh, H., and Tannous, F. E. (1999). Long-Term Behavior of Aramid Fiber Reinforced Plastic (ARFP) Tendons. *ACI materials Journal*, 96(3).
- Sallam, H., Ahmad, S., Badawy, A., and Mamdouh, W. (2006). Evaluation of steel I-beams strengthened by various plating methods. *Advances in Structural Engineering*, 9(4), 535-544.
- Sam, S., and Shome, M. (2010). Static and fatigue performance of weld bonded dual phase steel sheets. *Science and Technology of Welding & Joining*, 15(3), 242-247.
- Schnerch, D., Dawood, M., Rizkalla, S., and Sumner, E. (2007). Proposed design guidelines for strengthening of steel bridges with FRP materials. *Construction and Building Materials*, 21(5), 1001-1010.
- Schnerch, D., Dawood, M., Rizkalla, S., Sumner, E., and Stanford, K. (2006). Bond behavior of CFRP strengthened steel structures. *Advances in Structural Engineering*, 9(6), 805-817.
- Schnerch, D., Stanford, K., Sumner, E., and Rizkalla, S. (2005). *Bond behavior of CFRP strengthened steel bridges and structures*. Paper presented at the International Symposium on Bond Behaviour of FRP in Structures (BBFS 2005), International Institute for FRP in Construction.
- Sebastian, W., and Zhang, C. (2013). Observations from testing of indeterminate FRP-plated steel beams on flexible supports. *Composites Part B: Engineering*, 45(1), 200-214.
- Seleem, M., Sharaky, I., and Sallam, H. (2010). Flexural behavior of steel beams strengthened by carbon fiber reinforced polymer plates—Three dimensional finite element simulation. *Materials & Design*, 31(3), 1317-1324.
- Sen, R., Liby, L., and Mullins, G. (2001). Strengthening steel bridge sections using CFRP laminates. *Composites Part B: Engineering*, 32(4), 309-322.
- Shenoy, V., Ashcroft, I. A., Critchlow, G. W., and Crocombe, A. (2010). Fracture mechanics and damage mechanics based fatigue lifetime prediction of adhesively bonded joints subjected to variable amplitude fatigue. *Engineering Fracture Mechanics*, 77(7), 1073-1090.
- Siddique, M. A. A., and Damatty, A. E. (2013). Improvement of local buckling behaviour of steel beams through bonding GFRP plates. *Composite Structures*.
- Sika®CarboDurPlates. (2013). Product Data Sheet- Pultruded carbon fiber plates for structural strengthening, [Edition 2013-03_1].
- Sikadur®-30. (2014). Product data sheet, 2- part epoxy impregnation resin for bonding reinforcement [Edition 2014-01_1].
- Smith, S. T., and Teng, J. (2001). Interfacial stresses in plated beams. *Engineering Structures*, 23(7), 857-871.

- Society, C. (2000). Design guidance for strengthening concrete structures using fibre composite materials. Report of a Concrete Society Committee Crowthorne, UK.
- Suzuki, H. (2005). First application of carbon Fiber reinforced polymer strips to an existing steel bridge in Japan. *Advanced materials for construction of bridges, buildings and other structures*.
- Sweedan, A. M., Alhadid, M. M., and El-Sawy, K. M. (2016). Experimental study of the flexural response of steel beams strengthened with anchored hybrid composites. *Thin-Walled Structures*, 99, 1-11.
- Täljsten, B., Hansen, C. S., and Schmidt, J. W. (2009). Strengthening of old metallic structures in fatigue with prestressed and non-prestressed CFRP laminates. *Construction and Building Materials*, 23(4), 1665-1677.
- Tavakkolizadeh, M., and Saadatmanesh, H. (2001). Galvanic corrosion of carbon and steel in aggressive environments. *Journal of Composites for Construction*, 5(3), 200-210.
- Tavakkolizadeh, M., and Saadatmanesh, H. (2003). Fatigue strength of steel girders strengthened with carbon fiber reinforced polymer patch. *Journal of Structural Engineering*, 129(2), 186-196.
- Teng, J., Fernando, D., and Yu, T. (2015). Finite element modelling of debonding failures in steel beams flexurally strengthened with CFRP laminates. *Engineering Structures*, 86, 213-224.
- Teng, J., Fernando, D., Yu, T., and Zhao, X. (2011). Treatment of steel surfaces for effective adhesive bonding *Advances in FRP Composites in Civil Engineering* (pp. 865-868): Springer.
- Teng, J., Yu, T., and Fernando, D. (2012). Strengthening of steel structures with fiber-reinforced polymer composites. *Journal of Constructional Steel Research*, 78, 131-143.
- Tsai, M., and Morton, J. (1995). The effect of a spew fillet on adhesive stress distributions in laminated composite single-lap joints. *Composite Structures*, 32(1), 123-131.
- Vatandoost, F. (2010). *Fatigue Behaviour of Steel Girders Strengthened with Prestressed CFRP Strips*. (Master of Applied Science in Civil Engineering), The University of Waterloo, Waterloo, Ontario, Canada.
- Wahab, M. A., Ashcroft, I., Crocombe, A., and Shaw, S. (2001). Prediction of fatigue thresholds in adhesively bonded joints using damage mechanics and fracture mechanics. *Journal of Adhesion Science and Technology*, 15(7), 763-781.
- Walbridge, S. (2008). Fatigue analysis of post-weld fatigue improvement treatments using a strain-based fracture mechanics model. *Engineering Fracture Mechanics*, 75(18), 5057-5071.
- Wang, G., and Blom, A. (1991). A strip model for fatigue crack growth predictions under general load conditions. *Engineering Fracture Mechanics*, 40(3), 507-533.

- Wang, R., and Nussbaumer, A. (2009). Modelling fatigue crack propagation of a cracked metallic member reinforced by composite patches. *Engineering Fracture Mechanics*, 76(9), 1277-1287.
- Wenguang, L., and Guoping, C. (2010). *Analysis on fatigue life of cracked beam under forced vibration*. Paper presented at the Computer Engineering and Technology (ICCET), 2010 2nd International Conference on.
- Wu, Wang, X., Iwashita, K., Sasaki, T., and Hamaguchi, Y. (2010). Tensile fatigue behaviour of FRP and hybrid FRP sheets. *Composites Part B: Engineering*, 41(5), 396-402.
- Wu, G., Wang, H.-T., Wu, Z.-S., Liu, H.-Y., and Ren, Y. (2012). Experimental study on the fatigue behavior of steel beams strengthened with different fiber-reinforced composite plates. *Journal of Composites for Construction*, 16(2), 127-137.
- Wu, G., Wu, Z.-S., Luo, Y.-B., Sun, Z.-Y., and Hu, X.-Q. (2010). Mechanical properties of steel-FRP composite bar under uniaxial and cyclic tensile loads. *Journal of Materials in Civil Engineering*, 22(10), 1056-1066.
- Wu, Z., Wang, X., and Wu, G. (2011). Advancement of basalt fiber composites towards infrastructural applications (Keynote paper). *Proceedings of ISISS2011, Oct.*
- Xie, Y., and Wang, X. (2004). Application of G*-integral on cracked structural beams. *Journal of Constructional Steel Research*, 60(9), 1271-1290.
- Xie, Y., Xu, H., and Li, P. (1998). Crack mouth widening energy-release rate and its application. *Theoretical and Applied Fracture Mechanics*, 29(3), 195-203.
- Xiulin, Z., and Hirt, M. A. (1983). Fatigue crack propagation in steels. *Engineering Fracture Mechanics*, 18(5), 965-973.
- Yang, Q., and Thouless, M. D. (2001). Mixed-mode fracture analyses of plastically-deforming adhesive joints. *International Journal of Fracture*, 110(2), 175-187.
- Yasin, M. (2008). *Seismic Performance Assessment of Reinforced Concrete Frame Structures*. (M.Sc. Engg.), Bangladesh University of Engineering and Technology (BUET), Dhaka, Bangladesh.
- Yoon, S. H., and Lee, D. G. (2011). In situ crack propagation monitoring in tubular adhesive joints containing quartz nano-particles. *Journal of Adhesion Science and Technology*, 25(16), 1973-1985.
- Youssef, M. (2006). Analytical prediction of the linear and nonlinear behaviour of steel beams rehabilitated using FRP sheets. *Engineering Structures*, 28(6), 903-911.
- Yu, Q., Chen, T., Gu, X., Zhao, X., and Xiao, Z. (2013). Fatigue behaviour of CFRP strengthened steel plates with different degrees of damage. *Thin-Walled Structures*, 69, 10-17.

- Zhang, L., Hollaway, L., Teng, J., and Zhang, S. (2006). Strengthening of steel bridges under low frequency vibrations. *Proceedings of composites in civil engineering (CICE)*. Miami.
- Zhang, L., and Teng, J. (2010). Finite element prediction of interfacial stresses in structural members bonded with a thin plate. *Engineering Structures*, 32(2), 459-471.
- Zhao, X.-L., and Zhang, L. (2007). State-of-the-art review on FRP strengthened steel structures. *Engineering Structures*, 29(8), 1808-1823.
- Zhou, H., and Attard, T. L. (2013). Rehabilitation and strength sustainability of fatigue damaged concrete-encased steel flexural members using a newly developed polymeric carbon-fiber composite. *Composites Part B: Engineering*.
- Zhou, H., Attard, T. L., Wang, Y., Wang, J.-A., and Ren, F. (2013). Rehabilitation of notch damaged steel beams using a carbon fiber reinforced hybrid polymeric-matrix composite. *Composite Structures*.
- Zhou, H., Attard, T. L., Zhao, B., Yu, J., Lu, W., and Tong, L. (2013). Experimental study of retrofitted reinforced concrete shear wall and concrete-encased steel girders using a new CarbonFlex composite for damage stabilization. *Engineering Failure Analysis*.
- Zhou, H., Wang, Y., Shi, Y., Xiong, J., and Yang, L. (2012). Extremely low cycle fatigue prediction of steel beam-to-column connection by using a micro-mechanics based fracture model. *International Journal of Fatigue*.

LIST OF PUBLICATIONS AND PAPERS PRESENTED

1. Kamruzzaman, M., Jumaat, M. Z., Ramli Sulong, N., & Islam, A. (2014). **A Review on Strengthening Steel Beams Using FRP under Fatigue.** *The Scientific World Journal*, 2014. Vol. 2014, Article ID 702537, 21 pages (ISI-Q1).
2. Md. Akter Hosen, Mohd Zamin Jumaat, A. B. M. Saiful Islam, Mohamed Kamruzzaman, Md. Nazmul Huda and Mahmudur Rahman Soeb (2015). **Eliminating concrete cover separation of NSM strengthened beam by CFRP end anchorage.** *Structural Engineering and Mechanics*, Vol. 56, No. 6 (2015) 000-000 (ISI-Publication).
3. M. Kamruzzaman¹, M.Z. Jumaat, N.H.R. Sulong, I.M.I. Qeshta and K. Narmashiri (2017). **Effects of Lateral Bracing and Stiffeners on the CFRP Failure of Strengthened Steel Beams.** IOP Conf. Series: *Materials Science and Engineering* 210 (2017) 012021 doi:10.1088/1757-899X/210/1/012021.
4. Kamruzzaman, M., Jumaat, M. Z., Ramli Sulong, N (2016). **Flexural Behaviors of Strengthened Steel Beams using Different CFRP Plate End Shapes.** (Revision submitted: *Thin-Walled Structures*, ISI-Q1).
5. Kamruzzaman, M., Jumaat, M. Z., Ramli Sulong, N (2016). **Experimental Investigation on Fatigue Behavior of Wide-Flange Steel I-Beams Strengthened using Different CFRP End Cutting Shapes.** (Under review: *International Journal of Steel Structures*, ISI-cited publication).
6. Kamruzzaman, M., Jumaat, M. Z., Ramli Sulong, N (2016). **Nonlinear Analysis of Flexural Behavior of Strengthened Steel Beams with Different Boundary Conditions.** (Under draft) (Proposed ISI-cited publication)